CREEP2017

International Conference on
Creep and Fracture of Engineering
Materials and Structures (Creep2017)

BOOK OF ABSTRACTS

June 19–21, 2017; Saint Petersburg, Russia

organized by
POLYTECH — Peter the Great St.Petersburg Polytechnic University
Ural Federal University named after the First President of Russia
B.N. Yeltsin (Yekaterinburg)

POLYTECH
Peter the Great
St.Petersburg Polytechnic
University

Ural Federal
University

CREEP2017

14th International Conference on Creep and Fracture of Engineering Materials and Structures (Creep2017)

June 19-21, 2017; Saint Petersburg, Russia

BOOK OF ABSTRACTS

organized by

POLYTECH – Peter the Great St.Petersburg Polytechnic University

Ural Federal University named after the First President of Russia B.N. Yeltsin (Yekaterinburg)

POLYTECH
Peter the Great
St.Petersburg Polytechnic
University

Ural Federal
University

Creep and Fracture of Engineering Materials and Structures (Creep2017): Proceedings of the 14th International Conference on Creep and Fracture of Engineering Materials and Structures. June 19-21, 2017. – St. Petersburg: Polytechnical Publishing House. 2017. 170 p.

This book provides the Creep2017 Conference abstracts, provides the actual statement of recent developments in the creep analysis.

It will cover the following topics:

- Creep mechanisms;
- Modelling and simulation of creep;
- Experimental setups for creep type tests;
- Microstructure evolution and damage during creep;
- Creep of structures and creep – fatigue interactions;
- Creep under special conditions;
- The role of chemical composition on creep behaviour;
- Creep behaviour of Natural materials;
- Creep behaviour of Intermetallic compounds and alloys.

More than 100 papers are presented by the participants from USA, UK, Japan, Germany, France, Italy and other countries.

\

PREFACE

Dear Attendees!

We have the great pleasure to welcome you in Saint Petersburg, Russia, for the 14th International Conference on Creep and Fracture of Engineering Materials and Structures (Creep2017). The conferences series by founded by Professor Brian Wilshire in Swansea nearly forty years ago. This meeting happens in the first time in Russia and more than 100 attendees in Creep2017 coming from twelve countries over the world. The scientific program features more than 100 oral presentations organized in two parallel sessions running over the three days of the conference and covering several topics from creep mechanisms to design rules of structures, from experimental setup to the simulation of damage.

Building up the schedule the organizers met with the great problem dividing the time of attendees between the scientific program and the fortunate opportunity for the majority of them to visit the Northern Capital of Russia! However, we would like to hope that the delicious Venice of the North allows scientific discussions during the conference to be interesting and helpful as always it happened in these conferences.

We would like to thank the International Committee for their support and confidence, the sponsors and all the people involved in the organization of this conference.

Welcome to Creep2017 at Saint Petersburg!

Peter Panfilov and Georgii Kodzhaspirov
Creep2017 Chairs

CONFERENCE ORGANIZATION

CHAIRS:

Peter Panfilov (Yekaterinburg, Russia) and Georgii Kodzhaspirov (Saint Petersburg, Russia)

INTERNATIONAL COMMITTEE:

Lesley Cornish (South Africa),
Antonin Dlouhy (Czech Republic),
Gunther Eggeler (Germany),
Uwe Glatzel (Germany),
Hiroshi Harada (Japan),
Robert W. Hayes (USA),
Martin Heilmaier (Germany),
Haruyuki Inui (Japan),
Muthuswamy Kamaraj (India),
Michael Kassner (USA),
Kazuhiro Kimura (Japan),
Georgii Kodzhaspirov (Russia),
Michael J. Mills (USA),
Peter Panfilov (Russia),
Stefano Spigarelli (Italy),
Bernard Viguier (France),
Mark Whittaker (UK),
Alexandro Yawny (Argentina),
Zhufeng Yue (China).

ORGANIZING COMMITTEE:

Alexander Glezer (Moscow),
Georgii Kodzhaspirov (Saint Petersburg),
Andrey Kadomtsev (Saint Petersburg),
Vadim Korablev (Saint Petersburg),
Peter Panfilov (Yekaterinburg),
Artemiy Popov (Yekaterinburg),
Andrei Rudskoi (Saint Petersburg),
Nadejda Selezneva (Yekaterinburg),
Vladimir Starenchenko (Tomsk).

HISTORY OF THE CONFERENCES

CFEMS1 – Swansea, UK, 1981;

CFEMS2 – Swansea, UK, 1984;

CFEMS3 – Swansea, UK, 1987;

CFEMS4 – Swansea, UK, 1990;

CFEMS5 – Swansea, UK, 1993;

CFEMS6 – London, UK, 1995;

CFEMS7 – Irvine, USA, 1997;

CFEMS8 – Tsukuba, Japan, 1999;

CFEMS9 – Swansea, UK, 2001;

CFEMS10 – Pittsburgh; USA, 2005;

Creep2008 – Bayreuth, Germany, 2008;

Creep2012 - Kyoto, Japan, 2012;

Creep2015 – Toulouse, France, 2015;

Creep2017 – Saint Petersburg, Russia, 2017.

CONTENT

INVITED LECTURES

CREEP MECHANISMS AND MODELLING

EXPERIMENTAL SETUPS FOR CREEP TYPE TESTS

CREEP OF METALS AND ALLOYS

CREEP OF INTERMETALLICS AND ALLOYS

STEELS

CREEP UNDER SPECIAL CONDITIONS AND CREEP BEHAVIOR OF INORGANIC and NATURAL MATERIALS

INVITED LECTURES

Measurement of Power Law Creep Parameters by Nanoindentation

G.M. Pharr[1], R.S. Ginder[2], W.D. Nix[3]

[1] *Department of Materials Science and Engineering, Texas A&M University, College Station, TX, USA*

[2] *Department of Materials Science and Engineering, University of Tennessee, Knoxville, TN, USA*

[3] *Department of Materials Science and Engineering, Stanford University, Stanford, CA, USA*

Email: pharr@tamu.edu

Great progress has been made over the past decade in making mechanical property measurements by nanoindentation at elevated temperatures [1]. In addition to allowing one to measure the temperature dependence of those properties commonly investigated by nanoindentation such as hardness and elastic modulus, these advances have also paved the way for making small-scale measurements (micron and sub-micron) of the material parameters used to describe power law creep behavior such as the activation energy for creep, Q_c, and the stress exponent for creep, n. The ability to make such measurements by nanoindentation allows for high point-to-point spatial mapping of properties as well as the characterization of thin films, thin surface layers, and even small particles or the individual phases in complex multiphase microstructures. Despite this progress, significant experimental difficulties are still often encountered, and how one converts the data obtained in nanoindentation tests to the parameters normally used to characterize uniaxial creep is not at all straightforward because of the complex, non-uniform stress states produced during indentation contact.

In this presentation, we report on progress in making meaningful measurements of power law creep by nanoindentation based on recent experience with a new high temperature nanoindentation system capable of testing at temperatures up to 1100°C. Special attention is given to the models and data analysis procedures needed to convert nanoindentation load-displacement-time data, usually obtained with pyramidal indenters, into the creep parameters normally measured in uniaxial tension or compression testing [2-4]. The models and procedures are evaluated by comparison to several sets of creep data in which the material behavior has been probed both by nanoindentation and by uniaxial testing methods.

* Research sponsored in part by the National Science Foundation under grant number DMR-1427812.

References

1. J.M. Wheeler and J. Michler, *Review of Scientific Instruments* **84**, 045103 (2013).
2. A.F. Bower et al., *Proceedings of the Royal Society of London* **A441**, pp. 97-124 (1993).
3. C. Su et al., *Journal of the Mechanics and Physics of Solids* **61**, pp. 517-536 (2013).
4. R.S. Ginder, PhD Dissertation, University of Tennessee, December 2016.

Fundamentals of Creep in Aluminum Over a Wide Temperature Range

M.E. Kassner and K.K. Smith

University of Southern California

Los Angeles, CA. 90089-1453, USA

Email: kassner@usc.edu

This work describes creep research on pure aluminum including classic five power-law creep, Harper-Dorn creep, and an investigations of long-range internal stresses. Many of the models and theories for these phenomena persisted for a relatively long period of time due to the thoughtfulness of the works over the past decades. More recent developments in these phenomena are discussed that may lead to new interpretations in aluminum creep as well as other crystalline materials.

Harper-Dorn. Classic Harper-Dorn creep occurs at higher temperatures, very near the melting temperature [1-3]. Here, a stress exponent of about 1 is observed and this mechanism has been suggested at generally high temperatures for a wide variety of crystalline materials. Characteristics of Harper-Dorn creep include n=1, Q_c approximately equal to the activation energy for lattice self diffusion Q_{sd}, but many have suggested that unlike five power-law creep, the steady-state dislocation density is independent of the (modulus-compensated) stress. Interestingly, subgrains are generally not observed in the Harper-Dorn regime, and the Frank dislocation network would, by default, be the microstructural feature associated with the rate-controlling process for creep, as often suggested for five power-law creep. More recent works suggests that Harper-Dorn may not be observed in Al at these very high temperatures, but rather five-power-law creep extends into this temperature range uninterrupted by a "new" ""mechanism such as Harper-Dorn.

Five-power-law. A fairly well-accepted equation [2] for five power-law creep is:

$$\dot{\varepsilon}_{ss} = A_6 \left(\frac{\chi}{Gb}\right)^3 \left(\frac{D_{sd} Gb}{kT}\right) \left(\frac{\sigma_{ss}}{G}\right)^5 \qquad (1)$$

where □ is the stacking fault energy, A_6 is a constant, D_{sd} is the self diffusion coefficient, and G is the shear modulus. Although it is fairly well established that steady-state creep in pure metals and class M alloys is controlled by dislocation climb, the precise mechanism for creep is not well-established. There are two general lines of thinking with respect to the details of the rate-controlling process: 1.) subgrain obstacle-based theories and 2.) Frank network theories. Recent analysis suggests that the steady-state stress is predictable by the Taylor dislocation-hardening equation (2) independent of the subgrain size. The constant, □ is within the range of values observed at lower temperature where dislocation hardening is undisputed [4].

$$\sigma_y\big|_{\dot{\varepsilon},T} = \sigma'_\circ + \alpha M G b \sqrt{\rho} \qquad (2)$$

Long Range Internal Stresses (LRIS). Long range internal stresses, often suggested to be 3-20 times larger than the applied stress, have been suggested to exist in creep deformed aluminum. These high levels of LRIS have been proposed to be associated with subgrain boundaries and the rate controlling process for creep there. Convergent-

beam electron diffraction (CBED) and synchrotron x-ray diffraction experiments suggest that LRIS values are much lower than suggested by the early experiments and theoretical projections.

References

1. M.E. Kassner , P. Kumar and W. Blum, *International Journal of Plasticity*, **23**, pp. 980-1000 (2007).
2. M.E. Kassner, *Fundamentals of Creep in Metals and Alloys*, Elsevier, Third Edition, pp. 1-338 (2015)
3. K.K. Smith, M.E. Kassner. P. Kumar, *Encyclopedia of Aluminum and Its Alloys*, Taylor and Francis (2017) in press.
4. M.E. Kassner, *Acta Mater,* **52**, pp.1-9 (2004).
5. M.E. Kassner, M.-T. Pérez-Prado, M. Long, and K.S. Vecchio, *Metall. and Mater. Trans.*, **33A**, pp. 311-318 (2002).
6. T. Q. Phan, L. E. Levine, I-F. Lee, R. Xu, J.Z. Tischler, Y. Huang, T. G. Langdon, and M.E. Kassner, *Acta Mater*, **112**, pp. 231-241 (2016).
7. M.E. Kassner, P. Geantil and L.E. Levine, *Int. J. Pasticity*, **45,** pp. 44-60 (2013).

Fundamental modelling of creep in austenitic stainless steels and copper

Rolf Sandström

Materials Science and Engineering, Royal Institute of Technology, KTH

Brinellvägen 23, SE-10044 Stockholm, Sweden

Email: rsand@kth.se

Traditionally, creep and other mechanical test data have been represented with the help of empirical models that are fitted to the data with the help of a set of adjustable parameters. Such methods are usually easy to apply and they can directly give a good fit to the data. For a long time this was the only alternative for modelling of mechanical properties. However, in recent years basic models have been developed that do not require the use of adjustable parameters. In this presentation a survey of such models will be given. The advantage of the basic models is that they are predictive. New results can be proposed well outside the original set of data. Thus, the possibilities to extrapolate data to new conditions are much improved, and this is a task that has involved many scientists in the creep field. If you can develop a model that can describe available data without the use of adjustable parameters, you are assured that the model is based on the correct physical mechanisms. This is of course the main reason for the improved extrapolation capabilities. One should also be aware of that with traditional models, data can be accurately described without representing the relevant mechanisms. For example, for creep strain versus time curves, there are models that are at variance with the mechanisms involved, but the creep curves can still be accurately fitted with 3 to 4 parameters.

There are several important contributions to the creep strength from dislocations, particles, elements in solid solution, etc. Usually the contribution from the dislocations is the largest one. Various equations for the development of the dislocation density have been available for a long time. Detailed derivations of fundamental equations have recently been published [1]. There are three main contributions. Work hardening describes the generation of dislocations and recovery the annihilation of them. It has been shown that both dynamic and static recovery is of importance [2]. Dynamic recovery is strain dependent and forces dislocations together so they can annihilate each other. Static recovery is time dependent and describes how dislocations of opposite sign attract each other and again annihilate. Dynamic recovery is of particular significance during tertiary creep.

This fundamental model has been applied to copper [3],[4]. The creep curves can be well described. It is well known that cold working can significantly raise the creep strength in many cases. Recently it has been shown that the substructure plays an important role [2]. Stable structures can be formed in the cell walls that reduce the rate of static recovery and thereby raise the creep strength.

In Cu with about 50 ppm P (Cu-OFP), the small amount of P gives a large solid solution hardening effect. A quantitative modelling of this effect has recently been provided [5],[6]. Ab initio contributions have made it possible to model solid solution hardening in stainless steels [7].

It is well established that introducing particles in a material is a very powerful way to increase the creep strength. How to compute the particle strengthening at room temperature has been known for many years and a number of people have used the same equations at high temperatures, which is incorrect because climb of particles is not considered. A new procedure was proposed a few years ago. It has successfully been applied to austenitic stainless [8],[9]. It is based on a simple principle. If the particles are small enough, dislocations can climb across them without resistance. To enable the prediction of the particle hardening, the nucleation, growth and coarsening of particles must be described, which can be done with thermodynamic software.

The creep rupture can take place either by ductility exhaustion (ductile rupture) or as the result of creep cavitation (brittle rupture). Ductile rupture can be predicted with the help of ordinary creep models. However, brittle rupture requires that the cavitation is described in addition to the creep strain. Quantitative modelling of cavity nucleation has been a scientific riddle for a long time. However, basic models for grain boundary sliding are now available [10],[11]. In addition, the role of the substructure has been clarified. Cavities are assumed to form when subgrain boundaries on different sides of a sliding boundary meet [12]. Together with growth models [13], successful prediction of brittle creep rupture has been achieved [14].

All the models discussed in the present contribution are basic in the sense described in the introduction.

References

1. R. Sandström, The role of microstructure in the prediction of creep rupture of austenitic stainless steels, in: ECCC Creep & Fracture Conference, Düsseldorf, 2017.
2. R. Sandström, The role of cell structure during creep of cold worked copper, Materials Science and Engineering: A, 674 (2016) 318-327.
3. R. Sandstrom, Basic model for primary and secondary creep in copper, Acta Mater, 60 (2012) 314-322.
4. R. Sandström, J. Hallgren, The role of creep in stress strain curves for copper, J Nucl Mater, 422 (2012) 51-57.
5. R. Sandström, Influence of phosphorus on the tensile stress strain curves in copper, J Nucl Mater, 470 (2016) 290-296.
6. R. Sandström, Fundamental Models for Creep Properties of Steels and Copper, Trans Indian Inst Met, 69 (2016) 197-202.
7. P.A. Korzhavyi, R. Sandström, First-principles evaluation of the effect of alloying elements on the lattice parameter of a 23Cr25NiWCuCo austenitic stainless steel to model solid solution hardening contribution to the creep strength, Materials Science and Engineering: A, 626 (2015) 213-219.
8. R. Sandström, M. Farooq, J. Zurek, Basic creep models for 25Cr20NiNbN austenitic stainless steels, Materials Research Innovations, 17 (2013) 355-359.
9. S. Vujic, R. Sandstrom, C. Sommitsch, Precipitation evolution and creep strength modelling of 25Cr20NiNbN austenitic steel, Mater High Temp, 32 (2015) 607-618.
10. R. Sandström, R. Wu, J. Hagström, Grain boundary sliding in copper and its relation to cavity formation during creep, Materials Science and Engineering: A, 651 (2016) 259-268.
11. J. He, R. Sandström, Modelling grain boundary sliding during creep of austenitic stainless steels, J Mater Sci, 51 (2016) 2926-2934.
12. J. He, R. Sandström, Formation of creep cavities in austenitic stainless steels, J Mater Sci, 51 (2016) 6674-6685.
13. J. He, R. Sandström, Creep cavity growth models for austenitic stainless steels, Materials Science and Engineering: A, 674 (2016) 328-334.
14. J. He, R. Sandström, Brittle rupture of austenitic stainless steels due to creep cavitation, Procedia Structural Integrity, 2016, pp. 863-870.

Low-stress Creep of Creep Resistant Steels

L. Kloc[1*], P. Dymáček[1,2], N. Luptáková[1,2]

[1]Institute of Physics of Materials AS CR, Žižkova 22, 61662 Brno, Czech Republic

[2]CEITEC IPM, Institute of Physics of Materials AS CR, Žižkova 22, 61662 Brno, Czech Republic

Email: kloc@ipm.cz

Higher efficiency of power plants could be reached by higher temperatures of the working media, but this trend is limited by the creep life and corrosion resistance of the structural materials. So new materials are developed to meet the requirements of prospective A-USC plants, mainly austenitic steels and special alloys like Sanicro 25. The steels exhibit better creep properties and corrosion resistance than ferritic steels, but they are prone to thermomechanical fatigue due to lower thermal conductivity and higher expansion. Modelling of the stresses generated by the temperature gradients for particular parts of the plant is necessary. Since the creep mechnisms are relaxing theese stresses, reliable creep data at wide range of stresses are needed for the model formulation.

Process of creep deformation is too slow under conditions corresponding to industrial use of the steels. Laboratory experiments have to be accelerated by application of higher temperature and/or stress, and subsequent extrapolation process may be a source of potentially dangerous errors. Extrapolation can provide false results mainly if the creep deformation mechanism is changing. Evidences were presented that such change at very low creep rates occurs [1]. In most cases, both stress and temperature dependencies of the creep rate become weaker at low stresses. As was demonstrated by Kimura et al. [2], the creep life standards based on extrapolatin dangerously overestimate the real time to fracture for extremly long creep tests of about 100,000 hrs.

It is well known that cavities which are able to growth to dangerous sizes are nucleated during primary creep [3]. The primary stage can be assumed as an important indicator of overall creep properties. Thus, any models of creep life should be able to describe the primary creep stage correctly. Unfortunately, most current approaches tend to ignore the primary stage completely, which makes their reliability questionable.

Primary creep can be measured experimentally even at conditions close to application ones, if high strain sensitivity creep technique is employed. Helicoid spring specimens technique [4] have been used sucessfully for many materials.

Primary creep curve obtained for the creep resistant steels can be fitted by the Li equation [5] successfully.

(1)

where is creep strain, is secondary stage strain rate, is primary stage relaxation time, is initial strain rate and is time.

Though the primary creep curves at low stresses look similar as that at higher stresses, stress and temperature dependences of their parameters are completely different, indicating the difference in deformation mechanism. For instance, the creep deceleration in primary stage is strain controlled at higher stresses, but time controlled

at low stresses. Also temperature dependence of the creep rate at low stresses is much weaker than that at higher stresses. Last but not least, the ratio of the creep rates of different materials under the same conditions is much lower at low stresses than at higher stresses, as can be seen in the figure 1. This means the efficiency of the reinforcing elements in the microstructure is much lower with the low stress deformation mechanism [6].

Figure 1: *Comparison of creep rates of pure iron and two creep resistant steels at 600ºC and wide range of stresses.*

Acknowledgement: This work was supported by the Czech Science Foundation under contract no. 15-21394S, and partly accomplished in CEITEC – Central European Institute of Technology with research infrastructure supported by the Ministry of Education, Youth and Sports of the Czech Republic under the project CEITEC 2020 (LQ1601).

References

[1] L. Kloc, V. Sklenička, J. Ventruba, «Comparison of low stress creep properties of ferritic and austenitic creep resistant steels», *Mater. Sci. Eng.* A 319-321, 774-778, (2001).

[2] K. Kimura, K. Sawada, H. Kushima, «Assessment of long-term creep strength of grade 91 steel», in Lecomte-Beckers et al. (eds.) *Materials for Advanced Power Engineering 2010,* Forschungszentrum Julich GmbH., pp 162-171, (2010).

[3] A. S. Argon, «Intergranular cavitation in creeping alloys», *Scripta Metall.* **17**, 5-12, (1983).

[4] L. Kloc, P. Mareček, «Measurement of very low creep strains», *J. Test. Eval.* **37,** 53-57, (2009).

[5] J.C.M. Li, «A dislocation mechanism of transient creep», *Acta Metall.* **11,** 1269, (1963).

[6] L. Kloc, J. Fiala, V. Sklenička, «On the strengthening factors of structural steels under low stress creep regime», *Chem. Listy, Symposia* **96,** S212-S214, (2002).

Fraction-exponential operators in micromechanical modeling of creep processes in heterogeneous solids

Igor Sevostianov

Department of Mechanical and Aerospace Engineering, New Mexico State University, Las Cruces, NM 88003, USA

Email: igor@nmsu.edu

Modeling of the effective viscoelastic properties of heterogeneous hereditary materials has a very long history starting with remark of Eshelby (1957) that his results on elastic inclusion can be extended to linear viscoelastic materials. The standard approach to solve problems of viscoelasticity is based on elasticity-viscoelasticity correspondence principle: The problem is formulated in the Laplace domain, treated as the elastic one, and then, inverse transform gives the desired viscoelastic solution. The main challenge appearing in using elastic-viscoelastic analogy is to obtain analytical formulas for inverse Laplace transform. This difficulty constitutes the main reason to use the oversimplified dashpot-spring models. Unfortunately, the simplest models are not sufficiently flexible to match experimental data for real materials. An alternative approach has been proposed by Scott Blair and Coppen (1939, 1943) (based on experimental observations) and by Rabotnov (1948) (theoretically). They suggested to use fraction-exponential operators that, on one hand can describe experimental data of real materials with sufficient accuracy and, on the other hand, allow inverse Laplace transforms in explicit analytical form. This model has been rediscovered by Bagley and Torvic (1983, 1986) who called it “Cole-Cole model” since similar approach has been proposed by Cole and Cole (1941) to describe dispersive properties of dielectrics.

In this presentation, we show how the fraction exponential operators can be used in micromechanical modeling of heterogeneous hereditary solids. First, the history of the problem with analysis of the existing approaches is discussed and advantages of fraction-exponential operators are illustrated on several examples. Then we show how these operators can be used in micromechanics through creep and relaxation contribution operators of the inhomogeneities and implementation of the these operators into various homogenization schemes. The approach is illustrated on several examples that cover materials as different as fiber reinforced plastics, porous and micro-cracked ceramics, oolitic limestone, and dentin.

On Physical Basis of Larson-Miller Constant of 20

K. Maruyama[1], F. Abe[2], H. Sato[3], J. Shimojo[4], K. Yoshimi[1]

[1]. Department of Material Science, Tohoku University, Sendai, Japan

[2]. Structural Materials Division, National Institute for Materials Science, Tsukuba, Japan

[3]. Department of Mechanical Science and Engineering, Hirosaki University, Hirosaki, Japan

[4]. Energy & Nuclear Equipment Division, Kobe Steel, Takasago, Japan

Email. kouichi.maruyama@tohoku.ac.jp

The following Larson-Miller (LM) and Sherby-Dorn parameters are widely used when formulating stress-creep rupture life data as a function of stress and tempe

$$P = (\log t_r + C)\ T = f(\sigma) \quad (1)$$

$$P = \log t_r - (Q/R\ T) \log e = f(\sigma) \quad (2)$$

where t_r is the rupture life, R is the gas constant, and $f(\sigma)$ is a function of σ. The LM constant C and the activation energy Q characterize temperature dependence of t_r. $Q = Q_{LD}$ (Q_{LD}: activation energy for lattice self-diffusion) in creep of pure metals and pure metal type solid solution alloys. On the other hand, C is often assumed to be 20, but its physical basis is not obvious. Stress-rupture life data sets of nickel based alloy 617, 304H and 304J1 stainless steels, A3004N aluminum alloys and Mg-Al alloys were formulated with Eqs.(1) and (2) for determining C and Q of each data set. Based on the correlation between C and Q, it is discussed what is the C value corresponding $Q = Q_{LD}$. It is also examined how the C values change with melting temperature of the materials.

The values of C and Q change with the data sets even within the same material. In a material, C is related to Q by the following equation when the data sets were creep tested in a similar temperature and stress ranges:

$$C = (Q/R\ T_{av}) \log e - \log t_{rav} \quad (3)$$

where T_{av} and t_{rav} are the average values of testing temperatures and rupture lives of the material, respectively. The value of C corresponding to a given value of Q increases with decreasing T_{av} when t_{rav} is similar, or with decreasing t_{rav} when T_{av} is similar. The following relation, $Q_{LD} = a\ R\ T_m$ (a: a constant, T_m: melting temperature), is known in lattice self-diffusion. Creep tests are usually conducted at temperatures of similar T/T_m regardless of material. Therefore C takes similar values in all the materials. The value of C corresponding to $Q = Q_{LD}$ is 10 to 13 under usual creep test conditions. It is concluded that the assumption, $C = 20$, is not equivalent to $Q = Q_{LD}$.

Role of strain-induced particle coarsening in creep strength breakdown

R. Kaibyshev

Belgorod State University, Pobeda 85, 308015 Belgorod, Russia

E-mail: rustam_kaibyshev@bsu.edu.ru

Tempered martensite lath structure (TMLS) plays a vital role in creep resistance of 9-12wt.%Cr martensitic steels. Stability of TMLS under creep conditions is provided by concurrent operation of three agents: (i) a dispersion of boundary $M_{23}C_6$ carbides and Laves phase; (ii) a dispersion of M(C,N) carbonitrides, which are homogeneously distributed within ferritic matrix; (iii) substitutional alloying element within ferritic matrix. Decreasing efficiency of these agents facilitates transformation of TMLS to subgrain structure that deteriorates creep resistance and leads to the creep strength breakdown subdividing short-term creep range from long-term one. Depletion of W from solid solution is observed under both creep regimes, but the strain-induced coarsening of $M_{23}C_6$ carbides and Laves phase decreases and strain-induced transformation of nanoscale M(C,N) dispersoids to coarse particles of Z-phase are observed only under long-term creep conditions. These processes diminish Zener drag force that leads to the transformation of TMLS into subgrain structure. In contrast, under long-term aging no strain-induced coarsening of boundary particles occurs and the lath structure retains up to very high rupture times. Therefore, the strain-induced coarsening of boundary particles and phase transformations play an important role in the creep strength breakdown. Mechanisms providing strain-induced coarsening and strain-induced formation of Z-phase are discussed.

Low Temperature Creep in Metals

K.K. Smith and M.E. Kassner

University of Southern California, Los Angeles, CA. 90089-1453, USA

Email: kassner@usc.edu

Many crystalline materials are known to exhibit creep at low temperatures ($T < 0.3T_m$). Here we review and analyze the phenomenological relationships that describe primary creep (steady-state is usually not applicable). The discussion focuses on whether power-law (Eq. 1)

$$\varepsilon = at^n + c \qquad (1)$$

where $0 < n < 1$, or whether, alternatively, logarithmic (Eq. 2) descriptions better describes the experimental primary creep database at low temperatures.

$$\varepsilon = \alpha \ln t + c \qquad (2)$$

We compiled data from the literature as well as new experimental copper and silver primary creep data recently obtained by the authors. Depending on the material, it appears that the logarithmic form can somewhat better describe creep behavior at low temperatures, while the power-law behavior manifests at intermediate temperatures. The basic mechanism(s) of low-temperature creep plasticity is examined, as well. The Seeger forest-dislocation intersection mechanism may apply to lower stacking fault energy metals [1].

References

1. M.E. Kassner, *Fundamentals of Creep in Metals and Alloys*, Elsevier, Third Edition, pp. 1-338 (2015)

Basic model for creep of fcc metals: implementation for description of pure Aluminum and Al-Mg single phase alloys

S.Spigarelli[1], R. Sandström[2]

[1] *DIISM, Università Politecnica delle Marche, via Brecce Bianche, I-60131 Ancona, Italy*

[2] *Materials Science and Engineering, KTH, Binellvägen 23, S-100 Stockholm, Sweden*

Email. s.spigarelli@univpm.it

The description of the steady state creep rate dependence on applied stress and temperature is almost invariably based on the Norton equation or on derived relationships, which are phenomenological in nature and can seldom unambiguously be related to microstructural parameters such as dislocation density. This fact led to the development of a model with a physical basis that was successfully used to describe the creep response of fcc metals such as copper [1]. The model is based on the well-known Taylor equation, in which the free dislocation density (ρ) is related to the applied stress in the form

$$\sigma = \sigma_i + \alpha m G b \sqrt{\rho} \qquad (1)$$

where m is the Taylor factor (m=3.06 for fcc metals). The term σ_i , frequently defined as “internal stress”, represents the strength of pure annealed metal- that is, the stress required to move a dislocation in absence of other dislocations, although it could include the effect of solute, grain boundaries barriers etc- while α is a constant (α=0.2-0.4). The evolution of the dislocation density during straining can be expressed as

$$\frac{d\rho}{d\varepsilon} = \frac{m}{bL} - \omega\rho - \frac{2}{\dot{\varepsilon}} M_{cg} \tau_l \rho^2 \qquad (2)$$

where ω is a constant and L is the dislocation mean free path i.e the distance travelled by a dislocation before it undergoes a reaction, usually expressed as

$$L = \frac{C_L}{\sqrt{\rho}} \qquad (3)$$

being C_L the strain-hardening constant. In Equation 2, τ_l is the dislocation line tension ($\tau_l = 0.5Gb^2$), and M_{cg} is the climb and glide mobility, which is

$$M_{cg} = \frac{D_{0sd} b}{kT} \exp\left[\frac{(\sigma - \sigma_i) b^3}{kT}\right] \exp\left\{-\frac{Q_{sd}}{RT}\left[1 - \left(\frac{\sigma - \sigma_i}{R_{\max}}\right)^2\right]\right\} \qquad (4)$$

The first term on the right-side part of Eqn.2 represents the strain hardening effect due to dislocation multiplication, which is more rapid when L and, consequently, C_L assume low values and/or the dislocation density is very high. The second term at the right-hand side of Eqn.2 describes the effect of dynamic recovery. The view that creep in pure fcc metals is controlled by climb alone has been rarely challenged. Climb gives rise to static recovery which is taken into account in the third term on the right-hand side.

At steady state [2],

$$\dot{\varepsilon} = \frac{2M_{cg}\tau_I bC_L}{m - \omega C_L\left(\left(\sigma - \sigma_i\right)/\alpha mG\right)}\left(\frac{\sigma - \sigma_i}{\alpha mGb}\right)^3 \qquad (5)$$

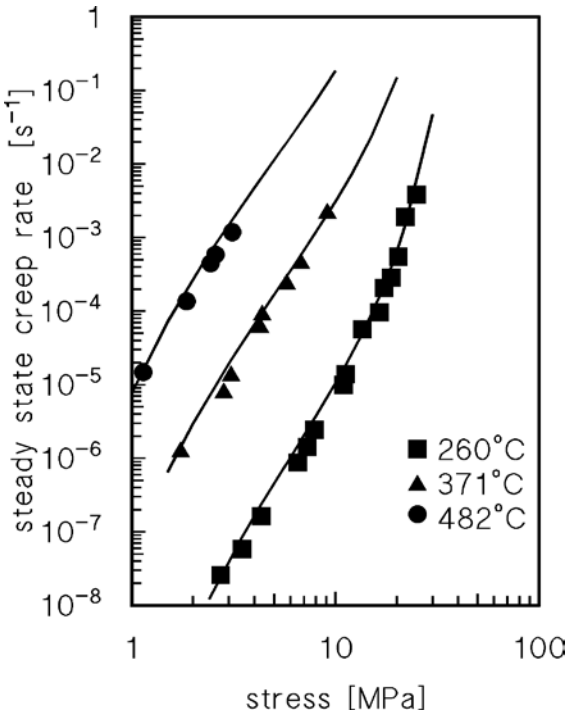

Figure 1. Steady state creep rate for high purity aluminium. Experiments from [3].

Equation 5 results in a stress exponent which is slightly larger than 3, and thus is in principle consistent with the observed n=4-5 values for pure metals and is able to describe creep results obtained in the low-temperature regime, which are characterized by larger *n* values.

The model above described was used to describe the steady state creep dependence on stress and temperature for high-purity Al [3] and for Al-Mg alloys [4]. Figure 1, as an example, shows very well the accuracy of the model in describing the experimental data.

1. R. Sandström, J. Hallgren, The role of creep in stress strain curves for copper, J.Nucl.Mater. **442**, pp. 51-57 (2012).

2. R. Sandström, The role of cell structure during creep of cold worked copper, Materials Science and Engineering: A, **674** pp. 318-327(2016).

3. I.S. Servi, N.J. Grant, Creep and Stress Rupture Behaviour of Aluminum as a Function of Purity. Journ. of Metals, Trans. AIME **191**, pp.909-916 (1951).

4. H.Oikawa, K. Honda, S.Ito, Experimental study on the stress range of class I behaviour in the creep of Al-Mg alloys, Mater.Sci.Eng**. 64**, pp. 237-245 (1984).

An investigation of creep under non-constant stress and temperature conditions in Waspaloy

Veronica Gray[1], Mark Whittaker[1], Steve Williams[2]

[1] *Institute of Structural Materials, Swansea University, Crymlyn Burrows, Swansea, SA1 8EN, UK*

[2] *Rolls-Royce plc, P.O. Box 31, Derby, DE24 8BJ, UK*

Corresponding Author: m.t.whittaker@swansea.ac.uk

In developing more accurate lifing models for critical aerospace components, knowledge of the development of evolving stress conditions is required to make appropriate predictions. Traditional approaches have been based around data conducted under isostress and isothermal conditions, enabling the development of constitutive relationships. However, in many applications both stress and temperature may vary, particularly during a full cycle, and results of these changes are not well understood, either in terms of microstructural behaviour or predictive capability.

Recently, Harrison *et al.* [1] conducted traditional and transient creep tests on Waspaloy over a range of conditions where the Theta lifing model was applied with limited success. More recent follow up tests of cyclic transitions from a Low Temperature High Stress (LTHS) to High Temperature Low Stress (HTLS), have shown that the LTHS cycle has decreasing or no pseudo–primary creep and increasing creep rate every cycle, whereas the HTLS cycle showed consistent pseudo-primary creep and a constant minimum creep rate.

This work takes a systematic approach to transient creep testing on Wasploy, a well understood material that can collate with previous work, in order to develop understanding. A test programme where creep conditions were cycled every 24 hours was undertaken examining the following variables:

- Constant Temperature: a test at constant temperature but with changing stress
- Constant Stress: a test at constant stress and changing temperature
- Constant Normalised Stress: cycling between two stress/temperature conditions with $\sigma/\sigma_{UTS}=0.6$
- Extreme conditions: cycling between conditions of extreme LTHS and HTLS
- Cycle order: all tests performed start with the LTHS condition, this test reverses the order.
- Traditional: all conditions used above were tested under isothermal/isostress creep for comparison

Interrupted tests were also performed and microstructural analysis was undertaken in order to further understand the creep damage mechanisms of different cycles and conditions.

[1] W. J. Harrison, M. T. Whittaker, and C Deen, “Creep behaviour of Waspaloy under non-constant stress and temperature”, Materials Research Innovation **17**(5), 2013.

Modelling tertiary creep of copper

Fangfei Sui, Rolf Sandström

Materials Science and Engineering, Royal Institute of Technology, KTH, Brinellvägen 23, SE-10044 Stockholm, Sweden

Email: fangfei@kth.se

Canisters made of oxygen free copper alloyed with 50 ppm phosphorus (Cu-OFP) are planned to be used to store spent nuclear fuel in Sweden. During the long term storage underground, the copper will be exposed to creep. It is critical that the controlling mechanisms and design procedures for creep are fully understood. A typical creep curve shows three stages. The creep rate decreases during primary stage, reaches a steady state value in secondary creep, accelerates during tertiary creep and terminates at rupture. For many materials the high initial creep rate is due to a low starting dislocations density and the accompanying low back stress. The work hardening gives rise to a decreasing creep rate. At the same time the recovery due to the annihilation of dislocations starts to become of importance. When recovery and work hardening balance, the stationary creep stage is reached. Based on the creep recovery mechanism, dislocation models were formulated. The primary and secondary creep of Cu-OFP can be represented by fundamental models [1]. In the present paper, the modelling of tertiary creep will be discussed.

There are several possible creep damage mechanisms including microstructure degradation, cavitation, necking instability and recovery which can accelerate the creep rate during tertiary creep. A model that takes substructure development during creep into account, which was derived for cold worked material can be used to represent a major part of tertiary creep [2].

In this model, dislocations in the cell walls are divided into two sets, balanced and unbalanced. In the former set, the number of dislocations with opposite sign is balanced. In the latter set, the dislocations are polarised, dislocations of only one sign are present. The unbalanced dislocations cannot annihilate each other since the opposite sign dislocations are missing. They do not contribute to static recovery. Both sets of dislocations will generate new unbalanced dislocations.

Since the balanced dislocations are exposed to static recovery, the dislocation density will be constant during secondary creep. At the same time the unbalanced dislocation density will continuously increase and so does the dynamic recovery, which explains the enhancement of the creep rate. A major back stress is built during secondary creep that matches the continuous increase of the true applied stress. At the end of the secondary stage the increase in the back stress is no more so pronounced and the effective stress is raised causing the increase of the creep rate in the tertiary stage.

Fig.1 shows the comparison of the model with experimental results. The three creep stages are reasonable well reproduced. It is interesting to note that the model can describe the logarithmic decrease in the strain rate in the primary stage, which has been observed for a number of materials. The rapid increase in the tertiary can also be represented.

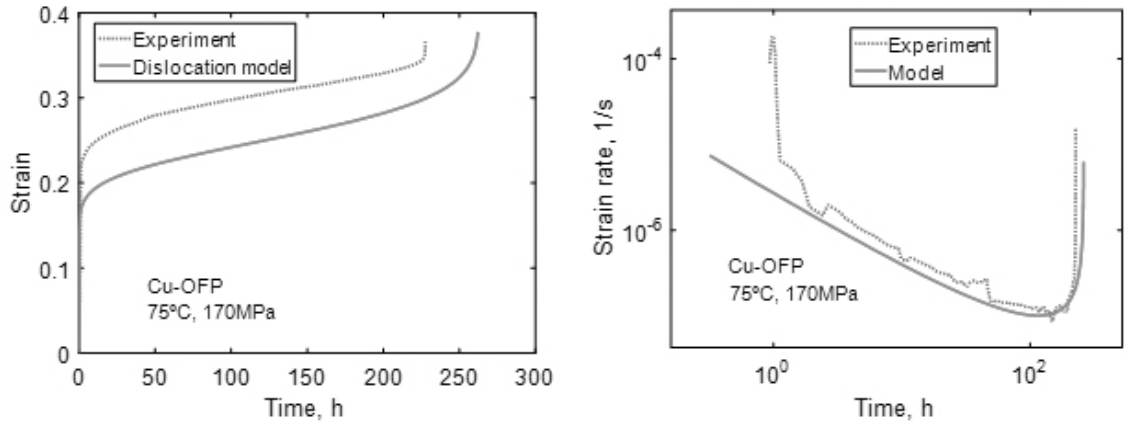

Fig. 1 Creep rupture curve for Cu-OFP at 75°C and 170 MPa. Annealed material; a) Creep strain versus time; b) Creep strain rate versus time. Experimental data from [1]

References

[1] R. Sandstrom. Basic model for primary and secondary creep in copper, *Acta Materialia* **60**, pp. 314-322 (2012).

[2] R. Sandström. The role of cell structure during creep of cold worked copper, *Materials Science and Engineering: A*, **674**, pp.318-327 (2016).

Four Regions in Low-Temperature Creep of Ultrafine-Grained Aluminum

E. Sato[1], K. Higane[1], H. Masuda[1], K. Kitazono[2]

[1]. Institute of Space and Astronautical Science, Japan Aerospace Exploration Agency, Japan

[2]. Graduate School of System Design, Tokyo Metropolitan University, Japan

Email. E. Sato. sato@isas.jaxa.jp

The present study investigated the low-temperature creep mechanisms in ultrafine-grained (UFG) aluminum manufactured by accumulative roll bonding. UFG aluminum with grain size 0.39 □m showed steady state creep even at room temperature under low stresses as confirmed by the creep curves in the □-□plot shown in Fig. 1. The low-temperature behavior was divided into four regions by three distinctive stresses, □, □ and □: □ (=45 MPa) is denoted as the micro-yielding stress with which dislocations start movement, □ (=85 MPa) the dislocation multiplication stress above which dislocations multiply with creep deformation, and □ (=171 MPa) the conventional yield stress above which macroscopic plastic strain is generated. As shown in Fig.2, during low-temperature creep, below □, negligible plastic strain is generated. Between □ and □, creep deformation with stress exponent 2.5 occurred, which is accommodated by dislocation absorption into grain boundary and by grain boundary sliding, similarly to the low-temperature creep of h.c.p. metals [1]. Between □ and □, creep deformation with stress exponent 7.0 occurred, whose mechanism is similar to the low-temperature creep of coarse-grained aluminum [2]. Above □, power-law breakdown occurred.

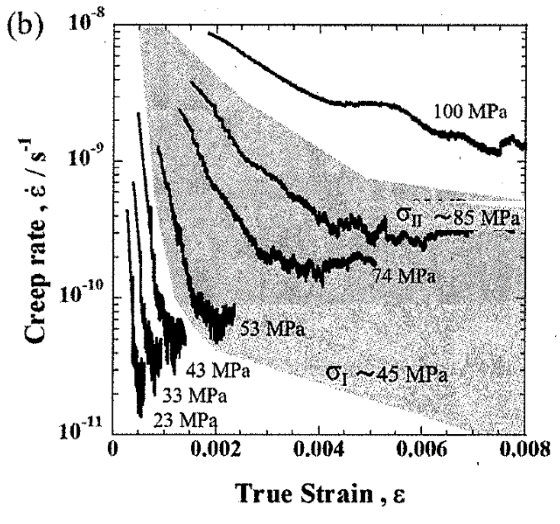

Fig. 1 creep curves in the □-□plot.

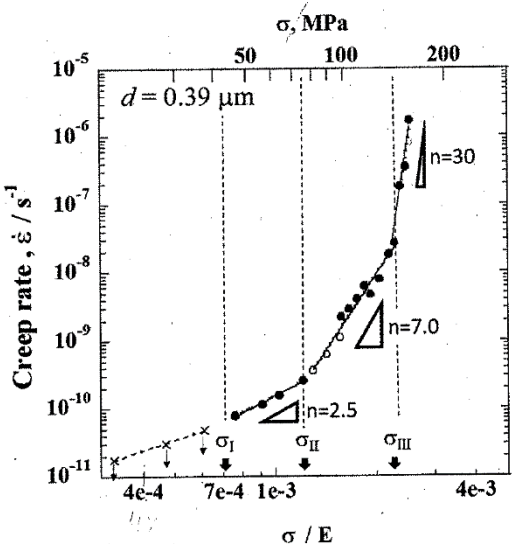

Fig. 2 Double logarithmic plot of creep rate and stress

References

1. T. Matsunaga et al., Phil. Mag. **90**, pp. 4041–1054, (2010).

2. T. Matsunaga et al., Scripta Mater. **63**, pp. 516–519, (2010).

The Crack-Tip Creep Damage Assessment Under Multi-Axial Stress State

V. Shlyannikov[1], A. Tumanov[1]

[1] Kazan Scientific Center of Russian Academy of Sciences, Kazan, Russia

Email. shlyannikov@mail.ru

Fields of stress, strain rate and process zone of a mode I creep crack growth are analyzed by employing damage evolution equations under multi-axial stress of state. Damage model for fracture of process zone represented by stress based formulation. Two expressions are derived to describe the stress-sensitive nature of multi-axial rupture behavior. The most general multi-axial creep rupture criterion is obtained as follows:

- in the tension-tension quadrant the behavior can be approximated by combination of the maximum hydrostatic stress and an octahedral shear stress criteria

$$D_f^{(+)} = (1-\chi) J_1 + \chi \sqrt{J_2'} \qquad (1)$$

- in the tension-compression quadrant the behavior can be approximated by combination of the maximum principal tensile stress and an octahedral shear stress criteria in the form of the Pisarenko-Lebedev limiting state theory [1]

$$D_f^{(-)} = (1-\chi) \sigma_{mp} + \chi \sqrt{J_2'} \qquad (2)$$

in which χ is the experimental material constant that is determined as the ratio of uniaxial tensile to compression strength $\chi=\sigma_t/\sigma_c$, where σ_{mp} is the maximum principal tensile stress, J_1 is the first stress invariant, J_2' is the second deviatoric stress invariant. We introduce a function for rate of accumulation of creep damage in the following form

$$\dot{\omega} = C \left[\frac{D_f^{(\pm)}}{(1-\omega)} \right]^m \qquad (3)$$

where *C* and *m* are material constants and multi-axial stress function $D_f^{(\pm)}$ described by Eqs.(1,2). By assuming that the creep strain rate is governing by the equivalent von Mises stress, the damage accumulation constitutive equation in multi-axial state of stress is used in the form given by Kachanov

$$\dot{\varepsilon}_{eqv} = B \left(\frac{\sigma_{eqv}}{1-\omega} \right)^n \qquad (4)$$

where *B* and *n* are constants of the Norton power law equation.

By the authors [2] one unified parameter in the form of a creep stress intensity factor (SIF) is introduced based on the asymptotic stress and strain the crack tip fields for elastic-nonlinear-viscous solid which gives more accurate the characterization of fracture resistant properties materials and structures

$$\overline{K}_{cr} = \left(\frac{C^*}{\dot{\varepsilon}_0 \sigma_0 I_n L} \right)^{1/(n+1)} ; \qquad (5)$$

The evolution of the creep crack-tip damage and variation of the creep stress-strain fields with time were analyzed by using the FE-model. Two cases of continuum solids state, i.e. undamaged creeping material and defective material with different degree of creep damage, were examined. A governing parameter of damage field for creeping solids under multi-axial stress state represented by the experimental constant in the form of ratio uniaxial tensile rupture strength to compression $\chi=\sigma_t/\sigma_c$ at an appropriate test temperature. In order to interpret of numerical results in the present study a current creep time t normalized by the transition time t_T.

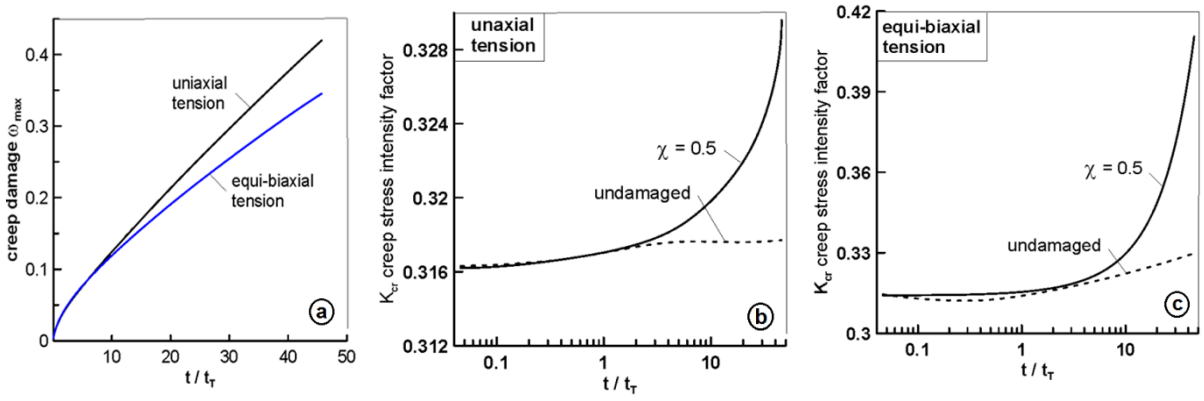

Figure 1. Creep damage and SIF behavior under multi-axial loading

In Fig.1,a the numerical results for the maximum size of creep damage zone behaviour are shown as a function of creep time under multi-axial stress state. Figs.1,b and 1,c represent the corresponding data for creep stress intensity factor behavior under uniaxial and biaxial loading according to Eq.(5). The curve concerns to the undamaged material for the steady state of secondary creep solution is also shown in these figures. It is clear that the effect of damage evolution appears at the extensive creep condition behind of the small-scale state when the transition time $t/t_T > 1$. It has been concluded that the creep holding time and multi-axial states of stress may be combined to produce a method on the basis of creep stress intensity factor for quantifying the damage effects on creep crack growth rate.

References

1. G. Pisarenko and A. Lebedev, *Naukova Dumka, Kiev,* 415p. (1976).
2. V. Shlyannikov *et al., Engineering Fracture Mechanics* 142, pp. 201–219, (2015).

Multi-scale modeling of dislocations behavior in molybdenum

V. Tseplyaev, S. Starikov, N. Serenko

Joint Institute for High Temperatures of RAS, Moscow 125412, Russia

starikov@ihed.ras.ru

Currently, there is a problem in Materials Science about accurate description and prediction of behavior of structural materials under extreme state. This task may be resolved by several methods, but the most perspective approach is the multi-scale modeling. Various techniques of modeling and theoretical physics are used for solution of subtasks on various time and spatial scales. The cooperation of different approaches (such as quantum calculations, atomistic simulation, dislocation dynamics, phase field modeling, kinetic equations and continuum mechanics) allows to predict the behavior of structural materials without use of experimental data. At the present time, the multi-scale model is at development stage. However, there are essential achievements in various methods of simulation of materials' properties at thermal, deformation and radiation impacts on various scales.

In this work, various types of computer simulation were performed for study of dislocations behavior in molybdenum. We used three different models: development of an interatomic potential on the basis of ab-initio calculations; molecular dynamics simulations; dislocation dynamics. Such multi-scale approach allows us to investigate the dislocation properties and compare the simulation results with the available experimental data. Particular attention is given to the link between models at various scales and calculations of macroscopic features (like stress-strain curve).

Monitoring of evolution process of microstructure for natural materials and prediction their fracture with AMD-methods

I.A. Migel[1], A.I. Kustov[2]

[1] Voronezh, Russia, Military Educational and Scientific Center of the Air Force Academy named after Professor N. E Zhukovsky and Y.A. Gagarin

[2] Voronezh, Russia, Voronezh State Pedagogical University

akvor@yandex.ru

Natural materials are among the surrounding materials leading place. One of the urgent problems of material science today is the problem of predicting the behavior of natural materials, including their manifestation in processes of creep. To solve this problem proposed to use a developing in the last 15-20 years the methods of acoustic-microscopy [1,2] or AMD-methods. They allow you to get with the help of acoustic waves (AB) structure of the image on the time-personal depth from the surface of the object (Figure 1a and 1b). It does not require any additional surface treatment, including chemical etching. Under the influence of the applied voltage is constantly changing structure of the object, and then change its properties. Thus, depending on the temperature conditions, humidity, time changing rate transformation test structures and material properties. AMD-methods allow us to assess the changes in the physical and mechanical properties of natural materials, observe the emergence of defects, identify areas of critical stress and the local destruction. The materials produced by powder technology forecasting the behavior of the material was carried out both on the analysis of the level of porosity of the acoustic image, and from the values of the velocity of acoustic waves and their level of absorption (Fig.1c and 1d) by the method developed earlier [3]. These results confirm the effectiveness of AMD, methods for analyzing processes of creep in natural materials.

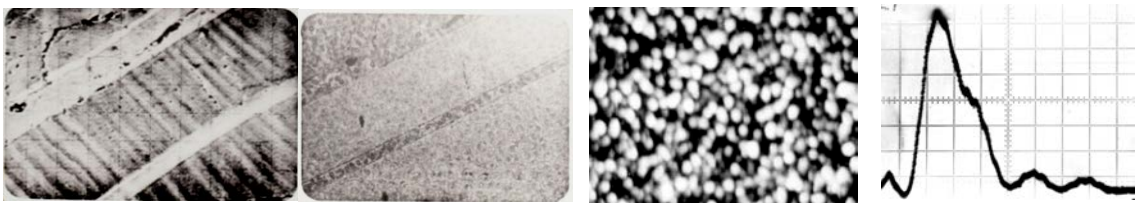

Fig.1. Comparative and acoustic a) and optical b) image area sphalerite of the sample (50 mkm / div;. Optics-120[x]) with inhomogeneities banded type with a characteristic size of 12-17 microns; c) The acoustic image of PZT-ceramics (ЦТС-19) at a depth of ~ 32 microns (the horizontal size of 250 microns); g) The experimental curves of ceramics PZT-22 (the horizontal scale of 5.2 micron / div., $\square Z_N$ = 10,09 mkm, $\square_R$ = 2,29·10 ^{3} m / s).

References

1. Kustov A.I., Migel I.A. Glass Physics and Chemistry, v.22., № 3., p. 245-247 (1996).
2. A.I. Kustov, I.A. Miguel. Material Science., №8., p. 15 - 19 (2011).
3. A.I. Kustov, I.A. Miguel, Fundamental Problems of Material Science, vol. 11, №4 / 2, p.592 - 598 (2014).

Development of methods for control of creep solid state materials based on the physical principles of the propagation of acoustic waves

V.M. Zelenev[1], A.I. Kustov[1], I.A. Migel[2]

[1]Voronezh, Russia, Voronezh State Pedagogical University

[2] Voronezh, Russia, Military Educational and Scientific Center of the Air Force Academy named after Professor N. E Zhukovsky and Y.A. Gagarin

akvor@yandex.ru

Creep processes play an important role in the natural phenomena, and in the technical and technological applications. They appear in the mother crystals of different nature - and in metals and dielectrics, and crystalline and amorphous materials. Actual materials science problem is that the objective control creep process. It can be successfully achieved on the basis of the analysis of structural building materials, a set of their physical characteristics, the study of the dynamics of the processes of nucleation and development of certain defects or their systems. This requires particular attention the prediction of the critical state of the material, including during creep.

Creep process control techniques in metallic materials using acoustic waves [1,2] have been developed. They allow you to obtain subsurface acoustic image material structure (Figure 1a), watch her transformation during deformation effects [3]. On the basis of the ray approach, developed the method of calculation of acoustic wave velocity samples and their level of attenuation from the characteristic of V (Z) -curves) (Figure 1b) [4]. The methods provide a calculation of the elastic modulus and their changes in the result of external influences, identification and characterization of defective structures, the identification communication of the grain size and the speed of the acoustic waves (Figure 1c).

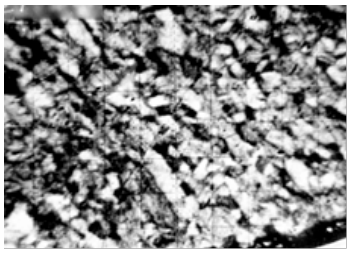

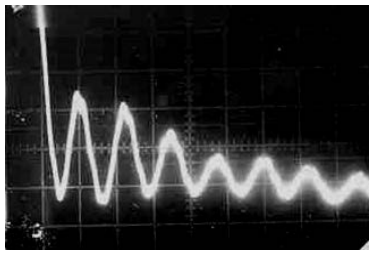

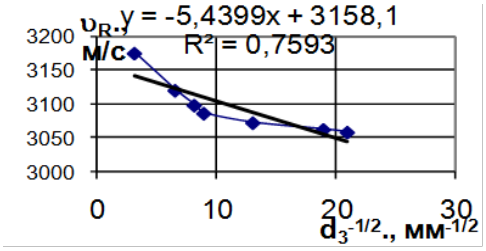

Fig.1. a) Acoustic Image of 10X12H2BMΦ- steel structure (scale: 20 micron / div, Z = - 17 micron), f = 407 MHz, α / f ^{2} = 29.102 dB / m·GHz^2; b) V (Z) - curve for steel 10X12H2BMΦ (horizontal: 14 micron / div, vertical: 0.25 V / div, $\square Z_N$ = 17,4 micron); c) The dependence of the SAW velocity ($\square_R$) on the grain size steel 18HGT.

References

1. Weglein R.D., Wilson R.F., J. Appl. Phys.,. v.55., №9., p.3261-3275. (1984).
2. B.L. Agapov, Kustov A.I. JETP Letters, t.20., Vyp.17., P. .51-55 (1994).
3. Kustov A.I., Miguel I.A. Vestnik of Tambov University., Ser. The natural and technical sciences. T. 18, 2. Vyp.4.Chast, s.1875-1877 (2013).
4. Kustov A.I., Miguel I.A. Material science, №8., p. 15 - 19 (2011).

Unified single crystal creep model with account of I, II and III stages

A. I. Grishchenko[1], A. S. Semenov[1], L. B. Getsov[2], E. R. Golubovski[3]

[1]. Peter the Great Saint-Petersburg Polytechnic University

[2]. Scientific and Development Association on Research and Design of Power Equipment

[3]. Central Institute of Aviation Motors

gai-gr@yandex.ru

The creep process is characterized by the presence of three stages. For polycrystalline nickel-based superalloys the second (steady state) stage of creep is dominant (more 50% time up to the failure). At the same time, single crystal nickel-based superalloys demonstrate domination of the third (accelerated) stage of creep (more than 80% time before the failure), whereas the first (decelerated) stage takes less than 5%. For such materials the phenomenological model, which describes only the second creep stage (for example, the power-type Norton's model), is insufficient to describe correctly behavior of such materials. The correct description of third stage of creep is based on the taking into consideration of the damage accumulation process. The alternative solution of this problem for single crystal Ni-based superalloy is based on the thermo-viscoplastic constitutive model for single crystal materials was described in [1].

The aim of the research is to develop fully coupled thermo-elasto-visco-damage phenomenological model for the single crystal nickel-based superalloys with taking into account of all (I, II and III) creep stages and to propose a procedure for the model parameter identification. The Nelder–Mead method [2] was used for the model parameter identification.

The generalized Kachanov-Rabotnov models used for the description of a third stage of creep:

$$\frac{d\varepsilon^c}{dt} = C\left(\frac{\sigma}{1-D}\right)^l \left(\varepsilon^c\right)^m, \tag{1}$$

$$\frac{dD}{dt} = K\frac{\sigma^p}{(1-D)^q}. \tag{2}$$

After integration of (1), (2) the following equation for the creep strain is obtained:

$$\varepsilon^c = \left\{A\sigma^\alpha\left[1-\left(1-Q\sigma^p t\right)^\nu\right]\right\}^\gamma,$$

where $A = \frac{1-m}{1-\frac{l}{1+q}}\frac{B}{K(q+1)}$; $\alpha = l-p$; $Q = K(1+q)$; $\nu = 1-\frac{l}{q+1}$; $\gamma = \frac{1}{1-m}$. (3)

Unfortunately the equation (3) can't describe correctly the first stage of creep (Fig. 1) due to impossibility to satisfy simultaneously the behavior at I and III stages. Therefore, we examined several modifications of (3) in form (4a) and (4b):

$$\varepsilon^c = B\sigma^\beta t^\eta + \left\{A\sigma^\alpha\left[1-\left(1-Q\sigma^p t\right)^\nu\right]\right\}^\gamma, \tag{4a}$$

$$\varepsilon^c = \begin{cases} A_1\sigma^{x_1}t^{\mu_1};\ 0 \le t \le t_I \\ \left\{\left(A_1\sigma^{x_1}t_I^{\mu_1}\right)^{\frac{1}{\mu}} + A\sigma^x\left[\left(1-K_1\sigma^p t_I\right)^{\nu} - \left(1-K_1\sigma^p t\right)^{\nu}\right]\right\}^{\gamma};\ t_I \le t \le t_f \end{cases}, \quad (4b)$$

t_I is the time at the end of first stage and t_f is *the* time before the failure

The constants of the creep models (3), (4a) and (4b) for single crystal alloy VZhM4, at 900ºC with crystallographic orientation <001> were determined on the base of experimental creep curves obtained by authors [3,4]. The creep model parameters by (3), (4a) and (4b) for single crystal alloy VZhM4 are given in Table 1. It found that the approximations (4a) and (4b) provide the same results. The experimental creep curves and their approximation by (3) and (4a) are shown in Fig. 1. The results of approximation of the up to 300 hours creep curves have shown a good accuracy.

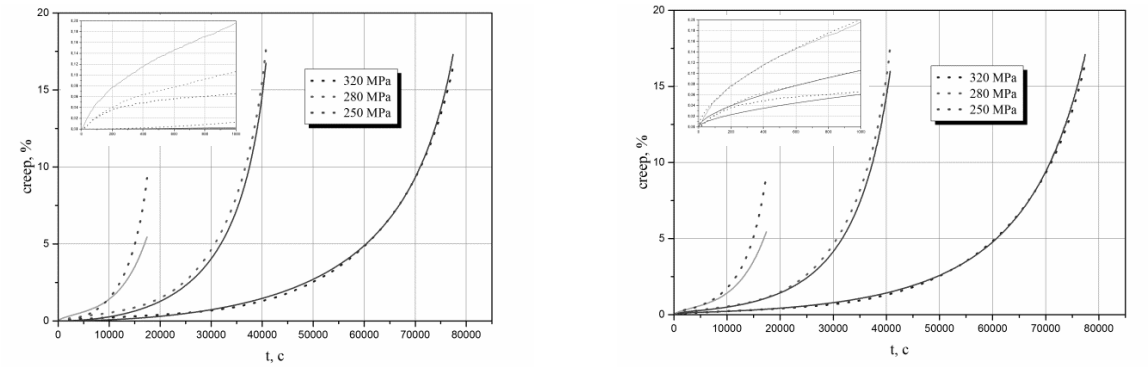

Fig.1. Experimental creep curves (points) for single crystal nickel-based superalloy VZhM4 and their approximation with using creep model (3) a) and (4a) b).

Table 1. The creep model parameters.

	T, ^{0}C	B	β	η	A	α	Q	p	ν	γ	MSD,%	R
(3)	900	-	-	-	2010	$1{,}39\cdot10^{-6}$	$1{,}58\cdot10^{-13}$	5,63	$9{,}6\cdot10^{-4}$	1,83	0,9	0,99
(4a)	900	$2{,}86\cdot10^{-10}$	4,69	0,589	25694	$2{,}81\cdot10^{-3}$	$2{,}50\cdot10^{-13}$	5,45	$6{,}62\cdot10^{-5}$	2,72	0,84	0,99
(4b)	900	$1{,}61\cdot10^{-10}$	4,83	0,609	25200	$2{,}47\cdot10^{-2}$	$2{,}37\cdot10^{-13}$	5,48	$4{,}28\cdot10^{-5}$	3,01	0,93	0,99

This research was supported by the RFBR (Grant No. 15-08-08779).

References

1. *A. Staroselsky, B.Cassenti, Mechanics of Materials **42**, pp 945-959 (2010)*
2. *J.A. Nelder, R. Mead, Comput. J **7**, pp 308–313 (1965)*
3. *L.B. Getsov, A.S. Semenov, E.A. Tikhomirova, A.I. Rybnikov, Materiali in Tehnologije **48(2)**, pp 255-260 (2014)*
4. *S.G. Semenov, L.B. Getsov, E.A. Tikhomirova, A.S. Semenov, Metal Science and Heat Treatment **57**, pp 11-12 (2016)*

Fraction-exponential description of the viscoelastic properties of dentin

S. Seyedkavoosi[1], D. Zaytsev[2], B. Drach[1], P. Panfilov[2], M.Yu. Gutkin[3,4,5], I. Sevostianov[1]

[1]. Department of Mechanical and Aerospace Engineering, New Mexico State University, Las Cruces, NM, USA

[2]. Department of Physics, Institute of Natural Sciences, Ural Federal University, Ekaterinburg, Russia

[3]. Institute of Problems of Mechanical Engineering, Russian Academy of Sciences, St. Petersburg, Russia

[4]. Department of Mechanics and Control Processes, Peter the Great St. Petersburg Polytechnic University, St. Petersburg, Russia

[5]. ITMO University, St. Petersburg, Russia

Email: m.y.gutkin@gmail.com; igor@nmsu.edu

Dentin represents the main part of tooth mineralized tissue with a rather complex hierarchical microstructure. It is characterized by the presence of tubules (~1.5 μm in diameter) that run from the dentin-enamel junction towards the pulp. The tubules are surrounded by highly mineralized cylinders of peritubular dentin, roughly 0.5-1 μm in thickness, composed largely of apatite. These tubules are separated by intertubular dentin that consists of a hydrated matrix of type I collagen which is reinforced with a nanocrystalline carbonated apatite.

Mechanical properties of dentin are governed by its microstructure. Quantitative understanding of the relationship between microstructure and mechanical properties of human dentin allows identification of the microstructural parameters governing the properties and leads to new methodologies in development of tissue equivalent materials. To the best of our knowledge the micromechanical model for viscoelastic properties of dentin has never been proposed in literature. This process is complicated by the lack of solid information on mechanical behavior of dentin, in general, and its creep-relaxation behavior, in particular.

We propose the fraction-exponential description of the viscoelastic properties of dentin. Creep tests are performed on specimens cut from the molar coronal part. Four parameters determining instantaneous and long term Young's moduli as well as the relaxation time are extracted from the experimental data. Physical meaning of the parameters and the difference between them for different sets of specimens are discussed.

Acknowledgement
Financial support from the FP7 Project TAMER IRSES-GA-2013-610547 (IS), Russian Science Foundation, research project No. 15-19-10007 (DZ, PP, and MYG), and New Mexico Space Grant Consortium contained in the NASA Cooperative Agreement NNX13AB19A to New Mexico State University (IS, SS) are gratefully acknowledged.

Data acquisition for stress analysis by Digital Image Correlation of nickel-based superalloys under tensile load at high temperatures

S. Reschka[1], L. Munk[2], D. Rodman[1], F. Nürnberger[1]

[1]. Leibniz Universität Hannover, Institut für Werkstoffkunde

[2]. Leibniz Universität Hannover, Institut für Kontinuumsmechanik

Email. reschka@iw.uni-hannover.de

Materials used in gas turbines are exposed to a harsh environment where they have to endure both high temperatures and loads for long durations. Hence, creep properties are of particular importance for a successful application. Nickel-based superalloys are widely used in such demanding environments since they feature a high creep resistance due to a high melting temperature of 1455 °C and a high fraction of up to 70 % of γ´-phase particles [1].
In order to improve existing creep models by considering a multi-scale behaviour, space-resolved information of local strains on different length scales during creep test would be beneficial. Though the use of Digital Image Correlation (DIC) during creep test can provide such information, its application is fairly challenging due to the altering surface properties caused by temperature loading resulting e. g. in a progressing oxidation of the surface.
To evaluate the applicability of various surface preparations regarding Digital Image Correlation of creep deformations, creep tests at various temperatures and tensile loadings were carried out at the example of the super alloy Nimonic 101. Since DIC-measurements require a temperature-stable surface pattern to be able to identify local strains, a pattern on the samples had to be achieved that is fine enough to resolve small deformations and to correlate these with microstructural features. Here, various methods were tested to prepare patterns of adequate quality. In addition, the forming of an oxide layer at high temperatures has to be considered, cf. Figure 1. Since the oxide layer of the sample surface and thus its visual properties evolve with the duration of the creep tests, the surface itself is rather unsuited for DIC-investigations.

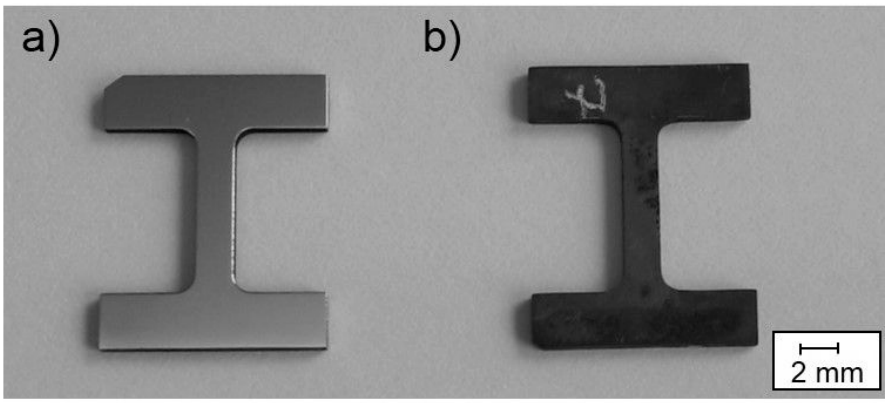

Figure 1: Sample before a) and after b) testing at high temperature

If additional patterns are added to the surface, the properties of the oxide layer still might prevent a successful DIC-measurement. Here, a pattern has to be applied that provides for sufficient contrast independent of the forming oxide layer. This pattern has to stick tight to the sample and is required to be sufficiently elastic to take part in the

deformations of the sample. Unfortunately, high temperature paint used here for the investigations was not suitable at higher strains. The creep deformation causes premature cracking in the paint itself, and thus, impedes an evaluation by DIC early on in the test, cf. Figure 2.

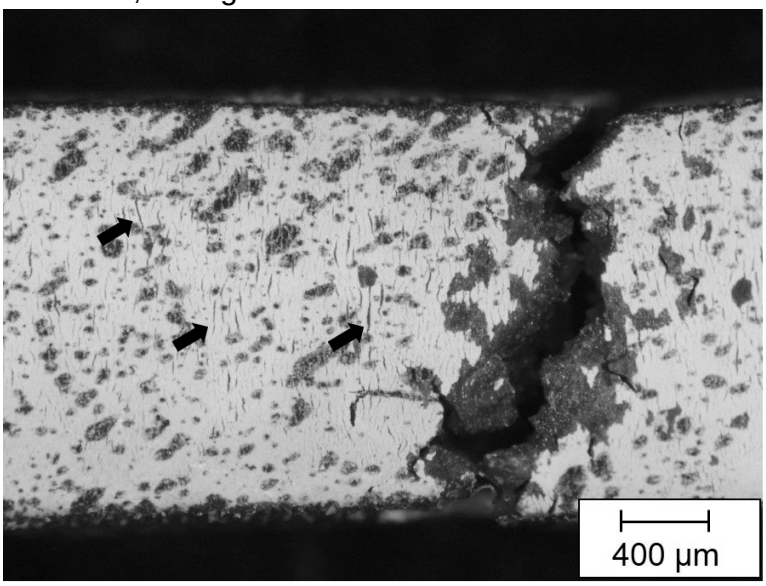

Figure 2: Fractured sample with high temperature paint DIC pattern after testing. The paint itself cracked all over in the specimen as highlighted by some arrows.

As alternative preparations of the pattern revealed, cracking of the high temperature paint can be overcome by generating white paint speckles on the surface roughened by a prior grinding instead of applying a closed paint layer. Afterwards, the sample has to be oxidised before taking pictures of the initial state in order to achieve a white pattern on a black sample.
After testing, the only cracks visible in the paint speckles continued in the unpainted sample surface. Therefore it was assumed that the pattern of the paint speckles is suitable for strain measurements by DIC.

Acknowledgement

Financial support for this work provided by the German Science Foundation (DFG) under Contract MA1175/63-1 and WR19/57-1.

References

1. H. M. Flower, *High Performance Materials in Aerospace*, Springer Science+Business Media, (1995)

Prediction of Creep Deformation by Bending

Syed Idrees Afzal Jalali*, Praveen Kumar, Vikram Jayaram

Department of Materials Engineering, Indian Institute of Science, Bangalore 560012, India

**Email. ali.idrees2@gmail.com*

Abstract. The present work aims to investigate the validity of creep data obtained from bending. Creep curves from bending tests are compared with uniaxial compression and tension data of commercially pure (CP) aluminum in the power law regime. Creep parameters like steady state creep rate, stress exponent and activation energy match well with uniaxial data (Fig. 1,2). However, for the extreme beam fibers, strain-strain rates calculated from tip deflection show a faster primary stage and prolonged secondary and tertiary stages (Fig. 3).

Introduction. Bending creep may be adapted to study the creep deformation of systems when the testing volume is very small. Under such conditions uniaxial testing becomes difficult due to problems of gripping and handling. Position dependent data may be obtained by testing samples in a gradient stress state such as cantilever beams. The validity of such data can be established by using techniques like digital image correlation (DIC) for strain measurement. With precision in strain measurement across a beam, a single sample can provide all the data in a particular deformation domain. Creep under bending involves the assumption of small deformations, linear variation in strain across beam height and material with no tension-compression asymmetry in creep properties. Linear variation of strain implies that plane sections of beams remain plane during creep [1]- [4]

Experimental details. Beams were machined from CP aluminum sheets by electro discharge machining. Cantilever beams with the same aspect ratio (length/height) held at a constant load and temperature were tested in a depth-sensing indentation system using wedge tip. Beams were also tested at a fixed load at different temperatures (200°C, 206°C and 210°C) to calculate the activation energy for creep. Standard ASTM protocol was followed for uniaxial samples.

Results and discussion. Bending results reveal that aluminum beams creep with a stress exponent of 4.5 (Fig. 1) and an activation energy for creep of 123 kJ/mole (Fig. 2) [5]- [7]. Steady-state creep rates obtained from beams of cross section 5 mm X 5 mm and above match with those obtained from uniaxial compression data for the same alloy (Fig. 1) in the tested stress regime. This suggests that if all the assumptions are met, bending creep can be used to predict creep behavior of a material. It is hypothesized that the reason for bending samples reaching steady state faster is the higher stress state at the beginning of the test. In the extreme fibers stress relaxes by about 30-35% from the elastic value to the steady state value [1]- [4] [8]. Stress during steady state has been shown to be constant [1]. Tests on small beams suggest a length scale effect, possibly due to the interplay between strain gradients [9] [7] and a small ratio of thickness: grain size. It is therefore important to account for the length scale effects to interpret creep data from small beams. Strains calculated from the bending creep model are compared with strains from DIC and allow verification of the assumptions made in bending creep models.

Conclusion.

1. Creep parameters like steady state creep rate, stress exponent and activation energy obtained from bending tests on end loaded cantilever beams match with

uniaxial data in absence of length scale and size effects.

2. Bending creep shows faster primary and prolonged secondary and tertiary stage.

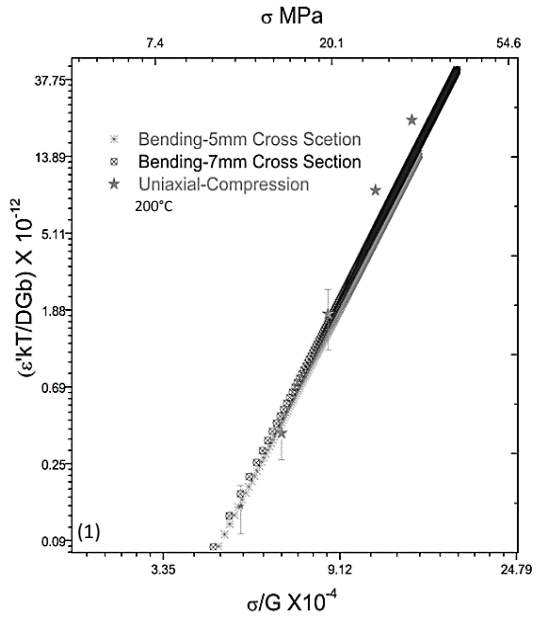

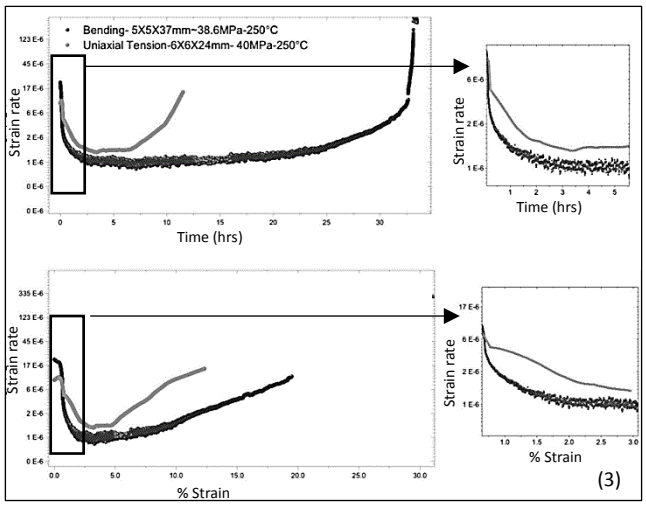

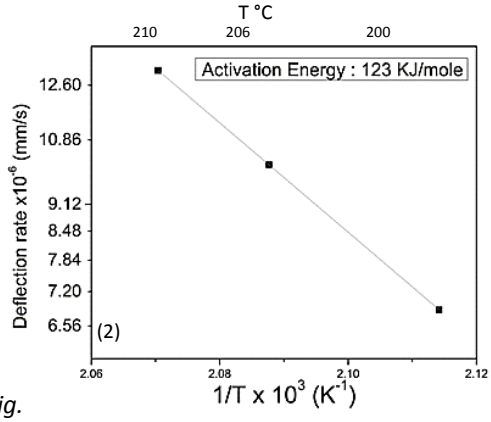

Fig.

1. *bending creep data verses uniaxial compression at 200°C*
2. *activation energy calculated from slope of deflection rate verses 1/T in beams*
3. *bending creep data verses uniaxial tension at 250°C*
   <u>note</u>: extended secondary and tertiary stages in bending relative to uniaxial

References

[1] H.J. Tapsell and A. E. Johnson, "An investigation of the nature of creep under stresses produced by pure flexure," *Journal of Intitute of Metals,* **vol. LVII**, pp. 387-405, (1935).

[2] A. Nadai, *Plasticity*, McGraw-Hill, p.160,(1931).

[3] Gleason H. McCullough, Worcester, MASS, "Experimental and Analytical Investigation of Creep in Bending," *American Society of Mechanical Engineers,* **vol. 55**, pp. 55-60, (1932).

[4] E. P. Popov, "Bending of Beams with Creep," *Journal of Applied Physics,* **vol. 20**, pp. 251-256, (1949).

[5] M. Ashby, "A report on the Deformation Mechanism Maps," *Acta Metallurgica*, **vol. 20**, p. 887, (1972).

[6] O.D. Sherby, "Activation Energies for creep of high purity aluminum," *Acta Metallurgica,* **vol. 5**, pp. 219-227, (1957).

[7] J. Dorn, "Viscous creep of aluminum near its melting temperature," *Acta Metallugica*, **vol. 5**, p. 654, (1957).

[8] F. K. Zhuang, S. T. Tu, G. Y. Zhoa and Q. Q. Wang, "A small cantilever beam test for determination of creep properties," *Fatigue Fracture of Engineering Materials & Structures*, **vol. 38**, p. 257–267, (2015).

[9] N. A. Fleck, G. M. Muller, M. F. Ashby and J. W. Hutchinson, "Strain gradient plasticty: thoery and experiment," *Acta Metallurgica*, **vol. 42**, p. 475-487, (1994).

[10] T. Courtney, *Mechanical Behaviour of Materials,* 2 ed., p. 166. (2005)

Creep rupture life prediction of a Nickel based Superalloy DS CM247 using θ -projection technique

C.M. Omprakash[1], M. Kamaraj[2], D.V.V. Satyanarayana[1]

[1]. Defence metallurgical Research Laboratory, Hyderabad, India

[2]. Indian Institute of TechnologyMadras,Chennai,India

Email.prakash6y@gmail.com

Creep resistance is an important design consideration for selection of materials in high temperature applications such as aeroengines, power plants etc. Accelerated tests under laboratory conditions do not provide exact deformation characteristics/ mechanisms encountered during service life. Therefore, a detailed understanding of the underlying creep and fracture mechanisms is essential to ensure safe life operation of these structural materials. Creep life prediction methodologies using conventional parametric methods based onLarson-Miller-Parameter (LMP) and Modified-Monkman-Grant (MGM)offer limited confidence in rupture life predictions on timescales required for real service applications as the predictions are outcome of limited data depending only on some specific parameters liketime to rupture (t_r), strain to rupture (□$_f$) and alsoempirical equations employ constants which upon investigation are often no longer constants over the conditions considered without any linkage to the underlying physical phenomena.However, models/techniques which account for underlying creep mechanisms and creep strain evolution with time are required for life assessment methods.

Hence it is practice to carry out several short term tests and then predict the long term behavior approaching service conditions. A variety of methods have been developed to predict the creep behavior. θ-projection technique is one of the most widely used approach for prediction of the entire creep curves as against “parametric” methods, which focus only on some aspects of creep curve such as time to rupture.And also, the θ-projection technique provides additional information on underlying deformation mechanisms within the selected domain of temperature and stress apart from rupture parameters. The theta projection approach has been extensively used for a variety of materials such as 1.25Cr-0.5Mo and 2.25Cr-1Mo steels, modified 9Cr-1Mo steel, austenitic stainless steels, eutectic Sn-Ag alloy, aluminium alloysand superalloysto successfully predict the entire portion of creep curves. The objective of the present effort is to investigate the ability of θ - projection approach to establish model parameters for prediction of the entire portion of creep curves of DSCM247 alloy and to compare the predicted values of time to rupture with the conventional method i.e., Larson Miller Parameter approach (LMP).

Constant load creep tests of DSCM247 alloy were conducted in air till rupture of the specimens. Creep strain measurements were made using extensometer and LVDT (linear variable differential transducer) assembly. Creep tests were conducted at 950°C in the stress range 100 to 350 MPa.

Confidence in this procedure is derived from the fact that the well- behaved nature of these θ functions with respect to stress has enabled predictions to be made of the entire creepcurves expected for the low stress levels relevant to service conditions. The predicted creep curves together with experimental creep curves are shown in Fig. 1.The predicted values of time to rupture obtained from θ - projection approach are compared

with the predicted values of time to rupture with the conventional method i.e., Larson Miller Parameter approach (LMP) as shown in Figs. 2. The predicted values of time to rupture using θ - projection approach in comparison to those obtained using Larson Miller Parameter approach (LMP) along with experimental results arepresented in Fig. 2. It can be observed that the predictions made by θ - projection approach are very close to the experimental valueseven at low stresses than those predicted using the conventional approach of Larson Miller Parameter approach (LMP).

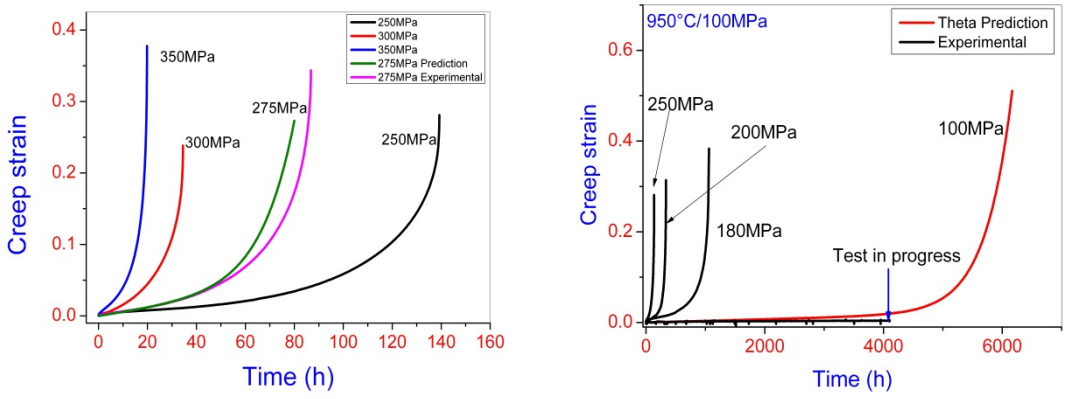

(a) (b)

Figure.1.Predicted creep strain-time curves of DSCM247 alloy together with experimental creep strain-time curves at 950°C (a) 275MPa & (b) 100 MPa.

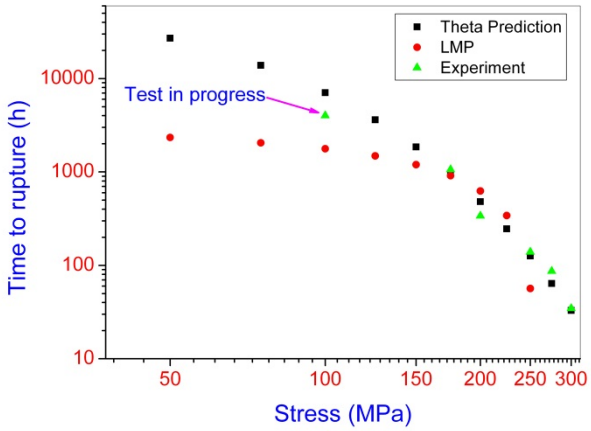

Figure.2. Predicted time to rupture curves of DSCM247 alloy using θ- projection approach and Larson Miller Parameter (LMP)approach for stress range 50-300 MPa.

Modelling the Viscoplastic Behaviour of a Martensitic Steel with a Mixture Approach

J. Eisenträger[1], K. Naumenko[1], H. Altenbach[1]

[1]Otto-von-Guericke Universität, Universitätsplatz 1, 39106 Magdeburg, Germany

Email. johanna.eisentraeger@ovgu.de

This contribution aims to analyze and model the viscoplastic behaviour of the tempered martensitic steel X20CrMoV12-1 (Alloy 1.4922), which has been used at elevated temperatures under creep conditions in power plants.

In a first part, the results of high temperature tensile tests at constant strain rates are presented. Six different temperature levels $673\,\mathrm{K} \leq T \leq 923\,\mathrm{K}$ and three different strain rates $\dot{\varepsilon} = \{5 \times 10^{-5}\mathrm{s}^{-1}, 1 \times 10^{-4}\mathrm{s}^{-1}, 1 \times 10^{-3}\mathrm{s}^{-1}\}$ have been taken into account.

Afterwards, a mixture model, which is based on microstructural processes, is discussed [1]. The microstructure is idealized such that only two constituents need to be taken into account by the mixture approach. The model applies an iso-strain concept and takes hardening and softening behaviour via macroscopic state variables into account. This results in a system of three differential equations with respect to time concerning the inelastic strain rate, the softening variable as well as the hardening variable.

Finally, the model is calibrated based on the results of presented tensile tests and on creep test results from literature [2]. For the calibration, one distinguishes an initial and a quasi-steady state and identifies the corresponding stresses and inelastic strain rates. Several advanced stress response functions for the inelastic strain rates are taken into account in order to model the power law breakdown. Furthermore, parameters for the hardening and softening variables are identified.

References

1. K. Naumenko, H. Altenbach, and A. Kutschke, «A Combined Model for Hardening, Softening, and Damage Processes in Advanced Heat Resistant Steels at Elevated Temperature», *International Journal of Damage Mechanics* **20,** pp. 578–597 (2011).
2. S. Straub, «Verformungsverhalten und Mikrostruktur warmfester martensitischer 12%-Chromstähle», *Dissertation*. Erlangen-Nürnberg: Friedrich-Alexander-Universität (1995).

Evaluation of Integrity and Estimation of Residual Creep Life for Aged Boiler Tubes Using Miniature Creep and Small Punch Creep Tests

R. Kaneko[1], D. Itoh[2] and K.I. Kobayashi [1]

[1.] *Department of Mechanical Engineering, Chiba University, 263-8522 Japan*

[2.] *Chiba University (now at Nippon Steel & Sumitomo Metal Co. Ltd)*

Email : k-cobayashi@faculty.chiba-u.jp

Some reasonable and reliable inspection tests are required to ensure the integrity of high temperature components and to extend their service lives.

Employing two types of aged boiler tubes that were used for 60,000 and 230,000 hours around at 470°C, miniature creep(MC) tests and small punch (SP) creep tests were carried out at 650°C. Creep lives of virgin materials were estimated employing massive NIMS creep data [1] and two TTP methods; Larson-Millar (LM) and Manson- Haferd (MH) parameters. After a series of miniature creep tests conducted using aged boiler tubes, the integrity of test materials was examined. Figure 1 is a comparison result employing LM parameter, and indicates that the creep rupture lives of 60,000 hours exposed tubes shown as solid circles exhibit nearly the same life as those of many virgin batches estimated using LM parameter (open symbols), or longer lives than them. This means that the aged tube still has the significant residual creep life.

After conducting the SP creep tests, a relationship between the MC and the SP creep tests were introduced; a ratio of applied load in the SP creep and stress in MC tests to the rupture time. Although this ratio gradually decreases a little with the rupture time, but nearly constant. Thus, it can help to estimate residual creep lives much easily because the SP creep test requires very small volume for sampling the specimen.

References

1. NIMS Creep data sheet, No.20B, pp.3-27, (1994).

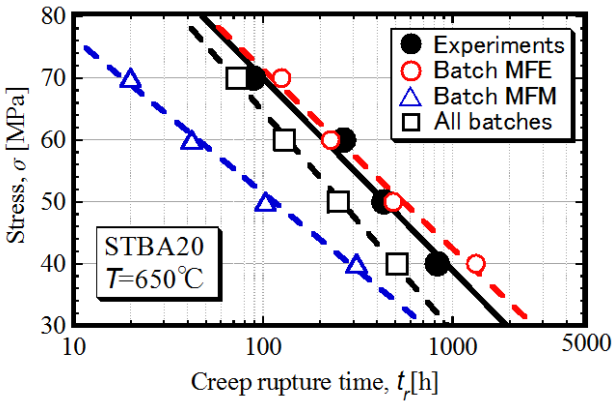

Figure 1 : *Comparison between miniature creep test results of age boiler tubes and estimation creep lives estimated using LM parameter.*

Zc method to predict creep deformation and rupture life based on short-term creep tests results

ZHAO Jie[1)] CAO Tieshan[1)], CHENG Congqian[1)], LI Huifang

1) School of Materials Science and Engineering, Dalian University of Technology, Dalian 116085

2) Avic Beijing Institute of Aeronautical Materials, Beijing 100095

E-mail: jiezhao@dlut.edu.cn

Key words：*HP heat resistant steel; creep; rupture life; Zc parameter*

Several methods have been proposed to estimate long-term creep rupture properties from short-term creep tests such as θ project and Ω methods. However, prediction accuracy problems are encountered because of scattering of experimental results. The current paper proposes a so-called Zc parameter to evaluate long-term creep deformation and rupture life based on short-term creep curves. Firstly the experimental data of various creep strain are normalized using time-temperature parameter(TTP parameter) to get various parallel regressive curves as shown in Fig.1. Secondly, by selecting a reference curve and proposing symbol Zc to represent the deviation of a curve with a certain creep strain from that reference curve, relationship can be built between the values of Zc and creep strain as shown in Fig.2. Finally, creep deformation as well as creep rupture life can be well predicted according to these analytic results as can be seen in Fig.3 and Fig.4. Besides the good agreement in predicting creep strain and rupture life, this method is also capable of performing probability analysis for the scattering of experimental data.

Supported by National Natural Science Foundation of China（Nos. 51171037and 51134013）

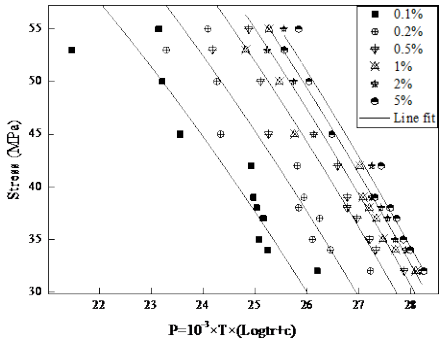

Fig.1 Stress-TTP parameter relationship for various creep strain

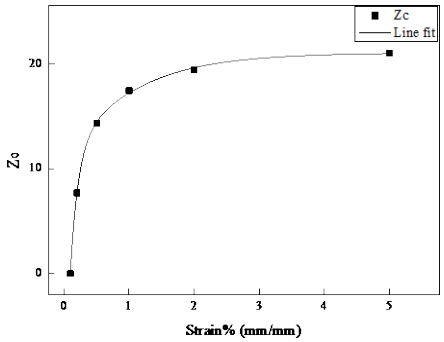

Fig.2 relationship between Zc and creep strain

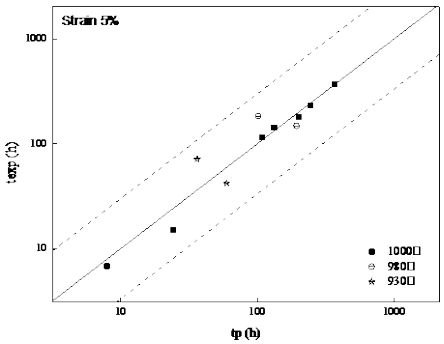

Fig.3 Comparison of experimental and predict times for 5% creep strain

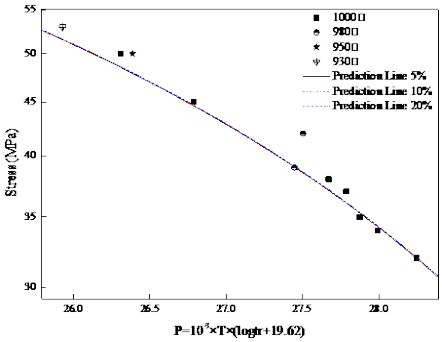

Fig.4 Comparison of experimental and predict rupture time

Investigation and Application of the Methods to Obtaining the Creep Properties of Thin Film/substract System by Using Three Points Bending Test

Shifeng Wen*, Zhufeng Yue

School of Mechanics and Civil & Architecture, Northwestern Polytechnical University, Xi'an, Shaanxi, 710129, PR China.

*Corresponding author, E-mail: wenshifeng@nwpu.edu.cn

There is a continued trend towards the progressive use of higher temperatures to achieve improved efficiencies in, for example, electric power generation equipment, gas turbines and chemical reactors in the last decades. This trend is resulting in an increased need for more reliable lifetime prediction methods for components subjected to creep loading [1-6].

In general, the standard technique to obtain creep parameters such as *n* (stress exponent) and *B* (the creep constant) is uniaxial tensile creep testing. This method is very conventional for the testing temperature below 1100^{o}C. But for the present technology, tensile creep testing is very difficult for higher temperature and for the thin film/substract system, such as at 1400^{o}C. The difficulties come not only from the limitation of specimen size (for the reason of materials), but also from the clamps (for it is difficult to get the materials for the clamps in such high temperature). As an alternative testing method, bending creep test has been attracted for its simple in specimen and loading fixture. For example, Hollenberg et al. [7] analyzed the relationships of creep strain, strain rate and applied stress for a ceramic material under bending creep. Based on the results of Hollenberg et al, Chuang [8], Krause and Chuang [9] and Chen and Chuang [10] investigated the relationships among neutral axis position, creep parameters and the bending moment. Recently, Chuang et al. [11] proposed multi-axial constitutive equations in a power-law creep form based on asymmetric creep responses under uniaxial creep. In addition, some other researchers have also studied the high temperature materials creep properties using the bending creep test by the finite element method or combining the test with numerical technique such as Lin et al [12], Ivankovic et al [13], Lim et al [14], Dusza et al [15] and so on. But the usual bending creep fixture in use is three-point bending test fixture or four-point bending test fixture [7-15]. However, theses fixtures are relative complex. Recently, a simpler bending creep texts fixture is designed, as shown in Fig.1 [16].

In this area, we have investigation the three point bending creep tests to obtain the characterization of the materials. Through the theoretical analysis, finite element simulation as well as the experimental verification, the main contributions of the dissertation are summarized as follows:

1. The three-point bending creep testing on thermal barrier coatings (TBCs) has been investigated with the aim of determining the creep parameters of TBCs. It consists of a superalloy substrate (SUB layer) and a bond coat (BC layer) and a termal barrier coating (TBC layer). The most important is that the grown oxide (TGO layer) which between the TBC and BC is considered. The present study also shows how bending creep testing of material can be used to determine the creep parameters of a material. A method is explored to determine the creep parameters of TGO layer with bending creep testing. It is the reverse numerical procedure, which allows extracting the creep parameters on the basis of two bending creep tests with two positions of loading pin and a series of finite element calculations. Finally it is discussed how different frictions between the loading pin and the specimen affect bending creep behavior and how different thickness of TGO layer affects the veracity of the creep parameters which obtain from the bending creep testing [16,17].
2. Understand the creep damage properties of thin film/substrate systems by bending creep tests. To this aim, a numerical study has been performed on the creep damage development of the thin film/substrate systems by implementing the Kachanov-Rabothov

damage law into finite element models. The part of work may shed some light on the influence of the modulus ratio of the substrate to the thin film, the thickness of the thin film and the bending load. Finite element method (FEM) results show that three obviously damaged zones are found. The first is at the edge of the loading pin, the second is at the interface between the film and the substrate ahead of the loading pin edge, the last is at the edge of the supporting pin A. The influence of the modulus ratio of the substrate to the thin film on the bending creep damage is not obvious at the preliminary stage of creep time. However, with the lapse of time, the damage rate decreases with the increase of modulus ratio of the substrate to the thin film. The change of the thickness of the thin film and the bending load also influence the creep damage behavior of the thin film/substrate systems [18].

3. One important method to predict the residual strength and residual life of materials and components is to predict the damage level of the materials. In this paper, two cases have been studied to explore the possibility to determine the damage levels of the materials by the bending test method with the help of the finite element method (FEM). One case uses Gurson model to study the prediction of the elastic-plastic damage. The other case uses a creep damage model, which is based on the Katchanov-Robotnov continuum creep damage law, to predict the creep damage. The analytical results show that the damage level of the damaged materials can be determined by the bending test experimental method [19].
4. The crystal plasticity slip creep theory was implemented into finite element (FE) model to simulate impression creep and uni-axial creep. The effect of crystallographic orientation on impression creep and uni-axial tensile creep behaviors. The stress conversion factor, which relates the impression creep data with those of tensile creep, was also investigated on its crystallographic orientation dependence. The impression creep technique is capable of yielding crystallographic creep stress exponent which is in consistent with that obtained from uni-axial creep test [20] .
5. Bending creep test (based on overhang beam geometry) is investigated by incorporating the important contribution of residual stress. Finite element simulations incorporating the residual stress are employed to investigate the residual stress behavior of bending creep specimen. We propose several methods to determine the creep parameters directly from the bending creep tests. We considering two cases of residual stress, one is tensile residual stress, the other is compressive residual stress. The work may shed some light on the influences during bending creep, as well as provide an efficient way of determining material residual stress characteristics.

Fig.1 The bending creep test fixture

References

[1] G.A.Webster and R. A. Ainsworth. High Temperature component Life Assessment. Chapman & Hall, London, UK.

[2] D.H. Sastry. Impression creep technique—An overview. Materials Science and Engineering A 409 (2005) 67.

[3] James C.M. Li. Impression creep and other localized tests. Mater. Sci. & Eng. A 322 (2002) 23-42.

[4] D. Dorothee, R. Klaus, S. Bridit, etc. Creep of a TiAl alloy: a comparison of indentation and tensile testing. Mater. Sci. & Eng. A 357 (2003)346-354.

[5] Z. F. Yue, B.Stockhert, G. Eggeler. A creep finite element analysis of indentation creep testing in two phase microstructures (particle/matrix-and thin film/substrate –systems).Computational Materials Science21 (2001)37.

[6] T. H. Hyde. K.A. Yehia, A.A. Becker. Application of the reference stress method for interpreting impression creep test date. Materials at High Temperature 13(3) (1995)133.

[7] G.W. Hollenberg, G.R. Terwilliger and R.S. Gordon, Ceram. Eng. Proe., I1 (54) (1971) 196.

[8] T.J. Chuang, J. Mater. Sei.. 21 (1986) 165.

[9] R.F. Krause and T.J. Chuang (eds.), Ceramic Today-Tr~morrow's Ceramics. Elsevier, 1991, p.1865.

[10] C.F. Chen and T.J. Chuang, J. Am. Ceram. Sot., Z~ (8) (1990) 2366.

[11] T.-J. Chuang and S.M. Wiederhorn, d. Am. Ceram. Soc., 74(199I) 2531.

[12] M.T. Lin, J.L. Shi, D.Y. Jiang, M.L. Ruan, T.R. Lai. High temperature creep of a hot-pressed b-sialon. Mater. Sci.& Eng. A300 (2001) 61.

[13] H.Ivankovic, E.Tkalcec, R.Rein, H.Schmidt. Microstructure and high temperature 4-point bending creep of sol–gel derived mullite ceramics. J. European Ceramic Society 26 (2006) 1637

[14] H.J. Lim, J.W. Jung, D.B. Han, K.T. Kim. A finite element model for asymmetric creep behavior of ceramics. Mater. Sci.& Eng. A 224 (1997) 125.

[15] J. Dusza, P.Hvizdog, W.Steinkellner and K.Kromp. Bending creep behaviour pf pressureless sintered MoSi2, Scripta Materialia, 37(1997)471.

[16] S.F. Wen, W.Z. Yan, J.X.Kang, J.Liu, Z.F. Yue. Simulation of the interface characterization of thin film/substrate systems by bending creep tests. Applied surface science.

[17] Shifeng Wen, Wuzhu Yan, Jiangxiong Kang, Jun Liu, Zhufeng Yue, Simulation of the Creep Damage Behavior of Thin Film/Substrate Systems by Bending Creep Tests. Materials & Design. 31(4): p.3531-3536.

[18] S.F.Wen, W.Z.Yan, X.S.Wang, J.Liu and Z.F.Yue, Prediction of strength using bending test method. Materials & Design.31(4): p.1828-1832.

[19] Shifeng Wen*, Wuzhu Yan, Jiangxiong Kang, Jun Liu, Zhufeng Yue, Investigation of Bending Creep Tests Part I: Effect of Residual Stress. Measurement. 2013 46(4):1592-1599.

[20] Shifeng Wen*, Xiaohu Zeng, Ziyi Kang, Zhufeng Yue, Investigation the effect of crystal orientation of nickel-based single crystal superalloys on bending creep tests, MATERIALWISSENSCHAFT UND WERKSTOFFTECHNIK, 2014 45(3): 200-206.

Study on Distribution of the Tensile Creep Stress and Strain of Smooth and Notched bars

ZHANG Juan[1] and WANG Xinmei[1]

[1]School of Mechanics, Civil. & Architecture, Northwestern Polytechnical University , China

Email:417185691@qq.com

Key words: creep; neat stress; notched specimen; FEM; stress and strain distribution; stress concentration; stress relaxation

Abstract: The tensile creep stress and strain characteristics of smooth and notched bars are analyzed in the paper. Six specimen are studied, which are model1, smooth bar, model 2, V-type notched bar, model 3, U-type notched bar with *R=1*, model 4, U-type notched bar with *R=3*, model 5, circular- type notched bar with *R=1*, and model 6, circular -type notched bar with *R=3*.

Fig. 1 FEM deformations of (a) smooth specimen; (b) V-notched specimen; (c) *R* = 1 U-notched specimen (d) *R* = 3 U-notched specimen; (e) *R* = 1 circular notched specimen;

(f) *R* = 3 circular notched specimen

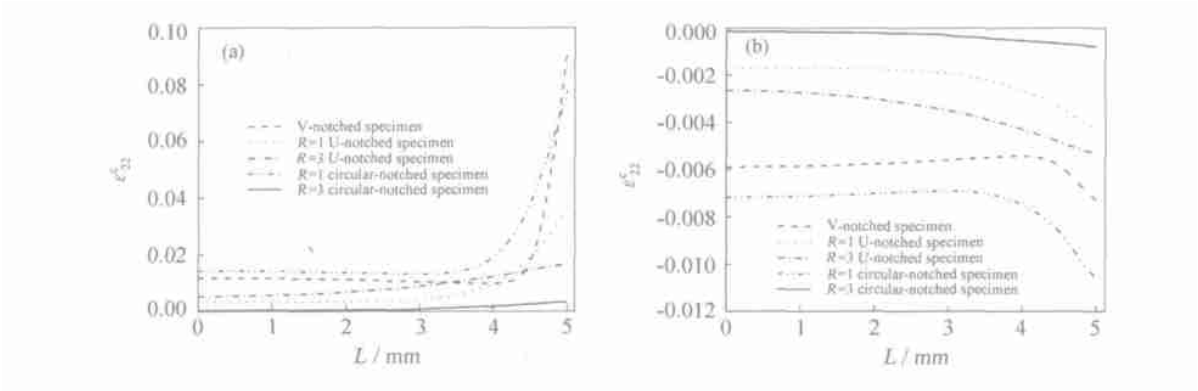

Fig. 2 Strains along minimum sections of (a) axial strain ; (b) radial strain ($t = 2 \times 10^6$ s)

Conclusion:

(1) The existence of the incision affects the stress state of the notched specimen. And the specimen appears multiaxial stress state. Moreover, the average Mises stress and axial stress on the minimum cross section are smaller than that of smooth specimen.

(2) In the notched specimens, the stress concentration of the v-shaped notched specimen is the most severe one. And u-shaped notched specimen is more severe than the same radius of the circular notched specimen. As while the notched specimen with radius R = 1 has more severe stress concentration than notched specimen with R = 3.

(3) In the process of creep, notched specimen produced stress relaxation locally, and different notched specimen stress relaxation rate are almost the same. The creep stress relaxations of u-shaped notched specimen is similar to the circular notched

specimen with the same radius. After creep stress relaxation, the stress value of U-shape notched specimen is smaller than corresponding circular notched specimen.

(4) In the process of creep, the redistribution of stress on the minimum cross section make the maximum stress of the sample not occur at the root of the notch, but move towards the center of the sample. The movement speed of v-shaped notched specimen is the slowest, while the u-shaped and circular notched specimen with the larger radius are the fastest. The stress distribution curve of u-shaped and circular notched specimen with the same radius are similar. Creep resulted in stress relaxation and stress redistribution, both can explain the influence of simple incision to the material life of fracture.

Time-dependent Stress Evolution and Growth of the Void in Single Crystal During Uniaxial Tensile Creep

Wuzhu Yan, Zhufeng Yue

School of Mechanics, Civil Engineering and Architecture, Northwestern Polytechnical University, Xi'an 710129, PR China

Email. *Corresponding Author: yanwuzhu@nwpu.edu.cn*

Abstract: The strong anisotropy and crystallographic orientation dependent mechanical properties brought difficulties in the application of single crystal super alloys. Micro-pore, a common drawback appearing in the directional solidification process, is generally known to be harmful to the mechanical properties of single crystal super alloys [1].

The present study aims at exploring the stress evolution and growth of the void embedded in single crystal super alloys during uniaxial tensile creep. To this aim, the crystallographic creep constitution relationship [2] was incorporated into three dimensional unit cell finite element simulations as shown in Fig. 1. The simulation results demonstrated that the stress distribution, stress evolution and void growth exhibited strong dependence upon creep time and crystallographic orientation. The potential nucleation sites of creep crack on the void surface associated with differently orientated single crystals were predicted as shown in Fig. 2.

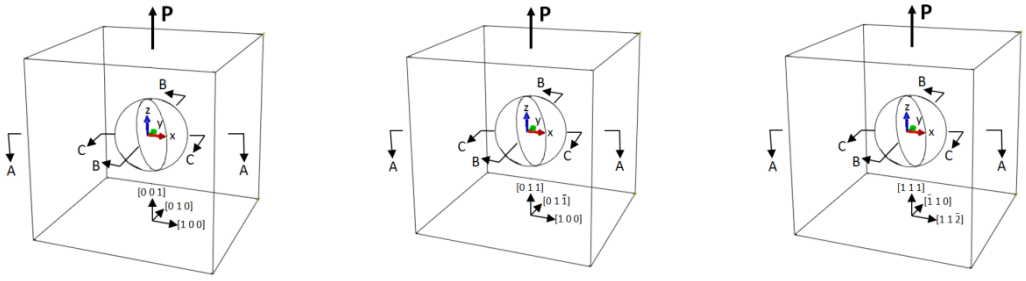

(a) (b) (c)

Fig. 1. Schematic view of the unit cell model. (a) [0 0 1] oriented; (b) [0 1 1] oriented; (c) [1 1 1] oriented.

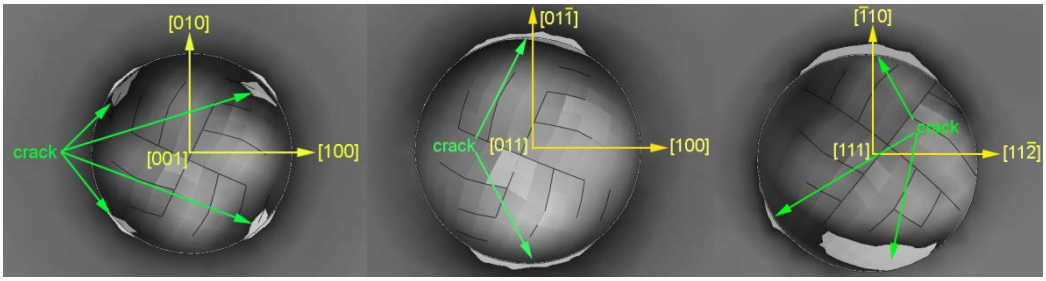

Fig. 2. Potential creep induced crack nucleation sites on the void surface for (a) [001]-, (b) [011]- and (c) [111]- oriented single crystals.

References

1. Y. Alinaghian, M. Asadi, A. Weck, *International Journal of Plasticity* **53**, pp.193-205, (2014).

2. W.Z. Yan, S.F. Wen, J. Liu, Z.F. Yue, *Mate. Sci. Eng. A* **527** pp.1850-1855, (2010).

Strain distribution measurements across dissimilar welded joints of Gr.91 under creep tests

Takuya Yamashita[1], Yuji Nagae[1]

[1]. Japan Atomic Energy Agency

Email: yamashita.takuya38@jaea.go.jp

Gr.91 / Inconel600 / 304SS dissimilar welded joint (DWJ) will be used in an advanced loop-type sodium cooled reactor at 550 °C which is the service temperature. The interface failure between the ferritic steels and the Inconel weld metal under creep tests at 550 °C have been reported [1,2]. However, the reason of interface failure has not been clarified. Interface failure isn't considered in the component design. Thus, it is necessary to prevent the interface failure. In this study, 2 types of DWJs were manufactured by Plasma Arc Welding (PAW) and Gas Tungsten Arc Welding (GTAW), respectively. DWJs by PAW (PAW_DWJ) and by GTAW (GTAW_DWJ) were formed different width and microstructure of Heat Affected Zone (HAZ), due to different heat input during welding to Gr.91, respectively. HAZ width in Gr.91 was identified by prior austenitic grain size, from interface to average of Gr.91 grain size (0.02 mm). HAZ width of PAW_DWJ and GTAW_DWJ were approximately 7 mm and 5 mm, respectively. HAZ width classified by grain size was the almost same as distance from interface to the most softening part which measured by the Vickers hardness test. Relatively coarse grained part in PAW_DWJ was formed adjacent to interface. HAZ was classified into 2 types depending on grain size: Larger than average grain size of Gr.91 was classified as Coarse Grain HAZ (CGHAZ), and that smaller than average grain size was classified as Fine Grain HAZ (FGHAZ). The width of CGHAZ and FGHAZ in PAW_DWJ were approximately 2 mm and 5 mm, those of GTAW_DWJ were approximately 0 mm and 5 mm, respectively. Specimens for creep tests were sampled from Gr.91 / Inconel600 part because creep ruptures of DWJs occurred at Gr.91 or the interface in many previous studies [1, 2]. In creep tests, GTAW_DWJs failed at the interface or Gr.91 part and PAW_DWJs failed at Gr.91 part i.e. the interface failure would not take place. It was assumed that width and microstructure of HAZ in PAW_DWJ were different from those in GTAW_DWJ. Therefore, strain distributions in HAZ of PAW_DWJ and GTAW_DWJ during creep tests were measured to investigate the failure behavior at 550 °C with applied stress 190 MPa where the interface failure occurred in GTAW_DWJ. Strain distribution in HAZ during creep test was measured by Speckle Image Correlation Analysis (SPICA). SPICA has been developed as a method for on-stream assessment of deformations of components in high temperatures [3]. Fig. 1 shows strain distribution measurements across Gr.91 / Inconel600 parts under creep tests. Strain distributions were different depending on constitutions and properties of HAZ. CGHAZ was hard to deform comparing to FGHAZ [2]. Therefore, strain around the interface in PAW_DWJ was small, and strain was concentrated far from the interface. As a result, PAW_DWJ clearly failed at FGHAZ. In contrast, such a strain concentration wasn't observed in GTAW_DWJ, strain gradually increased with distance from the interface in PAW_DWJ. A failure location couldn't be predicted from the strain distribution. Fig. 1 also shows the equivalent strain distribution obtained by elastoplastic finite element analyses. Obvious strain concentration was observed near the interface between Inconel and FGHAZ in GTAW_DWJ because of the large difference between the deformation resistance of

Inconel600 and FGHAZ. Since the adhesive property of the interface has not been characterized, interface failure cannot be evaluated. In contrast, strain concentrated at the boundary between CGHAZ and FGHAZ in PAW_DWJ, but failure assessment would be possible at the location because the material properties of CGHAZ and FGHAZ were obtained. Based on the above results, presence of CGHAZ between Inconel 600 and FGHAZ may enable to perform the failure assessment of the DWJ.

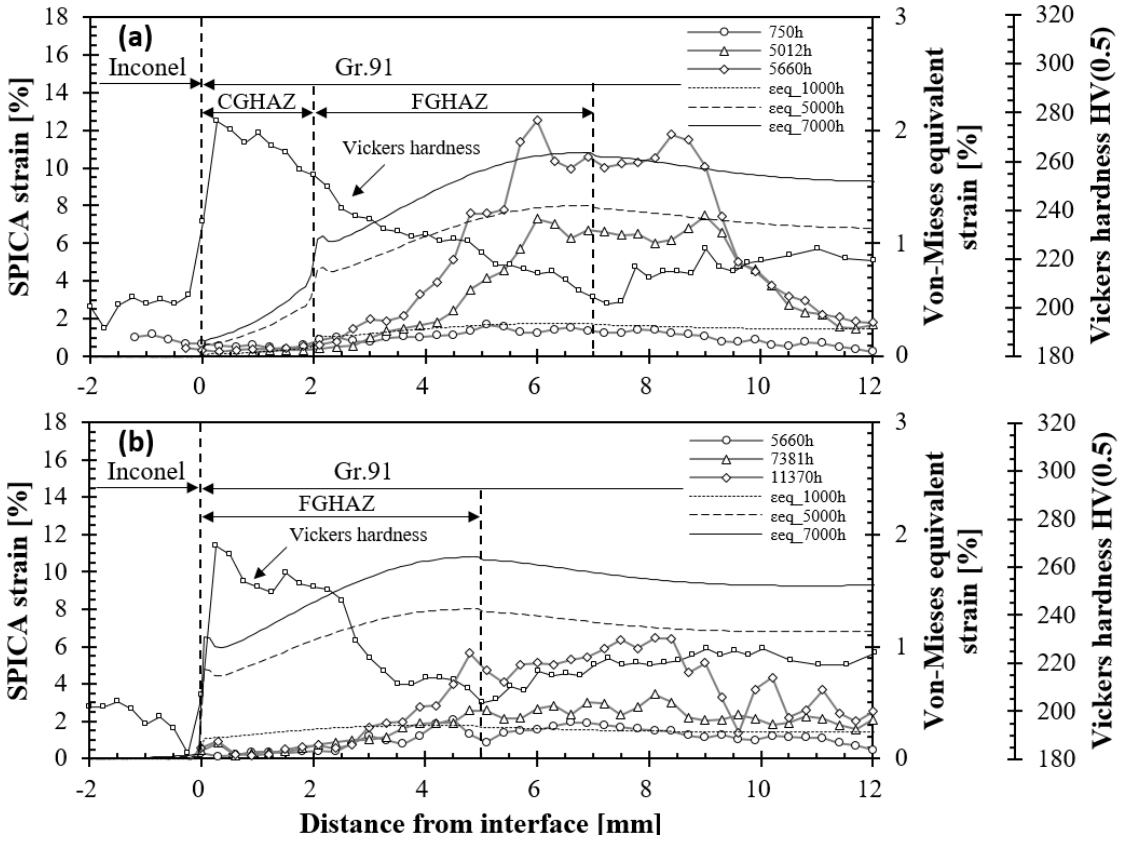

Fig. 1 strain distribution measurements across (a) PAW_DWJ and (b) GTAW_DWJ under creep tests (550 °C, 190MPa)

References

1. Yamazaki, M. et al., JEPE, Vol. **2**, pp. 1140-1149, (2007).
2. K. Laha et al., METALL. MAT. TRANS. A. Vol. **43A**, pp.1174-1186 (2012)
3. Hulshof, H. et al., ECCC, pp. 513-518, (2005).

Evaluation of Creep-Fatigue Damage in a Large-Scale Sodium Test Facility of the STELLA-2

Hyeong-Yeon Lee[1], Seok-Kwon Son[1], Jae-Hyuk Eoh[1], Ji-Young Jeong[21], Yong-Sun Ju[2]

[1]. SFR NSSS System Design Division, Korea Atomic Energy Research Institute

[2]. KOASIS. Inc.

Email: hylee@kaeri.re.kr

Abstract. A detail design on a large-scale sodium test facility is underway by Korea Atomic Energy Research Institute (KAERI). Elevated temperature design (ETD) evaluations were conducted for the main components including model reactor vessel (RV) and reactor internal(RI) according to ETD codes of ASME Section III Subsection NH and RCC-MRx. Quantification of conservatisms for the ETD codes has been conducted and technical issues were raised in elevated temperature design codes for 316L stainless steel components.

Introduction. KAERI has been developing Prototype Generation IV sodium-cooled fast reactor (PGSFR)[1]. Design evaluations on a large-scale sodium test facility of the STELLA((Sodium Test Loop for Safety Simulation and Assessment)-2 is underway at KAERI to demonstrate the plant safety and to support the design approval for the PGSFR and the facility is to be constructed by 2019. Since the STELLA-2 is a sodium test facility, high level of reliability in terms of structural integrity is required. Therefore, ETD codes of ASME-NH[2] and RCC-MRx[3] were used for design evaluation of the test facility to secure integrity with focus on creep-fatigue damage. The evaluation results and conservatism from both codes were compared. It was reported that ASME-NH is more conservative than RCC-MRx[4]. For design evaluation on creep-fatigue damage according to RCC-MRx, a web-based program of HITEP_RCC-MRx was developed and verification of the proram was performed.

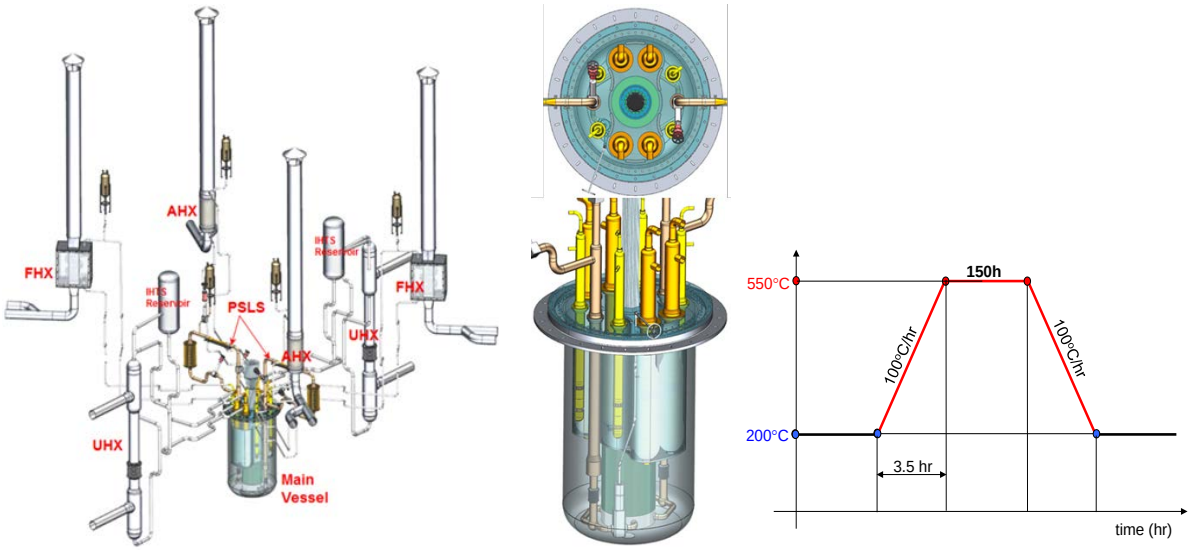

(a) (b) (c)

Figure 1. *Schematic of the STELLA-2 facility, model RV and operating transient of model RI*

Design feature of the STELLA-2 The STELLA-2 has model RV, reactor internal(RI), five heat exchangers (IHX, DHX, AHX, FHX, UHX), three kinds of tanks(sodium storage tank, expansion tank and reservoir). A schematic of the primary and secodnary system is shown in Fig. 1(a) and

model RV is shown in Fig. 1(b). The design transients of model RV is 550°C, 0.5MPa, and operating transients of model RV is 500°C, 0.1MPa while design transients of model RI is 600°C, 0.5MPa and operating transients of model RI is 550°C, 0.1MPa as shown in Fig. 1(c).

Evaluation results of creep-fatigue damage for model RV component Full 3D finite element analysis on the model RV and RI was conducted and the profile of stress intensity(S.I) under thermal load shows that the maximum S.I with the value of 336 MPa occurred as shown in Fig. 2(a) at the corner of redan structure which separates hot pool from cold pool. Calculation of creep-fatigue damage was conducted according to the procedures of ASME-NH and RCC-MRx. In equation (1), the first term is fatigue damage (D_f) and the second term is creep damage (D_c). The evalaution results showed that D_f and D_c as per ASME-NH was 0.070 and 0.0001, respectively while D_f and D_c as per RCC-MRx was 0.002 and 0.0102, respectively, which means ASME-NH was more conservative for fatigue damage and RCC-MRx was more conservative for creep damage. Those evaluation results were well within the allowable bi-linear limit as shown in Fig. 2(b).

$$\sum_{j=1}^{P}\left(\frac{n}{N_d}\right)_j + \sum_{k=1}^{q}\left(\frac{\Delta t}{T_d}\right)_k \le D \qquad (1)$$

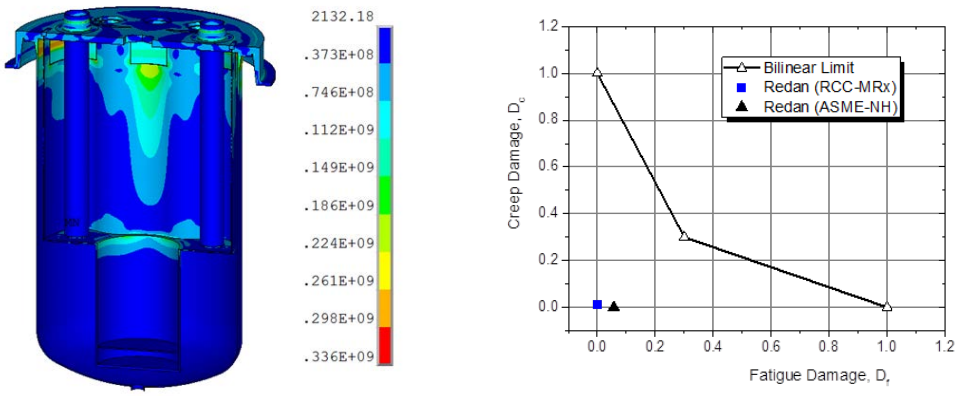

(a) (b)

Figure 2. *Distribution of stress intensity under thermal load and evaluation result of creep-fatigue damage according to ASME-NH and RCC-MRx*

Acknowledgements

This work was supported by an International Research & Development Program Foundation NRF grant (2013K1A3A7A03078195) and by a NRF grant (2012M2A8A2025635) funded by the Korea government (MSIP).

References

1. Y.I.Kim, *et.al.* KAERI/TR-4598/2012 (2012).
2. ASME Section III Subsection NH, Class 1 Components in elevated temperature service(2015).
3. RCC-MRx, Tome 1, Subsection B, Class N_{1Rx} Reactor Components, AFCEN (2015).
4. H.Y.Lee., Comparison of elevated temperature design codes of ASME Subsection NH and RCC-MRx, *Nuclear Engineering and Design* **308**, 142–153 (2016).

Method of Estimating the Temperature for 18Cr-9Ni-3Cu-Nb-N Austenitic Stainless Steel by Coarsening of the Sigma Phase

T. Kimura[1], Y. Shioda[1], K. Nomura[1], K. Kubushiro[1]

[1] IHI Corporation

Email.Corresponding. takahiro_kimura@ihi.co.jp

Introduction. 18Cr-9Ni-3Cu-Nb-N austenitic stainless steels (KA-SUS 304J1 HTB, ASME case 2328) are often used in USC boilers throughout the world. For safe and reliable power supply, it is significant to accurately evaluate the remaining creep life for this type of stainless steel. It is also important to estimate the operational temperature. Therefore, we studied a method for estimating the temperature of boiler tubes from microstructure changes.

Experimental procedure. Internal pressure creep tests were conducted at a temperature of 1023 K and a pressure of between 60 MPa and 100 MPa. The specimens used were made from tubes with an outer diameter of 50.8 mm and a thickness of 3.9 mm. The microstructures of ruptured specimens were observed using optical and scanning electron microscopes. The diameter of the σ phase particles at the grain boundaries was measured by means of five optical micrographs at a magnification of 500×, which were assumed to be a sphere of equivalent value.

Results. Fig. 1 shows backscattered electron images of the creep-ruptured specimens after 6486.4 h (1023 K × 60 MPa). Three phases were observed: σ phase (light grey), $M_{23}C_6$ carbides (dark grey), and Nb(C,N) (coarsened white particles). We focused in particular on changes in the σ phase. Fig. 2 shows the optical microstructures of the ruptured specimens within three stress ranges. The size of the σ phase rose dramatically in accordance with increases in the rupture time. We determined that in crept specimens the relationship between LMP and the particle sizes of the σ phase at G.B. could be approximated by means of one particular curve, and that the key point was that the relationship was satisfied even if at simple aged samples such as screw portions of uniaxial creep specimens. Therefore, we were able to investigate the just temperature for boiler tubes at operational power plants was being applied, by using just two factors, such as the plant's running time and the particle size of σ. This approach should prove to be an effective method of providing improved accuracy in evaluations of the remaining creep life for this type of stainless steel.

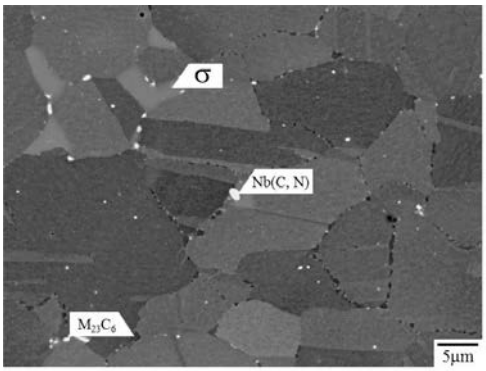

Figure 1. Backscattered electron images of a ruptured specimen (1023 K × 60 MPa, t_r = 6486.4 h)

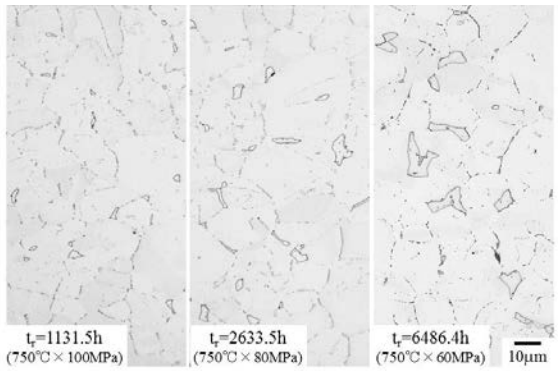

Figure 2. Changes in the size of the σ-phase in ruptured specimens. These rupture time were from 1131.5h to 6486.4h.

Method of Assessing Individual Creep Properties of Actual Piping Using Small Samples

M. Yaguchi[1], M. Tomobe[1], S. Komazaki[2], A. Kumada[3]

[1]. Central Research Institute of Electric Power Industry

[2]. Kagoshima University

[3]. Kobe Material Testing Laboratory Co., Ltd.

Email: yaguchi@criepi.denken.or.jp

In the analytical life assessment of creep strength enhanced ferritic (CSEF) steels, average creep properties are generally assumed, although there is a large amount of scatter in the creep properties of welded joints of the steels. It is important to estimate the individual creep properties of welded joints of materials used at power stations if analytical life assessment is quantitatively applied to the components of power stations. Thus, we have developed a new method of assessing the individual creep properties of welded portions of actual piping using small samples. This paper describes the concept and a preliminary examination of the assessment method for P91 steel, which has been used worldwide as a CSEF steel.

A series of creep tests was conducted on specimens taken from various P91 steel pipings in long-term use at USC plants [1], and it was found that variations in the creep characteristics of welded portions have a correlation with the creep characteristics of the base metals if the damage mode of the pipings is Type IV. This means that individual creep properties of welded joints of the pipings can be approximately predicted if we know the individual creep properties of the base metals of the pipings. Therefore, the authors proposed an assessment method for individual creep properties based on information obtained from small samples cut from the outer surface of the pipings. Using the method, we can assess the creep properties of the base metals on the basis of creep test results and precipitation density analyses of the small samples if the following assumptions are valid.

Samples are sufficiently small to be cut from the surface of the pipings without affecting the structural integrity of the pipings.

1) The properties obtained using small samples have a sufficiently strong correlation with those of standard test specimens.

2) The properties at the outer surface of pipings are almost the same as those inside the pipings.

We have examined these assumptions and obtained the following results.

1) The small punch creep test [2] is useful for evaluating the creep properties of materials because a test sample comprising a circular disc of 8 mm diameter and 0.5 mm thickness is sufficiently small to be taken from pipings without affecting structural integrity.

2) Small punch creep tests were conducted on P91 steel base metals used at USC Plant A and Plant B, where the creep rupture time for a standard-type specimen of the Plant A base metal is approximately ten times longer than that of the Plant B

base metal, while the hardnesses of both materials are almost the same. The results of the small punch creep test compared with those obtained with a standard test specimen are shown in Fig.1. While the results of the small punch creep test did not completely coincide with the standard test results, the small punch creep tests can evaluate the difference in the creep properties between Plant A and Plant B materials. Thus, it is considered that small punch creep tests have the capability to assess the individual creep properties of materials that are difficult to assess using a hardness method.

3) To evaluate the creep property distribution in the wall thickness direction, we investigated the microstructure, hardness and rupture time of the base metals in long-term use at the USC plants. We found that there was no difference in creep properties in the thickness direction except in the area of less than about 1mm from the surface of the pipings.

Therefore, it is considered that the proposed method has the potential to assess the creep properties of the base metals of pipings if small samples are taken from the pipings except from the surface area. Then, we can approximately predict individual creep properties of the welded joints of pipings on the basis of the creep properties of the base metals.

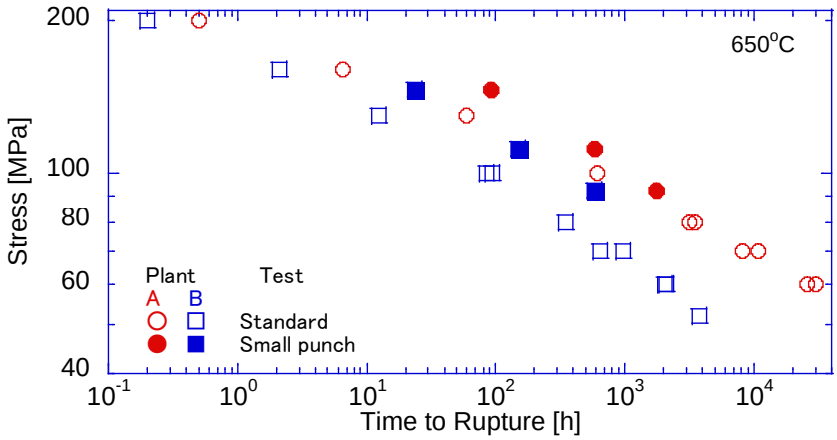

Figure 1 : Results of Small Punch Creep Test Compared with Standard Test Results

References

1. M. Yaguchi, S. Nagai, K. Sawada and K. Kimura, Advances in Materials Technology for Fossil Power Plants, Proc. 8th Int. Conf., Albufeira, Portugal, pp.447-458 (2016).
2. S. Komazaki, Y. Ohkawa and M. Yonemura, Advances in Materials Technology for Fossil Power Plants, Proc. 8th Int. Conf., Albufeira, Portugal, pp.623-632 (2016).

Evaluation of Cumulative Creep Rupture Life by Time-Fraction and Strain-Fraction Rules Using Small Punch Creep Tests

K.I. Kobayashi [1], S. Fukuda[1] and R. Kaneko[1]

[1.] Department of Mechanical Engineering, Chiba University, 263-8522 Japan

Email: k-cobayashi@faculty.chiba-u.jp

Small Punch (SP) creep test is an effective semi-destructive testing method to measure creep properties for very small areas of components, and was applied to evaluate residual creep lives using a ferritic stainless steel in this paper.

After preparing pre-crept uniaxial specimens that were interrupted at several lifetime ratios, disk-type SP creep specimens of 10 mm in diameter and 0.5 mm in thick were collected, machined and employed. Rupture lives by the SP creep test almost depended on the lifetime ratio of the uniaxial creep test even if the applied load level in the SP creep test was changed. Time-fraction (TF) rule based on each lifetime ratio of uniaxial and SP creep tests could estimate the residual lifetime below 0.5 of the uniaxial lifetime ratio, but it would not be validated over its lifetime ratio if the cumulative value was assumed as one (See Fig.1). Employing section areas in the SP creep specimen along the extruded ring edge on the fracture surface, strain-fraction (SF) rule based on each strain of creep exhaustion ratios was newly defined. An applied result of the SF rule was shown in Fig.2, and it reveals that the SF rule can estimate the residual lifetime of components more precisely than the TF rule except severely damaged level when the cumulative damage ratio was supposed to be one. Mixed fraction (MF) rule was introduced combining both the TF rule by the uniaxial creep and the SF rule by the SP creep. This MF rule was also verified to be effective to evaluate the residual life of aged components.

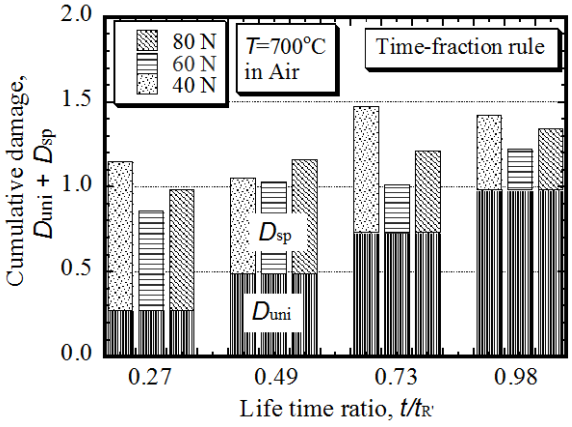

Fig.1 *Result of application of time fraction rule.*

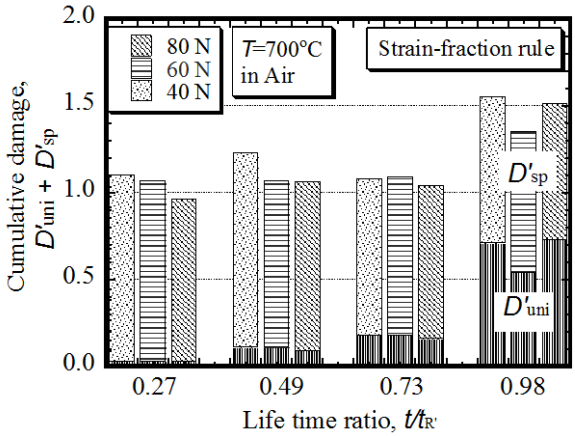

Fig.2 *Result of applicability of strain fraction rule.*

Small Ring Creep Testing of High Temperature Materials

C.J. Hyde

Department of Mechanical, Materials and Manufacturing Engineering, University Park,

The University of Nottingham, Nottingham, NG7 2RD,

Christopher.Hyde@nottingham.ac.uk, +44 (0)115 9513735

Components such as steam pipes, pipe branches, gas and steam turbine blades, etc. which operate in engineering applications such as power plant, aero-engines, chemical plant etc., can operate at temperatures which are high enough for creep to occur. Additional complexity is often also present in that the proportion of the material creep life consumed may vary from position to position within the component and only nominal operating conditions (i.e. pressure, temperatures, system load, etc.) known. Hence precise life predictions for these components, which may be complex in terms of geometry or weld characteristics, are not possible. Non-destructive techniques are therefore required in order to assist in the making of decisions on whether to repair, continue operating or replace certain components. Small specimen testing, of which there are several types, is a technique which can be used in this way. Small samples of material are removed from the component to make small creep test specimens, such as small ring specimens. These specimens can then be tested to give information on the remaining creep life of the component. This paper presents the results of Small Ring specimens tested under creep conditions and shows the comparison to standard (full size) creep testing for materials used under high temperature in industry. Also presented is a new update/improvement made to the testing technique since previously presented results.

High Temperature Creep Mechanisms and Anisotropic Creep of Zr-based Alloys

Nilesh Kumar, Boopathy Kombaiah and K. Linga Murty

Department of Nuclear Engineering, North Carolina State University, Raleigh NC 27695-7909, USA

Email: murty@ncsu.edu

We summarize here our research findings on basic creep mechanisms during high temperature deformation of Zr-based alloys, Zircaloy-4 (1.5Sn, 0.21Fe, 0.1Cr, 0.1O; wt.%) and HANA4 (1.5Nb, 0.4Sn, 0.2Fe, 0.1Cr; wt.%), with emphasis on transitions in creep mechanisms as a function of the applied stress and temperature. Deformation microstructures were investigated along with mechanical data for unequivocal determination of the underlying deformation mechanism(s). Moreover, anisotropic creep behaviors of these alloys in tubing form were investigated using internal pressurization superimposed with axial loads while monitoring hoop and axial strains using laser telemetric and LVDT extensometers respectively (Fig. 1). Zircaloy-4 behaved like a pure metal exhibiting dislocation climb at intermediate stresses along with cross-slip of screw dislocations at high stresses and Coble creep at low stresses. On the contrary, HANA4 revealed precipitation hardening mechanism along with dislocation climb at high stresses and Coble creep at lower stresses (Fig. 2).

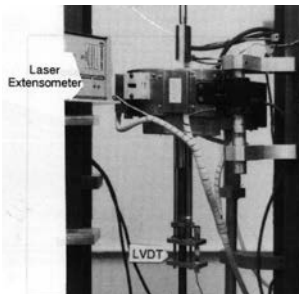

Fig. 1

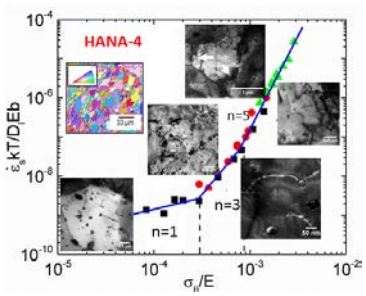

Fig. 2

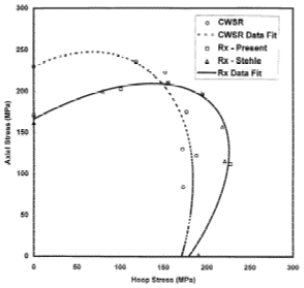

Fig. 3

Hexagonal closed packed crystal structure with limited number of slip systems rendered them textured exhibiting mechanical anisotropy resulting in different strain rates along hoop versus axial directions of the thin-walled tube. Our extensive studies on these materials revealed that Nb-addition has relatively minute effect compared to thermomechanical processing. Quantitative characterization of texture using crystallite orientation distribution functions (CODF) combined with single crystal slip models yielded correlations between model predictions and experimental results (Fig. 3) that could explain clearly the dominance of prism slip for the recrystallized Zircaloy-4. In contradiction, cold-work stress-relief resulted in apparent correlation with basal slip dominance albeit no such slip was noted in the deformation microstructures of low c/a ratio materials. Explanation for this lies in the fact that prior cold-work lead to saturation of prism planes leading to the possible operation of secondary or tertiary slip systems.

These various findings are used in predicting the dimensional changes of the cladding tubes in-reactor as well as those of the used nuclear fuel (UNF) during dry storage. Correlations clearly point out the importance of the experimental studies on creep during neutron radiation exposure which are currently limited.

This research is funded by the US National Science Foundation through grant DMR0968825 and the HANA4 alloy tubing was received from Korea Atomic Energy Research Institute.

Modelled and DIC-measured strains in notched specimen from Al-Cu-Mg-Si alloy with anisotropic creep behaviour

E. Gariboldi[1], K. Naumenko[2], O. Ozhoga-Maslovskaja[3], E. Zappa[1]

1. *Politecnico di Milano, Dipartimento di Meccanica, Milano (Italy)*
2. *Otto-von-Guericke-University Magdeburg, Institute of Mechanics, Magdeburg (Germany),*
3. *RWTH Aachen University, Laboratory for Machine Tools and Production Engineering (WZL), Aachen (Germany)*

Email. Elisabetta.gariboldi@polimi.it

Abstract

The study focuses on the validation of creep model able to describe anisotropic creep strain behaviour by means of experimental measurements of non-uniform strain field via Digital Image Correlation techniques. The investigated material was an Al-Cu-Mg-Si alloy with known anisotropic creep strain and for which a constitutive phase mixture model of high temperature behavior had been developed on the basis of uniaxial creep tests on specimen sampling orientations.

Flat notch specimens characterized by two notch radii (1 and 2.5mm) were sampled in different directions and constant load creep tests were carried out on them at 150°C at two different nominal stress levels. Before creep tests, the flat surface of the specimens was polished and a speckle pattern was obtained by means of air brush pen in order to allow Digital Image Correlation (DIC) analysis. The 3D DIC technique wasapplied in situ on selected samples in order to extract the displacement and strain field values on the surface of the notched specimens during creep tests as well at rupture. Finite element simulations of the stress redistribution and of creep strain development in different parts of the notched specimens were carried out for the different combinations of geometrical features (sampling orientation and notch radius) and nominal stress.

The analyses of DIC results showing the strain field evolution revealed a non-symmetrical damage and crack nucleation and propagation in some specimens. This observation suggested regions where proper comparisons with numerical results had to be carried out and gave the possibility to derive many pieces of information on damage forms and evolution from SEM microstructural analyses of crept specimens. Strain values around notches and in the vicinity of crack flanges once more clearly indicate anisotropic character of creep damage and, in the investigated alloy, the important role played by intermetallic particles at grain boundaries.

Effect of microstructural instabilities on high-temperature creep response of the 2024 aluminum alloy

M.Cabibbo[1], M.Regev[2], S.Spigarelli[1]

[1] DIISM, Università Politecnica delle Marche, via Brecce Bianche, I-60131 Ancona, Italy

[2] Mechanical Engineering Department, ORT Braude College, P.O.Box 78, Karmiel 2161002, Israel

Email. m.cabibbo@univpm.it

The creep response of a 2024 aluminum alloy has been investigated at 315°C, to quantify the effects of different instability phenomena, such as the evolution of secondary phase particle size and distribution, and early cracking in the Friction Stir Weld root. Figure 1 plots the experimental values of the minimum creep rate as a function of applied stress for three different experimental conditions: i. CL_b, i.e. constant load creep experiments carried out on the base metal; ii. VL_b, i.e. creep experiments on the base alloy in which the initial load (25 MPa) was abruptly increased after the minimum creep rate range was reached; iii. CL_{cw}, i.e. constant load creep experiments carried out on cross weld samples.

Figure 1 clearly shows the substantial difference observed when comparing the minimum creep rate in CL_b and VL_b samples. The reason for this discrepancy was identified in the different time of exposure at high temperature. In the VL_b samples, the increase in applied stress occurred after a given time of permanence at 315°C under 25 MPa, and resulted in the fracture of the specimen after a relatively short duration. In these conditions, all the VL_b samples underwent a roughly equivalent duration of exposure at 315°C. By contrast, the time corresponding to the minimum in creep rate in CL_b tests varied of orders of magnitude. Thus, while the microstructure of the VL_b samples, in terms of size, volume fraction and distribution of secondary phase particles, was substantially equivalent, in the case of the CL_b tests the microstructure of each sample underwent a different degree of overageing. This effect was quantified by introducing a threshold stress (σ_0), representing the strengthening contribution due to particle-dislocation interactions, into the well known Garofalo equation, i.e.

$$\dot{\varepsilon} = A(T)[\sinh \alpha(\sigma - \sigma_0)]^n \qquad (1)$$

where A(T) is a temperature-dependent parameter, α is a material constant, and n=4.4. The use of Equation 1 gave a good description of the experimental data for the base metal, with a constant value of the threshold stress for VL_b experiments; by contrast, in case of the CL_b experiments, the value of the threshold stress was observed to decrease with stress, i.e. with the increase of exposure time at 315°C, in qualitative agreement with the results of hardness measurements on crept samples.

This study also focused on the role of the Friction Stir Welding on the creep response of the 2024 alloy. This issue was addressed by taking into account that creep exposure caused the onset of root-cracks (Figure 2). These cracks invariably opened in otherwise undamaged cross-weld samples, whose integrity was tested before creep by X-rays analysis, and caused the reduction of the load-bearing section to about half of its original area. The high values of the minimum creep rate were thus caused by this reduction in area, which led to the stress redistribution in the unfractured portion of the

sample. Interrupted experiments were also used to investigate the crack nucleation and propagation stage, to be related with the microstructural inhomogeneities introduced by Friction Stir Welding.

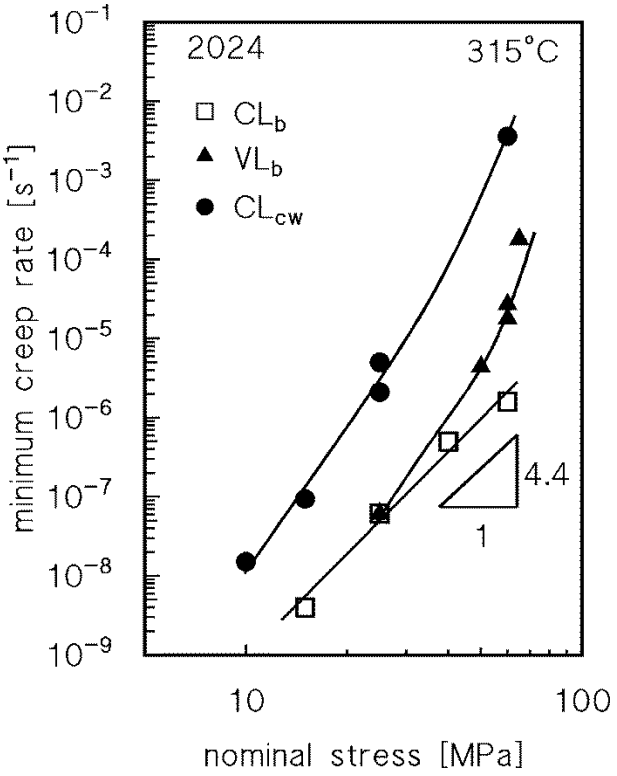

Figure 1. Minimum creep rate dependence on applied stress.

Figure 2. Root crack developed during creep at 315°C-25 MPa in cross-weld samples.

Correct Interpretation of Creep Rates: A Case Study of Cu

W. Blum[1], J. Dvorák[2], P. Král[2], P. Eisenlohr[3], V. Skleničk[2]

[1]. Institut für Werkstoffwissenschaften, University of Erlangen-Nürnberg, Martensstr. 5, D-91058 Erlangen, Germany

[2]. Institute of Physics of Materials, Academy of Sciences of the Czech Republic, Žižkova 22, CZ61662 Brno, Czech Republic

[3]. Department of Chemical Engineering and Materials Science, Michigan State University, East Lansing, MI 48824, USA

Email. eisenlohr@egr.msu.edu

Traditionally, the deformation resistance in creep is characterized by the minimum creep rate $\dot{\varepsilon}_{min}$ and its sensitivity to stress (stress exponent n) and temperature (activation energy Q). Various values of constant n have been reported in the literature and interpreted in terms of specific mechanisms. The present case study of coarse-grained Cu at 573 K yields a stress exponent n = 9 for $\dot{\varepsilon}_{min}$ in tension and a relatively low activation energy. The evolution of the deformation resistance with strain at constant tensile creep load and comparison with creep in compression without fracture indicates that the tensile $\dot{\varepsilon}_{min}$ result from transition from uniform deformation to strain localization during fracture. This is confirmed by the results of creep in compression where fracture is suppressed. Both the tensile $\dot{\varepsilon}_{min}$ and the compressive creep rate at strains around 0.3 can be described using existing equations for quasi-stationary deformation containing the subgrain boundary misorientation θ as structure parameter. While in the latter case constant θ leads to monotonic increase of n with stress, the tensile nine-power-law results from variable θ, and has no simple meaning. The result of this case study means that uncritical interpretation of minimum tensile creep rates as stationary ones bears a high risk of systematic errors in the determination of creep parameters and identification of creep mechanisms.

Modelling of creep and stress relaxation of the nickel-base alloy Nimonic 80A at isothermal and non-isothermal loading conditions

P. Hahn, M. Schwienheer, M. Oechsner

Institut fuer Werkstoffkunde TU Darmstadt
Email. hahn@mpa-ifw.tu-darmstadt.de

The design and dimensioning of new as well as the assessment of operating high temperature components requires a precise prediction of creep and stress relaxation. The increasing share of renewable energies forces fossil-fired power plants on increasing numbers of start-ups and shut-downs. Consequent transient loading conditions need to be taken into account. In order to meet this demand, non-isothermal creep equation are necessary, that enables a consistent prediction of creep strain and stress relaxation in a wide range of temperature and stress.

In this work the stress relaxation was modelled as change of reversible elastic strain to irreversible permanent strain. Analytic temperature-dependent equations of the different strain portions of the permanent strain: creep, initial plasticity and “negative creep” enables a consistent description of the material behaviour (Fig. 1) [1,2]. The efficiency and the accuracy of the numerical analysis using common finite element solvers (e.g. Abaqus®) are significantly affected by the used creep law. Therefore an enhancement of the successful in industrial application proved modified Garofalo creep equation [2,3] was developed. Optimized calculating times and a better robustness was achieved by the new implicit formulation of the Garofalo equation.

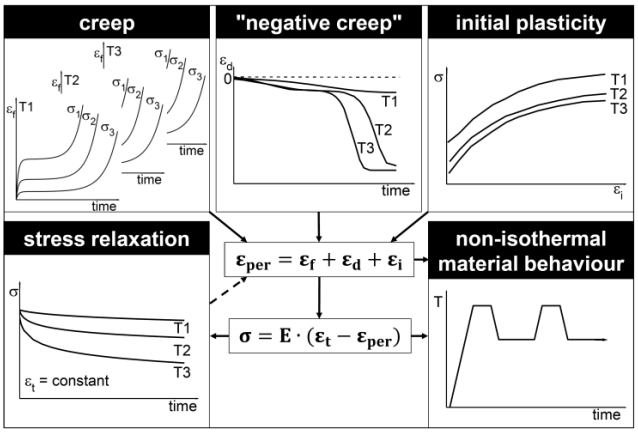

Figure 1. Schematic overview of the modelling process of stress relaxation

The adjustment of the phenomenological models was based on a wide database of hot tensile, creep and annealing tests of the nickel-base alloy Nimonic 80A. A temperature range of 450 °C up to 650 °C was examined. The developed material models were successfully validated with isothermal and non-isothermal relaxation experiments. Further the recalculation of a staged relaxation test demonstrates the capability of the defined material laws.

References

1. R. Fountain and M. Korchynsky, The phenomenon of “negative creep” in alloys, *Transactions of the ASM* **51**, pp. 108-122(1959).

2. K. H. Kloos et al., Direct creep curve assessment and optimization of creep equations for higher temperature alloys, *Materials technology - steel research* **67**, pp. 156-162(1996).

3. M. Monsees et al., Creep equations for heat resistant steels, *Steel research* 69, pp. 446-454(1998).

Creep and Low Cycle Fatigue Behaviors of Alloy 617 at Elevated Temperatures of 900℃ and 950℃.

S. J. Kim[1], R. T. Dewa[1], J. Y. Park[2], W. G. Kim[2], E. S. Kim[2]

[1]. Pukyong National University, 365 Sinseon-ro, Nam-gu, Busan 48547, Republic of Korea

[2]. Korea Atomic Energy Research Institute, 989-111 Daedeok-daero, Yuseong-gu, Daejeon 34057, Republic of Korea

Email. sjkim@pknu.ac.kr

A very high temperature reactor (VHTR) is one of the most promising Gen-IV reactor types for the economic production of electricity and hydrogen. The VHTR system is designed with a target life span of 60 years under operating conditions of 950℃ and 7 MPa in helium impurities. The intermediate heat exchanger (IHX) is a key component that links the reactors to the hydrogen production plant. The IHX component is directly exposed to a primary coolant of 950℃. The combination of high temperature operation and long duration of service requires structural materials with good thermal stability as well as high temperature creep resistance. Based on these material requirements, Alloy 617 is a leading candidate alloy for the high temperature components. Creep and low cycle fatigue (LCF) properties for Alloy 617 have been recently many studied; however, details of the deformation behavior during fatigue are not readily available [1-2].

In this study, creep rupture and LCF behaviors for Alloy 617 have been investigated at 900℃ and 950℃, the temperature range of particular interest for IHX. One of the goals of the current study is to understand the influence of temperature on creep rupture and LCF properties of this material.

Commercial grade nickel-based superalloy, Alloy 617 (Inconel 617) was used in this study. The material was solution treated hot rolled plate with a thickness of 25 mm. The initial microstructure of the parent metal is a fully austenitic face centered cubic structure. Creep specimens were fabricated in cylindrical form with a 30 mm gage length and 6 mm diameter. And LCF testing specimens were machined with shape and dimensions of 6.0 mm diameter in the reduced section with a gage length of 12 mm. Creep behaviour for Alloy 617 was investigated by a series of creep tests with different stress levels at 900^{o}C and 950^{o}C under different applied stresses. This stress represented 5-10% of the yield strength value of Alloy 617 at regarding temperatures. The Fully reversed ($R = -1$) total axial strain-controlled LCF tests have been conducted at four different total strain ranges of 1.5, 1.2, 0.9, and 0.6% at 900^{o}C and 950^{o}C on Alloy 617 in air environment by using a servo hydraulic machine (MTS, 100 kN) equipped at a constant strain rate of 10^{-3}/s.

Figure 1 shows the creep curves obtained for Alloy 617 at 900^{o}C and 950^{o}C. Creep rupture curve reaching less than 1600 h and 400 h were successfully obtained for 30 MPa at 900^{o}C and 950^{o}C, respectively. Little primary creep strain was observed at this creep condition. A well-defined secondary creep stage, found in austenitic stainless steels in the temperature range of 773 K - 873 K, was not observed. The onset of a tertiary creep was unclear, and tertiary creep stage started from a low strain level.

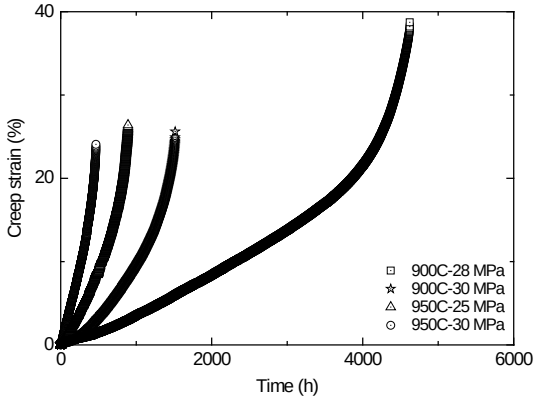

Figure 1. Creep curves obtained for Alloy 617 at 900ºC and 950ºC temperatures.

Figure 2 shows that at all the testing conditions the increased in temperature resulting in lower fatigue lives, and also the fatigue life are reduced with increasing in the total strain range. A good linearity are observed in the fatigue life curves for both temperature conditions.

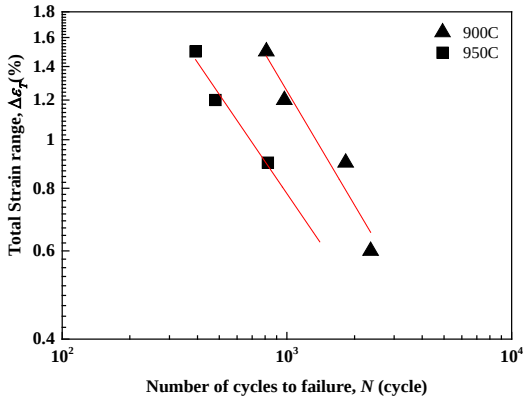

Figure 2. LCF lives of Alloy 617 at elevated temperatures and strain ranges.

In this conference, the creep and low cycle fatigue behaviors of Alloy 617 in the temperatures of 900 ºC and 950 ºC will be presented.

References

1. W. G. Kim *et al*., *Engineering Failure Analysis* **58**, pp. 441-451, (2015).
2. J. K. Wright *et al*., *Journal of Engineering Materials and Technology, Transactions of the ASME* **135**, pp. 1-8, (2013).

Creep of lamellar Fe-Al alloys

A. Schmitt[1,*], K.S. Kumar[2], X.Li[3], F. Stein[3], A. Kauffmann[1] and M. Heilmaier[1]

[1] Institute for Applied Materials (IAM-WK), Karlsruhe Institute of Technology (KIT), Karlsruhe, Germany

[2] School of Engineering, Brown University, Providence, USA

[3] Structure and Nano-/Micromechanics of Materials, Max-Planck-Institut für Eisenforschung GmbH, Düsseldorf, Germany

Email: anke.schmitt@kit.edu

Due to their low-density and oxidation-resistant iron aluminides are possible alternatives for steels in warm-temperature application. However, their usability is limited by a reduced ductility at room temperature and an intrinsically low creep resistance. As previously demonstrate for TiAl a lamellar microstructure can improve these properties simultaneously. In the Fe-Al system, a lamellar microstructure can be obtained through a eutectoid transformation in the composition range of 55 – 65 at.% Al. Specifically, the high-temperature ε-phase, Fe_5Al_8 decomposes into B2-ordered FeAl and triclinic $FeAl_2$.

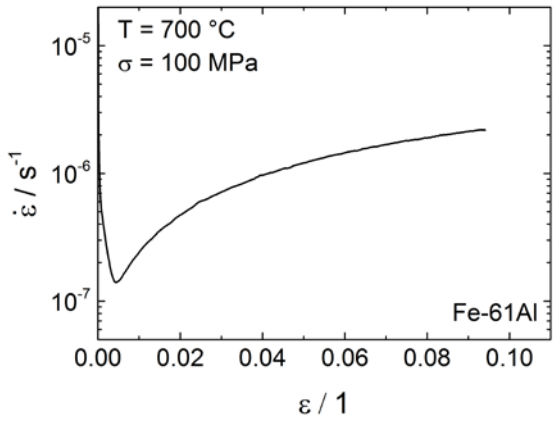

Fig. 1 Creep response of a lamellar Fe-61Al alloy at 700 °C and an applied stress of 100 MPa

The creep properties of these two-phase intermetallic alloys have not been investigated in detail to date. Thus, in this study, the constant-load compressive creep response of a binary, eutectoid Fe-Al alloy was examined. The resulting creep curve exhibit a characteristic minimum, follow by an increase of the creep rate with increasing time and strain. No pronounced steady state regime occurs. The minimum creep rate is temperature- and applied stress-dependent. The creep response at 700 °C and a nominal constant stress of 100 MPa for a fully lamellar eutectoid alloy is exemplary shown in Fig. 1. The minimal creep rate is at ~10-7 s-1 and, thus, roughly two orders of magnitude lower than that for single phase B2-ordered FeAl.

An increasing creep rate quite often indicative a microstructural instability and within a lamellar microstructure lamellar spacing might change. In order to verify a possible coarsening of the lamellae, the lamellar spacing was measured after different times and strains. However, a significant coarsening of the lamellae was noted. Therefore, the increase of the strain rate is caused by a different mechanism. It is also possible that the dominant creep mechanism might change.

As the material did not exhibit any indications for failure (e.g. cracking) during compressive creep, it may be assumed that both phases have to co-deform plastically. While it is known that the creep behavior of FeAl in a large composition range is primarily based on dislocation slip, knowledge on high temperature plastic deformation mechanisms of triclinic $FeAl_2$ phase is scarce. To determine the deformation behavior of the $FeAl_2$ phase, its creep behavior was studied in bulk single phase form. Various crept specimens were examined in the TEM to understand the underlying mechanisms of deformation of both phases during creep. In the early stages of creep, plastic deformation by slip appears to be restricted to the FeAl lamellae; the interface dislocation content increases as well to accommodate this plastic strain in FeAl, signaling dislocation-mediated sliding. Subsequently, signs of plastic deformation are noted in $FeAl_2$ and at even longer times, the lamellar morphology starts to destabilize.

On anisotropy factor assessment for aluminum alloys under high temperature creep

D. Kitaeva[1], Ya. Rudaev[2], Sh. Pazylov[2], G. Kodzhaspirov[1]

[1] Peter the Great St.Petersburg Polytechnic University, St.Petersburg, Russia

[2] Kyrgyz-Russian Slavic University, Bishkek, Kyrgyz Republic

Email. dkitaeva@mail.ru

The peculiarities of deformation behavior with deformation anisotropy for initially textured material and strong dependence of anisotropy factor ψ on the thermomechanical regimes of deformation, correlation of the regularities for it variation under the superplasticity conditions and boundary regions of thermoplasticity and high-temperature creep for aluminum alloy 1561 in [1–3] are established.

The studied structurization kinetics from initially textured state under temperature and high-rate effect in the regimes of thermoplasticity and high-temperature creep including superplasticity intervals is well correlated with regularities of change of deformation anisotropy of alloy 1561. Minimization of this indicator under superplasticity is explained by formation in material small equiaxial grains [3–6]. Therefore in [1–3, 6] it is rightly and reasonably offered to consider it as the macromechanical parameter of the material considering evolution of the structural changes happening under of thermopower effect. The model ratio describing kinetics of anisotropy factor for acceptance of the specified representation are formulated [6] and it interrelation with some physical quantity capturing the essence of structural and phase transformation of material is assiigned.

We will track temperature evolution of anisotropy factor with attraction of the one-dimensional Fokker-Planck's equation [7] belonging to the class of the parabolic equations and describing monotonous irreversible evolution of any initial distribution of probability density to an equilibrium state. Let's notice that Fokker-Planck's equation models superposition of friction and diffusion processes. For obtaining the closed solution of this equation in the form of Gaussian distribution we accept drift coefficient linearly depending on the order parameter [8]. We have

$$\psi(\eta,\xi) = (\pi a)^{1/2} \exp\left[-\frac{(\eta - b)^2}{a}\right]. \qquad (1)$$

Here η – the order parameter, ξ – reduced temperature [9],

$$a(\xi) = \frac{Q}{c}\left[1 - \exp(-2c\xi)\right] + a_0 \exp(-2c\xi);\ b(\xi) = b_0 \exp(-c\xi), \qquad (2)$$

and material functions $Q(\eta)$, $c(\eta)$, $a_0(\eta)$, $b_0(\eta)$, are defined from the following boundary conditions:

$$\left.\frac{d\psi}{d\xi}\right|_{\xi=\xi^*} = 0;\ \left.\frac{d\psi}{d\xi}\right|_{\xi=\frac{1}{2}} = 0;\ \left.\frac{d^2\psi}{d\xi^2}\right|_{\xi=0} = 0;\ \psi|_{\xi=\frac{1}{2}} = 1. \qquad (3)$$

It is emphasized by dependences (3) that under a temperature $\xi = \xi^*$ (or 693 K) there is a mathematical maximum on isotherms ψ □ ξ. The similar situation takes place and in the middle of the thermal range of superplasticity $(\xi = 1/2)$ [10, 11]. The third condition (3) by temperature of transition to superplastic range $(\xi = 0)$ is corresponded. The last equality (3) supposes that in the middle of a thermal interval of superplasticity material becomes isotropic. This well correlates with idea of superplasticity as about effect, happening during of indistinct irreversible structural transformation – dynamic recrystallization [9–14].

Acknowledgements

This work was supported by the Russian Foundation for Basic Research (Grant No.15-08-06531 a).

References

1. Sh.T. Pazylov, N.A. Omorov, Ya.I. Rudaev, On deformation anisotropy of aluminum alloys, *Tambov University Reports. Series Natural and Technical Sciences* **15 (3)**, pp. 974–975 (2010).

2. Sh.T. Pazylov, N.A. Omorov, A.K. Arzimatov, Deformation anisotropy and superplasticity of aluminum alloys, *Vestnik Kyrgyz-Russian Slavic University* **10 (10)**, pp. 144–149 (2010).

3. D.A. Kitaeva, Sh.T. Pazylov, Ya.I. Rudaev, Temperature-strain rate deformation conditions of aluminum alloys, *Journal of Applied Mechanics and Technical Physics* **57 (2)**, pp.352-358 (2016).

4. G.M. Amanbaeva, D.A. Kitaeva, Ya.I. Rudaev, Thermokinetic analysis of dynamic superplasticity parameters, *Vestnik Permskogo gosudarstvennogo tekhnicheskogo universiteta. Matematicheskoe modelirovanie system i protcesov* **14**, pp. 6–10 (2006).

5. D.A. Kitaeva, Ya.I. Rudaev, Macrokinetics heirarhies of states at dynamic superplasticity, *Materials Science Forum* **575-578**, pp. 340–344 (2008).

6. Sh.T. Pazylov, On anisotropy factor assessment, *Tambov University Reports. Series Natural and Technical Sciences* **21 (3)**, pp. 1216–1218 (2016).

7. R. Balesku, Equilibrium and nonequilibrium statistical mechanics, Vol.2, *Mir*, Moscow (1978).

8. H. Haken, Information and self-organization. A macroscopic approach to complex systems, *URSS*, Moscow (2014).

9. D.A. Kitaeva, Sh.T. Pazylov, Ya.I. Rudaev, On applications of nonlinear dynamics methods for mechanics of materials, *Vestnik Permskogo gosudarstvennogo tekhnicheskogo universiteta. Matematicheskoe modelirovanie system i protcesov* **15**, pp. 46–70 (2007).

10. A.I. Rudskoy, Ya.I. Rudaev, Mechanics of Dynamic Superplasticity of Aluminum Alloys*, Nauka,* St.Peterburg (2009).

11. D.A. Kitaeva, Ya.I. Rudaev, Synergetic Conceptions in Mechanics of Dynamic Superplasticity, *Nauch. Tekh. Vedom. St.-Peter. Gos. Politekhn. Univ.* **4-1 (183)**, pp. 274–283 (2013).

12. D.A. Kitaeva, Ya.I. Rudaev, About sensitivity to structural transformation at deformation of aluminum alloys, *Vestnik Kyrgyz-Russian Slavic University* **14 (7)**, pp. 60–63 (2014).

13. D.A. Kitaeva, G.E. Kodzhaspirov, Ya.I. Rudaev, On selforganization for thermomechanical deformation, *Tambov University Reports. Series Natural and Technical Sciences* **21 (3)**, pp. 1051–1054 (2016).

14. D.A. Kitaeva, G. Kodzhaspirov, Y. Rudaev, On the dynamic superplasticity, *Materials Science Forum* **879**, pp. 960–965 (2017).

Effect of Liquefaction of Low-Melting Bi Phase on the Creep Behavior of Cu-Bi Two Phase Alloy

Shobhit P Singh, Praveen Kumar

Department of Materials Engineering, Indian Institute of Science, Bangalore 560012, India

Email. shopasi@platinum.materials.iisc.ernet.in

Abstract. Cu-40 vol. % Bi is processed using liquid phase sintering (LPS). Compression creep tests of the alloy is conducted at various temperatures, including that above the melting temperature of Bi, $T_{m,Bi}$, in order to investigate the effect of liquefaction of Bi on the overall creep response of this alloy. Power-law creep with a stress exponent of 4 and 1 at high and low stresses, respectively, are observed below $T_{m,Bi}$, whereas the creep response above $T_{m,Bi}$ is anomalous, showing expansion at low stresses and regular power-law behavior at moderately high stress.

Introduction. Two phase alloys generally find their application in high temperature soldering and as phase change materials (PCMs) [1, 2]. Phase change materials comprising a low melting phase (LMP) material can be utilized in storing and releasing of the latent heat energy, when required, by liquefaction and solidification, respectively, of the LMP. One such proposed alloy consists of high volume fraction of Bi in Cu-Bi system [1].

Cu and Bi is a unique eutectic system which exhibits excellent wettability. Also, Bi has a very low solubility in Cu (≈0.003 at. % Bi at 800 °C) and there is no formation of any brittle intermetallic compound at all temperatures. This study investigates the compression creep of Cu-40 vol.% Bi at 200 °C, which is below $T_{m,Bi}$ and at 350 °C, which is significantly higher than $T_{m,Bi}$. The creep behavior of Cu-Bi alloy comprising such high-volume fraction of Bi at these temperatures has never been reported.

Experimental details. Cu-Bi alloy is prepared through LPS at 350 °C, i.e., above $T_{m,Bi}$. High purity Cu and Bi with spherical particles were utilized in preparation of the alloy. The details of alloy processing are discussed elsewhere [2]. Sintering of the alloy was carried out at high vacuum (~10^{-3} Pa). The experiments were conducted at constant load under compression at loads ranging from 3 to 25 MPa at 200 °C, and 3 to 10 MPa at 350 °C.

Results and discussions. Figure 1 (a) shows a few representative strain-time data for the samples tested at 200 °C. Fig. 1 (a) shows regular compression creep, showing distinct primary and secondary phases. Fig. 1 (b) shows the strain rate-stress data, showing a transition from a stress exponent of 4 to 1 at stresses below 10 MPa. Finite element analysis shows dominant role of Bi in overall deformation of this Cu-Bi alloy, thereby the stress exponent corresponds to that of Bi at these stresses. Figure 2 (a) shows strain-time data obtained from the experiments at 350 °C. Fig. 2 (a) reveals that at stresses >3 MPa, a short primary creep stage is observed followed by continued compression and rupture of the sample. The interesting fact to note is that the ruptured sample expanded for a long period of time, recovering the initial compressive strains. However, at 3 MPa, very short primary creep is observed which is followed by continuous expansion of the alloy. Three identical experiments were conducted using different Cu-Bi samples to confirm the observed phenomenon, and as shown in Fig. 2 (a), all three samples showed the anomalous expansion behavior. Interestingly, as shown in Fig. 2 (b), when the experiment at 3 MPa is conducted for very long periods,

the sample starts to creep normally once again after a certain period of time. This phenomenon occurs due to the effect of liquefaction of Bi at such high temperature.

(a) (b)

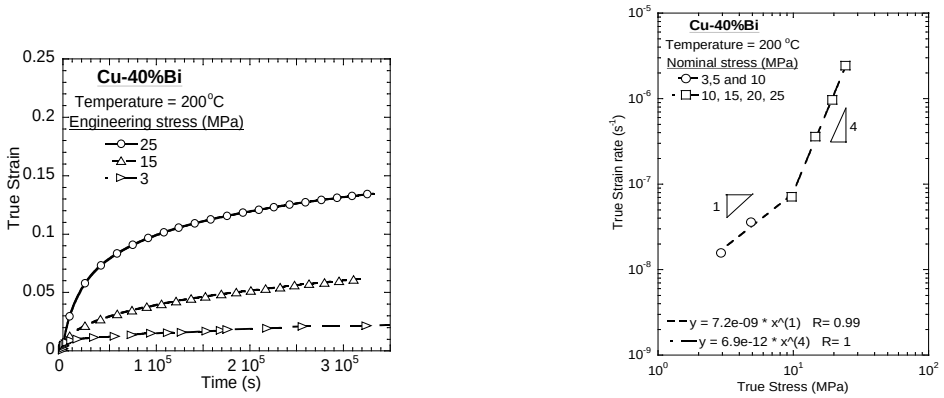

Fig. 2. (a) True strain versus time plot for creep at 200 °C, and (b) corresponding true stress versus true strain plot showing stress exponent values.

(a) (b)

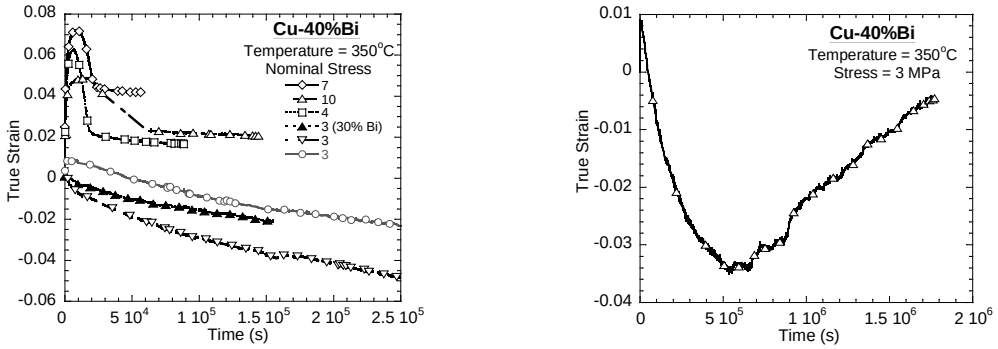

Fig. 2. (a) True strain versus time plot for Cu-Bi alloy tested at 350 °C, and (b) expanded time scale of a sample tested at 3 MPa.

Conclusion. Cu-Bi alloy is processed using LPS route. The alloy shows an anomalous creep behavior above $T_{m,Bi}$. This can be related to the effect of liquefaction of Bi on the overall creep response of the material; however, the phenomenon is not completely understood at present. It is established that this alloy can sustain moderate level of stresses under compression above the melting temperature of the LMP and hence can be used for energy storage and thermal surge protection.

References:

1. S.P. Singh, B.K.D. Barman and P. Kumar, Cu-Bi alloys with high volume fraction of Bi: A material potentially suitable for thermal surge protection and energy storage, *Materials Science and Engineering: A* **677**, pp. 140-152 (2016).

2. B.K.D. Barman, S.P. Singh and P. Kumar, Processing and mechanical behavior of Cu-Bi alloys with high volume fraction of Bi: Suitability for high temperature soldering application, *Materials Science and Engineering: A* **666**, pp. 339-349 (2016).

Effect of the Holding Stress in Stress-Holding Type Creep-Fatigue of Cu-Cr-Zr Alloy

K. Yamamoto[1], M. Deguchi[1], H. Tobe[2], E. Sato[2]

[1]. The University of Tokyo, Japan

[2]. Institute of Space and Astronautical Science, Japan Aerospace Exploration Agency, Japan

Email. sato@isas.jaxa.jp

Introduction. Japan Aerospace Exploration Agency (JAXA) is developing a new liquid rocket engine. It has been reported that the inner cylinder made of a Cu-Cr-Zr alloy suffers a stress-holding type creep-fatigue loading during engine operation [1]. The temperature and stress the alloy suffers in operation depend on design of the engine [2], and we need comprehensive understanding of stress-holding type creep-fatigue behavior to develop a higher performance liquid rocket engine. In this study, we carried out creep-fatigue tests with different holding stress, and discussed the effect of holding stress.

Experimental. A Cu-0.7Cr-0.09Zr alloy was used in this study, and creep-fatigue tests were carried out at a constant temperature of 750 K under vacuum (< 20 Pa). During one cycle of creep-fatigue test, the specimen was compressed by -1.5% at first, then was loaded with a constant stress for 410 s, and finally was extended by +0.5%. When the strain reached -10%, the test was interrupted.

Results and Discussion. Figure 1 shows the dependence of interrupted cycle on the holding stress. When the holding stress of -35 MPa was applied, negligible creep strain accumulated, and the test interrupted at 142nd cycle. In case of the holding stress of -50 MPa and -65 MPa, the interrupted cycle number was 60 and 41, respectively. At the first cycle of the test in which the constant load is -85 MPa, creep strain accumulates so much that the test stopped. This results can be explained by the results of tensile tests (Figure 2). If the holding stress is higher than tensile strength, creep strain accumulates rapidly and the test gets interrupted in the first cycle. If the holding stress between tensile strength and 0.2% proof stress is applied, creep strain accumulates. When the holding stress is below 0.2% proof stress, creep strain does not appear and thus the specimen shows much longer rupture life.

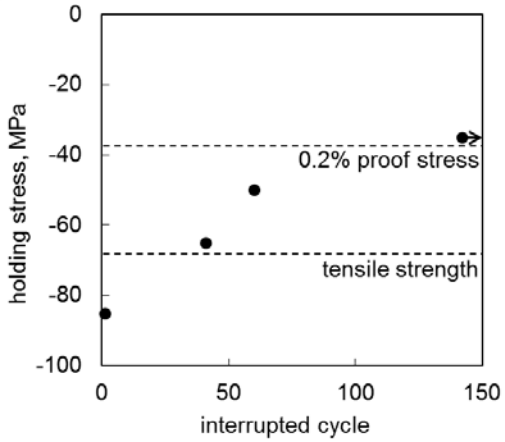

Figure 1. Holding stress vs. interrupted cycle.

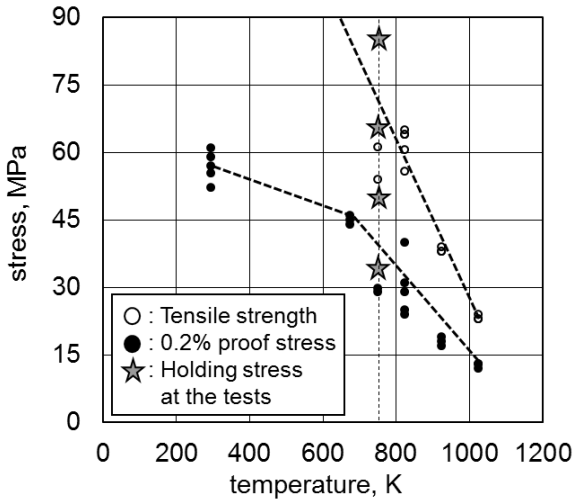

Figure 2. Tensile strength and 0.2% proof stress vs. temperature.

Conclusion. Various holding stresses were applied in stress holding type creep-fatigue test of Cu-Cr-Zr. When the holding stress is high enough, creep strain accumulates so rapidly that the test stops in first cycle. Creep strain accumulates under intermediate holding stress, and does not under too low holding stress. This results are in good agreement with the results of tensile tests.

References

1. M. Nishimoto, N. Yamanishi, S. Yoshimura, N. Kasahara and H. Akiba, *Trans. Jpn. Soc. Mech. Eng.*,**78A**, pp. 1534-1546 (2012)

2. M. Deguchi, H. Tobe, E. Sato, *International Journal of Fatigue*, **87**, pp. 351-358 (2016)

Microstructural Evolution during Creep of Al-Alloy 2618A

C. Rockenhäuser, S. Schriever, B. Skrotzki

Federal Institute for Materials Research and Testing (BAM), Berlin, Germany

birgit.skrotzki@bam.de

The aluminum alloy 2618A is an Al-Cu-Mg alloy with additions of Fe and Ni, which was designed for long-term operation at elevated temperature in transportation and aerospace industries. Typical applications include aircraft parts and structures (sheet material) or engine components such as turbo charger centrifugal compressor wheels (forged material). Such components are subjected to prolonged aging during service, (e.g. 50 000 h) at temperatures which are close to their age hardening temperature (ca. 190 °C).

The alloy 2618A has a nominal composition of Al-2.25Cu-1.5Mg-1.1Ni-1.15Fe (wt. %). Copper and magnesium contribute to strengthening through age hardening by forming nm-size rod shaped S' (or S) phase precipitates (Al_2CuMg). The rods form in three orthogonal orientations in the Al-matrix, as shown in Figure 1. Nickel and iron form the intermetallic compound Al_9FeNi, which is of µm-size (not shown in Figure 1) and causes dispersion hardening. It stabilizes the microstructure and improves the creep properties during long-term exposure at temperatures of 120 – 150 °C.

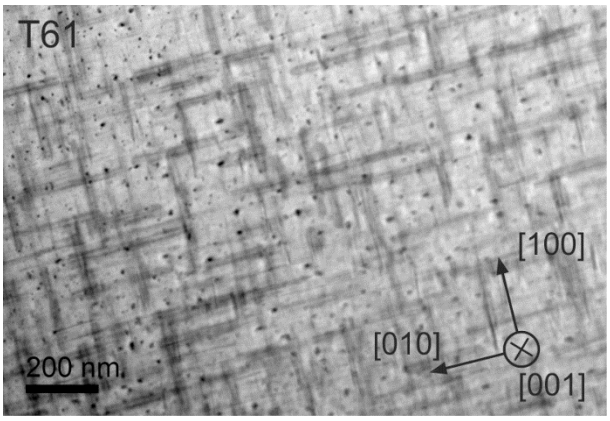

Figure 1: STEM-image of rod shaped S'/S (Al_2CuMg) precipitates in $<001>_{Al}$ orientation in the T61 condition: two orientations are lying in the image plane, one perpendicular.

The dispersoids do not change during the long-term exposure (at typical application temperatures) due to the low solubility of Ni and Fe in the Al-matrix. However, the S'/S-precipitates may change considerable in size, number density and volume fraction depending on service temperature and time, which may result in considerable degradation of mechanical properties. Therefore, we investigated the evolution of the hardening phase during creep at 190 °C and different loads and compared the size evolution to stress free isothermal aging at the same temperature.

Figure 2 shows the creep curves as creep strain vs. time for four different applied tensile stresses. Tests at the higher loads (230 MPa and 181 MPa) were terminated by fracture and are marked by "x". The two tests at lower loads (128 MPa and 79 MPa) were interrupted after 1,820 h and 4,172 h, respectively.

Samples for microstructural investigations were taken from the creep specimens perpendicular to the loading direction. Material states aged without stress to similar aging times were investigated for comparison. All samples were conventionally prepared for transmission electron microscopy (mechanical cutting of discs, grinding, electro-polishing). A JEM-2200FS TEM/STEM transmission electron microscope with a

field-emission gun was used and operated at 200 kV. At least 15 images were taken at different places of each sample and at least 300 precipitates were evaluated for each condition.

Dark-field transmission electron microscopy was used to selectively image the nm-sized precipitates along the <001>$_\alpha$ direction of the Al matrix. The resulting images were evaluated and allow the determination of radii distributions and the mean radius of the precipitates depending on aging time. Figure 3 summarizes the results and shows the average precipitate radius as a function of aging and creep time, respectively. The T61 state represents the initial state after peak aging treatment. The blue curve represents the results for stress free aging and clearly shows an increase of the particle radius with aging time by more than a factor of 3. Aging under applied load (orange curve) results in a ca. 15 % higher increase in radius as compart to conventional aging.

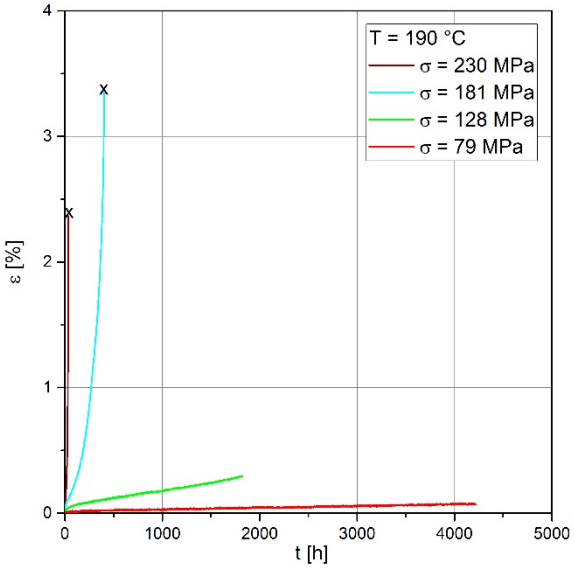

Figure 2: Creep curves at 190 °C and different applied stresses.

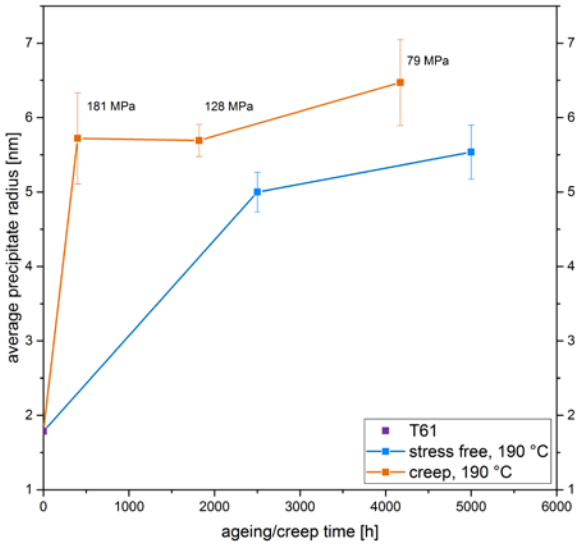

Figure 3: Average precipitate radius vs. ageing/creep time; blue: without stress; orange: with creep load.

This implies that the external load results in an accelerated coarsening of the hardening phase as compared to stress free aging and therefore in a faster degradation of mechanical properties, which should be taken into account for lifetime modeling of alloy 2618A.

Acknowledgements

The authors express their thanks to the Research Association for Combustion Engines (FVV, Frankfurt) for the selection of this research project as well as to the German Federal Ministry of Economic Affairs and Energy (BMWi) and the German Federation of Industrial Research Associations (AiF) for funding (IGF-No. 17734).

Creep behaviour of an Al-Si-Mg alloy with Er and Zr additions

E. Gariboldi[1], M. Colombo[1]

[1]. Politecnico di Milano, Dipartimento di meccanica (Italy)

Email. Elisabetta.gariboldi@polimi.it

Abstract

In recent years many efforts have been devoted to the development of innovative Al-based casting alloys with improved high temperature strength. Researches are often oriented to the investigation of the effects of minor element additions to widely diffused casting alloys. The alloy on which focuses the experimental study was selected within a range of alloys obtained by adding minor amounts of Er and Zr to the age-hardenable Al-7Si-0.4Mg alloy (A356 grade): In the heat treated condition the alloy displayed a good combination of microstructural features and short-time strength. The creep behaviour of the innovative alloy has been compared to that of conventional A356 alloy produced with the same casting route. Constant load creep tests were mainly carried out at 200 °C with rupture times ranging from a few to about 1000h. Some short tests were carried out at 300°C since this latter has recently become the reference temperature for comparisons among these innovative alloys. The quite promising test results have been discussed taking into account the microstructural features and microstructural stability of the investigated alloy.

Creep Behaviour of the Simulated P91 HAZ Regions at 600°C

M. Sondel[1,2], D. Schwarz[1,2], J. Koukal[1,2], V. Vodarek[1], Z. Kubon[3]

[1]. VSB - Technical University of Ostrava, Czech Republic

[2]. Czech Welding Institute Ltd., Ostrava, Czech Republic

[3]. MATERIALOVY A METALURGICKY VYZKUM s.r.o., Ostrava, Czech Republic

Email. martin.sondel@csuostrava.eu

Abstract

The aim of the paper is to describe the creep behaviour of the P91 steel heat affected zone (HAZ) regions at 600°C and explain why the creep rupture on welded joints at high temperatures is often observed in the HAZ, especially in the so called intercritical region (IC-HAZ). In modified (9-12)%Cr steels the creep rupture strength (CRS) of cross-weld specimens made of homogeneous welds is usually about 20 to 30% lower than that of the base material, depending on temperature and applied stress.

The different microstructures appearing in the HAZ of welded joints exhibit different properties, depending on the thermal parameters in the HAZ during welding. Considering the thermal cycle it is possible to identify several significant regions inside of the HAZ. The information about the thermal cycles of each of these regions of P91 welded joints were obtained by measuring on the real weld joint carried out by MMAW (Manual Metal Arc Welding).

The small size of each significant HAZ region in real welds does not allow any test on specimens extracted from the HAZ. The proposal is to reproduce the measured thermal cycles on larger specimens in order to allow mechanical and metallographic characterization of the basic HAZ regions. Suitable simulation technique makes it possible to simulate the properties of different regions in the HAZ. However, the effects of residual stresses in the real weldments are not reproducible when using this technique. The thermal cycles were reproduced in the specimens' central zone (± 10 mm from the centre of 11 x 11 x 70 mm specimens). All specimens were annealed at 750°C for 1h after simulation. The following temperature characteristics of single-pass and double-pass weld joints were simulated on specimens which were machined from the 60 mm thick P91 steel plate:

1. 1350°C/ 750°C/ 1h – corresponds to coarse-grained region + PWHT
2. 1050°C/ 750°C/ 1h – corresponds to fine-grained region + PWHT
3. 890°C/ 750°C/ 1h – corresponds to intercritical region + PWHT
4. 1350°C/ 1050°C/ 750°C/ 1h - coarse-grained + fine-grained + PWHT
5. 1350°C/ 890°C/ 750°C/ 1h - coarse-grained + intercritical + PWHT
6. 1050°C/ 890°C/ 750°C/ 1h – fine-grained + intercritical + PWHT

Real creep tests were carried out on specimens with HAZ simulated regions and on the P91 base material. All creep tests were carried out under constant load condition at 600 °C. The range of axial stresses was 80 - 240 MPa. The longest creep rupture tests of the HAZ simulated regions reached about 45 000 h. The creep rupture strengths of the simulated HAZ regions and of the P91 base material are shown in Fig. 1. The results prove that the creep resistance of the coarse-grained HAZ region is higher than that of either the fine-grained region or the intercritical region of the HAZ. The positive effect of the thermal cycle at 1350 °C on heat resistance of the HAZ was preserved

after application of the subsequent thermal cycle at 1050 or 890°C (double – pass). The creep resistance of both the fine-grained region and the intercritical region of the HAZ, as well as the FG + IC HAZ regions (double – pass), are approximately on the same level and are located at the lower bound of ± 20% scatterband of the P91 base material.

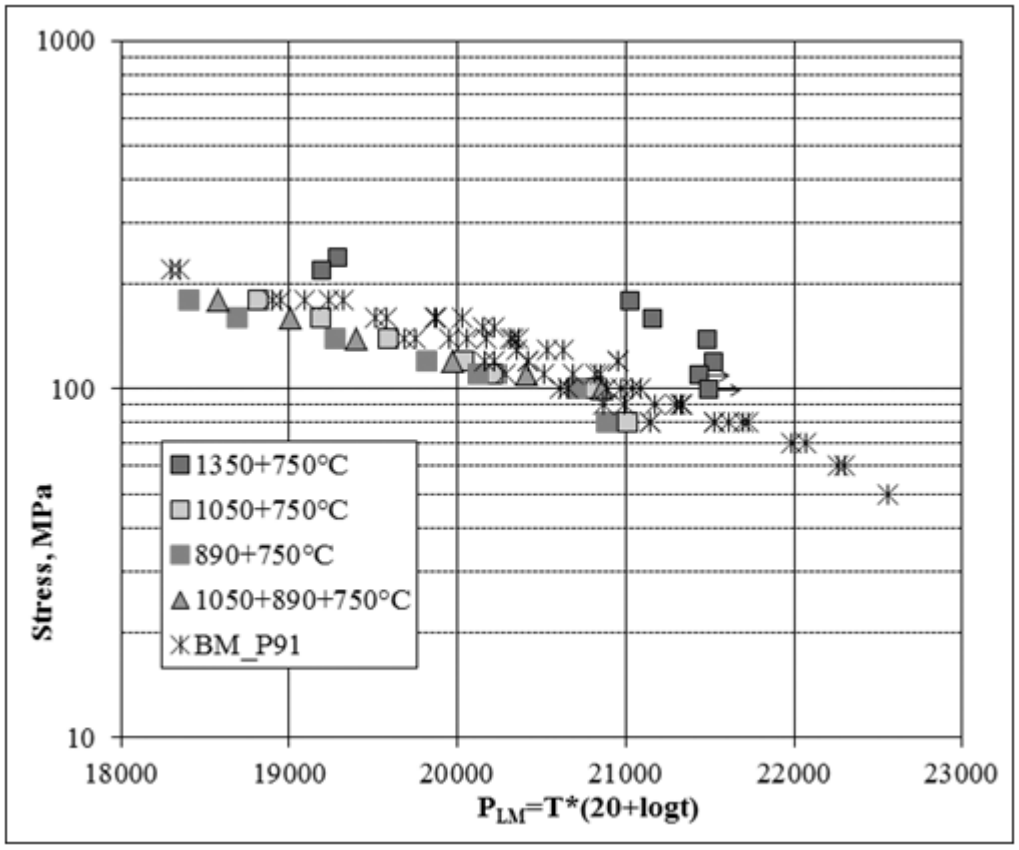

Figure 1. Results of Creep Rupture Tests of P91 Base Material and Simulated HAZ Regions

Microstructure of all simulated HAZ specimens was formed by tempered martensite. The prior austenite grain size in simulated HAZ regions was determined as follows: coarse-grained HAZ – G = 6, fine-grained HAZ – G = 8, intercritical part of HAZ – G = 9. Depending on temperatures in the simulated HAZ regions dissolution of minor phase particles occurred. Heating at 1350 °C resulted in dissolution of almost all precipitates, partial dissolution of minor phase particles took place at temperatures of 1050 and 890 °C. Subsequent PWHT at 750 °C resulted in re-precipitation of minor phases in simulated HAZ regions and precipitation processes continued during creep exposure at 600 °C. Identification of minor phases in simulated HAZ regions was carried out on crept specimens with time to rupture ca 10 000 hours. In each HAZ region the following minor phases were present: $M_{23}C_6$, M_2X, MX and Laves phase (Fe_2Mo). Creep exposure was accompanied by a gradual decrease of hardness in all simulated HAZ regions.

Creep Life Extrapolation of Alloy 617 Using a New Master Curve

W. G. Kim[1], J. Y. Park[1], S. J. Kim[2], E. S. Kim[2], M. H. Kim[1]

[1]. Korea Atomic Energy Research Institute, 989-111 Daedeok-daero, Yuseong-gu, Daejeon 34057, Republic of Korea

[2]. Pukyong National University, 365 Sinseon-ro, Nam-gu, Busan 48547, Republic of Korea

Email: wgkim@kaeri.re.kr

A very high temperature reactor (VHTR) is one of the most promising Gen-IV reactor types for the economic production of electricity and hydrogen. Alloy 617 is a leading candidate alloy for the intermediate heat exchanger (IHX) components [1]. Since the IHX component is directly exposed to a primary coolant of 950^{o}C, it is suffered from creep damage, and its creep life (or strength) will be gradually degraded under the high temperatures and long duration. Therefore, an accurate extrapolation of long-term creep life is very important in determining allowable design stress.

Many attempts have been made to formulate dependency of creep life to operating temperature and stress. A promising approach has been the use of time-temperature parameters (TTP). All of the various developed TTPs consist of a combination of time, temperature and suitable constants. With such parameters and for a given material, a single master curve of stress against the parameter can be obtained and this is of a great value for extrapolating test results. To accurately achieve the long-term life extrapolation, a “master rupture curve” (hereafter referred to as “master curve”) describing the relationships between log (stress) and parameter (*P*) should be suitably determined. So far, a master curve of polynomial form in the TTP methods such as the Larson-Miller (LM), Orr-Sherby-Dorn (OSD), and Manson-Harferd (MH) parameters, has been conventionally used well. However, the master curve of a polynomial form has the convex or concave curves in the extrapolation of the low stress ranges beyond experimental creep durations. Its master curve is overestimated or underestimated owing to intrinsic characteristics of the polynomials in the low stress region beyond experimental. To overcome this problem, in the master curve, a “sinh” (Hyperbolic Sine) form instead of polynomial form is newly proposed herein, as follows.

$$P(t_r, T) \Rightarrow f(\sigma) \tag{1}$$

$$P = b_0 + b_1 \log(\sigma) + b_2 \log(\sigma)^2 + b_3 \log(\sigma)^3 + ...b_n \log(\sigma)^n \tag{2}$$

$$P = b_0 - b_1 \sinh(b_2 \log\sigma) + b_3(\log\sigma) \tag{3}$$

In the time-temperature parameter, P is expressed as a function of stress as Eq. (1), and it is given as the polynomial form of Eq. (2). The “sinh” function of Eq. (3) was used instead of Eq. (2). The curves defined as sinh (x) = (e^{x}-e^{-x}) /2 can be plotted, as shown in Fig. 1(a). A slashed region can be used for creep life prediction. Namely, since sinh(x) function has always an inflection point at x (stress)=0, its master curve can extrapolate stably for up to very low stress level of x=0. The “sinh” master curve using LMP fitted for creep rupture data (n=260 data points) of Alloy 617 is stably extended without convex or concave in the low stress level, as shown in Fig. 1 (B). Thus, Eq. (3) is reasonable as a master curve in the extrapolation of the low stress ranges beyond the experimental test durations for Alloy 617. The predicted plot of log σ vs. log t_r is presented up to 10^6 h for Alloy 617 from 800 ^{o}C to 1000^{o}C, as shown in Fig. 2. This predicted curve showed a good agreement with the experimental data of each

temperature. In addition, it was verified that a new master curve using “sinh” function was comparable to Wilshire’s approach [2] known a good method in creep life prediction.

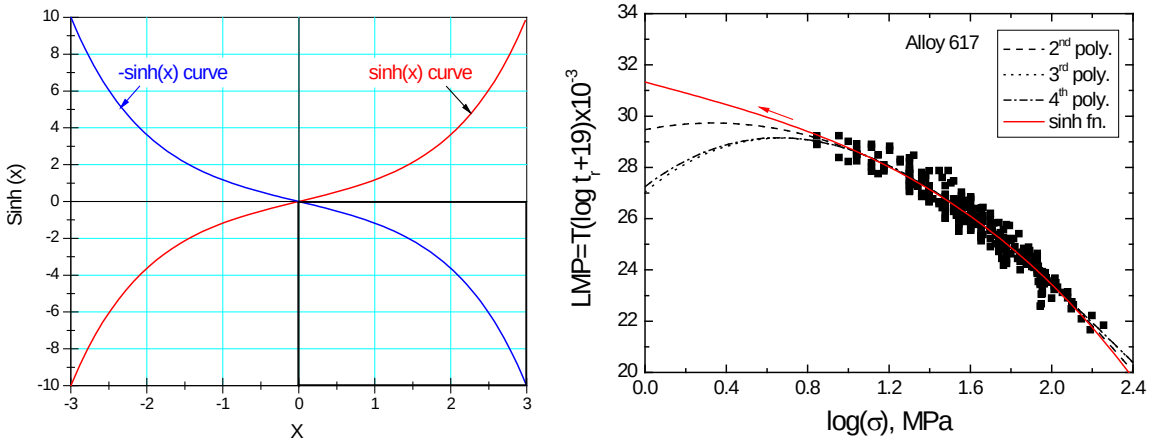

(a) Curves of sinh (x) function (b) Master curve fitted by “sinh” function

Figure 1. Definition of “sinh” function and a master curve fitted by “sinh” function for creep rupture data of Alloy 617.

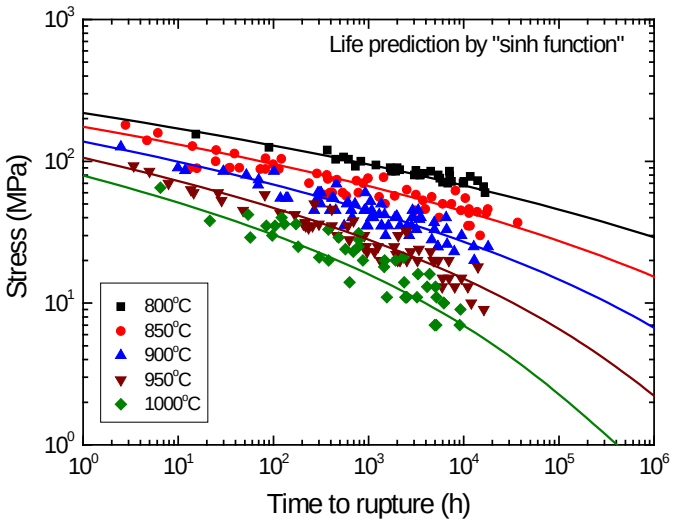

Figure 2. Extrapolated curves for “sinh” in LMP at each temperature for Alloy 617.

References

1. W. G. Kim *et al*., *Engineering Failure Analysis* **58**, pp. 441-451, (2015).

2. B. Wilshire *et al*., *International Materials Reviews* **53**, pp. 91-104, (2008).

Creep behavior of an Al-Cu-Mg-Ag alloy subjected to T6 treatment

Marat Gazizov[1], Rustam Kaibyshev[1]

[1]. Laboratory of Mechanical Properties of Nanostructured Materials and Superalloys, Belgorod State University, Pobeda 85, Belgorod, 308015, Russia

Email. gazizov@bsu.edu.ru

Al-Cu-Mg-Ag alloys exhibit superior creep strength that make it possible to use them as a material for aviation structures operating at elevated temperatures [1,2]. The addition of silver to Al-Cu-Mg alloys promotes the formation of the Ω-phase [1-3]. This precipitate forms as a uniform dispersion of thin, hexagonal plates with large aspect ratios (diameter/thickness) on $\{111\}_\alpha$ habit planes and has a coherent structure of broad faces. Several structures for the Ω-phase have been proposed, although the most widely accepted structure is orthorhombic (*Fmmm*, a = 0.496 nm, b = 0.859 nm, c = 0.848 nm), which has very small differences in its atomic coordinates compared with the equilibrium θ-phase (Al_2Cu, body-centered tetragonal lattice, *I4/mcm*, a=b=0.6066 nm, c=0.495 nm) in Al-Cu alloys [1-3]. It was established that the Ag and Mg atoms segregate on the board interfaces of the Ω-phase plate and provide a coherence structure of current boundaries [3]. The edges of the Ω plates can lose coherency through thickening of the plates during ageing.

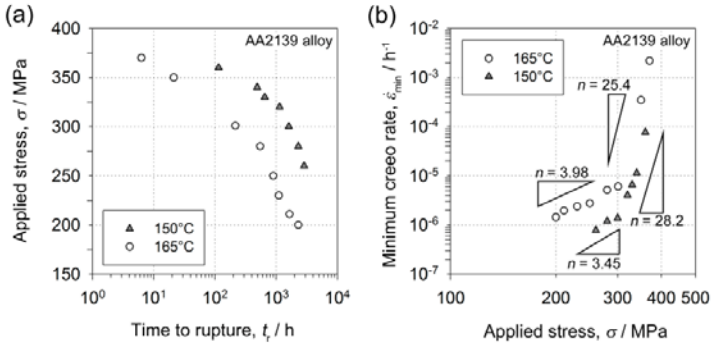

Fig. 1 Creep rupture data (a) and stress dependence of minimum creep rate (b) at 150 and 165°C for AA2139-T6 alloy

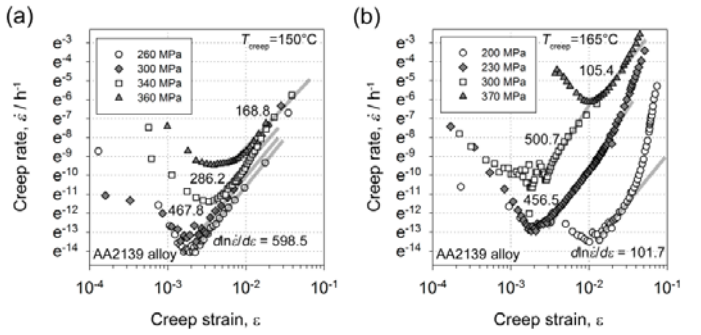

Fig. 2 Creep rate *vs*. strain curves and evaluation of $d\ln\dot{\varepsilon}/d\varepsilon$ for AA2139-T6 alloy at 150°C (a) and 165°C (b)

Despite the importance of improved creep strength, most of the published work on this alloy has concentrated on characterization of the Ω-phase and its evolution at elevated temperatures. Only limited experimental results have been published in the open literature about the alloy's creep behavior [4,5]. The purpose of the present research is to investigate the effect of applied stress on creep resistance of a AA2139 alloy by analyzing creep strength and creep strain curves.

The AA2139 alloy with the chemical composition of Al-4.5Cu-0.56Mg-0.77Ag-0.42Mn-0.12Ti-0.05V-0.02Fe (in wt. %) was prepared using a direct-chill, semi-continuous casting process with a high cooling rate. The ingots were homogenized at 510°C for 24 h, extruded at ~400°C and then hot-rolled along the main ingot axis into plates with a thickness of ~20 mm. The 20-mm plates were machined, after that solution treated for 1 h at 510°C, water quenched and finally peak-aged for 2 h at 190°C (T6 treatment). Computer-controlled ATS Lever Arm Testers, model #2330, with WinCCS II software equipped three zone furnace were used for the creep testing at temperatures of 150 and 165°C with applied stress range (σ) from 200 MPa to 370 MPa, and times to rupture, (t_r) from 6.3 to 2862 hours.

Analysis of experimental data shows that the creep strength takes place at applied stresses of ~280 and ~320 MPa or times to rupture of ~550 and ~1150 h at creep temperatures of 150 and 165°C, respectively (Fig. 1a). The stress dependences of minimum creep rate $\dot{\varepsilon}_{min}$ for the alloy are shown in Fig. 1b. The $\dot{\varepsilon}_{min}$ is described by a power law:

$$\dot{\varepsilon}_{min}=A\times\sigma^n, \quad (1)$$

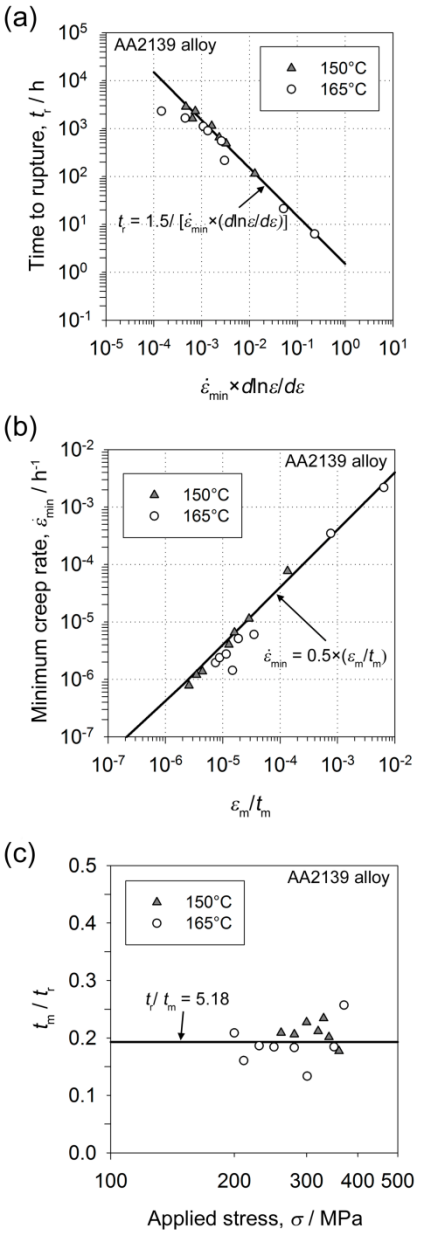

Fig. 3 Relationship between time to rupture and minimum creep rate $\dot{\varepsilon}_{min}$ times acceleration of creep rate $d\ln\dot{\varepsilon}/d\varepsilon$ in acceleration creep region (a), stress dependence of strain to minimum creep rate (b) and $g=t_m/t_r$ (c) for AA2139-T6 alloy

where A is a constant and n is the stress exponent [6,7]. The stress exponent n is evaluated to be about 3.4/3.5 and 25/28 at high and low stresses at temperatures of 150 and 165°C, respectively. The, the creep strength breakdown is steady state phenomenon in Al-Cu-Mg-cu alloys. The higher $\dot{\varepsilon}_{min}$ results in shorter time to rupture and lower creep rupture strength of the AA2139 alloy (Fig. 1b). Abe's approach to characterization of creep strength prediction of steels at long times [6,7] was applied to describe correlations between other creep deformation parameters for the AA2139-T6 alloy. It was shown that the t_r reasonably correlates with the $\dot{\varepsilon}_{min}$ that confirms the aforementioned conclusion. The acceleration of creep rate by strain in the acceleration region $d\ln\dot{\varepsilon}/d\varepsilon$ at 150 and 165°C (Figs. 2a and b, respectively), as [6,7]:

$$t_r=B/[\dot{\varepsilon}_{min}\times(d\ln\dot{\varepsilon}/d\varepsilon)], \quad (2)$$

where B is a constant equal 1.5 (Fig. 3a), and $\dot{\varepsilon}_{min}$ and $d\ln\dot{\varepsilon}/d\varepsilon$ reflect the creep behavior in the transient and acceleration regions, respectively [6,7]. The $\dot{\varepsilon}_{min}$ is inversely proportional to the time to minimum creep rate t_m, while it is proportional to the strain to minimum creep rate ε_m (Fig. 3b)., as [6,7]:

$$\dot{\varepsilon}_{min}=C\times(\varepsilon_m/t_m) \quad (3)$$

where C is a constant equal 0.5. The duration of acceleration region is proportional to the duration of transient region, while the $d\ln\dot{\varepsilon}/d\varepsilon$ is inversely proportional to the ε_m [6,7]. The t_r is also correlated with the t_m, as [6,7]:

$$t_r=g\times t_m, \quad (4)$$

where g is a constant equal to ~5.18 for the AA2139 alloy (Fig. 3c). The present creep life equations allow reasonably predicting the degradation in creep rupture strength of the AA2139-T6 alloy.

The work was supported by joint project between USATU (Ufa State Aviation Technical University) and UMPO (Ufa Engine Industrial Association), which is entitled "Elaboration and industrial development of high-precision shaping coordinated technologies and superficial hardening of responsible details from Al-alloys with heightened constructional energy efficiency". This project was implemented under contract №40/10-30976/NCh-NCh-01-13-KhG and was sponsored by the Ministry of Education and Science of the Russian Federation (contract №02.G25.31.0010 between UMPO and the Ministry of Education and Science of the Russian Federation).

References

1. I.J. Polmear *et al.*, «After Concorde: evaluation of creep resistant Al-Cu-Mg-Ag alloys», *Materials Science and Technology* **15**, pp. 861-868 (1999).
2. S.C. Wang and M.J. Starink, «Precipitates and intermetallic phases in precipitation hardening Al-Cu-Mg-(Li) based alloys», *International Materials Reviews* **50 (4)**, pp. 193-215 (2005).
3. C.R. Hutchinson *et al.*, «On the origin of the high coarsening resistance of Ω plates in Al-Cu-Mg-Ag alloys», *Acta Materialia* **49**, pp. 2827-2841 (2001).
4. D. Bakavos *et al.*, «The effect of silver on microstructural evolution in two 2xxx series Al-alloys with a high Cu:Mg ratio during ageing to a T8 temper», *Material Science Engineering* **A491**, pp. 214-223 (2008).
5. J. Wang *et al.*, «Creep behaviour at elevated temperatures of an Al-Cu-Mg-Ag alloy», *Material Science Engineering* **A234-236**, pp. 287-290 (1997).
6. F. Abe, «Creep behavior, deformation mechanisms, and creep life of mod.9Cr-1Mo steel», *Metallurgical and Materials Transactions* **46(12)**, pp. 5610-5625 (2015).
7. F. Abe, «Effect of quenching, tempering, and cold rolling on creep deformation behavior of a tempered martensitic 9Cr-1W steel», *Metallurgical and Materials Transactions* **34A**, pp. 913-925 (2003).

High Temperature Titanium Sheets of Ti6242 and VT18U

M.S. Kalienko, A.V. Volkov, A.V. Zhelnina

PSC VSMPO-AVISMA CORPORATION, V. Salda, Sverdlovskaya Oblast, Russia

Email: kamak@yandex.ru

One of the principal trends in engine building is continuous improvement of propulsive efficiency, generally by means of increasing fan diameter and by-pass ratio and also reduction of gas generator and increase of thermal efficiency. The last, in its turn, leads to rising of working temperature and forming new requirements for materials used in engine and aircraft construction. Titanium alloy sheet semi-finished products are widely used in aircraft industry in virtue of inimitable combination of its properties. One of the most famous titanium alloys for usage at elevated temperatures is Ti6242 used for production of a wide product range, but this alloy has certain operational limits. This Report represents a comparative evaluation of mechanical properties of sheets made of Ti6242 alloy and Russian alloy VT18U: mechanical properties of sheets at room temperature; mechanical properties at elevated temperatures within 550÷685°C; creep; evaluation results of surface gas saturation of titanium alloys after long-term exposures at elevated temperatures. Isothermal oxidation experiments were performed in the temperature 625°C for 1000h., and then the samples were investigated by different methods.

Based on the results of properties comparative assessment of titanium alloy sheets, Russian alloy VT18U could successfully replace Ti6242 alloy and expand operational limits of products usage.

Contributions of Different Hardening Mechanisms on Creep Strength of Single Crystal Ni alloys - Pure Ni to Ni Solid Solution to Ni-Based Superalloys -

Uwe Glatzel, Ernst Fleischmann, Christian Konrad, Fabian Krieg, Rainer Völkl

Metals and Alloys, University Bayreuth, 95447 Bayreuth, Germany

E-mail: uwe.glatzel@uni-bayreuth.de

Five different alloys were cast in single crystalline (SX) state using a Bridgman vacuum induction furnace. After heat treatment of the single crystal samples creep testing at 980°C was conducted. The behavior of polycrystalline pure Ni, take from [1] was compared to our SX data [2,3]. The single crystal samples vary from pure Ni to Ni solid solution (single-phase) to Ni-base superalloys (two-phase, precipitate hardened alloys).

The SX Ni solid solution samples can again be divided in a Re free solid solution and in a 9 wt.% Re containing solid solution. Care has been taken to use compositions, which are in single-phase state at creep testing temperature.

The SX Ni-base superalloys are CMSX-3 (no Re content) and CMSX-4 (3 wt.% Re). The composition of the matrix phase of the superalloys corresponds to the above mentioned solid solution alloys.

With the creep experiments at 980°C on single crystals and in comparison with the literature poly crystalline data, several strengthening contributions to creep can be quantitatively determined. There is an increase in creep strength in increasing order by:

1. prevention of grain boundary sliding
2. solid solution strengthening without Re
3. solid solution strengthening with Re
4. precipitate hardening without Re
5. precipitate hardening with Re

These strengthening mechanisms can be qualitatively explained by simple models:

2. and 3. by solid solution strengthening models, dependent on atomic size misfits and changes in elastic constants.

4. by Orowan, coherency and back stress theories due to precipitates.

5. as combination of 2, 3 and 4, with an additionally strengthened matrix phase.

References

[1] H.J. Frost, M.F. Ashby, *Deformation-Mechanism Maps*, Pergamon Press (1982).

[2] E. Fleischmann, C.H. Konrad, J. Preußner, R. Völkl, Ernst Affeldt, U. Glatzel: Met. Mat. Trans. A, 46A (2015) 1125-1130.

[4] E. Fleischmann, M.K. Miller, E. Affeldt, U. Glatzel: Acta Mat., 87 (2015) 350-356.

Thermodynamic properties in NiAl system by a first-principles renormalized potential

Ryoji Sahara[1], Toshio Osada[1], Swastibrata Bhattacharyya[2], and Kaoru Ohno[2]

[1] Research Center for Structural Materials, National Institute for Materials Science, Tsukuba, Ibaraki 305-0047, Japan

[2] Yokohama National University, Japan

Email: SAHARA.Ryoji@nims.go.jp

Ni-based superalloys with γ/γ' two-phase structures are widely used as structural materials for high-temperature applications such as turbine disk materials in advanced aircraft engines and land-based gas turbines. This is because they show excellent tensile strength and creep properties in high temperature regions (1).

In order to theoretically study thermodynamic equilibrium and metastable phases near the order-disorder phase transition temperature, a lattice Monte Carlo method (MC) provides one of the most powerful methods. While, one of the problem of the model is how to determine a reliable many-body interactions to be used. That is, even if it is decided by first principles calculations, the model neglect the vibrational entropy as well as the elastic energy, which result in overestimation of the phase transition temperatures and underestimation of the width of single phase fields compared with experimental data (2).

In the present study, the thermodynamic properties of the alloys are evaluated using a face-centered-cubic (fcc) lattice-gas model. In order to obtain quantitatively accurate results, the results of first principles calculations are mapped onto the fcc lattice using the renormalization technique, which can overcome some shortcomings of lattice-gas models such as neglecting vibrational entropy (3)-(7). The fundamental idea of the scheme is making the new (renormalized) potential function for discretized space without changing the value of the partition function for continuous space.

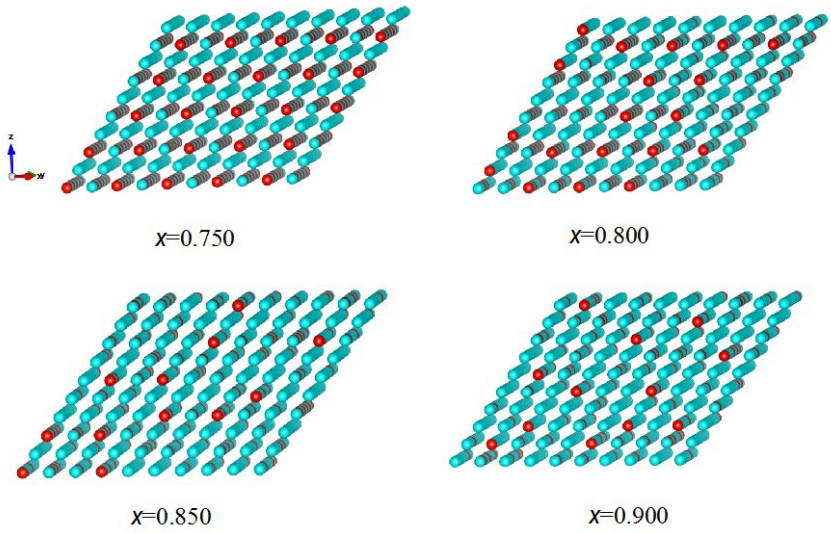

Figure 1. Typical atomic distributions obtained by MC simulations (0.75≦x≦0.90). 10×10×10 atoms of 20×20×20 primitive fcc cells are shown. Ni and Al atoms are expressed by dark and thin gray colored marks.

We show that the renormalized potential gives quantitative phase diagram by using the scheme. As an example, Fig. 1 shows snapshots of atomic distribution obtained by MC simulations using the renormalized potential in Ni_xAl_{1-x} system at 900K. It is shown that the phase transition between single phase and coexistence phase (γ/γ') occurs between x=0.80 and 0.85, which is comparable with experimental value, around x=0.83.

References:

(1) T. Osada, Y. Gu, N. Nagashima, Y. Yuan, T. Yokokawa, H. Harada, Acta Mater. 61 (2013) 1820.

(2) T. Horiuchi, S. Takizawa, T. Suzuki, and T. Mohri, Metall. Mater. Trans. A26 (1995) 11.

(3). K. Ohno, Sci. Rep. Res. Inst. Tohoku Univ. A 43, (1997) 17.

(4). K. Ohno, K. Esfarjani, and Y. Kawazoe, Introduction to Computational Materials Sciences: From Ab Initio to Monte Carlo Methods, Solid-State Sciences (Springer-Verlag, Berlin, 1999), pp. 188–197.

(5). R. Sahara, H. Mizuseki, S. Uda, K. Ohno, T. Fukuda, and Y. Kawazoe, J. Chem. Phys. 110, (1999) 9608.

(6). R. Sahara, H. Ichikawa, H. Mizuseki, K. Ohno, H. Kubo, and Y. Kawazoe, J. Chem. Phys. 120, (2004) 9297.

(7). Y. Misumi, S. Masatsuji, R. Sahara, S. Ishii, and K. Ohno, J. Chem. Phys. 128, (2008) 234702.

Some Critical Issues for the Development of High-Temperature Co-Based Superalloys with $L1_2$ Cuboidal Precipitates

Haruyuki Inui[1, 2], Norihiko L. Okamoto[1, 2]

[1]. Department of Materials Science and Engineering, Kyoto University, Sakyo-ku, Kyoto 606-8501, Japan

[2]. Center for Elements Strategy Initiative for Structure Materials (ESISM), Kyoto University, Kyoto 606-8501, Japan

Email. inui.haruyuki.3z@kyoto-u.ac.jp

The recent discovery of the stable $L1_2$-ordered intermetallic compound, $Co_3(Al,W)$ coexisting with the solid-solution based on fcc Co has opened up a pathway to the development of a new class of high-temperature structural material based on cobalt, 'Co-base superalloys'. We have experimentally investigated physical and mechanical properties of both $L1_2$ single-phase and fcc/$L1_2$ two-phase alloys with and without quaternary alloying. Those include tensile properties at room temperature, elastic constants, temperature dependence of yield stress and dislocation structures, and creep properties at 1000°C [1]. Dislocation dissociation has been examined fully by weak-beam microscopy in each of temperature domains of the yield stress-temperature curve. We have also investigated effects of quaternary alloying elements on the volume fraction, lattice constants and $L1_2$ solvus temperature of some Co-Al-W ternary base alloys [2]. The general trend of creep properties of single crystals of fcc/$L1_2$ two phase alloys made at 137 MPa and 1000°C is that the alloy with the higher $L1_2$ volume fraction and the higher $L1_2$ solvus temperature exhibits a better creep resistance [3]. The best creep properties obtained for the two-phase single-crystal alloy (with a high $L1_2$ volume fraction and high $L1_2$ solvus temperature through higher-order alloying) is only comparable to that of the Ni-base superalloy of the 1 st generation. We believe that the insufficient high-temperature mechanical properties of Co-based alloys with $L1_2$ cuboidal precipitates are due to the low strength of the constituent $L1_2$ compounds at high temperatures [4], which comes from the very low complex stacking fault (CSF) energy, as is evident from the four-fold dissociation of <110> dislocations. We will discuss some critical issues to be addressed as well as strategies for strengthening Co-based alloys with $L1_2$ cuboidal precipitates in the lights of our experimental findings.

References

1. N.L. Okamoto, T. Oohashi, H. Adachi, K. Kishida, H. Inui and P. Veyssiere, Philosophical Magazine **91**, pp. 3667-3684 (2011).

2. M. Ooshima, K. Tanaka and H. Inui, Journal of Alloys and Compounds **508**, pp. 71-78 (2010).

3. K. Tanaka, M. Ooshima, N. Tsuno, A. Sato and H. Inui, Philosophical Magazine 92, pp. 4011-4027 (2012).

4. Z-H. M.T. Chen, N.L. Okamoto, M. Demura and H. Inui, Scripta Materialia121, pp. 28-31 (2016).

On the Effect of Particle Coarsening on the Creep Activation Parameters n and Q

G. Eggeler[1], G. Kausträter[2], S. Mogharebi[1], F. Richter[1], O. Kastner[3]

[1]. Institute for Materials, Materials Science, Ruhr-University Bochum, Bochum, Germany

[2]. Aluminiumwerk Unna AG, Unna, Germany

[3]. Leibniz Universität Hannover, Hannover, Germany

E-Mail. Gunther.Eggeler@rub.de

Creep is a deformation mode which occurs at high temperatures and which shows a very strong stress and temperature dependence. These dependencies are often captured by a phenomenological law with a power law stress dependence (stress exponent: n) and an Arrhenius type of temperature dependence (apparent activation energy: Q). The present study considers whether particle coarsening has an effect on the activation parameters n and Q. For this purpose we extend a qualitative model which was put forward by Ilschner [e.g. 1,2]. He proposed a control circuit which explained the increase and decrease of creep rate. In Ilschner's control circuit, creep rates were governed by the effective stress, which is given by the difference between the applied stress and an internal back stress. The internal back stress changed when dislocation densities evolved. In the present work we consider the case where particles also contribute to the back stress term. We assume that particles can undergo Ostwald ripening, which effects a particle back stress term. Our model allows to switch particle coarsening on and off. It is shown that particle coarsening can indeed affect n- and Q-values. The results of the numerical model are presented, which show that higher apparent creep activation energies are observed with (as compared to without) particle coarsening.

Two cases are discussed where particle coarsening is an essential part of creep. One case is the coarsening of carbides in tempered martensite ferritic steels [3]. Another is the rafting of the γ'-phase in Ni-base superalloys [4]. It is shown that in both cases one can experimentally observe values for apparent creep activation energies which are much higher than those for self diffusion. These findings are interpreted in the light of Ilschner's extended control circuit of creep.

1. B.Ilschner, *Hochtemperatur-Plastizität*, Springer-Verlag, Berlin (1973)

2. B.Ilschner, «Plastic deformation and failure of crystalline materials at high temperature», *Comportamento meccanico e termico dei materiali metallici*, Societa italiani di fisica, Bologna, Italy, pp. 217-229 (1982)

3. G. Eggeler, B. Ilschner, P. Schepp und R. Zohner, «Kurzzeitkriechverhalten des warmfesten Stahls X20 CrMoV 12 1 bei 500 bis 60000», *Material und Technik*, **14** pp. 187-195 (1986)

4. P. Wollgramm, H. Buck, K. Neuking, A. B. Parsa, S. Schuwalow, J. Rogal, R. Drautz, G. Eggeler, «On the role of Re in the stress and temperature dependence of creep of Ni-base single crystal superalloys», *Mat. Sci. Eng. A*, **628** pp. 382-395 (2015)

Influence of Temperature on Stacking Fault Energy and Creep Mechanism of A Single Crystal Nickel-Based Superalloy

S. G. Tian, S. Liang, X. J. Zhu, D. L. Shu, B. S. Zhang

School of Materials Science and Engineering, Shenyang University of Technology, Shenyang, 110870, China

Email: Tiansugui2003@163.com

Single crystal nickel-based superalloys have an excellent mechanical and creep properties at high temperature, which has been widely applied in preparation of blade parts in advanced aero-engines [1]. But the alloys with different composition have various stacking fault energy (SFE), and the alloys with different SFE display the various mechanical and creep properties [2] due to the different moving pattern of dislocation during deformation [3]. In the paper, by means of creep properties measurement of a single crystal alloy at various temperatures, contrast analysis of dislocations configuration, based on thermo-dynamics method, SFEs of containing- Re alloy at different temperatures are calculated to investigate the influence of temperatures on the SFE and deformation mechanism of the alloy during creep.

The SFE (γ_{SF}) of alloy with FCC structure may be expressed as [4]:

$$\gamma_{\mathrm{SF}} = \frac{1}{8.4V^{2/3}}\Delta G_{\mathrm{b}}^{\gamma\to\varepsilon} + \Delta G_{\mathrm{s}}^{\gamma\to\varepsilon} \qquad (1)$$

The mixed surplus free-energy of the alloy is expressed as :

$$\Delta G_b^{\gamma\to\varepsilon} = \sum [T(x_i x_j a_{ij} - \Delta S_i) + \Delta H_i + x_i x_j c_{ij}] \qquad (2)$$

SFE of the alloy at 760 °C, 980 °C and 1070 °C are calculated, a

Table 1 SFE of the alloy at different temperatures

Temp., ℃	760	980	1070
Stacking Fault Energy, (mJ/m^2)	128.1	281.2	349.1

Results show that deformation mechanism of alloy during creep at 760 ºC is γ′ phase sheared by <110> super-dislocations which is decomposed to form the configuration of Shockley partials plus SISF. While the deformation mechanism of alloy during creep at 1070 ºC is the screw or edge super-dislocations shearing into rafted γ′ phase. During creep at 760 ºC and 980 ºC, some super-dislocations shearing into γ′ phase may cross-slip form {111} to {100} planes for forming the K-W locks to restrain their slipping, which may enhance the creep resistance of alloy at high temperature.

References

1. J.L. Liu, T. Jin, J.H. Zhang, et al., *Acta Metall. Sin.* 37, pp. 1233 (2001).

2. D.M. Knowles, Q.Z. Chen. *Mater. Sci. Eng.* A 340, pp. 88 (2003).

3. S. Gourdet, F. Montheillet. *Acta Mater*. 50, pp.2801 (2002).

4. T. Ericsson. *Acta Metall.* 14, pp. 853 (1966).

Creep parameter determination based upon element segregation in Ni-SX superalloys

C.Schwalbe[1], E.Galindo-Nava[1],N.Jones[2], C.M.F.Rae[1]

[1] Rolls-Royce University Technology Centre, Department of Materials Science and Metallurgy, University of Cambridge, Cambridge, UK

[2]Rolls-Royce plc, Derby, UK

Email cs798@cam.ac.uk

Ni-base SX-Superalloys are the state of art materials currently used for the turbine blades in the jet engine. Superalloys contain around ten alloying element, each adding beneficial properties to the compound [1]. The different chemical properties result in element segregation arising during the dendritic growth in the casting process. This segregation has been shown to persist in high refractory containing alloys after the standard solution heat treatment [2],[3]. This leads to slightly different element compositions that influence microstructure and creep parameters locally.

The chemical composition determines the most common creep parameters, such as the APB-Energy [4], Interfacial Energy [5], the Lattice Misfit {Caron:2001tw} and Solid Solution Hardening Resistance [6]. Each parameter is evaluated using established methodologies as referenced. Thus, these creep parameters will vary throughout the dendritic structure of an alloy as a function of the elemental segregation.

Using EPMA-Analysis the local element composition across the dendritic structure was assessed and quantified (see Figure 1a). Using the EPMA-maps of the elements with the highest segregation coefficient (Rhenium), the map compositions were then subdivided into a limited number of bins, balancing compositional complexity with computational efficiency. As a result, the dendritic regions of each alloy can be identified by their local mean composition (see Figure 1b), location (see Figure 1a) and frequency (see Figure 2).

As a result the magnitude of each creep parameter can be estimated for every region across the microstructure. This lays the foundation for a full-field creep model that can more accurately describe the natural scatter in creep life, which is thought mostly to be attributed to small element chemistry differences arising naturally in the, casting and heat treatment processes [7].

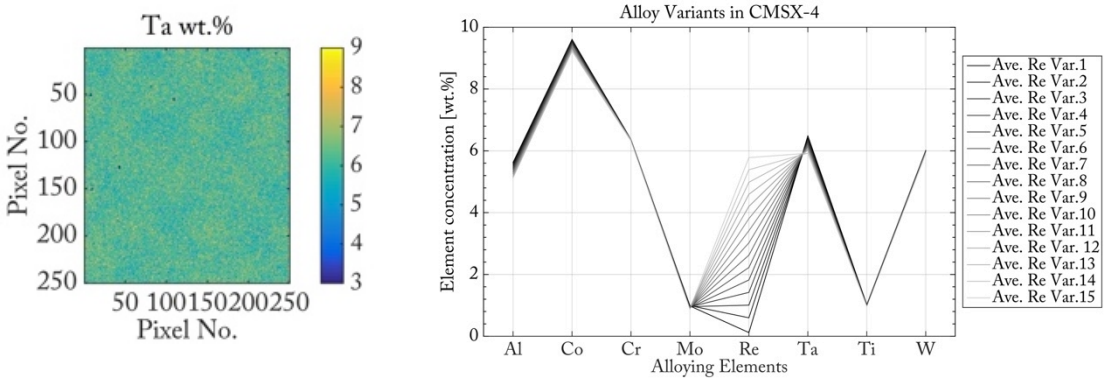

Figure .1a (left) – EPMA element concentration map across the analysed microstructure.
Figure 1b (right) – Element concentration across the different element variants

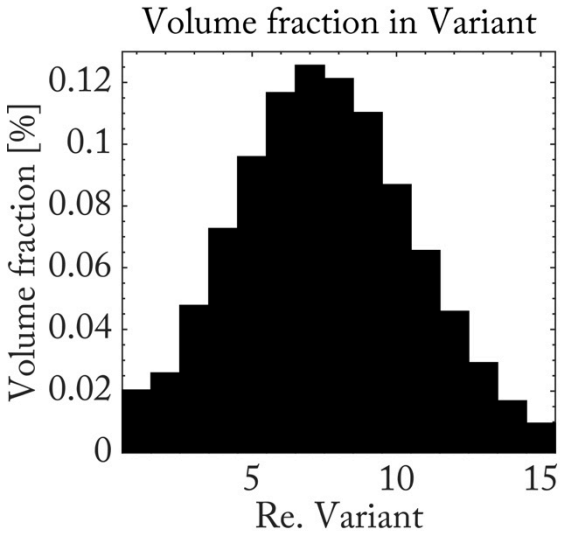

Figure 2 – Histogram of the volume fractional frequency of each variant in the microstructure

References

1. A. K. Jena and M. C. Chaturvedi, J Mater Sci **19**, 3121 (1984).
2. M. S. A. Karunaratne, C. M. F. Rae, and R. C. Reed, Metall and Mat Trans A **32**, 2409 (2001).
3. A. Szczotok and B. Chmiela, Jmep **23**, 2739 (2013).
4. D. J. Crudden, A. Mottura, N. Warnken, B. Raeisinia, and R. C. Reed, Acta Materialia **75**, 356 (2014).
5. B. Sonderegger and E. Kozeschnik, Metall and Mat Trans A **40**, 499 (2009).
6. R. Labusch, Physica Status Solidi (B) **41**, 659 (1970).
7. B. C. Wilson, E. R. Cutler, and G. E. Fuchs, Materials Science and Engineering: A **479**, 356 (2008).

Simulation of creep of directionally solidified NiAl-based eutectics with local and non-local material models

J. Albiez[1], I. Sprenger[2], D. Weygand[2], M. Heilmaier[2], T. Böhlke[1]

[1]Institute of Engineering Mechanics, Karlsruhe Institute of Technology (KIT), Karlsruhe, Germany

[2]Institute for Applied Materials, Karlsruhe Institute of Technology (KIT), Karlsruhe, Germany

Email: juergen.albiez@kit.edu

The B2-ordered intermetallic compound NiAl is of interest for high temperature applications due to its promising material properties, such as high oxidation resistance, high melting temperature, high thermal conductivity and relatively low density [1]. Its low creep resistance and its weak room temperature fracture toughness, however, limit the applicability of NiAl for structural applications [1]. One way to improve these two properties simultaneously is the use of the directional solidification (DS). The directionally solidified NiAl-9Mo eutectic consists of well-aligned Mo-10Al-4Ni fibers embedded in a Ni-45.2Al matrix [2] (each in at. %). The minimum creep rate of this DS eutectic can be more than five orders of magnitude lower compared to the monolithic NiAl, together with a twice as high room temperature fracture toughness (e.g., [3,4]).

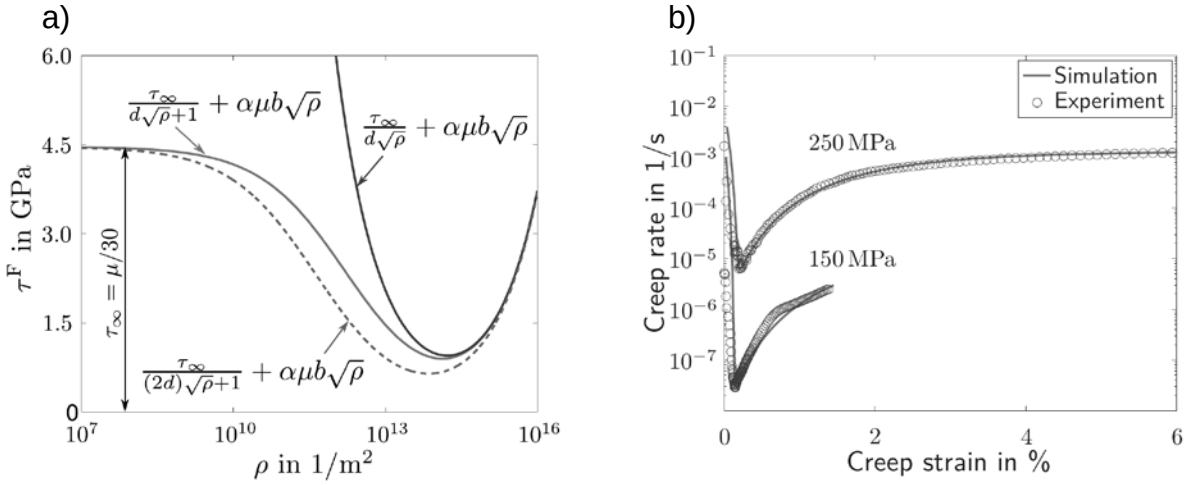

Fig. 1: *a) Comparison of the two size-dependent hardening models of [7,8]. The modified hardening model (eq. (1)) fulfills the limit by the theoretical strength for a defect free crystal. b) Experimentally measured creep curves and predicted ones at 1000°C.*

To study the deformation behavior as well as the composite effect, a local finite element model is established. High temperature compression tests of single crystal Ni-40Al, which serves as a model material for the NiAl matrix of the composite, reveal a lack of significant hardening, therefore, the matrix is modeled by an ideal plastic behavior. For the fiber, however, micro-pillar experiments of exposed fibers show a transition of the yield strength from theoretical strength to a dislocation-based strengthening mechanism with increasing dislocation density [5,6]. A generalized size-dependent model for the transition from dislocation-source strengthening to forest-dominated strengthening was proposed by El-Awady [7] and is shown in Fig. 1a. This

model, however, neglects the limitation by the theoretical strength for a defect-free material (Fig. 1a). A possible regularization results in

$$\tau^{\mathrm{F}} = \frac{\tau_\infty}{d\sqrt{\rho}+1} + \alpha\mu b\sqrt{\rho} \tag{1}$$

which considers the limit case of theoretical strength ($\tau_\infty = \mu/30$) for a defect-free material (Fig. 1a) [8], thus, all parameters have a physical meaning. The local finite element model is evaluated by comparing the predicted creep curves to experimentally measured ones for different applied stresses, different fiber diameters and two different temperatures [8]. Due to the comparison, one can conclude that the model is able to reproduce the effects of (i) a change of the applied stress, (ii) a change of the fiber diameter, and, (iii) a modification of the temperature. Exemplary, the simulated creep curves are plotted together with the experimentally observed ones for two different applied stresses (Fig. 1b) [8].

To account for the possibility of dislocation transfer from the matrix to the initial defect-free fibers, a gradient plasticity model in the sense of [9] is used. The simulated creep curves of this non-local finite element model are discussed with the focus on the influence of the interface resistance against plastic slip.

References

1. R. Noebe, R. Bowman, M. Nathal, Physical and mechanical properties of the B2 compound NiAl, *Int. Mater. Rev.* **38** pp. 193-232 (1993).

2. H. Bei, E.P. George, Microstructures and mechanical properties of directionally solidified intermetallic composites, *Mater. Sci. Forum* **539-543** pp. 1495-1500 (2007).

3. M. Dudová, K. Kuchařová, T. Barták, H. Bei, E.P. George, C. Somsen, A. Dlouhý, Creep in directionally solidified NiAl-Mo eutectics, *Scr. Mater* **65** pp. 699-702 (2011).

4. A. Misra, Z.L. Wu, M.T. Kush, R. Gibala, Deformation and fracture behaviour of directionally solidified NiAl-Mo and NiAl-Mo(Re) eutectic composites, *Philos. Mag. A* **78** pp. 533-550 (1998).

5. H. Bei, S. Shim, G.M. Pharr, E.P. George, Effects of pre-strain on the compressive stress-strain response of Mo-alloy single-crystal micropillars, *Acta Mater* **56** pp. 4762-4770 (2008).

6. P. Sudharshan Phani, K.E. Johanns, G. Duscher, A. Gali, E.P. George, G.M. Pharr, Scanning transmission electron microscope observations of defects in as-grown and pre-strained Mo alloy fibers, *Acta Mater* **59** pp. 2172-2179 (2011).

7. J.A. El-Awady, Unravelling the physics of size-dependent dislocation-mediated plasticity, *Nat. Commun.* **6** pp. 1-9 (2015).

8. J. Albiez, I. Sprenger, C. Seemüller, D. Weygand, M. Heilmaier, and T. Böhlke, Physically motivated model for creep of directionally solidified eutectics evaluated for the intermetallic NiAl-9Mo, *Acta Mater.* **110** pp. 377-385 (2016).

9. S. Wulfinghoff, E. Bayerschen, T. Böhlke, A gradient plasticity grain boundary yield theory, *Int. J. Plast.* **51** pp. 33-46 (2013).

On the Influence of Triaxial Stress States on Microstructural Evolution in Ni-base Superalloy Single Crystals

L. Cao, D. Bürger, P. Wollgramm, G. Eggeler

Institut für Werkstoffe, Ruhr-Universität Bochum, Universitätsstr. 150, 44801 Bochum, Germany

E-mail: lijie.cao@rub.de

Ni-base single crystal superalloys are used for turbine blades which operate in the creep regime, where they are exposed to high temperature and complex stress states. While many studies address the evolution of microstructure during uniaxial creep [1,2], much less effort has been devoted to the effect of multiaxial stress states. Therefore, in our present work, we use a novel circular notched miniature tensile creep specimen to investigate creep of Ni-base single crystal superalloys (SXs) under multiaxial loading conditions.

Firstly, it is briefly explained how circular notches affect the stress state in the notch root under tensile loading, and why stresses redistribute under creep conditions [3]. Finite element creep stress calculations (FEM) were conducted assuming isotropic material behavior to study how the stress states evolve during creep. A new circular notched miniature creep specimen was then designed and manufactured using electro discharge machining (EDM) and subsequent high precision turning. An image of the circular notched miniature creep specimen which was used in the present work is shown in Fig. 1.

Figure. 1: *Circular notched miniature creep specimen right after machining.*

In the present work uniaxial and circular notched creep tests were performed on the Ni-based single crystal superalloy ERBO1C (CMSX 4 type) in a precise <100> loading direction (± 1°). The specimens were creep deformed at a temperature of 950°C at a stress / net section stress of 300MPa. Macroscopic experimental displacements of notched specimens were interpreted on the basis of local deformations calculated by

FEM. FEM was also used to identify regions of different stress states, where rafting was investigated using scanning electron microscopy (SEM). The evolution of the γ/ γ' microstructure was studied using quantitative metallography. Special emphasis was placed on relating the details of rafting to the local stress state in dendritic regions of the microstructure. A case is presented where the different stress states in the cross section of the notched specimens produce significantly different raft microstructures. It is also shown that these differences decrease as creep proceeds and as stresses redistribute during creep. The results are discussed in the light of previous work on stress redistribution in circular notched specimens and on rafting under multiaxial stress states. Areas in need of further work are highlighted.

References

[1] R.C. Reed, *The superalloys: fundamentals and applications*, Cambridge university press, (2008).

[2] R. Bürgel, H. J. Maier, T. Niendorf*, Handbuch Hochtemperatur-Werkstofftechnik*, Wiesbaden, (2011).

[3] G. Eggeler, C. Wiesner, A numerical study of parameters controlling stress redistribution in circular notched specimens during creep, *J. Strain Anal. Eng. Des* **28***,* pp. 13–22, (1993).

Modeling Creep of Ni-Base Superalloys by Integrating Phase-Field and Dislocation-Based Crystal Plasticity at Mesoscale

P. Y. Zhao[1], C. Shen[2], S. R. Niezgoda[1] and Y. Wang[1]

[1]Department of Materials Science and Engineering, The Ohio State University, Columbus, Ohio, USA

[2]GE Global Research, One Research Circle, Niskayuna, NY 12309, USA

Email. Corresponding. Wang.363@osu.edu

Creep performance is a key aspect of design for high-temperature structural applications of Ni-base superalloys, with its assessment usually involving costly long-term experimental testing. Accelerated design and alloy development can be achieved using theoretical modeling and computer simulations, but currently it is still challenging due to the lack of creep models that can incorporate realistic material heterogeneities and predict subsequent microstructural and micromechanical evolution. In this study, we develop a computer simulation technique for creep deformation that integrates a dislocation-density based crystal plasticity (CP) model with phase-field (PF) model for precipitate and grain microstructure evolution. The linkage between CP and PF is through the dislocation density that serves as both a plasticity carrier and a microstructure descriptor. The validity of small-strain approximation in creep allows us to formulate both approaches in a unified framework, and the usage of spectral method allows us to perform long-term large-scale simulations in three-dimension.

The model is first calibrated against Haynes 282, showing consistent predictions on both tensile and creep performance as compared with experiments. Then microstructural heterogeneities such as non-uniform precipitate distribution in grain boundary (GB) denuded zones, which has been largely seen in welded materials, are introduced in a parametric way and the results show significantly nonlinear correlation between those microstructural heterogeneities and mechanical properties. Predictions on the spatial distribution of micromechanical fields provide useful information on analyzing the correlation between stress/strain concentration and local microstructural features such as interface and channel width up to the secondary creep.

Further assessment of tertiary creep requires quantitative modeling of failure mechanisms. In this study we focus on the diffusive growth of creep cavity by using a comprehensive PF model that account for bulk diffusion, surface diffusion and GB diffusion. Simulation results show that the elastic anisotropy at GB can significantly influence the evolution of GB cavity during creep.

This work is supported by the National Energy Technology Laboratory under Grant No. DE-FE0027776 (P.Z., Y.W. and S.R.N.) and the National Science Foundation DMREF program under Grant No. DMR-1534826 (Y.W. and S.R.N.).

Long time annealing of the nickel-based superalloy Waspaloy

K. Firlus[1], S. Kinzel[1,2], J. Gabel[3], U. Glatzel[1]

[1] University Bayreuth, Metals and Alloys, Germany

[2] now at: H-O-T Härte und Oberflächentechnik, Buttenheim, Germany

[3] MTU Aero Engines AG, Munich, Germany

e-mail: uwe.glatzel@uni-bayreuth.de

Turbine components made of Ni-based superalloys show contraction at moderate and high temperature (450°C - 800°C) and low stress. Thus size tolerance of these parts are undershot. This effect is not fully understood yet. The contraction or negative creep is often associated with the convergence towards thermodynamic equilibrium. Thereby phase fractions may vary and changes in crystallographic structure may occur, which leads to contraction of the specimen.

The nickel-based superalloy Waspaloy which is known since the 1950s and is used for gas turbines and aerospace components is investigated in this study. To determine thermodynamic stable phases and phase fractions at the annealing temperature, the CALPHAD-method was used with ThermoCalc TTNi7 and TTNi8 database.

Very precisely manufactured rods with a diameter of 10 mm and a length of 100 mm were measured with high precision. Additionally, Disks with a thickness of about 2 mm with the same diameter were produced to examine structural changes. Afterwards, rods and disks were annealed for different times with maximum of 10,000 h. At every time step, rod specimens were air cooled and the length was measured. Changes in the lattice parameter were determined by X-Ray diffraction and shifts in the microstructure were characterised by SEM.

On the Evolution of Microstructure during Creep of a Polycrystalline Ni base Superalloy

H. Sommer[1], J. Kiese[2], M. Ersanli[1], N. de Boer[3], J. Klöwer[3], G. Eggeler[1]

[1]. Institute for Materials, Materials Science, Ruhr-University Bochum, Bochum, Germany

[2]. VDM Metals GmbH, Werdohl, Germany

[3]. VDM Metals GmbH, Altena, Germany

E-Mail: Hannah.Sommer@rub.de

Creep is the time dependent plastic deformation of materials, which shows a strong dependence of stress and temperature [1,2]. Creep strongly depends on microstructure and it is well known that the microstructures of engineering materials evolve during creep. In the present study we investigate a polycrystalline Ni-base superalloy, which is used for different high temperature components (e.g. combustion chambers, liners, casings, exhaust ducting). Its creep behavior was studied at stresses ranging from 60 to 250 MPa in the temperature range between 760 and 950 °C. The features of individual creep curves are discussed. Minimum creep rates are measured and their stress and temperature dependencies are described using Arrhenius and Norton plots.

The volume fraction, morphology, spatial arrangement and size distribution of γ' precipitates (size s: 20-200 nm) has a strong influence on creep. In order to investigate this influence, pre-creep stress free ageing experiments were performed to establish different γ/γ' microstructures and to document their effect on creep. Ageing experiments were performed in the temperature range of 750 – 900 °C for periods between 1 and 900 h. The effect of ageing was studied using scanning and transmission electron microscopy. In addition micro hardness experiments (HV 10, indent diagonal d > 100 µm) were used to study the extent of ageing. An attempt was made to rationalize the evolution of the particle population on the basis of the kinetics which governs Ostwald ripening. Special emphasis was placed on how the superposition of an applied stress affects particle coarsening and on how particle coarsening effects creep rates. The results are discussed in the light of previous results published in the literature.

References

1. J. Čadek: *Creep in Metallic Materials*, Elsevier, Amsterdam (1988)

2. F. R. N. Nabarro, H. L. de Villiers, *The Physics of Creep*, Taylor and Francis, London (1995)

Localised deformation during high temperature creep of a Ni based single crystal superalloy.

B. Viguier[1] and C. Josse[2].

[1] CIRIMAT, INP/ENSIACET, Université de Toulouse

[1] UMS Castaing, Espace Clément Ader, Université de Toulouse

Email. bernard.viguier@ensiacet.fr

Single-crystal nickel-based superalloys are extensively used in the aeronautic industry, particularly in the hottest parts of turbo-reactors for aircraft and helicopters. The optimized microstructure consists of an array of ☐' cubi
<100> cubic directions and coherently embedded in an austenitic matrix ☐. Cre
high temperature leads to changes in this microstructure where cubes coarsen to form platelets aligned along {001} planes, this is rafting [1]. We have shown in a previous paper [2] that depending on the local stress state and local strain amount the morphology and orientation of rafts may vary. Especially rafts oriented 45° off the load axis were observed in areas with a large plastic strain (over 10%). In the present work these particular areas are characterized in more details using SEM/EBSD analysis and FIB. It appears that the reorientation of the rafts does not seem to be related to the rotation of the crystal but instead to the localization of the plastic strain inside limited bands.

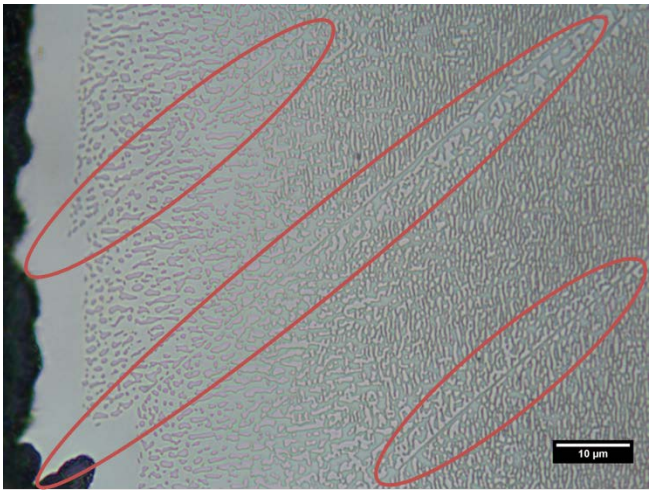

Figure 1. Optical microscope observation of rafts in MC2 superalloy after high temperature creep test at 1100°C. Localized bands of rotated rafts are circled (the load axis is along horizontal direction).

References

1. F.R.N. Nabarro and H.L. De Villiers, *The physics of creep*. Taylor & Francis, London, (1995).

2. F. Touratier, E. Andrieu, D. Poquillon, and B. Viguier, *Mater. Sci. Eng. A*- **510-11** p. 244 (2009).

Double minimum creep in the rafting regime of a single crystal Co-base superalloy with positive lattice misfit

S. Neumeier, F. Xue, C. Zenk, L. Freund, M. Göken

Friedrich-Alexander-University Erlangen-Nuremberg, Department Materials Science & Engineering, Institute I, Erlangen 91058, Germany

Email. steffen.neumeier@fau.de

The microstructural evolution and the creep deformation mechanisms in the rafting regime of a Ta-containing single crystal γ/γ′ Co-base superalloy has been investigated by SEM and TEM investigations. Neutron diffraction measurements revealed that the large lattice misfit is positive and decreases from room temperature (+0.72%) to 1000 °C (+0.40%), which is approximately 100 °C lower than the γ′ solvus temperature. This leads to an initially cuboidal γ′ morphology.

During creep deformation at 950 °C and 150 MPa a pronounced directional coarsening of the γ/γ′ microstructure occurs. SEM investigations reveal that the γ′ rafts form normal to the external compressive stress axis due to the positive lattice misfit. This rafting behavior is similar to that of Ni-base superalloys with a negative lattice misfit that are creep deformed at high temperatures by applying external tensile stresses.

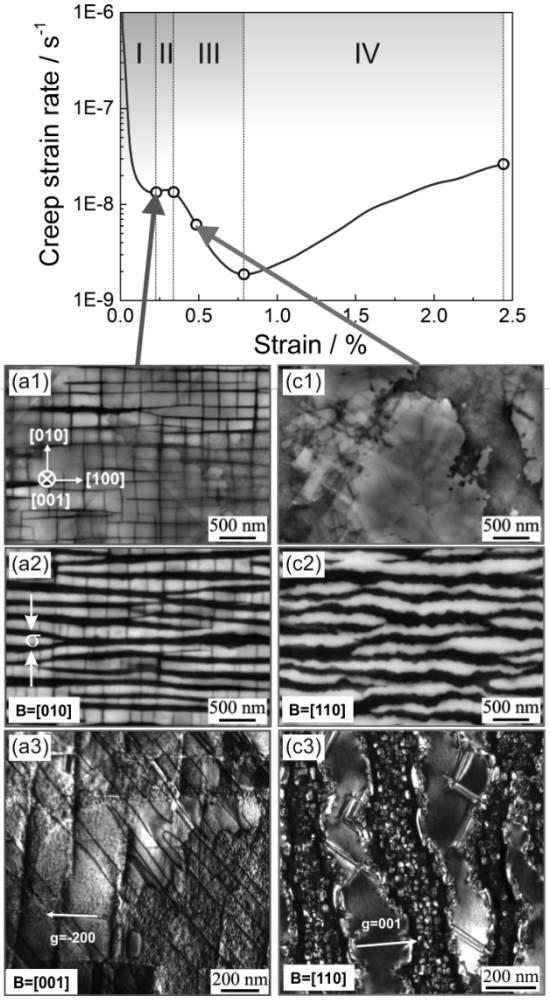

Figure 1. Representative creep curve with different creep stages of single crystal Co-base superalloy ERBOCo-2Ta at 950 °C and 150 MPa.

The creep curves of the Co-base superalloy show four distinct creep regimes including a double minimum creep rate, which has not been reported in Co-base superalloys before (see Figure 1). Similar behavior was found for single crystal γ/γ′ Ni-base superalloys in the low stress / high temperature regime at 1100 °C [1].

Interrupted creep tests show that in the first stage, as found by TEM investigations, a/2<110> type dislocations glide in the horizontal γ channels and deposit at the γ/γ′ interface. With ongoing creep deformation these dislocations start to enter the vertical γ channels by cross slip and climb and, different to the deformation behavior of Ni-base superalloys in the rafting regime, also <112> type partial dislocations cut occasionally the γ′ phase and create stacking faults. This results in a slight rise of creep rate. In the third stage the vertical γ channels get closed due to the rafting of the γ′ phase. The creep rate decreases further again until the vertical γ channels were completely closed and the rafted structure is well established at the global minimum. This indicates a creep hardening effect due to rafting similar to Ni-base superalloys in the high temperature creep regime [1]. With ongoing creep deformation

the γ/γ′ rafts coarsen continuously and become more irregular and wavy and the creep rate increases again. The stacking faults start to form in the early stages of creep, but they appear more frequent beyond the global minimum at a large accumulated strain. The consecutive shearing by partial dislocations and the diffusion of alloying elements lead to the formation of microtwins as well as the formation of $D0_{19}$-Co_3W phase on the (111) planes during the late stages of creep. These mechanisms may influence the creep behavior as well which will be also discussed in the paper.

References

1. W. Schneider and H Mughrabi, Investigation of the creep and rupture behavior of the single-crystal Nickel-base superalloys CMSX-4 between 800°C and 1100°C*, Proc. of the 5th International Conf. on Creep and Fracture of Engineering Materials and Structures",* edited by B. Wilshire and R.W. Evans, The Institute of Materials, London, pp. 209–219 (1993).

Creep of the single-crystal nickel-base superalloy CMSX-4 at a super-solvus temperature

A. I. Epishin[1], T. Link[1], G. Nolze[2], B. Fedelich[2], T. Feldmann[2], B. Viguier[3], D. Poquillon[3], Y. Le Bouar[4], A. Ruffini[4], A. Finel[4]

[1]. Technical University of Berlin, Berlin, Germany

[2]. Federal Institute for Materials Research and Testing (BAM), Berlin, Germany

[3]. CIRIMAT/ University of Toulouse, Toulouse, France

[4]. Laboratoire d'Etude des Microstructures, CNRS/ONERA, Châtillon, France

E-mail: alex_epishin@yahoo.de

Data about the creep of metals and their alloys at temperatures close to the melting point are very limited. The reason is that most engineering alloys are used at temperatures below 0.6-0.8 of their melting point, so, investigation of creep at higher temperatures has usually no practical relevance. For some special applications however it is important, in our case hot isostatic pressing (HIP) of single-crystal turbine blades cast from nickel-base superalloys. In order to remove porosity the blades are HIPed at temperatures above γ'-solvus where superalloy has no strengthening γ'-phase and therefore is very soft. E.g., the company Howmet Castings hips the superalloy CMSX-4 at 1288°C, which corresponds to a homologous temperature of about 0.97=1561 K/1612 K (solidus temperature). Knowledge about the creep of CMSX-4 at this temperature and understanding of the creep mechanisms are necessary to model the kinetics of pore closure during HIP.

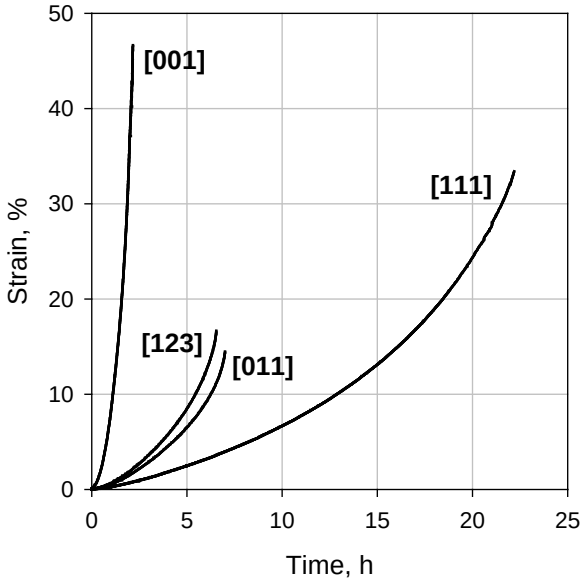

Figure 1. Creep curves of CMSX-4 single-crystals of different orientations at 1288°C/10 MPa.

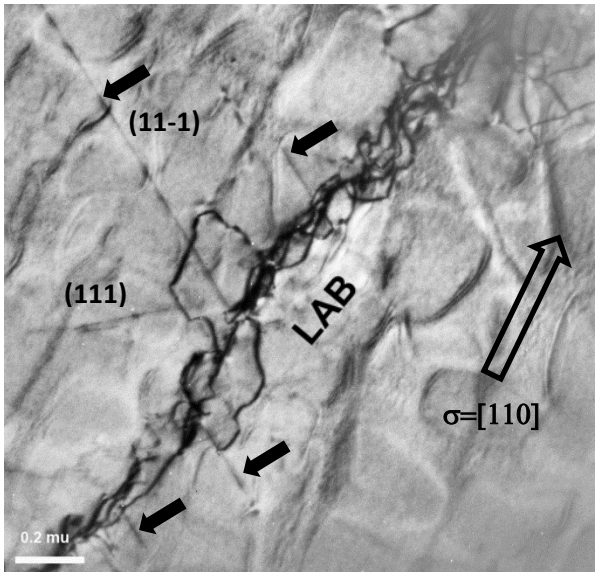

Figure 2. Retarding of slipping dislocations (marked by black arrows) by a LAB in a [011] single-crystal of CMSX-4 during creep at 1288°C/10 MPa.

CMSX-4 single-crystals of [001] orientation and few single-crystals of different orientations, [011], [123] and [111], were tested under creep conditions at 1288°C in the stress range between 4 and 16 MPa. At this temperature which is above the γ'-solvus (for CMSX-4 1280°C) the superalloy has single phase structure representing the γ-solid solution of nickel

strengthened by solute atoms. Creep curves of CMSX-4 single-crystals of different orientations measured at 1288°C/10 MPa are shown in Fig. 1. It is seen that despite such a high homological temperature, 0.97, CMSX-4 shows very high anisotropy of creep rate. The average creep rate of [001] single-crystal in the range 0-30% strain is about 11.5 time faster than that for [111], a ratio, which is even higher than at the practically relevant temperatures 750-1100°, see e.g. [1]. Approximation the strain rate – stress dependence by the Norton power law gave a stress exponent *n* of about 6 which is reasonable for dislocation creep. The specimen shape after testing, analysis of traces of plastic deformation by electron backscatter diffraction (EBSD) and transmission electron microscopy (TEM) investigations (see Fig. 2) indicate on dislocation slip on the octahedral system ⟨011⟩{11-1}.This result however does not support the current doctrine that at high temperatures creep of metals and alloys are climb controlled [4]. It is concluded from the obtained results that even at such a high homologous temperature, 0.97, dislocation movement by slip is more preferable than by climb if only relatively week obstacles are present like solute atoms and low angle boundaries (LABs).

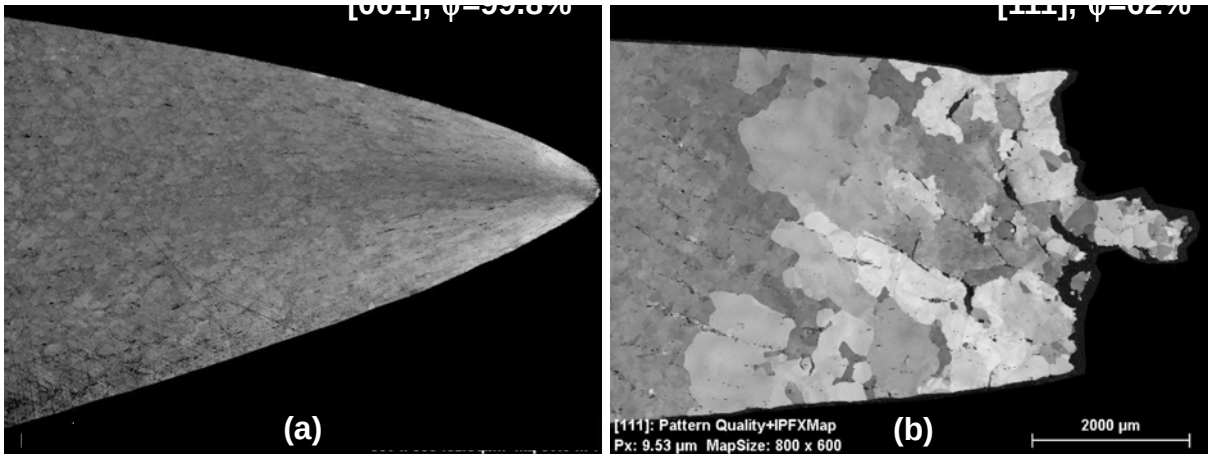

Figure 3. Necking and recrystallization behavior of CMSX-4 single-crystals of different orientation during creep at 1288°C/10 MPa, EBSD.

It is remarkable that under used testing conditions the necking and recrystallization behavior of differently oriented single-crystals is very different. E.g., the [001] single-crystal showed very large local strain during necking, ψ=99.8%, and no recrystallization (see Fig. 3a), while the [111] single-crystal small necking, ψ=62%, accompanied by recrystallization. Such a specific deformation and recrystallization has to be undestood.

The obtained creep data of CMSX-4 which was introduced in a finite element model in order to simulate pore closure during commercial HIP at a temperature of 1288°C [3, 4].

References

[1] V. Sass et al., *Acta Mater.,* 44, pp. 1967-1977 (1996).

[2] J. Weertman, J. R. Weertman, Chapter 20, pp. 1309-1340, in: *Physical Metallurgy*, Vol. 2, ed. by R. W. Cahn, P. Haasen, North-Holland Physics Publishing, 1983.

[3] A. Epishin et al., *Mater. Sci. and Eng. A*, **586**, pp. 342–349 (2013).

[4] A. I. Epishin et al., *Eurosuperalloys 2014, MATEC Web of Conferences*, **14**, 08003 (2014).

Creep Behaviour of overaged Nimonic 263 Superalloy

G. Angella[1], R. Donnini[1], M. Maldini[1], D. Ripamonti[1]

[1] National Research Council, Institute of Condensed Matter Chemistry and Technology for Energy

dario.ripamonti@cnr.it

Nimonic 263 is a precipitation hardened nickel base superalloy often employed in stationary components of gas turbine (e.g. combustion chambers). Its creep strength is mainly related to the precipitation of *γ'* – $(Ni,Co)_3(Ti,Al)$ particles, which develop during ageing, after solution treatment. Microstructural studies and thermodynamic calculation [1] point out that *γ'*, whose solvus temperature is about 925°C, is a metastable phase which, after prolonged soaking coarsen and, eventually, is replaced by needles of *η* − $(Ni,Co)_3Ti$ phase. It was shown elsewhere [2] that *γ'* coarsening during creep tests does not account for creep acceleration, which increases roughly linearly with strain for samples subjected to the usual heat treatment routine (2h/1150°C, water quench, 8h/800°C – peak ageing), In this condition, samples show small decelerating stage followed by a long accelerating stage (Fig. 1).

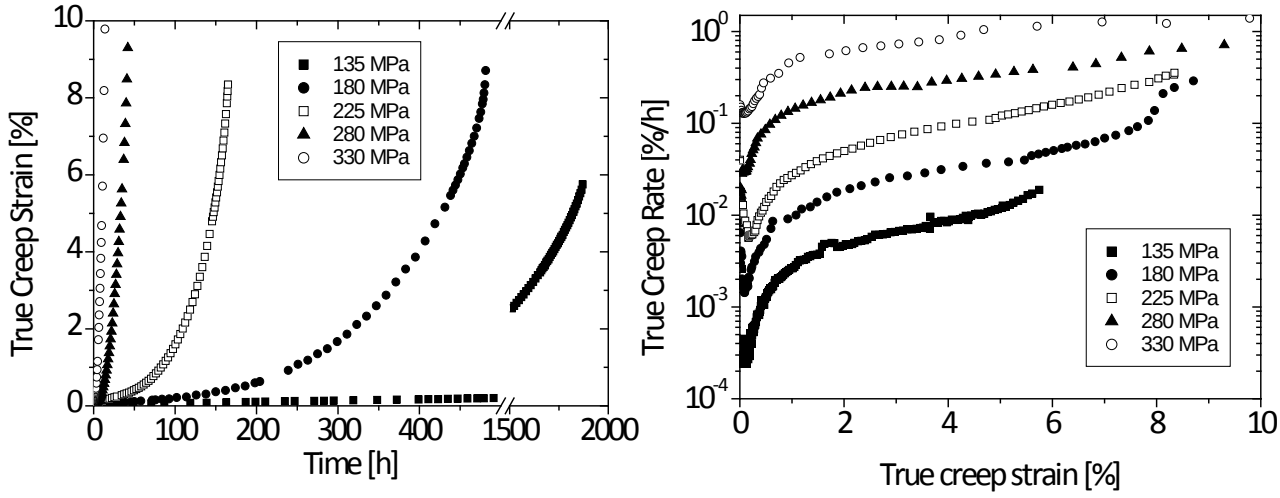

Fig. 1: Creep strain versus time (on the left) and creep rate versus creep strain (on the right) for 800°C/8h (peak) aged samples crept at 800°C.

Overageing not only reduces time to rupture and increases minimum creep rate, but also affects the shape of the entire creep curve, reminding the shape of regular class M materials. This effect becomes visible for longer ageing times as stress decreases (Fig. 2a-f). At low stresses, though, this transition is no longer shown, even for very long overageing (up to 3500 h), when *η* phase needles start to replace *γ'* particles. This behaviour may be explained taking into account that when particles coarsen their mutual distance decreases, such that creep deformation may be controlled by dislocation interaction.

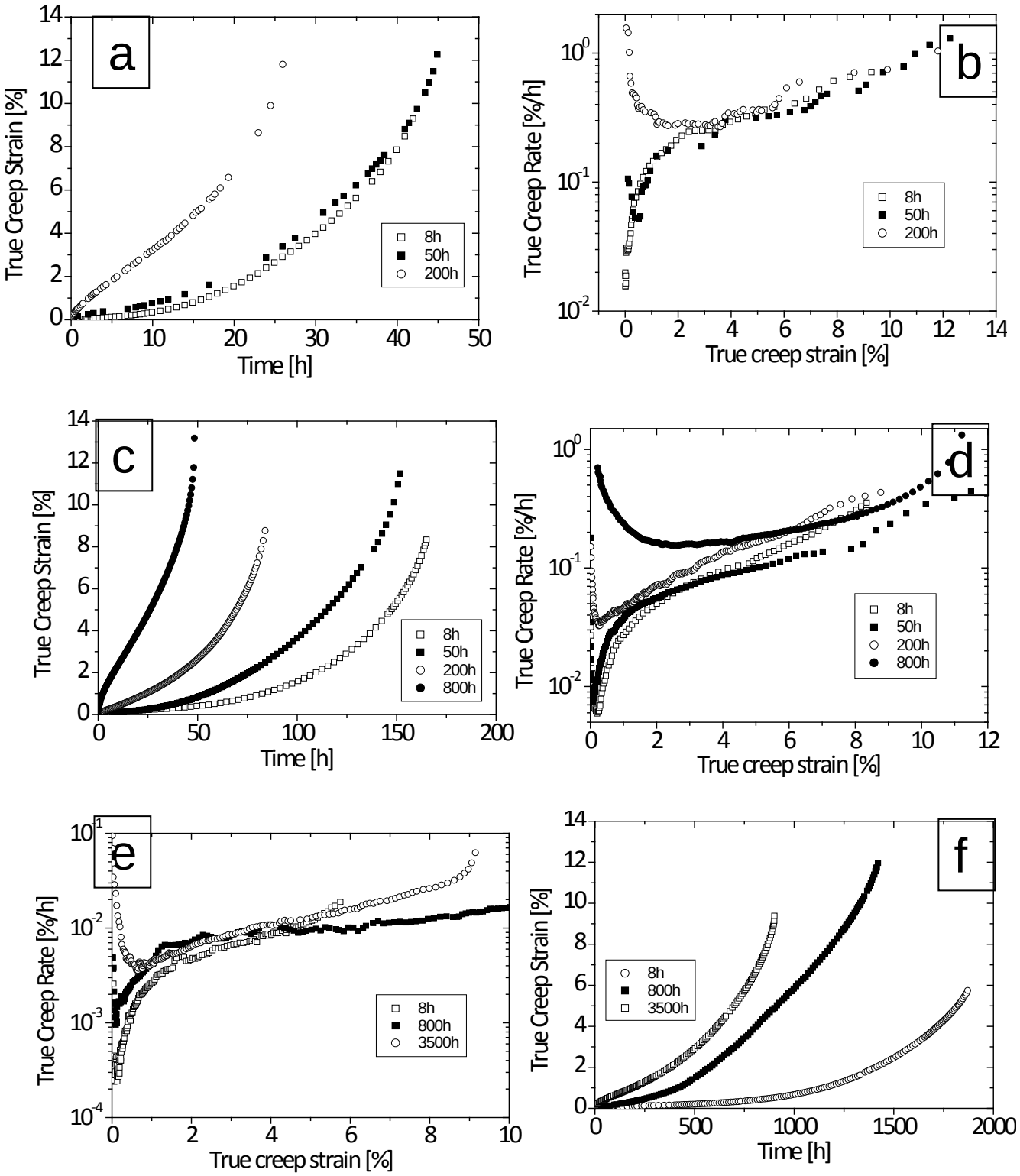

Fig. 3: Creep strain versus time (on the left) and creep rate versus creep strain (on the right) for aged samples crept at 800°C/280 MPa (a-b), 800°C/225 MPa (c-d), 800°C/135 MPa (e-f). (Ageing times in the legend)

References

[1] J.C. Zhao, V. Ravikumar, A.M. Beltran, «Phase precipitation and phase stability in Nimonic 263» *Metallurgical and Material Transactions A*, **32A**, 1271-1282 (2001)

[2] G. Angella, R. Donnini, D. Ripamonti, M. Maldini, «The role of particle ripening on the creep acceleration of Nimonic 263 superalloy», *MATEC Web of Conferences*, **14**, 14001-6 (2014)

High-Temperature Creep-Sag Deformation of a Full-Sized Zr-2.5Nb Pressure Tube

R.W.L. Fong and T. Nitheanandan

Fuel & Fuel Channel Safety Branch

Canadian Nuclear Laboratories, 286 Plant Road, Chalk River, Ontario,

Email: randy.fong@cnl.ca

CANDU® power reactors use natural-uranium fuel and heavy water moderator. In these reactors, the horizontal zirconium alloy fuel channels are the main pressure boundary. The fuel channel consists of two concentric tubes: (i) an internally pressurized Zr-2.5Nb tube that contains the uranium fuel bundles and the re-circulating heavy-water primary coolant, and (ii) a Zircaloy-2 calandria tube that separates the pressure tube from the heavy-water moderator. The full weight of the pressure tube, fuel and coolant is supported by spacers tightly-fitted around the pressure tubes outside surface and resting on the bottom of the calandria tube. In a hypothetical event of a large loss of coolant accident (large LOCA) and a coincidental loss of emergency core cooling (LOECC), the pressure tube in the fuel channel overheats and deforms. With negligible internal pressure, the pressure tube deformation occurs via a creep-sag mechanism.

The high temperature creep-sag deformation characteristics of a full-sized Zr-2.5Nb pressure tube have been investigated experimentally using 5 equally spaced fixed point loading (Figure-1). The pressure-tube test section was internally heated slowly (≈2.5°C/s) to high temperatures up to 1000°C, while the vertical deflection was continuously monitored until it contacted the calandria tube. The sagging of the pressure tube became increasingly pronounced when the temperatures exceeded 800°C.

This paper summarizes the measured deformation from the tube sag experiment and describes a comparison with analytical results, to improve the understanding of pressure tube sag phenomena when subject to high temperature transients.

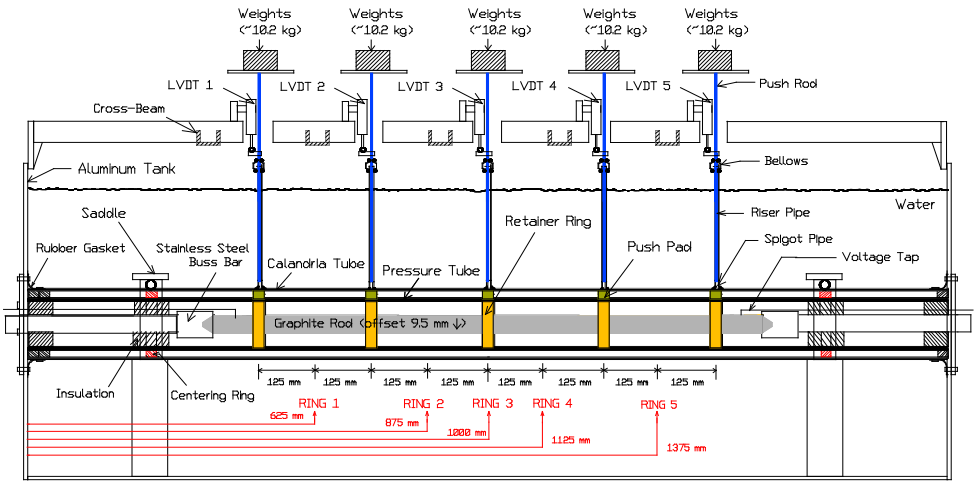

Figure 1. Experimental investigation of creep-sag deformation of a full-sized CANDU® Zr-2.5Nb pressure tube.

® Registered Trademark of the Atomic Energy of Canada Limited

New Insights Into Rate Limiting Deformation Processes in Ni-Base Superalloys

T. M. Smith, A. Eagan, M. Ghazisaeidi, S.R. Niezgoda, Y. Wang, and M.J. Mills

[1] Center for Electron Microscopy and Analysis, The Ohio State University, Columbus, OH 43212, USA

[2] Department of Materials Science and Engineering, The Ohio State University, Columbus, OH 43210, USA

Polycrystalline Ni-based superalloys are vital materials for disks in the hot section of aerospace and land-based turbine engines due to their exceptional microstructural stability and strength at high temperatures. In the drive to increase operating temperatures and hold times in these engines, hence increasing engine efficiency and reduction of carbon emissions, creep properties of these alloys becomes increasingly important. At these higher temperatures, new deformation modes become active. Twinning and stacking fault shearing are important operative mechanisms in the 600-800°C temperature range. Advanced characterization techniques--based on scanning transmission electron microscopy using diffraction contrast imaging, high resolution imaging, and energy dispersive spectroscopy--have been used to gain new insights into these mechanisms and the rate-limiting processes during high temperature deformation. Several alloy compositions and microstructure variants of commercial disk alloys are being explored to enhance creep behavior models and provide insights that can lead to higher temperature capabilities in these alloys.

Phase stability during creep of CoCrFeMnNi and CoCrFeNi compositionally complex high- and medium-entropy alloys

N. Luptáková[1], T. Záležák[1], I. Kuběna[1], G. Laplanche[2], E.P. George[3,4], A. Dlouhý[1]

[1]. Academy of Sciences CR, Institute of Physics of Materials, Zizkova 22, 616 62 Brno, Czech Republic

[2]. Institut für Werkstoffe, Ruhr-Universität Bochum, 44 780 Bochum, Germany

[3]. Oak Ridge National Laboratory, Materials Science and Technology Division, Oak Ridge, TN 37831-6115, USA

[4]. University of Tennessee, Department of Materials Science and Engineering, Knoxville, TN 37996-2100, USA

Email : dlouhy@ipm.cz

We have investigated creep in two equiatomic, compositionally complex alloys CoCrFeMnNi and CoCrFeNi both of which crystallize as FCC solid solutions. Arc-melted and drop-cast ingots of these alloys were thermo-mechanically processed and recrystallized prior to creep. The creep behaviours of both alloys are similar with the reduced compositional complexity of the quaternary alloy compared to the quinary alloy having only a minor effect. Creep tests performed at 1073 K clearly showed that the stress dependence of the creep rate can be fitted by a phenomenological Norton law with a stress exponent close to 3 for both alloys. Therefore, they exhibit a Class I creep behaviour over a wide range of applied stresses in which the accumulation of creep strain is solid solution controlled. Our experiments also addressed long-term phase stability of the two FCC solid solutions subjected to creep loading. The results obtained at 1073 K suggest that the most reactive element in the two investigated alloys is chromium, which separates from the solid solution to form Cr-rich precipitates, mainly at grain boundaries in CoCrFeMnNi (Fig. 1a) but at both grain

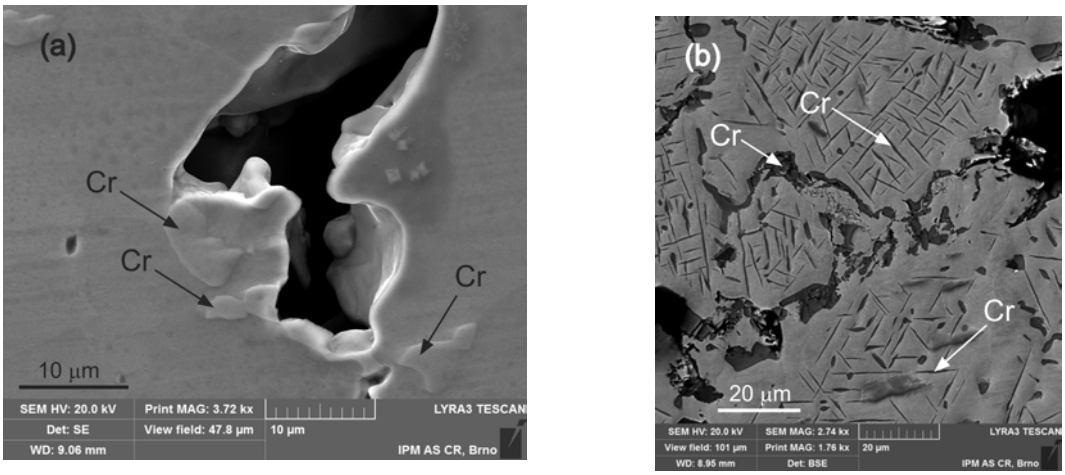

Figure 1: *Precipitation of Cr-rich phases during creep at 1073K in (a) CoCrFeMnNi and (b) CoCrFeNi*.

boundaries and within the grains in CoCrFeNi (Fig. 1b). The grain boundary Cr precipitates often facilitate nucleation and growth of creep cavities. The crystallography of the Cr particles was investigated using advanced SEM and TEM techniques and rather unexpected results were obtained, which are presented and discussed. Based on these findings, and those of previous studies [1-3], it can be concluded that creep

deformation facilitates the decomposition of CoCrFeMnNi and CoCrFeNi and limits their FCC solid solution stability above 1073 K.

Acknowledgement. This research was supported by CSF under the contract no. 14-22834S. GL acknowledges support from the German Research Foundation (DFG) through project LA 3607/1-1, and EPG from the U.S. Department of Energy, Basic Energy Sciences, Materials Sciences and Engineering Division.

References

1. F. Otto et al., *Acta Mater.* **112**, pp. 40 - 52 (2016).

2. E.J. Pickering, R. Munoz-Moreno, H.J. Stone, N.G. Jones, *Scr. Mater.* **113**, pp. 106-109 (2016).

3. B. Schuh et al., *Acta Mater.* **96**, pp. 258-268 (2015).

Influence of microstructural parameters on creep properties of the Nickel-Based superalloy AD730™

Winnie Vultos[1*], Florence Pettinari-Sturmel[1], Muriel Hantcherli[1], Joël Douin[1], L. Thébaud[2,3], Patrick Villechaise[2], Jonathan Cormier[2] and Alexandre Devaux[3]

[1] CEMES-CNRS, BP 94347, 29 rue Jeanne Marvig, 31055 Toulouse cedex 4, France

[2] Institut Pprime, UPR CNRS nº 3346, CNRS – Université de Poitiers – ISAE-ENSMA, Physics and Mechanics of Materials Department, ISAE-ENSMA, 1 avenue Clément Ader, BP 40109, 86961 Futuroscope - Chasseneuil, France

[3] Aubert & Duval, Site des Ancizes BP1, 63770 Les Ancizes Cedex, France

**Email corresponding author : winnie.vultos@cemes.fr*

For more than 30 years, several studies have been performed to understand and improve the mechanical properties of Ni-based superalloys designed for turbine blades as well as turbine disks application. These alloys experience severe using condition combining tensile test, creep and fatigue at different temperatures.

The development and the optimization of these materials have been possible through multiscale approaches combining experiments and modeling. Thanks to these researches, the mechanical behavior of polycrystalline Ni-based superalloys, the understanding of the relation between the macroscopic behavior and the characteristics of the microstructure are well known.

In the current competitive aeronautic context, in order to increase the aero-engine efficiency, the engine makers have to propose new materials for higher operating temperature.

Aubert & Duval has developed the Ni-based superalloy AD730™ for turbine disks. This superalloy is able to withstand higher operating temperatures while being less expensive due to its chemical composition and its capability to be manufactured through the cast and wrought route [1-2].

But the data available on AD730™ are still rare, especially at the microscopic scale, because of its recent development. However, one may expect that its mechanical properties are highly dependent on microstructural parameters such as the hardening γ' precipitates characteristics (size, distribution and chemistry) as shown in previous studies on NR3, N18 and Udimet™ 720Li alloys [3-5] during creep around 700 °C.

The microstructure of AD730™ was first characterized using conventional TEM. It consists in multimodal γ' precipitates. Then, post mortem TEM observations and in situ straining experiments have been performed to identify the pertinent deformation micromechanisms, which control the macroscopic creep deformation.

This study is focused on the influence of microstructural parameter and the applied stress on creep deformation micromechanisms.

References

1. A. Devaux *et al.*, AD730™ « A New Nickel-Based Superalloy for High Temperature Engine Rotative Parts », *Superalloys 2012* ; 911-919 (2012).

2. A. Devaux, E. Georges and P. Heritier, « Development of New C&W Superalloys for High Temperature

Disk Applications » *Adv. Mater. Research.* : **278 :** 405-410 (2011)

3. T. Billot, P. Villechaise, M. Jouiad and J. Mendez*.,* « Creep–fatigue behavior at high temperature of a UDIMET 720 nickel-base superalloy », *Int. J. Fatigue* ; **32:**824-829 (2010)

4. S. Raujol, F. Pettinari, D. Locq, P. Caron, A. Coujou and N. Clement, « Creep straining micro-mechanisms in a powder-metallurgical nickel-based superalloy» , *Mater. Sci. Eng.*; 387-389 **:** 678-682 (2004).

5. J. Douin, F. Pettinari-Sturmel and A. Coujou*,* Dissiociated dislocations in confined plasticity, *Acta Mater.* ; **55 :** 6453-6458 (2007).

Creep and Oxidation Behavior of Coated and Uncoated Thin Walled Single Crystal Samples of the Alloy PWA1484

Fabian Krieg[1], Mike Mosbacher[1], Markus Fried[2], Ernst Affeldt[2], Uwe Glatzel[1]

[1]. Metals and Alloys, University Bayreuth, Ludwig-Thoma-Str. 36b, 95447 Bayreuth, Germany

[2]. MTU Aero Engines AG, Dachauer Straße 665, 80995 Munich, Germany

Email: fabian.krieg@uni-bayreuth.de

To achieve a higher efficiency of a turbine a higher gas inlet temperature behind the combustion chamber is needed. One way of improvement is the applying of MCrAlY- or NiAl-coatings on the blade alloys. Another method is an active cooling of the turbine blade by air which requires complex internal cooling channels. This results in lower wall thicknesses. An advantage of thin-walled and consequently lighter blades is the lower centrifugal force with constant rotation speed in a turbine. This has a big impact on the overall turbine weight since discs, shafts, bearings and casings can be reduced in dimensions. Thereby the thrust to weight ratio is increased. Nevertheless the reduction of the part thickness has a negative effect on the service life. This alloy dependent decrease of creep resistance is known in literature as thickness debit effect [1-6].
The aim of the present work is to investigate the combined effect of NiAl coatings and small sample thicknesses (1 mm and below). Therefore aluminized and uncoated samples of the single crystal Ni-based superalloy PWA1484 were tested in creep and oxidized up to 1000 h.

For determination of the creep resistance a high temperature creep-setup according to [7] was used. The creep sample is heated resistively by direct electrical current, the temperature is measured by a thermocouple and controlled using a PID controller. The strain is recorded contactless using a video extensometer. The gauge section has a cross section of 2.9 mm and a thickness in between 0.3 mm and 1.0 mm with varying stresses up to 170 MPa. The crystallographic orientation of the samples is close to the [001]-orientation with a maximum deviation of 4%.

The oxidation and the creep tests were carried out at temperatures of 980°C and 1100°C in ambient air. To get an insight of the present work some of the results of the oxidation test at 980°C and the creep test at 1100°C are shown.

The initial state of the creep and oxidation specimen is shown in figure 1. The layer structure of the aluminized samples is as follows: The outer-most first layer is the NiAl-coating with an average thickness of 25-30 µm, followed by the diffusion zone with the same thickness. The diffusion zone is followed by the unchanged microstructure of the Ni-based superalloys with the γ-matrix and the cuboidal γ´-precipitates, see Figure 1 a, b. The uncoated samples show the microstructure of Fig. 1b.

Figure 2 shows the results of the creep experiments at a temperature of 1100°C and an applied stress of 70 MPa for the aluminized and 80 MPa for the uncoated samples. 9 creep tests with the aluminized and 3 with uncoated samples were performed with this set of parameters.

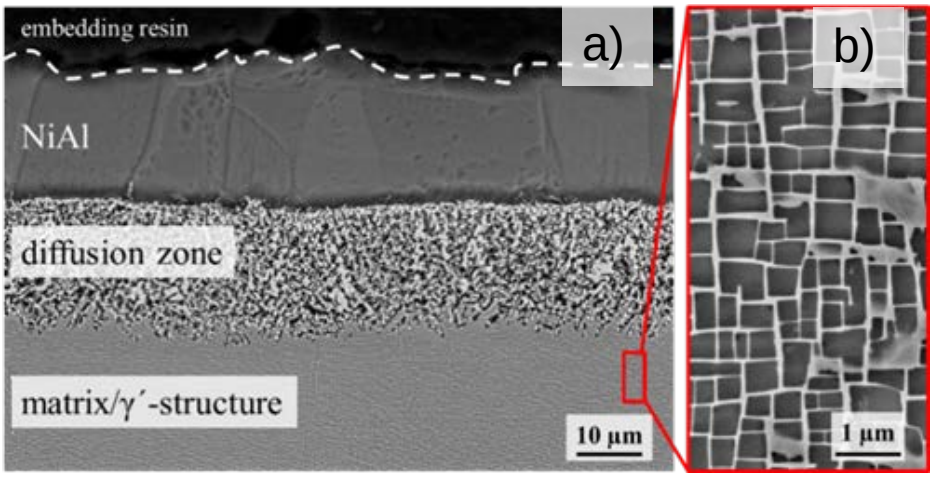

Figure 1. Initial state of the creep and oxidation samples. a) aluminized and b) uncoated microstructure.

The creep curves (Figure 2) show a primary, secondary and tertiary creep regime for both types of samples (aluminized and uncoated). The thickness debit effect is clearly observable for uncoated and aluminized specimen. It shows a significant decrease in creep resistance with decreasing sample thickness. The aluminized samples show a small scattering regarding rupture life and rupture strain.

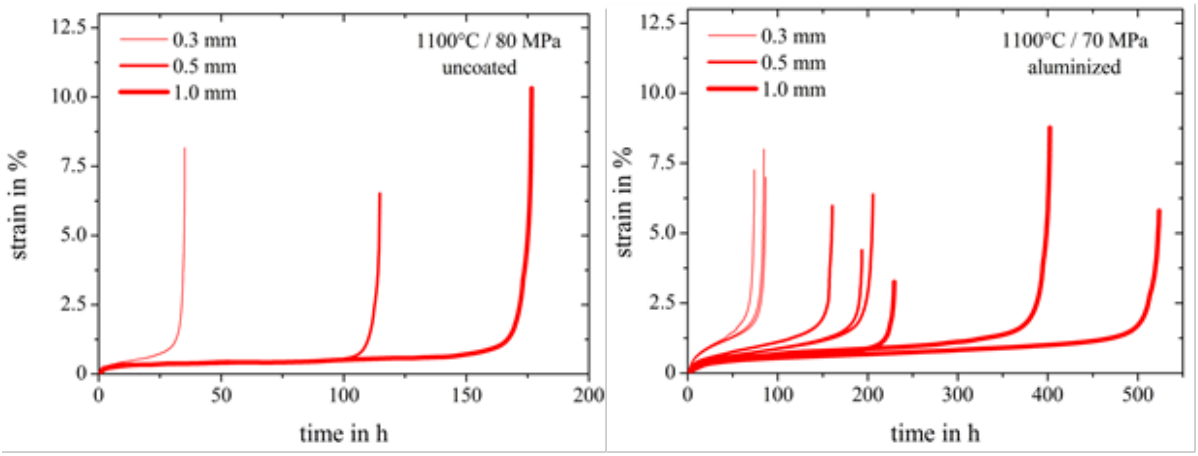

Figure 2. Creep experiments at a temperature of 1100°C and a stress of a) 80 MPa for uncoated and b) 70 MPa for aluminized specimen.

References

[1] A. Srivastava et al., *Acta Materialia* **60**, pp. 5697-5711 (2012).

[2] M. Bensch et al., *Acta Materialia* **58**, pp. 1607-1617 (2010).

[3] B. Cassenti and A. Staroselsky, *Materials Science and Engineering A* **508**, pp. 183-189 (2009).

[4] R. Hüttner et al.,*TMS Superalloys* **2008**, pp. 719-723 (2008).

[5] V. Seetharaman and A. D. Cetel, *TMS Superalloys* **2004**, pp. 207-214 (2004).

[6] M. Brunner et al., *Materials Science and Engineering A* **550**, pp. 254-262 (2012).

[7] R. Völkl et al., *Materials Science and Engineering A* **483–484**, pp. 587-589 (2008).

Interrelation of FEM Simulation to Superplastic Forming Experiments for Ti-6Al-4V

Bibhavendra Kumar Singh[1]*, S.S. Bhattacharya[1], Uday Chakkingal[1] and Sergey A Aksenov[2]

[1]Materials Forming Laboratory, Department of Metallurgical and Materials Engineering, Indian Institute of Technology, Madras, Chennai – 600 036, India

[2] Moscow Institute of Electronics and Mathematics, National Research University "Higher School of Economics", 34 Tallinskaya, Moscow 123458, Russia

**Email: bibhu32@gmail.com*

Superplastic forming has become an indispensable process in aircraft and automobile parts manufacturing. It is a low tolerance fabrication process, widely used to produce turbine blades, seat structures, compressor blades and chassis [1]. Low production rate and constricted predictive capabilities of stability during deformation are its major drawbacks. Under such circumstances, finite element method (FEM) can be considered to be most reliable both for analyzing complex geometries and criticality involved in the manufacturing process [2].

In the present study, FEM simulation of superplastic forming process for Ti-6Al-4V sheet into square-shaped box was conducted using ABAQUS®, to analyze actual forming process [3] and to predict the formability of the material into a complex shape. The simulation results were then compared with those obtained with material characteristics from tensile jump test. Special subroutine was linked to FE simulation in order to verify the correctness of the superplastic material characteristics. While performing simulations, it was assumed that the titanium alloy is a rigid-plastic material with isotropic and homogeneous properties, while the die was considered to be a rigid body. FEM analysis was carried out considering constitutive equations based upon Power law equation. Furthermore, in the present research, effects of important factors such as temperature, co-efficient of friction, strain rate sensitivity index upon the optimum forming pressure-time and thickness distribution of rectangular component were analyzed systematically using the FE model. The accuracy and reliability of the FEM model was validated with experimental data, which confirmed the suitability of the finite element approach for modelling superplastic forming of Ti-6Al-4V. Alloy sheet of thickness 1mm and 2mm was used, with temperature ranging from 875˚C to 980˚ C

References

[1] P. Pradeep and S Ayyanar, *Journal of Applied Sciences* **12(10)**, pp. 1048–1052 (2012).

[2] L Carrino and G Giuliano*, International Journal of Mechanical Sciences* **39(2)**, pp. 193-199 (1997).

[3] R K Rayudu, "Superplastic Forming and Diffusion Bonding of Titanium Alloy Ti-6Al-4V," *Ph.D. thesis*, Indian Institute of Technology-Madras, (2014)

Modeling of nickel-based superalloys in a crystal plasticity framework

L. Munk[1], S. Reschka[2], Dr. S. Löhnert[1], Prof. P. Wriggers[1]

[1]. Gottfried Wilhelm Leibniz Universität Hannover, Institut für Kontinuumsmechanik

[2]. Produktionstechnisches Zentrum der Leibniz Universität Hannover, Institut für Werkstoffkunde

Email. munk@ikm.uni-hannover.de

Many commercial nickel-based superalloys, single- or polycrystalline, have one common feature: particles of the $L1_2$-structured γ' phase are embedded into a nickel-matrix. Under loading, these particles give rise to many coupled microstructural effects that range from dislocation interactions, interface phenomena to phase transformations.

The length scale of γ' precipitates is lower by orders of magnitude when compared to the scale of grains. In the context of standard finite element simulations, resolving precipitates within a grain and, at the same time, modeling dozens to hundreds of grains is not manageable on single computer frameworks. In order to approximate the complex behavior of these alloys under loading, modeling must either follow a multiscale or a phenomenological path – the latter is pursued in this work.

A wealth of different material descriptions exist in the literature, in particular for the single crystalline case. Most of these models are based on statistical and physical arguments, though, different flow rules, hardening laws, dislocation density evolutions have been postulated and have successfully captured material behavior [1, 2, 3].

This work focuses on models of polycrystalline alloys under constant load. In the final framework, grains are constituted by a rotation of the glide normal and burgers vector, geometry is generated by Voronoi-tesselation. The mechanical and constitutive equations are solved in a large deformation fully-implicit FE-simulation. This study attempts to compare the models' ability to reproduce macroscopic creep curves.

References

1. J.-B. le Graverend, J. Cormier, F. Gallerneau, P. Villechaise, S. Kruch, J. Mendez, «A microstructure-sensitive constitutive modeling of the inelastic behavior of single crystal nickel-based superalloys at very high temperature», *International Journal of Plasticity* **59**, pp. 55-83 (2014).

2. M. Shenoy, Y. Tjiptowidjojo, D. McDowell, «Microstructure-sensitive modeling of polycrystalline IN 100», *International Journal of Plasticity* **24**, pp. 1694-1730 (2008).

3. B.F. Dyson, «Microstructure based creep constitutive model for precipitation strengthened alloys: theory and application», *Materials Science and Technology* **25**, pp. 213-220 (2009).

Creep of Mo-Si-B-Al-Ge alloys at ultra-high temperatures

P. Kellner[1], R. Völkl[1], U. Glatzel[1]

[1]Metals and Alloys, University Bayreuth, Germany

Email. peter.kellner@uni-bayreuth.de

At high temperatures metallic materials deform by creep under a constant load. For ultra-high temperatures above the temperature limit of superalloys refractory metals and their alloys in general and Mo-Si-B alloys in particular show great potential. Alloying with Zr [1] or / and Ti [2] is used to improve the creep properties of Mo-Si-B alloys. Though most of these studies are based on compression creep tests. In addition commonly applied powder metallurgy manufacturing processes provoke formation of internal SiO_2 due to relatively high oxygen contents.

Little is reported in literature about Mo-Si-B alloys prepared by melting metallurgy. G. Hasemann et al. [3] directionally solidified a near-eutectic Mo-17.5Si-8B alloy consisting of Mo_{ss}, Mo_3Si and Mo_5SiB_2 by zone melting (ZM) achieving a remarkably low SiO_2 content. However a comparison of high temperature mechanical properties of melted and sintered alloys is missing. Therefore high temperature tensile creep tests of spark plasma sintered as well as argon arc melted specimens are performed in this work.

4 and 5 components Mo-9Si-8B-xAl-yGe (x = 0, x = 2; y = 0, y = 2; all concentration are given in at.%) alloys are investigated. Aluminum and germanium are added in order to reduce the melting points. All alloys are three phase, a Mo solid solution (α-Mo) and two intermetallic phases Mo_3Si (A15) and Mo_5SiB_2 (T2). Alloys are homogenized and coarsened by a subsequent heat treatment for 24 h at 1850 °C under vacuum. Microstructures are investigated using SEM, EDS, WDS, XRD, XRF and ICP analysis. Tensile creep tests on miniature specimens are performed at 1250 °C up to 1400 °C and stresses from 50 MPa up to 250 MPa with a proprietary creep testing device under vacuum of $8 \cdot 10^{-4}$ Pa.

Specimens produced by argon arc melting show superior creep properties compared to specimens produced by powder metallurgy. Much higher grain sizes of the former are identified as the main reason for the better creep properties, shown in Figure 1. Doubling the grain size of the microstructure results in a 10 times lower minimum creep rate.

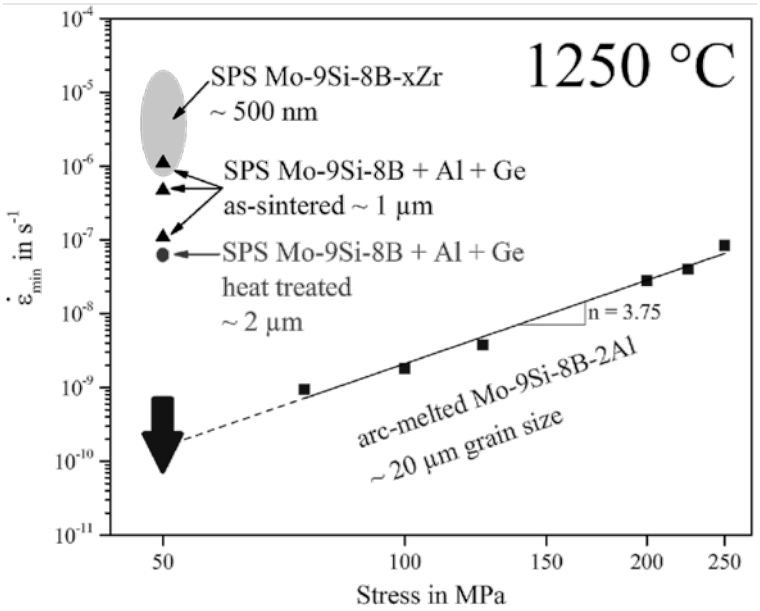

Figure 3. Grain size effect on the minimum creep rate.

References

1. C. Hochmuth, D. Schliephake, R. Völkl, M. Heilmaier, U. Glatzel, Influence of zirconium content on microstructure and creep properties of Mo-9Si-8B alloys, *Intermetallics* **48**, pp. 3–9 (2014)

2. M. A. Azim, D. Schliephake, C. Hochmuth, B. Gorr, H.-J. Christ, U. Glatzel, M. Heilmaier, Creep-Resistance-and-Oxidation-Behavior-of-Novel-Mo-Si-B-Ti-Alloys, *Journal of the Minerals Metals & Materials Society* (JOM) **67**, pp. 2621–2628 (2015).

3. G. Hasemann, I. Bogomol, D. Schliephake, P. I. Loboda, M. Krüger, Microstructure and creep properties of a near-eutectic directionally solidified multiphase Mo-Si-B alloy, *Intermetallics* **48**, pp. 28–33 (2014).

Role of non-random metal site occupation in the formation stability of γ-$Cr_{23-x}Fe_xC_6$ (x = 0–3) carbide phases by high resolution TEM and *ab initio* calculations

M. Souissi [1], T. Matsunaga[1,2], R. Sahara[1], M. H. F. Sluiter[3], M. Tabuchi[1], M. J. Mills[2]

[1]. Computational Structural Materials Design group, Research Center for Structural Materials, National Institute for Materials Science,1-2-1 Sengen, Tsukuba, Ibaraki 305-0047, Japan.

[2]. Department of Materials Science and Engineering, The Ohio State University, Columbus, OH 43221, USA.

[3]. Department of Materials Science and Engineering, Delft University of Technology, Mekelweg 2, 2628 CD Delft, The Netherlands.

Email. SOUISSI.Maaouia@nims.go.jp

Nano-sized precipitates such as γ-$M_{23}C_6$ play a crucial role in the physical properties of high Cr heat resistant steels. The creep resistance of the steels strongly depends on the carbide composition, stability and distribution [1]. Although there are some theoretical works on the phase stability and the electronic structures in γ-$M_{23}C_6$ [2-3], their formation mechanism and stability are still unclear. The γ-$M_{23}C_6$ crystal is a face centered cubic (fcc) structure, with space group (*Fm-3m*). The supercell contains four ($M_{23}C_6$) unit cells consisting of 92 metal atoms occupying four inequivalent metallic sites, namely, 4a, 8c, 32f, and 48h sites and 24 non-metallic sites on 24e sites, using Wyckoff notations (*see* Fig.1(a)). The stability of these precipitates is very sensitive to the site occupancy of metal atoms and their magnetic setting in multicomponent systems [4]. Herein, first-principles calculations have been performed to study those effects on the stability of γ-$Cr_{23-x}Fe_xC_6$ (x = 0–3), in Cr-rich region.

Calculations using supercell technique within the density functional theory (DFT) based on the plane-wave method (PAW) were performed for describing the ion interactions, using Vienna ab initio Simulation Package (VASP). A spin-polarized magnetic approach with generalized gradient approximation (GGA) formulated by Perdew, Burke, and Ernzerhof (PBE) was employed for the exchange and correlation energy terms.

The formation stability of the precipitate is deduced by accounting the formation enthalpy, ΔH_f (meV/atom), given by the following formula whereby the zero-point vibration contribution is ignored:

$$\Delta H_f = \left[E(M_mC_n) - \left(mE(M) + nE(C)\right)\right] / \left(m+n\right) \quad (1)$$

where the first term on right-hand site is the total energy of the precipitate. While, the second and third terms are the total energies of elemental solids α-Fe [5], α-Cr, and graphite [5]. *m* and *n* are the number of metal and carbon atoms, respectively.

Figure 1(b) shows the results of the formation enthalpy of γ-$Cr_{23-x}Fe_xC_6$ (x = 0–3) as a function of Fe content and site occupation. As annotation, for each configuration we indicate the number of Cr sites which are substituted by Fe atoms, with superscripts to indicate the substituted sites. For example, the configuration ($4Fe^{(4a)}$+ $4Fe^{(48h)}$) has 4 Fe

atoms in 4a sites and 4 Fe atoms in 48h sites. We found that iron did not randomly substitute chromium on the four independent metal atom sites. The formation enthalpy of γ-$Cr_{23}C_6$ is higher than the lowest formation enthalpy of γ-$Cr_{22}Fe_1^{4a}C_6$, about –73.7 meV/atom. This value is quantitatively within the experimental enthalpy range. Iron prefers to substitute to chromium 4a site, consistent with early works [2,3,6]. However, for x > 1, iron atoms began to enter 48h sites, followed by 32f. The 8c are last-substituted sites. Details of the lattice distortion, the electron density distribution and the

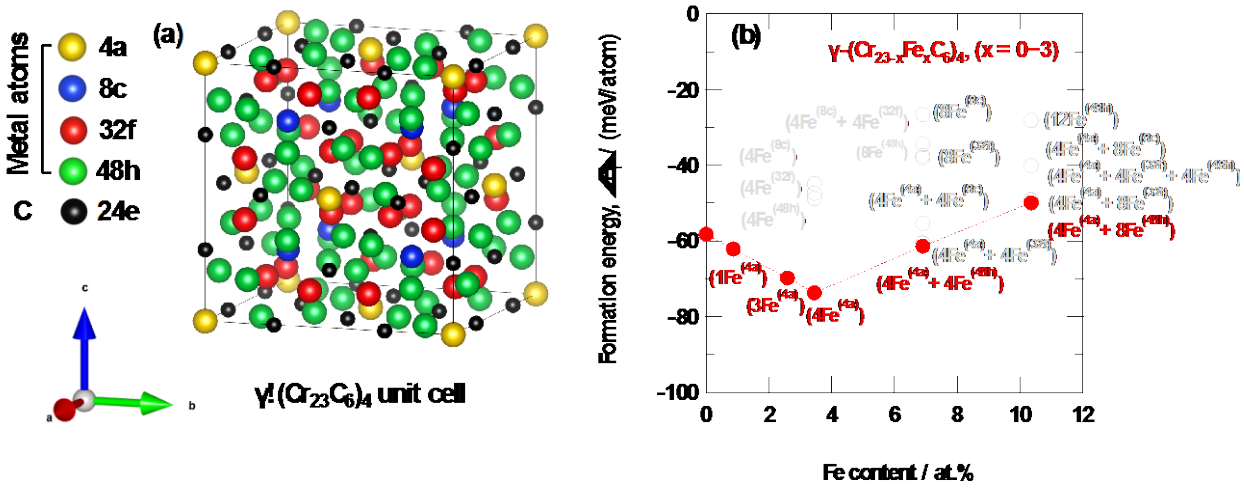

magnetic transition state will be presented.

Figure 1. (a) The unit cell, and (b) the formation enthalpy of γ-$Cr_{23-x}Fe_xC_6$ (x = 0–3) as function of Fe content and site occupation. Filled circles indicate the most stable configurations.

References

[1] T. Matsunaga *et al., Mater. Sci. Eng. A* **655**, pp. 168–174 (2016).

[2] J. J. Han *et al., J. Phys. : Condens. Matter* **24**, pp. 505503 (2012)

[3] N. I. Medvedeva *et al., Comput. Mater. Sci.* **96**, pp. 159–164 (2015)

[4] R. Sahara *et al., Metall. Mater. Trans.* **47A**, pp. 2487–2497 (2016).

[5] M. Souissi *et al., Comput. Mater. Sci.* **124**, pp.249-258 (2016).

[6] C. Fang *et al., Acta Mater.* **103**, pp. 273–279 (2016).

Creep behavior of newly developed Fe-Al-O powder based alloy

S. Fintová, I. Kuběna, Milan Jarý, Natália Luptáková, Tomáš Záležák, Luděk Stratil, Filip Šiška

Institute of Physics of Materials, Academy of Sciences of the Czech Republic v. v. i., Žižkova 22, 616 62 Brno, Czech Republic

Email. kubena@ipm.cz, siska@ipm.cz

Newly developed Fe-Al-O powder based alloy was produced at the Institute of Physics of Materials AS CR. The experimental alloy was prepared from Fe and Al powders with the purity of 99 % (11 wt. % of Al in 3 kg mass) by milling for 4 weeks in an oxygen atmosphere. The prepared material was encapsulated into the tubular container in Argon atmosphere. The tube was rolled at 900°C to form the plate of the thickness of 7 mm. The steel container was removed by machining after processing.

Three different types of heat treatment were applied to improve mechanical properties of material. Fine grained microstructure (300 - 500 nm) is characteristic for a basic state of the material and the material state after the annealing at 1100°C for 3 and 24 h, Fig. 1a-c. Grain coarsening resulting in final bimodal microstructure containing also 100 - 500 μm grains was observed after annealing at 1200°C for 24 h, Fig. 1d. Dispersed oxides particles were observed in the microstructure. The oxides were introduced into the microstructure due to the chemical reaction of the milled powder with the oxygen atmosphere.

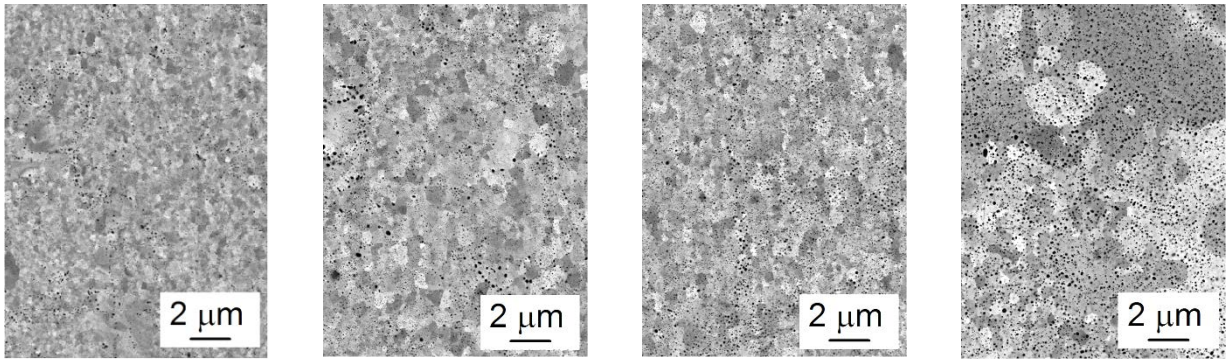

a) basic state *b) 3 h / 1100 °C* *c) 24 h / 1100 °C* *d) 24 h / 1200 °C*

Fig. 1 Typical microstructure of the developed Fe-Al-O alloy

Creep tests were performed at 800°C in tensile loading mode applying 60 % of the proof stress value measured at 800 °C. The loading axis of specimens was parallel to the rolling direction.

Results: Similar creep behavior was observed for the basic state and the material treated at 1100 °C, Fig. 2 and Table 1. Creep behavior was improved by annealing for 24 h at 1200 °C, Fig. 2 and Table 1.

Table 1 Creep characteristics of the developed Fe-Al-O alloy

specimen	loading [MPa]	time to fracture [h]	average secondary creep rate [h^{-1}]	creep fracture strain [%]
basic state	96.6	17.44	5×10^{-4}	2.00
3 h / 1100 °C	70.8	20.63	9×10^{-4}	3.42
24 h / 1100 °C	60.0	32.49	9×10^{-4}	4.97
24 h / 1200 °C	52.2	306.72	3×10^{-5}	2.05

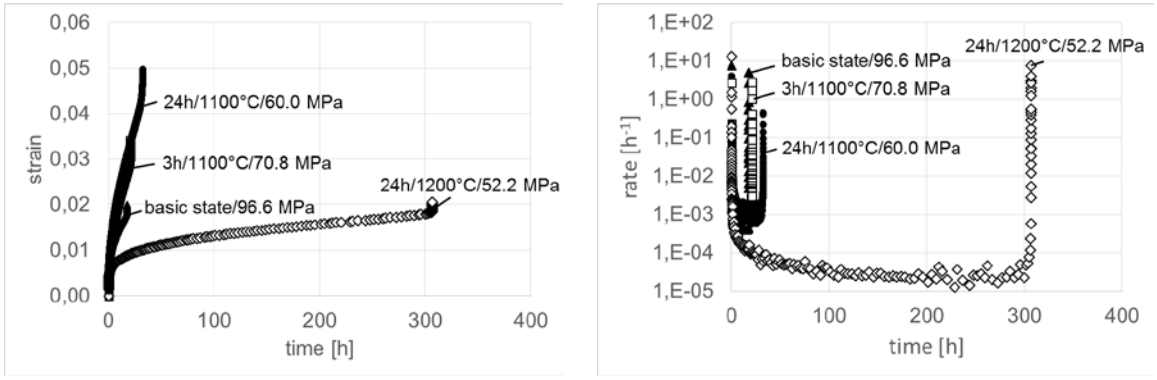

a) creep strain *b) creep rate*

Fig. 2 Creep behavior of the developed Fe-Al-O alloy

The damage mechanism of the specimens subjected to the creep tests is shown in Fig. 3. No diffusion based cavitation mechanism was observed in the specimens polished gauge length. Present defects were created due to the tensile loading applied during the creep test. Cavities were created due to the material decohesion on the oxides/metallic matrix interface. Cavities coalescence and consequently defects growth occurred during the progress of the creep test. The presence of defects corresponds to observation of the fracture surfaces of all the tested specimens (see Fig. 4). The mechanism was the same for both materials, the fine grained material and the material with bimodal microstructure.

a) basic state *b) 24 h / 1200 °C*

Fig. 3 Damage mechanism of the developed Fe-Al-O alloy during the creep test

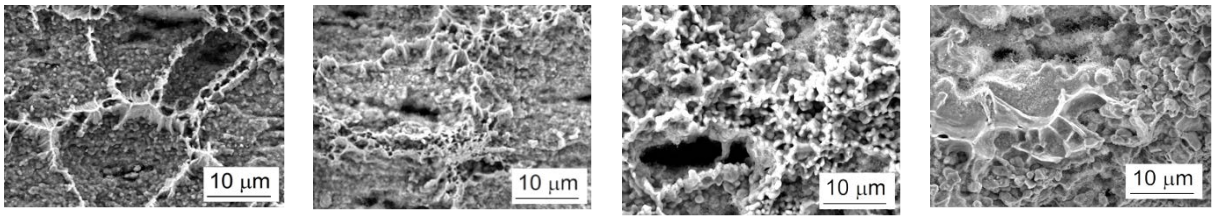

a) basic state *b) 3 h / 1100 °C* *c) 24 h / 1100 °C* *d) 24 h / 1200 °C*

Fig. 4 Fracture surface of the developed Fe-Al-O alloy specimens after the creep test

Conclusions: The newly developed fine grained Fe-Al-O powder based alloy strengthened by dispersed oxides is characteristic by low creep properties. Creep behavior of the experimental alloy was improved due to the heat treatment at 1200°C for 24 h resulting in grain coarsening. No diffusion caused cavitation mechanism was observed. Cavitation creation, connection and following defects growth due to the tensile loading was the reason for specimen failure during the creep tests for all the tested specimens.

Acknowledgement: This study has been supported by the Czech Science Foundation via the project 15-21292Y.

Double Shear Creep Testing of Single Crystal Ni-Base Superalloys

D. Bürger[1], X. Wu[1], P. Wollgramm[1], A. Dlouhy[2], G. Eggeler[1]

[1].*Institut für Werkstoffe, Ruhr-Universität Bochum, 44801 Bochum, Germany*

[2]. *Institut of Physics of Materials, ASCR, Žižkova 22, 616 62 Brno, Czech Republic*

E-mail: david.buerger@rub.de

In the present work we study the shear creep behavior of single crystal Ni-base superalloys (SXs). Shear testing is attractive because it allows to directly activate specific crystallographic slip systems, which facilitates the investigation of elementary deformation processes. Moreover, it represents a simple case of multiaxial loading (σ_1=-σ_3, σ_2=0) and can be exploited to validate reference stress procedures. Double shear creep testing has a number of advantages over other shear test techniques and it has been used at several occasions to study creep of engineering materials [e.g. 1-3]. The specimen consists of two outer loading wings and an inner central loading grip. In between are two shear zones which deform in parallel. The shear stress is introduced by pulling the two bottom surfaces of the outer loading sections upwards while simultaneously pushing the top surface of the central loading section in the opposite direction.

In the present work we use double shear creep testing to contribute to the discussion on the formation of planar faults during low temperature and high stress creep. For this purpose we compare the creep behavior of the macroscopic crystallographic <11-2>{111} and <01-1>{111} shear systems, which differ in the activation of the underlying microscopic slip systems. It turns out that the <11-2>{111} shear systems deforms significantly faster than the <01-1>{111} system. This is due to the fact that two dislocation families are required to initiate the cutting of the γ'-phase by planar faults []. In the case of <11-2>{111} shear testing the two dislocation families have similar large resolved shear stresses, while in the case of the <01-1>{111} system only one dislocation family experiences sufficient mechanical driving force. The results of the present work contribute to a better understanding of the processes which govern the "opening of the Rae window" [4,5] during the early stages of low temperature and high stress creep.

References

1. C. Mayr, G. Eggeler, G.A. Webster, G. Peter, *Mat. Sci. Eng. A* **199**, pp. 121-130 (1995)

2. G. Eggeler, *Material Science and Technology* **25,** 236-241 (2009)

3. G. Kaustrater et al., *Creep and Fracture of Engineering Material and Structures,* pp. 207-217 (2001)

4. G.L. Drew, R.C. Reed, K. Kakehi, C.M.F. Rae, *Superalloys 2004,* pp. 127-135 (2004)

5. X. Wu et al., *Acta Materialia* **112,** pp. 242-260 (2016)

Uniaxial Creep of Superalloy Single Crystals – On Microstructural and Crystallographic Scatter and the Effect of Pre-Exposure and Different Thermo-Mechanical Treatments on Creep

P. Wollgramm[1], B. Ruttert[1], D. Bürger[1], L. Heep[1], A. B. Parsa[1], G. Eggeler[1]

[1].Institut für Werkstoffe, Ruhr-Universität Bochum, 44801 Bochum, Germany

E-mail: philip.wollgramm@rub.de

In the present work we present novel uniaxial creep results on the mechanical behavior of single crystal Ni-base superalloys (SXs) at elevated temperatures. A miniature creep test technique is used which allows to apply tensile loads in precise crystallographic directions [1], [2]. To establish common ground, a short introduction into special aspects of miniature creep testing and overview of the creep behavior in the entire stress and temperature range relevant for SXs is given. The different deformation scenarios which govern the microstructural evolution in the different stress and temperature regimes are briefly summarized.

Special emphasis is placed on some technologically important aspects which are not widely covered in the open literature. Thus, it is shown how creep properties scatter when specimens are taken from different positions of a cast and heat treated laboratory plate [3]. It is shown how creep properties vary when specimen orientations deviate from targeted directions (like for example <100>). We also present preliminary results on the effect of a HIP treatment on creep properties [4].

References

1. Malzer, G., et al., *Miniature specimen assessment of creep of the single-crystal superalloy LEK 94 in the 1000 degrees C temperature range.* Metallurgical and Materials Transactions a-Physical Metallurgy and Materials Science, 2007. **38a**(2): p. 314-327.

2. Wollgramm, P., et al., *The effect of stress, temperature and loading direction on the creep behaviour of Ni-base single crystal superalloy miniature tensile specimens.* Materials at High Temperatures, 2016. **33**(4-5): p. 346-360.

3. Parsa, A.B., et al., *Advanced Scale Bridging Microstructure Analysis of Single Crystal Ni-Base Superalloys.* Advanced Engineering Materials, 2015. **17**(2): p. 216-230.

4. Mujica Roncery, L., et al., *On the Effect of Hot Isostatic Pressing on the Creep Life of a Single Crystal Superalloys* Advanced Engineering Materials, 2016. **18**(8): p. 1381-1387.

Examination of thermo-physical properties and strain rate behaviour of honeycomb alloys to study the effect of rub in in outer air seals

Sonun Ulan kyzy[1], Oliver Munz[2], Tim Fischer[3], Uwe Glatzel[1]

[1] Metals and Alloys, University of Bayreuth, 95447 Bayreuth Bavaria, Germany

[2] Institute of Thermal Turbomachinery, Karlsruhe Institute of Technology, 76131 Karlsruhe Baden-Württemberg, Germany

[3] Institute of Materials Science and Mechanics of Materials, Technical University of Munich, 85748 Garching Bavaria, Germany

Email. sonun.ulan-kyzy@uni-bayreuth.de

Overall, efficiency of gas turbines is closely associated with sealing systems between rotor and stator. Most widely used are labyrinth seals with honeycomb liners, which allow for minimum leakage and tolerate rub events. During rubbing wear should only occur on the honeycomb side, to avoid severe damage. Therefore it is important to study wear mechanisms and microstructure changes in the honeycomb structure. Complex stress, strain and temperature loadings in jet engines hinder the analysis of the main influencing parameters on wear of honeycomb seals.

In this study we build up thermo-mechanical deformation on typical honeycomb sheets with a servo-hydraulic tensile machine and we will in future compare with results of a rub in test rig. Tests with various strain rates (from 10^{-2} to 10^{2} 1/s) and within a broad temperature range (from room temperature to close to the melting point) help us to determine relations between deformation and microstructure of the typical honeycomb alloys Haynes 214 and Hastelloy X. Furthermore, the microstructure of the test specimen is compared to out of service honeycomb liners from an engine. Microstructure examination of tensile specimens and honeycomb seals we carried out using SEM, EDX and EBSD.

The study reveals that, available published data poorly describe thermo-physical properties of honeycomb alloys. After an extensive quantitative study of physical properties on thin walled honeycomb alloys we observed a characteristic phase of transformation of temperatures until close to the melting point. Thermo-physical properties of alloys were studied by using: Laserflash, Dilatomery, DSC and elastic constants determined by Resonant Ultrasound Spectroscopy.

Based on these experimental data we aim to build a multiscale finite element model of rub in order to predict wear of honeycomb seals.

The influence of thickness on the creep behavior of the thin-walled cylindrical sample of nickel-based single crystal superalloys

X.M. Wang, X.Z. Wang, Y. Wang, Y.Y. Hou, L. Li, Z.F. Yue

School of Mechanics, Civil Engineering and Architecture, Northwestern Polytechnincal University, Xi'an 710072, China
Email:wangxinmei@nwpu.edu.cn

The creep behavior of Nickel-base single crystal alloy is one of the key features for the application of gas turbine blades which must withstand very high temperatures. In order to achieve high firing temperature and high-efficiency gas turbine engines, cooling technology is usually introduced during the blade design. The wall thickness of the blade is small to get good cooling efficiency. At most part of the blades, the wall thickness is less than 2mm and it can be as small as 0.5mm at some positions. It is known that thickness debit takes place when the specimen thickness is less than 2.0mm in nickel-based single crystal superalloys. Therefore, the influenced of the thickness on the creep behavior of the cooled turbine blade is studied with a thin-walled cylinder to simulate the structure of the blade. Temperature gradient caused by the cooled air from the inside surface of the blade is also considered.

Three models with the same internal diameter and different outer diameters are analyzed. The wall thicknesses are 0.5 mm, 1.0 mm and 2.0 mm. Firstly, the flow-field analysis was performed using software CFX to obtain the temperature distributions. The boundary conditions were set according to the service conditions of the turbine blades. Then the creep behavior of the three samples was simulated using a damage model developed from Kachanov-Rabotnov damage equations with the consideration of cavitations and degradation of material together. The model was implemented into UMAT of software ABAQUS. The material parameters were calibrated at several temperatures by comparing the simulation results and experimental results. The material parameters at other temperatures were obtained by interpolation method during the calculation. Results show that the temperature gradient decreases with the increases of the wall thickness. Stress redistribution takes place due to the temperature gradient. After 160h creep, the von Mises stress and maximum shear stress are larger at the lower temperature position, i.e. the inside of the cylinder. However, the cavitation damage is larger at the high temperature position, i.e. the outside of the cylinder. The crack initiation time increases with the increase of the wall thickness, which imply that the crack is easy to occur from the position with small wall thickness in the blade.

STEELS

Aging effect on creep properties of type 310 austenitic stainless steel during isothermal and non-isothermal creep tests at 870°C. Experiments and modelling.

C. Parrens[1], J.-L. Dupain[2], B. Malard[1], D. Poquillon[1]

[1]. CIRIMAT ENSIACET, 4 Allée Emile Monso, BP44362, 31030 Toulouse, France

[2]. Safran Landing Systems, Safran group, 9 Rue Guynemer, 64400 Bidos, France

Email. coralie.parrens@ensiacet.fr

310 sample removed from heat treatment furnaces intern parts after 500h of service evidenced high sigma phase contents, up to 12%, and unusual creep strain. Given the significant microstructure evolution due to phase transformations $\delta \rightarrow \sigma$ and $\gamma \rightarrow \sigma$ at 870°C, the aim of this study is to explore aging effects on the mechanical behavior, especially viscoplasticity. Sigma phase is an inter-metallic phase composed mainly of iron and chromium, which forms in austenitic stainless steels during exposure at the temperature range 500°C to 950°C [1, 2]. Usually, this precipitation causes a loss of ductility and toughness, so that it is involved in numerous industrial issues [3-6].

The studied components are parts of thermal treatment furnaces. So they endure a succession of thermal cycles of 2h between room temperature and 870°C, including quenching. Due to the loading and to the temperature, these devices are submitted to creep. Therefore, the mechanical behavior at high temperature of this alloy is investigated. Many data are available in the literature about isothermal creep [7] but few take into account the effects of thermo-mechanical cycles and microstructure evolution due to aging.

Samples are extracted from real component after 257 in-service cycles, corresponding to 514h = 21.4 days. They exhibit higher σ phase content than expected by thermodynamic predictions, and isothermal contents measured after a 60 days long heat treatment at 870°C. The critical effect of thermal cycles on σ phase kinetic of precipitation was evidenced through σ phase quantification on isothermally and anisothermally heat treated samples. The effect of thermal cycling on nucleation and growth on □phase particles was investigated.

In addition to metallurgical characterizations, mechanical characterizations are carried out: RFDA, tensile tests and creep tests at 650°C, 780°C and 870°C. As-received material and materials after various aging treatment, and so different □phase contents, are investigated.

Not only the Young modulus and the yield strength are modified. They increase due to aging, but more surprising, creep rates increase as illustrated in (1). This result is investigated for different loading and 3 temperatures.

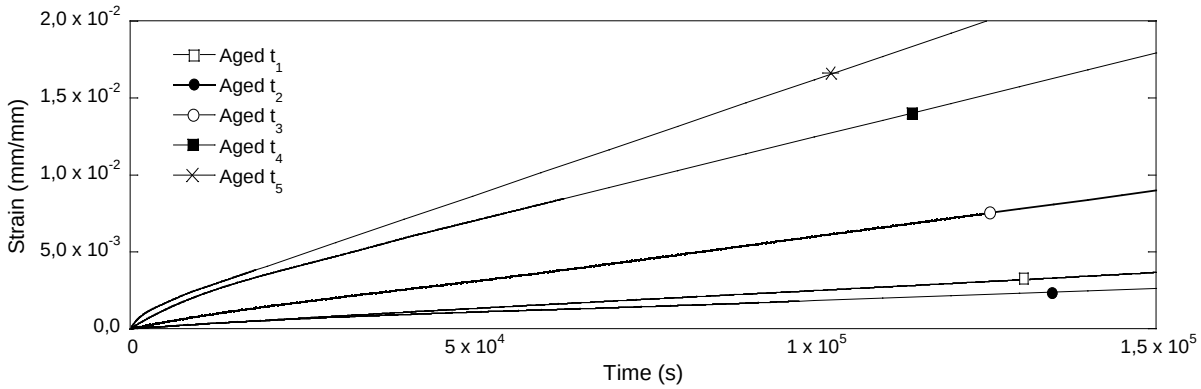

Figure 1: Effect of metallurgical aging on creep tests at 870°C for □ = 15MPa (t_1<t_2<t_3<t_4<t_5)

Associating mechanical tests results to the measured σ phase kinetic, we are able to propose a model to predict creep strain rates of 310 stainless steel into in service conditions, taking into account metallurgical evolution during anisothermal and isothermal aging.

References

1. D.M.E. Villanueva et al., *Materials Science and Technology* **22**(9), pp. 1098-1104 (2006).

2. A. V. Kington and F.W. Noble, *Materials Science and Technology* **11**(3), pp. 268-275 (1995)

3. J. Brozda and J. Madej, *Engineering Failure Analysis* **15**, pp. 368-377, (2008).

4. A.Y. Al-Kawaie and A. Kermad, *Saudi Aramco Journal of Technology*, (2011).

5. A.V. Kington and F.W. Noble, *Materials Science and Engineering A* **138**, pp. 259-266, (1991).

6. E. O. Hall and S.H. Algie, *Metallurgical Reviews*, **11**(1), pp. 61-88 (1966).

7. Nickel Development Institute, A.I.S.I., *High-Temperature Characteristics of Stainless Steels*, in *A Designers' handbook series*. 2011.

Substructural evolutions accelerated by 2D grain boundary sliding in ODS ferritic steel

H. Masuda[1], H. Tobe[1], E. Sato[1], Y. Sugino[2], S. Ukai[3]

[1]. Institute of Space and Astronautical Science, Japan Aerospace Exploration Agency

[2]. Kobelco Research Institut,. Inc.

[3]. Hokkaido University

Email: masuda.hiroshi@ac.jaxa.jp

Introduction

Grain boundary sliding (GBS) is well known as one of the most important deformation modes during creep in polycrystalline materials. Although GBS is generally considered to be accommodated by lattice or grain boundary diffusion, it can accelerate dislocation activities and substructural evolutions in the transient regime between GBS creep and dislocation creep [1]. The aim of this study is to characterize the interaction among GBS, dislocation activities and substructural evolutions in a 2D model material, oxide-dispersion-strengthened (ODS) ferritic steel which causes an ideal 2D GBS due to an anisotropic grain structure [2].

Experimental

A rolled sheet of 15Cr–ODS ferritic steel (Fe–15Cr–0.03C–2W–3.8Al–0.32Zr–0.12Ti–0.35Y_2O_3) was annealed at 1423 K for 4 h to obtain a recrystallized microstructure with the anisotropic grains elongated and aligned in the rolling direction (RD). Figure 1a and b show a shear test specimen made by electric discharging and 2D GBS occurs in shear perpendicular to the grain longitudinal direction. As shown in Fig. 1c, surface markers were drawn by focused ion beam (FIB) on the RD plane to detect GBS. The post-FIBed specimens were crept in shear until fracture at 1173 K under vacuum (< 10^{-3} Pa) with constant loads. After the shear tests, the microstructure was observed by scanning electron microscopy (SEM), electron back-scattered diffraction (EBSD) and electron channeling contrast imaging (ECCI) to evaluate the deformation mechanisms.

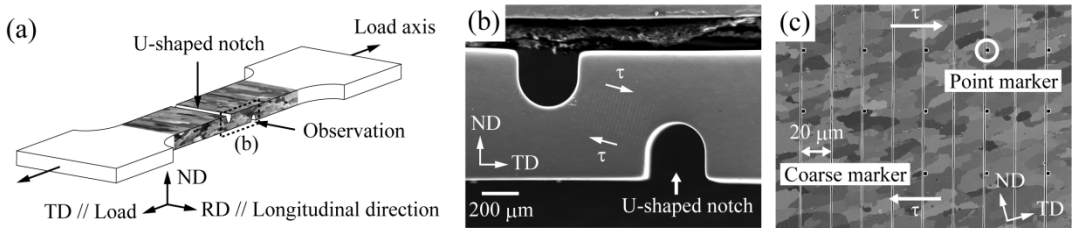

Figure 1 (a) Schematic of a shear test specimen and (b) (c) SEM images on the RD surface.

Results

Figure 2 shows a relation between strain rates and stresses. The stress exponent, *n*, changed around 50 MPa, which might correspond to the transient regime between GBS creep (region II, $n \sim 3$) and dislocation creep (region III, $n \sim 12$).

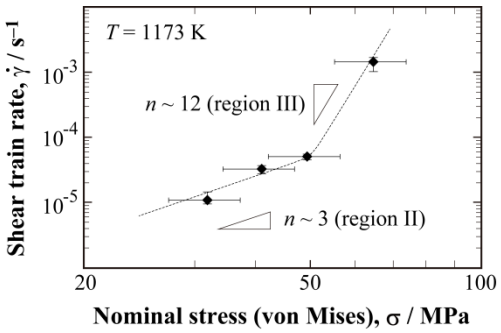

Figure 2 Shear strain rate *vs.* nominal von Mises stress at 1173 K.

Figure 3 shows an equivalent microstructure before and after deformation to 11.4% in region III (1173 K, 63 MPa), where GBS was frequently observed in spite of the increase in *n* value, contrary to expectations. GBS significantly triggered dislocation activities and accelerated substructural evolutions rather than dislocation creep alone. In Fig. 3b, GBS triggered a slip band belonging to a $[1\bar{1}1]$ $(21\bar{1})$ slip system. In Fig. 3c, on the other hand, GBS triggered sub-boundary formation along {110} planes. Both of these phenomena can be explained by the "Ball–Hutchison model" (Fig. 3d [3]); GBS was relaxed by dislocation activities. In addition, these dislocation activities were followed by different microstructural evolutions (slip bands or sub-boundaries) depending on the angle θ between GBS and dislocation slippage. The slip bands were triggered with small θ, while the sub-boundary formation was triggered and then continuous dynamic recrystallization was accelerated with large θ.

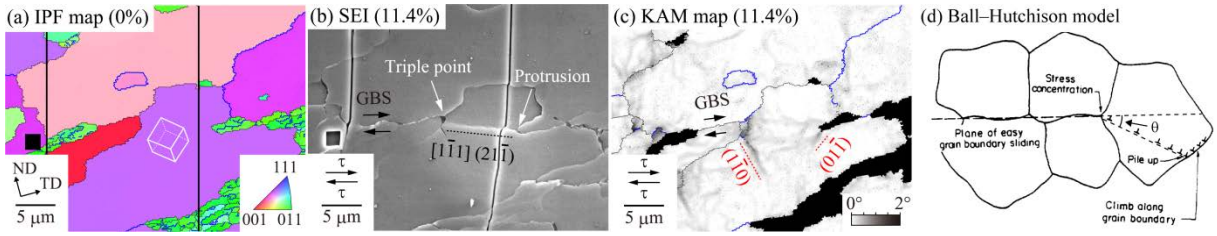

Figure 3 (a) EBSD map before deformation, (b) SEM image and (c) kernel average misorientation (KAM) map after deformation to 11.4% in region III (1173 K, 63 MPa) and (d) schematic of the "Ball–Hutchison model".

Reference

1. H. Masuda, H. Tobe, E. Sato, Y. Sugino, S. Ukai, Acta Mater. 120 (2016) 205–215.

2. H. Okada, S. Ukai, M. Inoue, J. Nucl. Sci. Technol. 33 (1996) 936–943.

3. A. Ball, M.M. Hutchison, J. Met. Sci. 3 (1969) 1–7.

Threshold stress for grain boundary sliding in FeCrAl-ODS steels

S. Ukai[1], R. Kamikawa[1], N. Oono[1], H. Masuda[2], E. Sato[2]

[1]. Materials Science and Engineering, Faculty of Engineering, Hokkaido University

[2]. Institute of Space and Astronautical Science, Japan Aerospace Exploration Agency

Email: s-ukai@eng.hokudia.ac.jp

Introduction

Aiming for preventing hot steam oxidation with Zircaloy cladding and thus significantly improving safety at severe accident in light water reactors (LWR) [1], we have developed FeCrAl-ODS steels with forming stable alumina scale on the cladding outer surface [2]. Creep deformation mechanism of FeCrAl-ODS steel was investigated at 1273 K and at low strain rate of around 10^{-5} s^{-1}, which are simulated condition in loss of coolant accident (LOCA).

Experimental

The FeCrAl-ODS steels containing 15Cr, 6Al and 0.5Y_2O_3 with/without 0.4Zr (mass %) have been manufactured by mechanical alloying (MAing) and hot extrusion of MAed powder at 1423 K. The extruded bars were subsequently cold-rolled with 85 % and annealed at 1423 K for 1 h to obtain a recrystallized microstructure. The creep tests were conducted at 1273 K under argon gas atmosphere at strain rate ranging 10^{-7} to 10^{-2} s^{-1}, corresponding stress level is 20 to 150 MPa. After the creep tests, the microstructure was observed by scanning electron microscopy (SEM), electron back-scattered diffraction (EBSD) and transmission electron microscope (TEM) to evaluate the deformation mechanisms.

Results and discussion

The creep curves at 1273 K have been acquired, and minimum creep strain rates were derived at each stress level. Figure 1 shows the minimum creep strain rate as a function of stress in a double logarithmic diagram. A slop of this curve corresponds to a stress exponent, *n*. For the specimens without Zr addition, *n*–value becomes 5-10 in a Region-III, demonstrating that a deformation is dominated by a dislocation creep mechanism, while approaching 2 for *n*–value in the Region-II suggesting that deformation process changes to grain boundary sliding (GBS) that was verified by step changes of scratch, drawn before creep test, at grain boundaries. With decreasing strain rate and stress, the slop, *n*–value, again slightly increases. This corresponds to Region-I. These behaviors are more obvious for the specimens with Zr addition.

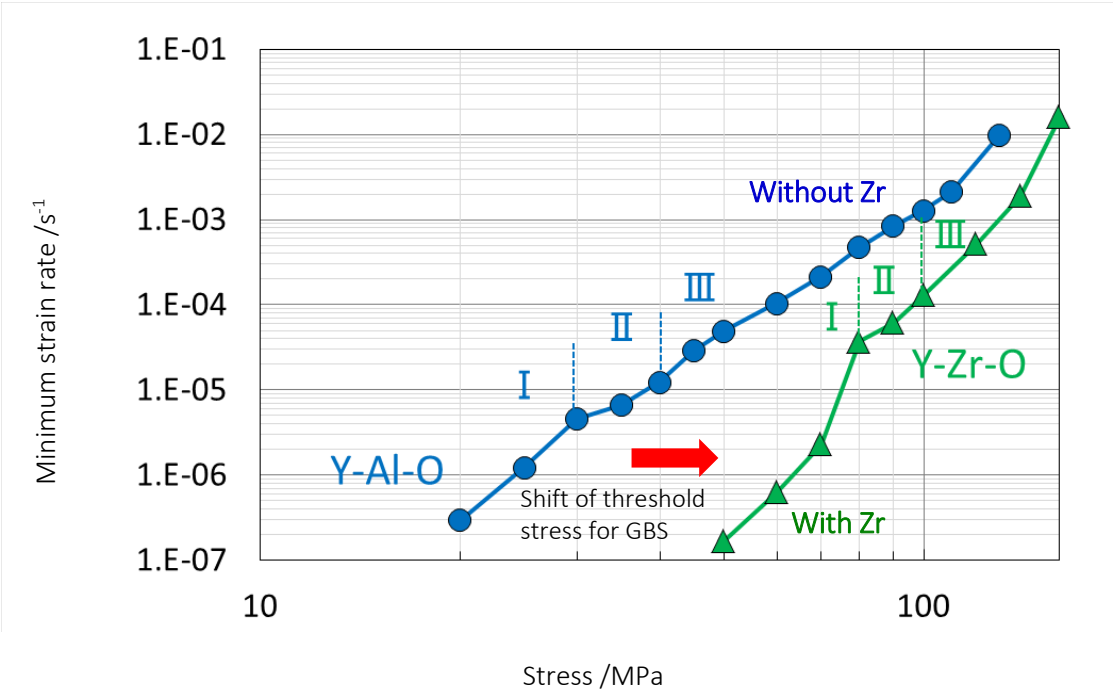

Figure 1 Minimum creep strain rate *vs.* stress at 1273 K for specimens with/without Zr addition, showing Region-I, II and III.

There are several hypotheses for deformation mechanism in Region-I [3]. Considering that Region-II is mainly dominated by GBS, Region-I could be related to a threshold stress for GBS. The specimens without Zr addition contain larger size of Y-Al complex oxide particles, while extremely finer Y-Zr complex oxide particles are formed in the Zr added specimens. An increased number density of the oxide particles by the reduced size distribution leads to the shortened distance between particles in the Zr-added specimens; resultantly results in strongly strengthening a pining force for the moving dislocation. The stress accumulated by GBS at the grain boundary triple junction (GBTJ) should be relaxed by dislocation movement in order to that GBS continuously proceeds. It is considered that stress shift for Region-I toward higher stress in Zr-added specimens is attributed to the increased threshold stress for GBS, because higher stress could be required for dislocation to overcome oxide particles and to relax the accumulated stress at GBTJ.

Reference

1. K.A. Terrani, S.J. Zinkle, L.L. Snead, J. Nucl. Mater., 448 (2014) 420-435.

2. S. Ukai, N. Oono, T. Kaito, T. Torimaru, A. Kimura, S. Hayashi, TOP FUEL 2016, Boise Center, Idaho, USA, Sep. 11-16, 2016.

3. T.G. Langdon, Materials Science and Engineering, A137 (1991) 1-11.

Microstructural evolution in advanced 12Cr steels during creep

C.R. Das and John Hald

Materials and Surface Engineering, Department of Mechanical Engineering

Technical University Denmark

E-mail.crdas@mek.dtu.dk

9-12Cr steels are in use in power plants and heat transport systems due to their very good mechanical properties compared to austenitic stainless steels up to temperature of 620°C and good thermo physical properties. Transformation of MX types of precipitates in to Z phase in these steels during service causes breakdown in creep strength. This calls for development of advance 12Cr steel for 650°C applications. One of the authors had initiated the development of advance 12Cr steel based on Z phase in early 2000. Use of Z phase as a strengthening phase would reduce the thermodynamic driving force which would enhance the microstructural stability.

Chromium increases the kinetics of MX into Z phase transformation whereas carbon decreases this. This calls for reduction in carbon content substantially resulting lower content of $M_{23}C_6$ precipitates. W is added to achieve Laves phase which would provide boundaries strengthening. Ni and Mn have been reduced in these steels whereas Co and Cu have been used to achieve relatively higher A_{c1} transformation temperature. Sudden creep strain (~3%) jump was observed in these steels during tests at 650°C. Reason for this jump is not understood yet and it is necessary to understand the origin of this creep strain jump. Therefore, the objective of the present investigation is to understand the origin of this behavior.
Two 12Cr steels are chosen for the current study. These steels were normalized at 1050°C for 1h followed by tempering at different temperatures. Tempering temperature was selected based on equilibrium A_{c1} temperature of the steel. Creep curves of one of the steels are shown in Figure 1.

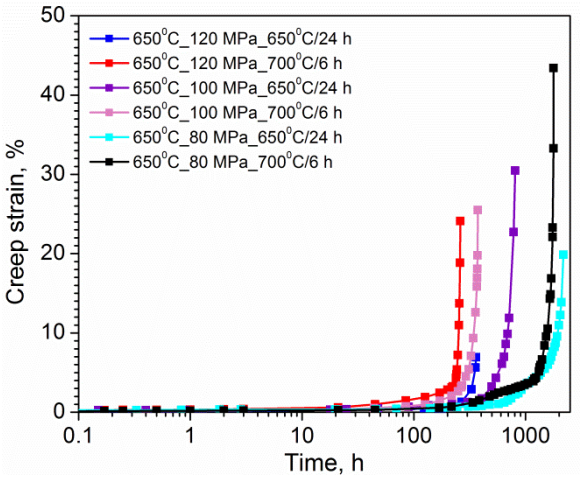

Figure 1: Creep curves of steel 1.

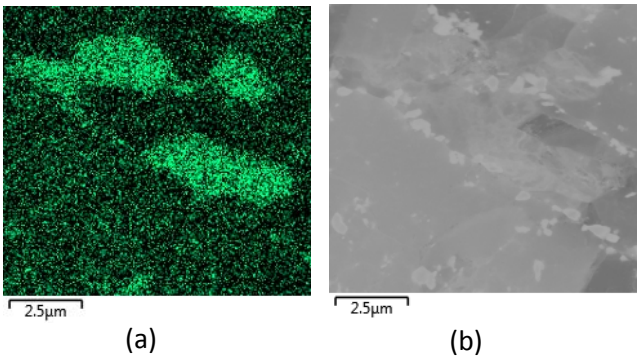

Figure 2: (a) Electron image and (b) Ni map of steel 1.

Energy dispersive spectroscopy (EDS) study of crept specimens (steel 1) reveals partitioning of alloying elements in the microstructure. Partitioning is significant in a specimen which was tested for longer time. Electron image and EDS map of Ni in steel 1 are shown in Figure 2(a,b). In the current paper, microstructure evolution during creep would be discuses to illustrate reason for creep strain jump using optical, scanning electron microscope and transmission electron microscope.

ORIGIN AND NATURE OF CREEP STRENGTH BREAKDOWN IN 9%Cr STEELS

A.Fedoseeva[1], N. Dudova[1], R. Kaibyshev[1]

[1] Belgorod State University, Pobeda 85, 308015 Belgorod, Russia

E-mail: fedoseeva@bsu.edu.ru

9%Cr martensitic steels are used as structural material for elements of fossil power plants working at ultra-supercritical parameters of steam (T=600-620°C, P=25-30 MPa). High creep resistance of these steels is achieved by superposition of substructure strengthening associated with low thickness of laths, long-range stress fields originated from lath boundaries and high density of lattice dislocations with precipitation hardening. Service temperature of these steels is limited by creep strength breakdown which deteriorates long-term creep strength. Analysis of creep strength and microstructural evolution in a P92-type steel, a 3wt.%Co modified P92 steel; and a 3wt.%Co and 1wt.%W modified P92 steel showed that the creep strength breakdown is tertiary creep phenomenon attributed to three process of evolution of microstructure and a dispersion of secondary phases: (i) the transformation of fine V-rich MX carbonitrides to coarse Z-phase particles; (ii) the strain-induced coarsening of $M_{23}C_6$ carbides and the Laves phase particles; (iii) transformation of lath structure to subgrain one. It was shown that these processes take place only in range of long-term-creep and are not observed under short-term creep. In addition, the creep strength breakdown correlates with the depletion of excess W from the solid solution under long-term aging while strain-induced depletion of W is observed under short-term creep.

Role of Ti and Nb on creep rupture properties of stainless steels

F. Abe

National Institute for Materials Science (NIMS), 1-2-1 Sengen Tsukuba 305-0047, Japan

E-mail: ABE.Fujio@nims.go.jp

The creep rupture properties are compared between 9 heats of JIS SUS 321HTB stainless steel (18Cr-10Ni-Ti) containing 0.39 to 0.55 mass % Ti and 9 heats of JIS SUS 347HTB stainless steel (18Cr-12Ni-Nb) containing 0.72 to 0.88 mass % Nb at 600 to 750 ^{o}C for about 100 to 200,000 h in NIMS Creep Data Sheets, by taking the effect of Ti and Nb into account. For the both steels, the heat-to-heat variation in time to rupture is very large of about one order of magnitude difference between the strongest and weakest heats even at a short time of about 100 h to long times exceeding 100,000 h at 600 to 700 ^{o}C. The heat-to-heat variation in time to rupture of the 321HTB is correlated with the heat-to-heat variation in grain size, while that of the 347HTB is mainly explained by the effect of impurity boron. During creep, TiC, $M_{23}C_6$ and σ phase are observed to have precipitated in the 321HTB, while NbC, $M_{23}C_6$ and σ phase have precipitated in the 347HTB. The precipitated $M_{23}C_6$ carbides in the 321HTB became dissolved in favor of further precipitation of thermodynamically more stable TiC carbides in the matrix but not in the 347HTB. The dissolution of grain boundary $M_{23}C_6$ carbides results in the disappearance of grain boundary precipitation hardening, indicating that the grain boundaries act as weak region and that finer the grains, shorter the time to rupture in the 321HTB. In the 347HTB, boron enhances fine distributions of $M_{23}C_6$ carbides along grain boundaries, which enhances the grain boundary precipitation hardening, increasing the time to rupture. The different origins of heat-to-heat variation in time to rupture for the 321HTB and 347HTB is correlated with the different precipitation behavior in the steels during creep.

Creep and Microstructure in Boron Added 9% Chromium Heat Resistant Steel

T. Matsunaga[1,2], H. Hongo[1], M. Tabuchi[1], M. Souissi[1], R. Sahara[1],

H. C. Whitt[2], T. K. Payton[2], W. Zhang[2], M. J. Mills[2]

[1]*National Institute for Materials Science, Tsukuba, Ibaraki 305-0047, Japan*

[2]*Department of Materials Science and Engineering, The Ohio State University, Columbus, OH 43221, USA*

Email: MATSUNAGA.Tetsuya@nims.go.jp

Creep strength of high chromium (Cr) heat-resistant steels in ultra super-critical power generation system is decreased by Type IV fracture at heat-affected zone (HAZ) after welding. To resolve this problem, NIMS developed new 9Cr steels, so-called B added 9Cr steel, with a low amount of boron (B) and nitrogen (N), which showed longer creep rupture time than conventional Gr. 91 steel. The chemical composition of the new steel is Fe-0.12C-0.31Si-0.51Mn-0.001P-0.001S-9.04Cr-<0.01W-0.99Mo-0.21V-0.071Nb-0.011B-0.010N in wt%. Although the welded sample of the new steel also showed longer creep rupture time than that of Gr. 91 steel [1], the strengthening mechanisms not only in base metal but also in welded sample with the addition of B has been unclear. Previous papers claimed that because B segregates to prior austenite grain boundaries (PAGBs), the GB energy and the phase transformation was retarded during welding [2]. However, B was detected in $M_{23}C_6$ near PAGB in other series of B added 9Cr steels [3]. Therefore, the present study focuses on the effect of B on the precipitate and microstructure in base metal and welded sample before and after creep tests at 873 K.

Figure 1 shows a double logarithmic plot of time-to-rupture and applied stress in base metal (circles) and simulated HAZ (rectangles) for the B added 9Cr steel and Gr. 91 steel. For base metal, the B added 9Cr steel shows higher creep strength than the conventional steel. Next, scanning electron microscope observations were performed to evaluate grain boundary coverage by precipitates at PAGBs, and precipitate size distribution in the B added 9Cr steel. Grain boundary coverage was about 30% for the initial condition, then increased up to about 40% until about 1,000 h, and was almost stable after that. Figure 2 shows precipitate size distribution before and after creep tests. Before creep testing, the peak appeared at the size of 0.1-0.15 □m and its number fraction reached about 40%. The peak shifted to larger size and the deviation became large after creep tests. Precipitate size also changed quickly for times less than 1,000 h, but increased slightly at the long time up to about 20,000 h. Although the precipitate morphology changes remarkably in the early stage of creep, it is relatively unchanged during the latter stage of creep. Thus, high microstructural stability might lead to high creep strength in 9Cr steel.

Figure 1 also shows creep rupture time of simulated HAZ samples of each steel at 873 K. Because it is well known that Type IV fracture appears at fine-grained HAZ, the simulated HAZ samples show shorter life time than base metal for both steels. However, creep rupture time in the B added 9Cr steel is seven times longer than that in Gr. 91 steel. Because first-principles calculations showed the stability of $M_{23}C_6$ was

increased by B addition [4], $M_{23}(BC)_6$ might pin the interface migration associated with phase transformation during welding, suppressing grain refinement [5]. Therefore, creep deformation was suppressed at fine-grained HAZ in the B added 9Cr steels, and exhibited increased creep strength compared with Gr. 91 steel after welding.

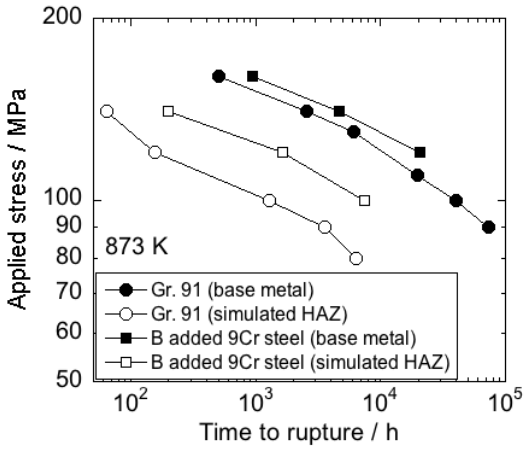

Figure 1. Double logarithmic plot of time to rupture and stress of B added 9Cr steel and Gr.91 steel.

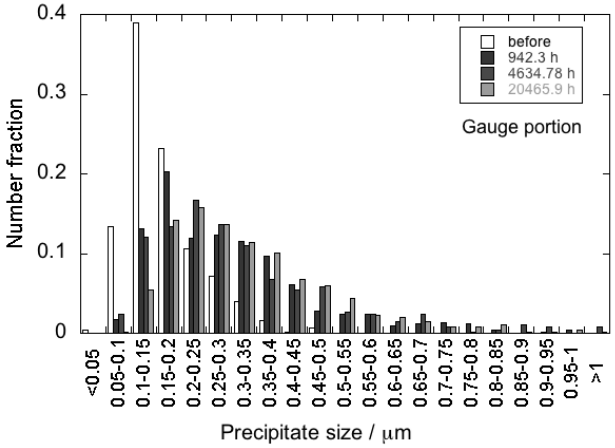

Figure 2. Change of precipitate size before and after creep tests at 873 K in gauge portion of B added 9Cr steel.

Reference

[1] M. Tabuchi, H. Hongo, Y. Takahashi, *J. Soc. Mater. Sci. Japan* **58**, pp. 108-114 (2009).
[2] M. Kondo, M. Tabuchi, S. Tsukamoto, F. Yin, F. Abe, *Sci. Technol. Weld. Join.* **11**, pp. 216-223 (2006).
[3] F. Abe, *Sci. Technol. Adv. Mater*. **9**, 013002 (2008).
[4] R. Sahara, T. Matsunaga, H. Hongo, M. Tabuchi, *Metall. Mater. Trans. A* **47**, pp. 2487-2497 (2016).
[5] T. Matsunaga, H. Hongo, M. Tabuchi, R. Sahara, *Mater. Sci. Eng. A* **655**, pp. 168-174 (2016).

Change in Hydrogen Thermal Desorption Characteristic of Heat Resistant Ferritic Steel with Creep

S. Komazaki[1], H. Yamashita[1], K. Sato[1] and K. Kimura[2]

[1]. Kagoshima University

[2]. National Institute for Materials Science

Email: komazaki@mech.kagoshima-u.ac.jp

It is well known that hydrogen is trapped by a variety of defects and microstructures in steels such as vacancies, vacancy clusters, dislocations, grain boundaries, precipitates, voids and microcracks, and it is easily released from those trap sites by heating. However, the temperature range of hydrogen desorption varies according to the kind of trap sites, because of different binding energy between hydrogen and each trap site. This interesting nature of hydrogen may be available for detecting and evaluating damages accumulated in the steels.

With those points as background, preliminary to the present study, the authors measured the hydrogen evolution curve for the creep ruptured specimens of 9%Cr ferritic steel, Gr.91 (Mod.9Cr-1Mo) steel, using the thermal desorption analysis (TDA). The experimental results revealed that a clear single peak existed on the curve, and the peak height increased significantly as the applied stress decreased resulting in the increase of rupture time [1]. Since this hydrogen thermal desorption characteristic showed almost no variation only by the thermal aging, the above increase in peak height reflected the creep damage. Furthermore, as shown in Fig. 1 [2], the amount of desorbed hydrogen, C_H, increased monotonously with increasing Larson-Miller parameter (LMP), *i.e*., consuming creep life, depending on the stress level. There was an almost linear correlation between the log C_H measured on the creep ruptured and the LMP, which was approximated by "log C_H = 0.39 LMP – 13.4". This was a kind of criterion for creep rupture or fracture, and this equation meant that as far as the C_H did not reach this line, the fracture never occurred.

In this study, the change in hydrogen thermal desorption characteristic of 18Cr-2.5Si steel due to creep was investigated to examine the applicability of hydrogen as a tracer for creep damage evaluation of ferritic heat resistant stainless steel. The hydrogen charging into the interrupted creep specimens with a wide variety of degrees of damage was conducted by means of cathodic electrolysis. Next, the hydrogen-charged samples were subjected to the TDA for measuring the hydrogen evolution curve. The experimental results revealed that the overall shape of curve varied with creep depending on the test conditions as well as Gr.91 steel. However, this change in desorption characteristic reflected not only the creep damage but also the microstructural changes such as precipitation/coarsening of NbC and change in dislocation density. In an attempt to separate their effects on the change in desorption characteristic and extract that of creep damage, the measured curve was decomposed into several small curves by comparison with the curves of thermally aged and solution treated steels. As a result, the amount of desorbed hydrogen, which was likely to be associated with defects like a void and/or vacancy cluster, was found to increase with increasing creep damage, and it was successfully arranged with the parameter derived based on the creep void growth's law.

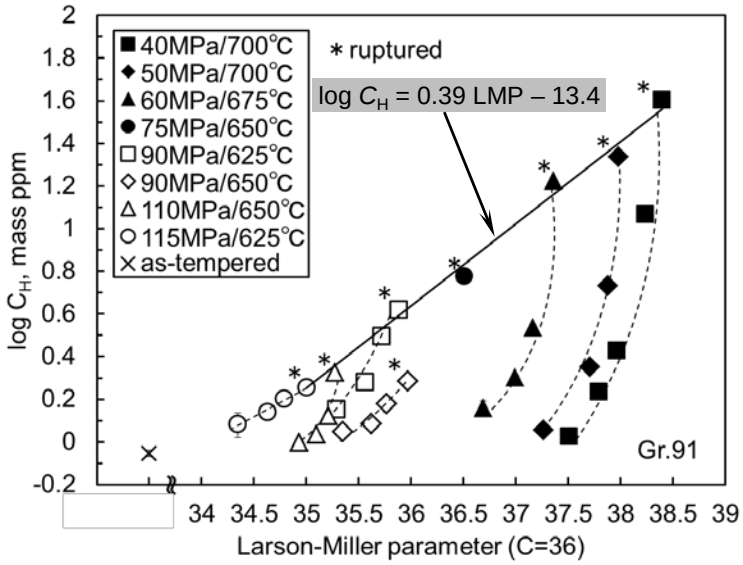

Figure 1. Change in C_H measured on creep specimens of Gr.91 [2].

References

1. S. Komazaki, T. Honda, T. Sakamura, K. Sawada, K. Kimura and Y. Kohno, Tetsu-to-Hagané, Vol.96, 2010, pp.614-619.
2. S. Komazaki, H. Yamashita, M. Yonemura and M. Igarashi, Advances in Materials Technology for Fossil Power Plants, 2013, pp.744-753.

Modelling Creep-Rupture Properties for Austenitic Steels Undergone Neutron Irradiation and High Temperature

A.A. Buchatsky, A.G. Gulenko, B.Z. Margolin

Central Research Institute of Structural Materials "Prometey", Saint-Petersburg, Russia

E-mail: crism@mail.ru

Some structural components of fast reactor with sodium coolant of BN type are undergone high neutron irradiation (~1 dpa/year). Operation temperature of such components corresponds to creep regime of austenitic steels (500-600°C). At present Russian NORM and RCC-MR (A16) code do not allow to calculate damage when creep deformation and neutron irradiation happen simultaneously. Experimental determination of creep rupture properties (CRP) under irradiation may be performed using intra-reactor test results. Such tests are very expensive and may be carried out practically for the short time. That's why approaches for prediction of creep rupture properties under irradiation have to be developed.

The aim of this work is to propose physical and mechanical model for prediction of the irradiation effect on CRP and to construct the design curves.

The proposed model includes equations of nucleation and growth of voids on grain boundaries and uses, as a local fracture criterion, the so-called criterion of micro-plastic collapse or plastic instability of unit cell. It is known that neutron irradiation intensifies the diffusion processes in a material, increases the creep rate and also results in the increase of yield strength. With increasing the yield strength, i.e. strengthening the grain body, the fraction of strain caused by grain boundaries sliding increases and, as a result, the rate of void nucleation on grain boundaries grows. Acceleration of diffusion process increases voids growth rate.

Thus, neutron irradiation accelerates damage caused by grain boundary voids.

The proposed model permits to predict CRP at various temperatures allowing for the influence of irradiation under deformation. For the calibration of the model parameters, the experimental data on CRP without and with neutron irradiation during short time (of order of 100÷1000 hours) were used. On the basis of the proposed model, CRP were calculated for 16Cr-11Ni-3Mo and 18Cr-9Ni steels (Russian analogs of 316 and 304 steels, respectively) for various levels of neutron flux.

Microstructure and creep properties of 9%Cr steel containing boron.

E. Tkachev, A. Belyakov, R. Kaibyshev

Belgorod State University, Pobeda 85, Belgorod, 308015, Russia

Email: tkachev_e@bsu.edu.ru

The creep properties and structural changes under conditions of creep at 650°C of a 0.1C-9Cr-1.5W-0.5Mo-3Co-NbV steel with 13 ppm boron and 7 ppm nitrogen were studied. Creep tests were carried out at 650°C in the stress range of 180 to 100 MPa. The creep rupture strength at 650°C is shown in Figure 1 in comparison with P92 and P92+3%Co steels [1]. The studied steel exhibits a remarkably higher creep resistance than the P92 and P92+3%Co steels.

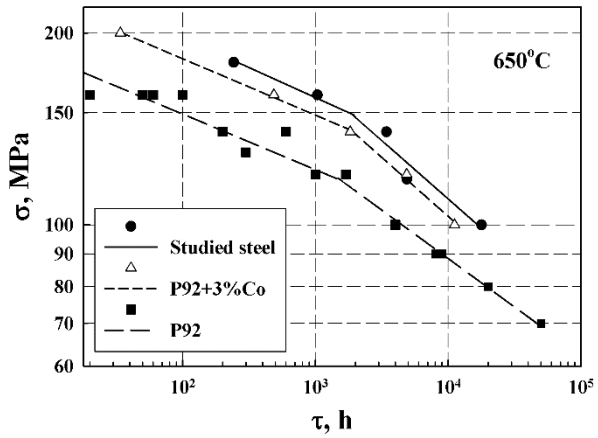

Figure 1. Creep rupture strength of P92, P92+3%Co and studied steels at 650°C

Based on the observations of transmission electron microscopy, precipitates of $M_{23}C_6$ (M=Cr, Fe), MX (M: Nb, V, Ti X: C, N), and Laves phase were identified after creep. Any evidences of BN precipitates were not observed.

The precipitation of relatively coarse particles of Laves phase was observed even after creep for 243 h. The Laves phase particles were observed at high- and low-angle boundaries. The MX-type particles did not change significantly their size during creep. Mainly spheroidal Nb-rich carbonitrides were observed within the martensite laths. The crystallographic investigation revealed specific orientation relationships (OR) between $M_{23}C_6$ carbides and ferrite matrix:

$(110)_\alpha||(111)_{Cr_{23}C_6}[1\bar{1}\bar{1}]_\alpha||\ [01\bar{1}]_{Cr_{23}C_6}$ (Kurdjumov-Sachs OR);

$(110)_\alpha||(111)_{Cr_{23}C_6}[00\bar{1}]_\alpha||\ [01\bar{1}]_{Cr_{23}C_6}$ (Nishiyama-Wassermann OR);

$(001)_\alpha||(001)_{Cr_{23}C_6}[110]_\alpha||\ [100]_{Cr_{23}C_6}$ (Bain OR).

In additional, small amount of Z-phase particles was observed after long-term creep with a rupture time of 17863 h.

Recovery was observed in gauge portions of each crept sample. Subgrains tended to approach the equiaxed shape during creep tests. The regions of a homogeneous ferritic matrix (about 10 μm^2 in area) were locally observed in the creep tested specimen after 17 863 h.

The strengthening due to grain and sub-grain boundaries is one of the most effective mechanisms for achieving high creep resistance in high-chromium martensitic steels [2]. Stabilization of the tempered martensite lath structure is associated with the particle-stabilized substructure hardening [3]. It was shown that the pinning pressure exerted by $M_{23}C_6$ carbides is significantly higher than that by other precipitates. These carbides are therefore much more important than the other types of particles for the creep resistance of the studied steel. In the studied steel the coarsening rate of $M_{23}C_6$ carbides during creep exposure is relatively small. This can be associated with the effect of high boron content [4]. Then superior creep resistant of the studied steel was attributed to the addition of boron, which reduces the coarsening rate of $M_{23}C_6$ carbides.

References

1. Fedoseeva, A., Dudova, N., & Kaibyshev, R. (2016). Creep strength breakdown and microstructure evolution in a 3% Co modified P92 steel. *Materials Science and Engineering: A*, ***654***, 1-12.

2. Dudko, V., Belyakov, A., Molodov, D., & Kaibyshev, R. (2013). Microstructure evolution and pinning of boundaries by precipitates in a 9 pct Cr heat resistant steel during creep. *Metallurgical and Materials Transactions A*, ***44***(1), 162-172.

3. Kostka, A., Tak, K. G., Hellmig, R. J., Estrin, Y., & Eggeler, G. (2007). On the contribution of carbides and micrograin boundaries to the creep strength of tempered martensite ferritic steels. *ActaMaterialia*, ***55***(2), 539-550.

4. Abe, F. (2008). Effect of boron on creep deformation behavior and microstructure evolution in 9% Cr steel at 650 C. *International Journal of Materials Research*, ***99***(4), 387-394.

Low Temperature Creep of Martensitic Steels under Tension and Torsional Loading

Mathias Münch[1], Nagarjuna Remalli[1], Robert Brandt[1]

[1]. University of Siegen, Germany

Email: mathias.muench@uni-siegen.de, nagarjuna.remalli@uni-siegen.de, robert.brandt@uni-siegen.de

High strength martensitic steels with tensile strength grades from 2000 MPa upwards are applied in the powertrain of vehicles due to their excellent fatigue strength and high creep deformation resistance. However, an increasing demand to downsize combustion engines requires an even higher resistance of steels. Especially a high creep deformation resistance is needed when considering elevated temperatures up to 150°C.

Low temperature creep occurs at stresses below the macroscopic yield strength [1]. Most theories suggest that high strength steels obey a logarithmic creep law and the driving force for creep is provided by a thermally activated process [2]. The mechanism of the transient creep section in the mentioned temperature range is identified as pure dislocation glide [3].

The purpose of this research is to investigate the low temperature creep behavior of martensitic steels. The creep tests are conducted below the yield strength in a temperature range of 75 °C – 150 °C. Each test is performed for 16 hours. To exploit the advantage of a homogeneous stress distribution, the samples are strained under tension load. The influence of stress, temperature and tensile strength has been well studied and the dependency of the creep parameters is discussed. The obtained results are discussed considering a dislocation glide mechanism.

Furthermore, the samples are strained under torsional load as well. The correlation between torsional and tensional low temperature creep is shown up and discussed. Comprehensive residual stress measurements have been conducted in order to quantify structural changes resulting from low temperature creep in martensitic steels.

References

1. M.E. Kassner and K. Smith, Low temperature creep plasticity, *Journal of Materials Research and Technology* **3**, pp. 280 – 288 (2014).
2. R.W. Neu and H. Sehitoglu, Low-Temperature Creep of a Carburized Steel, *Metallurgical Transaction A* **23A**, pp. 2619 – 2624 (1992).
3. A. Oehlert and A. Atrens, Room Temperature Creep of high strength steels, *Acta metall. mater.* **42**, pp. 1493 – 1508 (1994).

Microstructural Investigations of Low Temperature Creep in Martensitic Steels

Nagarjuna Remalli[1], Mathias Münch[1], Robert Brandt[1]

[1]. Institute of Materials Engineering, University of Siegen, Germany

Email. nagarjuna.remalli@uni-siegen.de, mathias.muench@uni-siegen.de, robert.brandt@uni-siegen.de

Martensitic steel shows creep at low homologous temperature ($T/T_m < 0.3$) and at stress levels below the yield stress $\sigma_{0.2}$. Most of the theories show up that the creep strain of these steels follow a logarithmic creep law. By this the conclusion is drawn that the low temperature creep (LTC) deformation mechanism is pure dislocation glide [1]. The driving force is to be provided by a thermally activated process [2].

The creep rate is strongly influenced by the mechanical properties of the steel, i.e. a steel comprising a high yield strength shows a relatively low creep rate. Furthermore, LTC seems to be strongly controlled by microstructural and structural properties of martensitic steel. Absence of ferrite, a refined precipitate distribution and the structural uniformity decreases the creep rate significantly [3]. However, the mechanism of LTC in martensitic is still unclear and a matter of scientific investigations.

It has been shown up in [4] that a hypothesis implies that slip localization or inhomogeneous slip near the grain and phase boundaries is a major contribution to LTC. Therefore, this work is elucidates the microstructural changes that occurred during LTC in the temperature range of 75 °C – 150 °C in tension and torsional loading methods.

Phase analysis of samples that are strained under tension and torsional loading has been carried out by X-ray diffraction method. It was determined that the samples contain martensite in body centered cubic crystal structure and retained austenite in face centered cubic crystal structure. In order to observe the possibility of stress induced martensitic transformation during creep, phase quantification was done by a Rietveld refinement method. The microstructural changes occurred during the creep under tension and torsional loading is well studied by scanning electron microscopy (SEM). The prior austenite grain size (PAGBs) was determined and the influence of adding Vanadium as an alloying element over the changes in PAGBs was observed. Furthermore the morphological and compositional changes of precipitated carbides are investigated by SEM equipped with energy dispersive spectroscopy.

References

[1] A. Oehlert and A. Atrens, Room Temperature Creep of high strength steels, *Acta metall. mater.* **42**, pp. 1493 – 1508 (1994).

[2] R.W. Neu and H. Sehitoglu, Low-Temperature Creep of a Carburized Steel, *Metallurgical Transaction A* **23A**, pp. 2619 – 2624 (1992).

[3] C. Liu, Z. Zhaoe, and D.O. Northwood, Effect of Heat Treatments on Room Temperature Creep Strain of a High Strength Steel, *Key Engineering Materials Vols*. **171-174**, pp. 403- 410 (2000).

[4] C. Liu, S. Bhole, and D. Northwood, The Effects of Ferrite Content and Morphology on the Mechanical Properties and Room Temperature Creep of Quenched and Tempered SAE 4340 Steel, *JSME International Journal* **46A**, No. 3, pp. 272- 277 (2003).

Effect of Stress Multiaxiality on Creep Life of High-Chromium Ferritic Heat Resisting Steels

K. Yoshida[1], H. Tsuruta[1], M. Tabuchi[2] and K. Kobayashi[3]

[1]. Research Laboratory, IHI Corporation, Isogo-ku, Yokohama 235-8501, Japan

[2]. National Institute for Materials Science, Tsukuba 305-0047, Japan

[3]. Graduate School of Engineering, Chiba University, Inage-ku, Chiba 263-8522 Japan

Email: kimiaki_yoshida@ihi.co.jp

High-chromium ferritic heat resisting steels have been used for structural components at elevated temperature, because of their excellent creep properties. In general structural components are subjected to multi-axial stress state. It has been pointed out that the stress multiaxiality has an influence on creep damage evolution of high-chromium steels. It is, therefore, needed to identify the effect of multi-axial stress state on creep damage of the high-chromium steels.

In this study, circumferentially notched bar creep rupture tests were conducted for Grade 91 and Grade 92 steels in order to examine the effect of multi-axial stress state on creep rupture and damage behavior. Base metal and simulated fine grained heat affected zone material were tested for both steels. From the experimental results, it was confirmed that multi-axial stress state had significant and different effects on the creep rupture and creep damage behavior of these materials.

Finite element predictions based on ductility exhaustion approach were applied to predict the creep rupture time and the creep damage in notched bar specimens. It was concluded that a ductility exhaustion approach with empirical model of rupture strain provided reasonable creep life and damage predictability almost in a scatter band of a factor of 2.

Effect of thermomechanical processing on the high temperature tensile and creep-rupture strength of austenitic stainless steel

A. Rudskoy, G. Kodzhaspirov

Peter the Great St.Petersburg Polytechnic University, St.Petersburg, Russia

Email: gkodzhaspirov@gmail.com

The effect of High Temperature Thermomechanical Processing (HTMP) using rolling with combination of temperature – strain - time parameters on the structure and mechanical properties at the high temperature including creep rupture strength applied to austenitic stainless steel AISI 321 type has been studied. It was analyzed the dependence of structural transformations from temperature-strain-time parameters of HTMP. Both short and long-term strength at temperatures in the range 20 to 400^0 C have been estimated. The HTMP treated metal with a fragmented substructure has shown to be more advantageous with respect to the tensile and creep rupture strength in compare with work hardened and recrystallized structure. It was found that the HTMP treated steel with the relaxed by dynamic recovery and polygonization mechanism structure can provide higher functional loads and has a much less tendency to creep at 400^0C compared to steel subjected to conventional heat treatment (quenching from 110^0C).

References

[1] Jonas J.J., Barnett M.R. And Hodgson P.D. Thermomechanical Processing; *Materials ProcessingHandbook*, CRC (Chemical Rubber Corp.) Handbook series, *Taylor & Francis;* eds. J.R. Groza, J.F. Shackelford, E.J. Lavernia and M.T. Powers,(2007), 29, p.1.

[2] G E.Kodzhaspirov, A. I. Rudskoy, V. V. Rybin, Physical fundamentals and resource-saving technologies in the production of parts by plastic deformation [In Russian], *Nauka*, St. Petersburg , (2007), 350 p.

[3] Kodzhaspirov G.E., Rybin V.V., Apostolopoulos H. Role of mesostructured in thermomechanical treatment of metallic materials. *Metal Science and Heat Treatment*, (I2007), Vol.1-2, pp.24-28.

[4] C. M Sellars.50th Hatfield Memorial Lecture: The University of Sheffield, (2002).

[5] G. Kodzhaspirov, A. Borowikow, And M. Terentyev, Modeling the hot deformation stress–strain curve of a Ni-based superalloy, *Materials Scince Forum* (2013),762, pp.753–756.

Long-term creep strength and rupture ductility of Grade 92 steel

K. Kimura[1], K. Sawada[1]

[1]. National Institute for Materials Science

Email: kimura.kazuhiro@nims.go.jp

Creep strength enhanced ferritic (CSEF) steels have been widely used as high temperature structural components in the modern thermal power plants, however, remarkable drop in not only creep rupture strength, but also creep rupture ductility of CSEF steels are recognized in the long-term. Significant drop in creep rupture strength and ductility of the steels become obvious in the stress regime lower than 50% of 0.2% offset yield stress (Half Yield) at the temperatures [1]. A half yield is regarded to be an elastic limit of the steels, therefore, creep deformation mechanism of CSEF steels is considered to be different in high- and low-stress regimes divided by a half yield. High ductility in the high-stress regime above half yield should be provided by a plastic deformation, which easily takes place with the assistant of external stress above elastic limit. Generally, alloying elements including impurities, non-metallic inclusions and precipitation of intermetallic compounds such as Laves phase are considered to be a cause of ductility drop. On the other hand, a remarkable drop in ductility in the low-stress regime is considered to be derived from a concentration of creep deformation into a tiny recovered region formed at the vicinity of grain boundary. Preferential recovery along grain boundary is speculated to be caused by poor creep strength due to plastic deformation introduced during late stage of martensitic phase transformation, since creep strength of CSEF steels are reduced by plastic deformation prior to creep exposure [2].

New heat treatment process with intermediate tempering on partially transformed dual phase microstructure obtained by cooling from normalizing temperature to the temperature between Ms and Mf, retains the potential to improve creep rupture ductility without loss of creep rupture life. Improvement in creep rupture ductility of Grade P92 steel has been obtained by a modified heat treatment process with an intermediate tempering on partially quenched dual phase which reduces residual stress introduced by martensitic phase transformation accompanied with shape change and volume expansion [3].

References

1. K. Kimura, K. Sawada and H. Kushima, Proceedings of ASME 2010 PVP Conference, Bellevue, Washington, USA, July 18-22, PVP2010-25297, (2010).

2. F. Arav, H.J.M. Lentferink, C.F. Etienne, J.C. van Wortel, Proceedings of the Fifth Int. Conf. Creep of Materials, Lake Buena Vista, Florida, USA, May 18-21, pp.117-125, (1992).

3. K. Kimura and K. Sawada, Proceedings of the 23rd IFHTSE Congress, Savannah, Georgia, USA, April 18-21, (2016).

Creep behavior of n-ODS-18Cr steel

J. Rajesh[1], P. Suresh Babu[2], R. Vijay[2], S. Ganesh Sundara Raman[1] and G. Sundararajan[1]

[1]. Department of Metallurgical and Materials Engineering, Indian Institute of Technology Madras, Chennai-600036, India

[2]. International Advanced Research Centre for Powder Metallurgy and New Materials, Hyderabad-500005, India

Email: rajeshjarugula@gmail.com

Nano oxide dispersion strengthened steels (n-ODS) are being considered as high temperature structural materials in super critical thermal power plants and in advanced nuclear reactors. In the present study, n-ODS steel containing 18 Cr (Fe-18Cr-2W-0.25Ti-0.3Y_2O_3) prepared by mechanical alloying of the powder and subsequent extrusion, has been selected for evaluation of its creep behavior.

Tensile creep tests were carried out at temperatures in the range of 923 – 1073 K and the stresses in the range of 150 - 400 MPa. Minimum creep rate was calculated from the creep curves and the minimum creep rate data was utilized to assess the stress and temperature dependence of creep rate. The stress exponent and activation energy obtained in this study were greater than the values normally obtained in pure metals. This difference can be attributed to the threshold stress generated due to the dislocation-particle interaction. Transmission electron microscope (TEM) analysis were carried out on the crept samples to understand the influence of long term creep exposure on particle coarsening, dislocation/particle interaction and grain growth.

From the creep curves it was observed that the samples crept at higher stresses showed a tertiary stage creep behavior whereas at lower stresses the samples failed in the secondary stage itself. Observations made on creep fractured samples using the Scanning electron microscope (SEM) indicated a transgranular failure mode in the samples tested at high stresses and mixed-mode failure in the samples tested at low stresses.

Creep Crack Initiation in Carburised 316H Austenitic Stainless Steel

M.Callaghan[1], J.Eaton-McKay[1], A.Wisbey[1], P.Deem[1], M.Chevalier[2]

[1] Amec Foster Wheeler, Walton House, Birchwood Park, Warrington, Cheshire, WA3 6GA. UK

[2] EDF Energy Nuclear Generation, Barnwood, Gloucester, GL4 3RS. UK

Email: Andrew.wisbey@amecfw.com

Introduction - The UK operates a fleet of high temperature advanced gas-cooled nuclear reactors (AGRs), operating in the creep regime of their structural materials (450-650°C). In service there have been a number of examples of cracking in 316H austenitic stainless steel and this provides the impetus for the following study.

Experimentally it was observed that high levels of surface cracking occurred on ex-service 316H material following laboratory creep deformation, especially on the surface that had been previously exposed to the CO_2 coolant used in the AGRs (Figure 1a). Post testing metallography and micro-hardness testing indicated significant increases in surface hardness (Figure 1b) and other work showed high carbon levels at the surface [1] – attributed to a carburisation process. For experimental ease and to better control the surface condition, a pre-conditioning treatment was developed to replicate this surface carburisation.

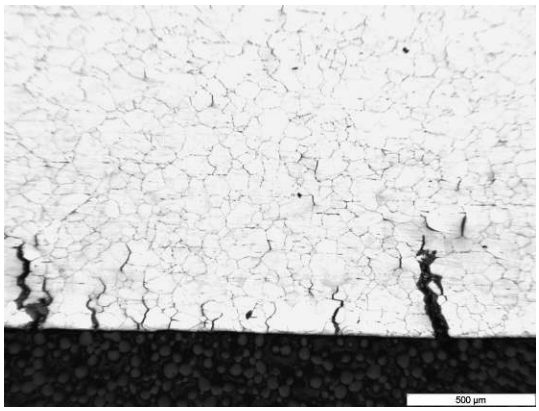

a)

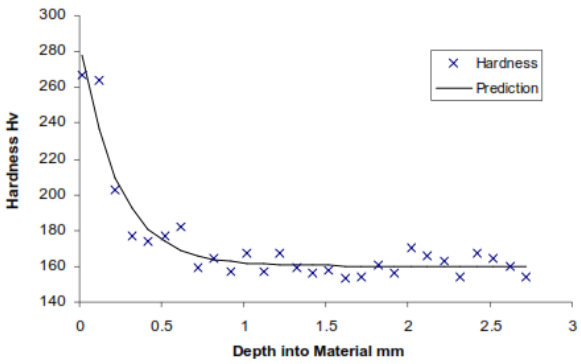

b)

Figure 1. Ex-service 316H material after creep testing at 525°C – a) metallographic section through the gauge length and – b) the micro-hardness profile from the surface of the material.

Experimental – The pre-conditioning used ex-service forged 316H material with a highly polished surface on the gauge length of standard uniaxial creep samples. These samples were then exposed to a simulated reactor gas atmosphere at 600°C, with 41.4 bar pressure and for 3000 hours. This was found to produce a significant hardened layer on the outer surface of the gauge length (i.e. not the end fixtures), similar to that found after service exposure.

Creep testing at 550°C was undertaken in lab air of the pre-conditioned 316H. Tests were interrupted at various creep strains, cooled to room temperature and initially the surface was non-destructively inspected using dye penetrant. Subsequently destructive metallography was used to detect surface cracking and was found to be substantially more sensitive than the dye penetrant.

Results & Discussion – Surface cracking has been observed following creep testing of pre-conditioned 316H at 550°C and the crack paths have mainly followed grain boundaries, as observed with ex-service material. The maximum crack length for

various creep strains is shown in Figure 2. No cracking was observed after the initial loading at a test stress of 260 MPa and presumably no cracking occurs below this stress. 339 MPa produced immediate cracking (3.55% plastic strain) but the boundary of the cracking behaviour upon initial plastic loading continues to be refined. There appears to be a different cracking response to the creep and plastic deformation – with cracking occurring after a creep strain of 0.33% (+0.41% plastic deformation, i.e. total strain of 0.74%) but none was seen after an initial plastic deformation of ~0.8% (prior to creep deformation). Thus there is a suggestion that creep deformation is more damaging than the plastic strain, possibly an effect of the differing interactions with the microstructure – i.e. creep damage accumulation at grain boundaries. There is a modulus mismatch at 550°C between the bulk 316H (~158 GPa) and the surface carburised layer (~205 GPa – assuming uniform layer characteristics) [2], leading to higher stresses in the carburised layer, compared to the bulk material. This will enhance the propensity for cracking in the outer surface.

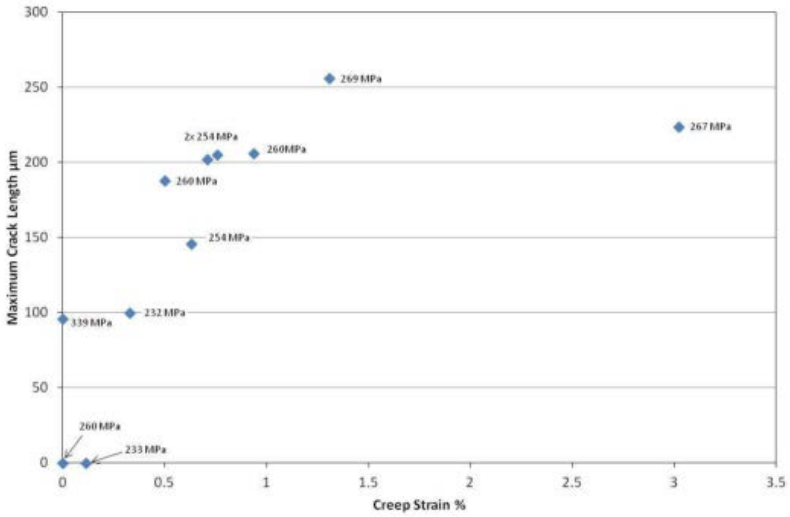

Figure 2. The effect of creep strain on the crack length in carburised 316H surfaces.

The data generated here supports the safe operation of the UK AGR fleet, identifying crack lengths to be assumed for structural integrity assessments and, in time, the creep strain tolerated prior to cracking.

References

1. C.Younes, “Oxidation & carburisation of type 316H stainless steels in AGR environments”, University of Bristol report, CMY/IAC/14/C04, June 2014.
2. A.Wisbey, M.Chevalier, D.Dean, P.Deem, M.Lynch, J.Eaton-McKay, M.Turnock, “The fatigue behaviour of carburised 316H stainless steel and the application to nuclear plant assessment” in proc. conf. Fatigue 2017, Cambridge, UK, 3-5 July 2017.

Creep Behavior of a 10%Cr Martensitic Steel

N. Dudova, R. Mishnev, R. Kaibyshev

Belgorod State University, Belgorod 308015, Russia

Email. dudova@bsu.edu.ru

Creep behavior and microstructure evolution of a 10%Cr martensitic steel with high B (0.008%) and low N (0.003%) contents were examined at 650°C. Deformation behavior was analyzed at apparent steady state in terms of threshold stresses at applied stress ranging from 120 to 180 MPa. The tempered martensite lath structure (TMLS) strengthened by fine $M_{23}C_6$-type carbides with an average dimension of 70 nm and MX carbonitrides with size ranging from 30 to 40 nm evolved after tempering at 770°C. The threshold stress is high and exceeds approximately 4 times the values of Orowan stress and detachment stress originated from MX particles which are distributed within laths. Mechanism of threshold stress attributed to boundary $M_{23}C_6$-type carbides was proposed. High threshold stress can be induced by $M_{23}C_6$-type carbides mainly located at high- and low-angle boundaries. These carbides exhibit high coarsening resistance and remain their orientation relationship with ferritic matrix unchanged under long-term creep. As a result, TMLS remains stable and no formation of subgrain structure occurs even after long-term creep at 120 MPa for approximately 40000 h.

Long Term Microstructural Evolution in a 10%Cr High Creep Resistant Martensitic Steel

R. Mishnev, N. Dudova, R. Kaibyshev

Belgorod State University, Belgorod 308015, Russia

Email. mishnev@bsu.edu.ru

Evolution of microstructure and dispersion of secondary phases were studied in a low-nitrogen 10%Cr martensitic steel with 3% Co and 0.008% B additives under creep conditions at 650°C and an applied stress of 120 MPa. Creep tests were interrupted at different creep stages and transmission and scanning electron microscopy were applied for structural characterization. It was shown that superior creep resistance of this steel was attributed to slow increase in creep rate at the first stage of tertiary creep whereas the rapid acceleration of creep rate took place only at the short second stage of tertiary creep. Transition from minimum creep rate stage to tertiary creep was found to be accompanied by coarsening of Laves phase particles, whereas $M_{23}C_6$ – type carbides demonstrated high coarsening resistance under creep conditions. The tempered martensite lath structure (TMLS) remains nearly unchanged under creep. Threefold increase in lath thickness is accompanied by an insignificant decrease in lattice dislocation density. $M_{23}C_6$–type carbides were found to give the main contribution to hindering the transformation of interlath boundaries to subgrain boundaries, impeding the migration of low-angle boundaries by exerting a large pinning pressure. A high Zener drag pressure is maintained up to rupture. $M_{23}C_6$ carbides retain their orientation relationship with ferritic matrix up to rupture providing a high drag pressure. Partial transformation of V-rich carbonitrides to Z-phase was revealed in the gauge portion of crept specimen, only. This strain-induced formation of Z-phase does not affect the creep strength under applied stress of 120 MPa due to nanoscale size of Z-phase particles.

CREEP UNDER SPECIAL CONDITIONS AND CREEP BEHAVIOR OF INORGANIC and NATURAL MATERIALS

Application of Shear-Lag Model in Creep of Random Planar Fibre Composites

F. Dobeš, P. Dymáček

Institute of Physics of Materials, Academy of Sciences of the Czech Republic, Žižkova 22, 616 62 Brno, Czech Republic

Email: dobes@ipm.cz

Mechanical properties of discontinuous fibre composites are dependent on fibre orientation. Ryu and Hong [1] suggested describing this dependence by means of the effective aspect ratio of fibres

$$S_{\text{eff}} = \frac{l}{D}\cos^2\theta + \left(\frac{3\pi - 4}{3\pi}\right)\left(1 + \frac{D}{l}\right)\sin^2\theta, \qquad (1)$$

where l and D are length and diameter of fibres, respectively and θ is the angle between stress direction and fibre axis. The effective aspect ratio is then incorporated into strengthening coefficient of the shear-lag model. In our contribution, we will apply this approach for an interpretation of creep of composites reinforced by planar isotropic distribution of fibres.

Two different techniques are used for creep testing: uniaxial compression and small punch tests. Both techniques are able to test reduced volume of material in comparison with conventional tensile creep tests. Specimens for uniaxial tests can be cut from the bulk with two basic orientations: (i) with the fibres plane perpendicular and (ii) parallel to the stress direction. The calculation of S_{eff} for orientation (i) is simple ($\theta = 90°$). The angle θ can have all values from 0° to 90° for stress direction parallel to the plane of fibres. The effective aspect ratio is then obtained by integrating Eq. (1) under assumption of random distribution of angles,

$$S_{\text{eff}} = \frac{2}{\pi}\int_0^{\frac{\pi}{2}}\left(\frac{l}{D}\cos^2\theta + \left(\frac{3\pi - 4}{3\pi}\right)\left(1 + \frac{D}{l}\right)\sin^2\theta\right)d\theta = \frac{l}{2D} + \frac{3\pi - 4}{6\pi}\left(1 + \frac{D}{l}\right). \qquad (2)$$

Disc specimens for small punch testing can be also prepared in two basic orientations. For small punch specimens with disc plane parallel to the plane of fibres, the effective aspect ratio is the same as in the above case (ii). For specimens cut in perpendicular direction to the plane of fibres a double integration is necessary. The obtained formulas are then compared with the results of testing composites prepared by squeeze casting of Al-based alloys into preforms consisting of planar randomly distributed Saffil fibres.

Acknowledgements. The research was conducted in the frame of IPMinfra supported through project No. LM2015069 of MEYS (Ministry of Education, Youth and Sports of the Czech Republic).

References

1. H.J. Ryu, S.H. Hong, *Creep Behavior of Advanced Materials for 21st Century*. R.S. Mishra, A.K. Mukherjee, K.L. Murty, (eds.), pp. 159-170, (1999).

Tensile and Creep Anisotropy in ODS Steel Tubes for Nuclear Cladding Applications

T. Jaumier[1,2], S. Vincent[1], L. Vincent[1], R. Desmorat[2]

[1]. DEN-Service de Recherches Métallurgiques Appliquées, CEA, Université Paris-Saclay, F-91191, Gif-sur-Yvette, France

[2]. LMT-Cachan (ENS Cachan, CNRS, Université Paris-Saclay), 94235 Cachan cedex, France

Email. thibaud.jaumier@cea.fr

The development of advanced nuclear systems such as Gen. IV sodium cooled fast reactors relies upon the availability of reliable structural materials. In particular, oxide dispersion strengthened (ODS) steels are suitable candidates for fuel cladding applications due to low irradiation induced swelling and good creep strength and corrosion resistance [1][2]. Ferritic Fe-14Cr-1W-0.3Ti and martensitic Fe-9Cr-1W-0.3Ti ODS steel tubes are studied, obtained by means of hot extrusion and pilger cold rolling. Tensile and creep tests are performed on tile and ring specimens.

While higher chromium content benefits corrosion resistance, the α {001}<110> stable texture formed by cold rolling prevents proper recrystallization during heat treatments [1]. Thus the anisotropic microstructure created during the fabrication processes cannot be modified properly and the ferritic ODS steel tube exhibits anisotropic tensile properties, with higher yield strength in the extrusion direction in the range 400-750°C. While the ductility seems better at intermediate temperatures in this longitudinal direction, it falls at higher temperatures and becomes better in the transverse direction (Fig. 1a). Furthermore, another anisotropic behavior can be seen with uniaxial creep tests, as shown in Fig. 1b. At a given stress the time to rupture (at 650°C) is much larger in the longitudinal direction than in the hoop one. These anisotropic features can be reduced on martensitic ODS steels with lower Cr content [3], though achieving an overall lower creep resistance along the extrusion direction but similar in the transverse/hoop direction (Fig. 1b).

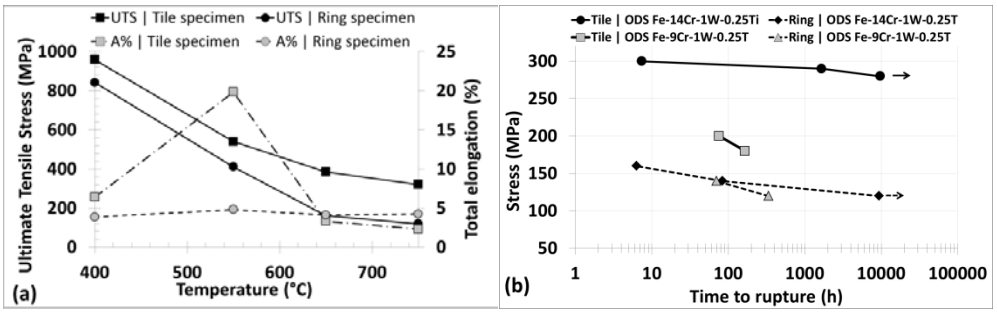

Figure 1. (a) Evolution with respect to the temperature of the ultimate tensile strength (UTS) and the total elongation for tensile tests performed at $1.10^{-5}s^{-1}$ on Fe-14Cr-1W-0.3Ti ODS steel tube. (b) Time to rupture/stress plot of uniaxial creep tests on ODS steel tubes. Arrows indicate ongoing tests

Examination of the fracture surfaces (tensile specimens) suggests damage is intra-granular at low temperatures (<550°C) and intergranular above. Fracture surfaces on creep specimens will be presented as well. Further work will be the development of a model describing the mechanical/damage behavior of these ODS steel tubes.

References

[1] S. Ukai et al., *Structural Materials for Generation IV Nuclear Reactors*, pp. 357-414, (2017)
[2] A. Alamo et al., *Journal of Nuclear Materials* **329-333 A**, pp. 333-337, (2004)
[3] L. Toualbi et al., *Journal of Nuclear Materials* **442,** pp. 410-416, (2013)

Creep Rupture and Damage Behaviors for Welded Pipe of Ni-based Alloy Using Full Thickness Specimen

S. Zhang[1], H. Fukutomi[1], T. Nishii[2], K. Satoh[3]

[1]. Materials Science Research Laboratory, Central Research Institute of Electric Power Industry, 2-6-1 Nagasaka, Yokosuka-shi, Kanagawa, 240-0196, Japan

[2]. Research & Development Dept., Electric Power Development Co., Ltd., 15-1, Ginza 6-Chome, Chuo-ku, Tokyo, 104-8165, Japan

[3]. Chubu Electric Power Co., Inc., 1, Higashishin-cho, Higashi-ku, Nagoya, 461-8680, Japan

Email: zhangsd@criepi.denken.or.jp

HR6W is currently considered as one of the leading candidate material for A-USC power plant due to its excellent creep strength and good ductility [1]. This paper investigates creep rupture and damage behaviors of HR6W weldment using full-thickness specimen cut from the circumferentially welded pipe. Creep test was conducted at 750°C and 114MPa, and was interrupted to observe the surface crack.

Circumferential welding of the pipe was performed with narrow gap hot wire switching TIG (HST) using MG 617 (⏥1.0mm) weld metal. The pipe was solution annealed followed by water quenching prior to welding and the weldment was subjected to a post weld heat treatment. Figure 1 shows shape and dimension of full-thickness specimen with macrostructure of side surface.

The creep test was finally stopped at 1800h in order to clarify the creep damage behavior. Time to creep rupture of full-thickness specimen predicted by Ω method [2] is about 1823h, which is longer than that of the standard welded joint specimen [3]. Figure 2 shows the surface cracks observed at 1800h. Many small cracks were also found on the inner surface in base metal. On the other hand, there was no crack on the side surface, but significant deformation zones were observed on both side surfaces inclined approximately at angle of 45 degrees to the axial direction of specimen.

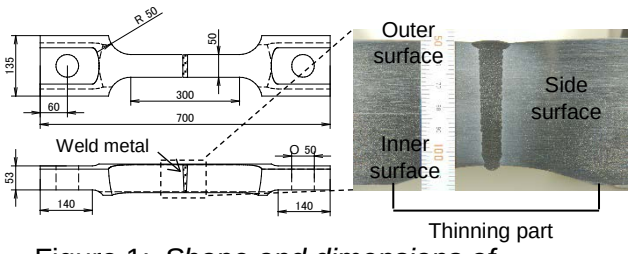

Figure 1: *Shape and dimensions of specimen tested (mm).*

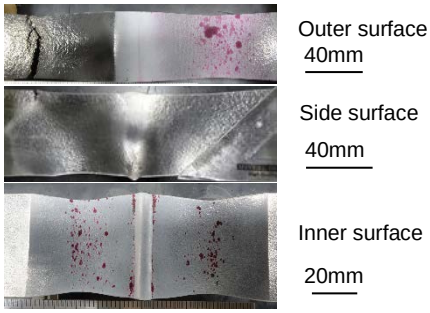

Figure 2: *Surface cracks observed at 1800h.*

REFERENCES

1. M. Fukuda, *Journal of the Japan Society of Mechanical Engineers* **114**, pp. 244-247 (2011).

2. M. Prager, *J. Pressure Vessel Technology* **117**, pp. 95-103 (1995).

3. T. Tokairin and M. Kitamura, *Report of the 123rd Committee on Heat-Resisting Materials and Alloys JSPS* **56(3)**, pp. 299-310 (2015).

Creep Behavior and Microstructure Evolution in Two Designs of P23/P91 Heterogeneous Welds

V. Vodárek[1], J. Holešinský[2], L. Střílková[3], Z. Kuboň[3]

[1] VŠB – Technical University of Ostrava, Ostrava, Czech Republic

[2] ArcelorMittal Ostrava, Ostrava, Czech Republic

[3] Materials and metallurgical research Ltd., Ostrava, Czech Republic

Email. vlastimil.vodarek@vsb.cz

Dissimilar welds usually represent critical locations of power plant structures and that is why a much of effort has to be devoted to studies on microstructural stability and creep resistance of these joints [1]. P23 and P91 steels are often used in modern blocks of fossil fired power plants. Heterogeneous welds between these steels can be used for compensation of different temperatures and steam pressures in different parts of components. This paper is dealing with creep behavior of two designs of P23/P91 dissimilar welds at temperatures of 500, 550 and 600 °C. Detailed microstructural characterization of crept specimens was carried out in order to understand differences in creep resistance of both P23/P91 weld designs.

P23 and P91 steel pipes of dimensions ϕ219 x 25 mm were welded by GTAW and SMAW technologies. A P91 matching filler metal (E CrMo 9 1B) was used in the Weld A and a P23 matching consumable (Thyssen Cr2WV) was applied to the Weld B. Chemical compositions of parent materials and fillers are shown in Table 1.

Table 1. Chemical compositions of parent materials and fillers (WM), in wt.%

Material	C	Mn	Si	Ni	Cr	Mo	V	Ti	Nb	W	N
P23	0.08	0.55	0.27	0.08	2.11	0.07	0.23	0.06	0.01	1.70	0.013
P91	0.11	0.51	0.38	0.42	8.67	1.00	0.23	0.01	0.07	0.01	0.048
WM91	0.11	0.66	0.21	0.82	9.50	1.02	0.22	N.A.	0.04	0.06	0.028
WM23	0.07	0.44	0.20	0.17	2.47	0.06	0.25	N.A.	0.02	1.62	0.018

Uni-axial creep rupture tests of both weld designs were carried out using “cross-weld” specimens (ϕ = 6 mm) at temperatures of 500, 550 and 600 °C. Five levels of stress in the range from 55 to 200 MPa were applied. Failure locations were identified using light microscopy. Detailed investigations on microstructure evolution in both weld designs during long-term creep/thermal exposure were carried out using scanning and transmission electron microscopy. Thermodynamic (Thermocalc) and kinetic (Dictra) modelling of carbon redistribution and minor phase evolution was performed and experimentally validated [2].

Results of creep rupture tests are summarized in Fig. 1. In addition to the experimental data points, mean and –20 % (low) standardized creep rupture strength curves for the P23 steel are shown. Results of creep rupture tests are close to or below the -20 % creep strength curve. The most pronounced drop in creep resistance occurred at low applied stresses and temperature of 600 °C. Furthermore, creep resistance of Weld A was slightly better for all temperatures of creep testing.

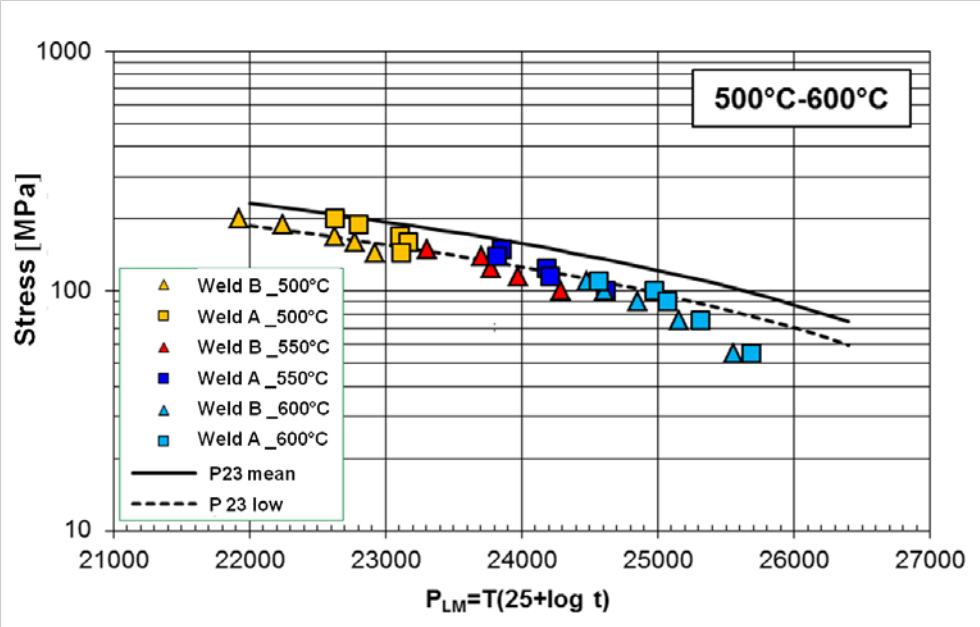

Figure 1. Results of creep rupture tests on Welds A and B

Metallographic investigations have demonstrated that during creep exposure the development of creep damage can simultaneously take place in several critical areas of welds but the final failure position is determined by the “weakest area” for given testing parameters. Specimens of the Weld B were more prone to failure in the partly decarburized zone, i.e. in the WM23 close to the WM23/P91 fusion line. EBSD investigations proved that specimens of the Weld B were less resistant to recovery/recrystallization processes in the partly decarburized zone than specimens of the Weld A. Decarburization of the WM23 or P23 steel during long-term creep exposure was accompanied by dissolution of carbides. Stability of MX phase in the P23 parent material was higher than that in WM23. It was related to differences in chemical composition of MX phase in both materials - MX particles in the P23 steel contained besides vanadium also titanium. Un-dissolved MX particles in the partly decarburized zone of the P23 steel slowed down recovery/recrystallization processes in bainite.

Acknowledgement

The authors wish to acknowledge the financial support from the project No. LO1203 "Regional Materials Science and Technology Centre - Feasibility Program" funded by Ministry of Education, Youth and Sports of the Czech Republic.

References

[1] H. Heuser, C. Jochum, W. Bendick, B. Hahn, Welding of New Pipe Steels in Modern High Efficiency Power Stations with High Steam Parameters, In: *Safety and Reliability of Welded Components in Energy and Processing Industry*, Verlag TU Graz, pp. 67 – 74 (2008).

[2] J. Holešinský, *Microstructural Stability and Creep Resistance of Steels for Energy Industry*, PhD Dissertation, VŠB – TUO, Ostrava, p. 113 (2015).

Creep damage and strain accumulation in steam-methane reformer catalyst tubes

J. M. Brear, J. Williamson

John Brear – Plant Integrity. Abergefryn, Capel Seion, Drefach, Llanelli, UK

Email: john.brear@johnbrear-plantintegrity.com

Steam-methane reformers provide a primary source of hydrogen for refining and process purposes. The highly endothermic reaction takes place in directly-fired, vertical, catalyst-filled tubes, 120-150mm diameter. Due to the severe operating conditions, these tubes are fabricated from centrifugally cast, thick section material, typically to the generic specifications HK40 and HPNb or their proprietary derivatives.

The dominant tube loading is the through-wall thermal stress generated on each start-up. Life consumption is by cyclic creep relaxation of these thermal stresses augmented by forward creep under the sustained pressure stress, the relative proportions being governed by the design and operational pattern of the unit. The combination of multiaxial stress and thermal gradients, coupled with microstructural variation through wall, leads to damage initiation typically at the quarter radius position. Creep cavities nucleate and grow, linking to form cracks which propagate to the inner and outer surfaces. It is usual to find a dense network of parallel cracks, of similar length, spaced radially by the width of the columnar grains (Fig. 1). Experience shows that significant service life is available after crack initiation [1].

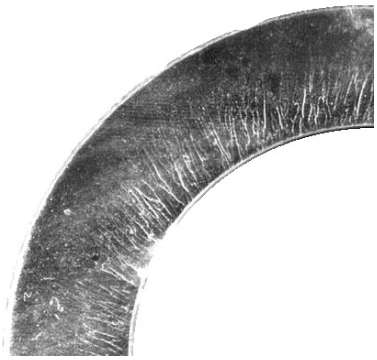

Figure 1 – HK40 reformer tube at end of life

A damage-front propagation approach, based on a primary-modified continuum damage mechanics formulation [2], has been shown suitable for modelling damage and strain development in these tubes. It has been validated against rigorous finite element analysis [3]. Uniaxial creep and rupture data provide the intrinsic strain and damage rate kinetics, and the resultant constitutive law is integrated numerically through the operational history of the tubes.

This paper explores the effects of materials, design and operational parameters on the creep process. Model predictions of damage and strain are compared with actual diametral measurements and NDE estimates from plant inspections. Results from reformers that have experienced serious fault conditions are included. Good agreement between prediction and observation is seen (Fig. 2).

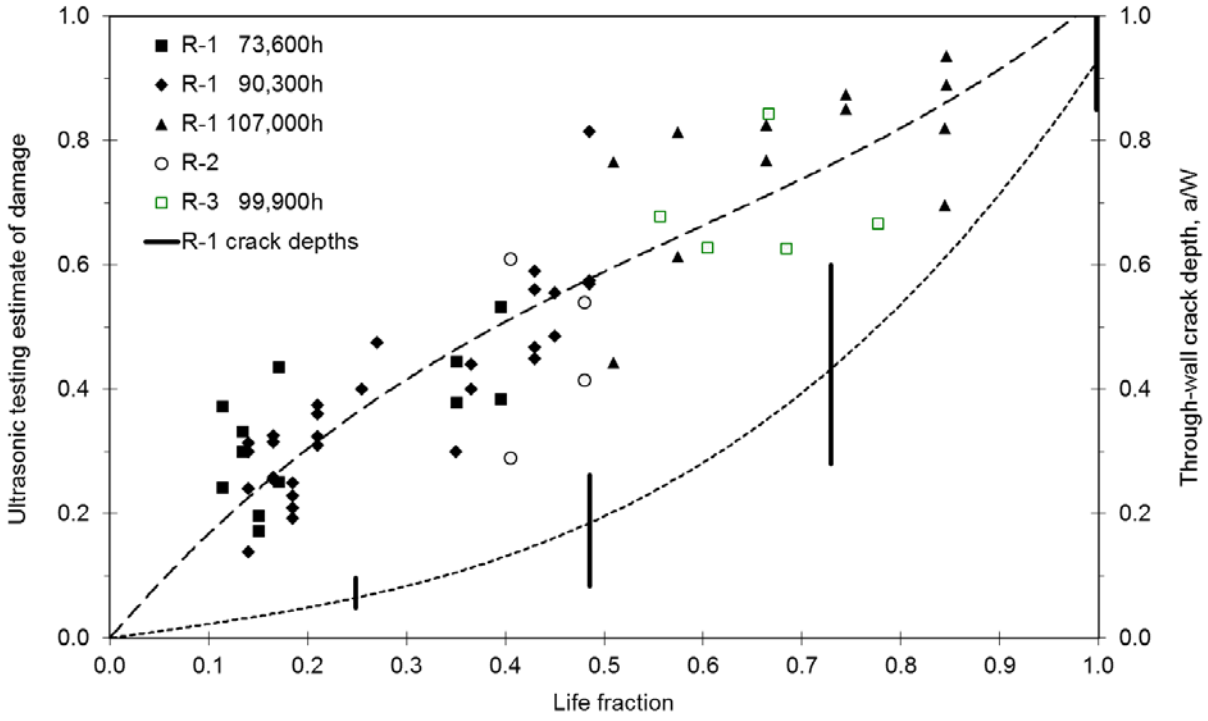

Figure 2 – Observed and predicted damage levels and crack depths in three reformers

Under service conditions, damage accumulation and cracking rates are enhanced at higher operating cycle frequencies, whereas under predominantly steady operation tube life is largely strain controlled. Small differences in tube temperatures and process conditions within a reformer are seen to explain observed variations in failure location and time.

It is concluded that the creep modelling approach adopted provides a realistic and robust basis for prediction of through-life damage and strain accumulation that can be validated and progressively refined using periodic inspection data.

References

1. J. Williamson and J.M. Brear, "Risk-based life management of steam-methane reformer pressure parts", *CRU 30th Conference 'Nitrogen + Syngas 2017'*, London, (2017)
2. L.M. Kachanov, *'Introduction to Continuum Damage Mechanics'*, Kluwer Academic, (1990)
3. J.M. Brear, J.M. Church, D.R. Humphrey and M.S. Zanjani, "Life Assessment of Steam Reformer Radiant Catalyst Tubes – the use of damage front propagation methods" *Int J Pressure Vessels and Piping*, **78**, Issue 11-12, pp.985-994, (2001)

Time-depend properties of human dentin and enamel

D. Zaytsev, P. Panfilov

Ural Federal University, Institute of Natural Sciences and Mathematics (Russia)

Email: dmitry.zaytsev@urfu.ru

A comprehensive study of time-depend properties of human dentin and enamel under compression and bending were carried out. Thirty intact human molars and premolars without caries and visible damages were used in this work. The teeth were extracted from mature (25-40 years old) male and female subjects according to the Ethical Protocol of Urals State Medical University (Ekaterinburg, Russia). Shimadzu AGX-50kN testing machine was used for the uniaxial compression and three-points bending. The shape of the samples were parallelepipeds of square cross section 2x2 mm^2 and 0.7 mm in height for uniaxial compression and with cross section 2x0.8 mm^2 and 12 mm in length for bending. The samples were tested at different rate of loading (10mm/min, 1mm/min, 0.1mm/min, 0.01mm/min and 0.001mm/min) under compression and bending. Ten samples per each rate of loading were compressed for both dentin and enamel samples. Ten dentin samples per each rate of loading were tested under bending also. In addition, five samples per each stress were tested under creep condition when constant stress applied to them during 5 hours (100MPa, 200MPa, 300MPa, 350MPa, 400MPa and 450MPa for compression of the dentin and enamel samples and 50MPa, 80MPa, 100MPa, 120MPa and 140MPa for bending of the dentin samples). Five samples per each constant stress were compressed for both dentin and enamel whereas five samples per each constant stress were bending for dentin. Scanning electron microscope (SEM) JEM 6390LV was applied for examination of the fracture surfaces of pieces of dentin samples after bending.

It was shown that the mechanical properties of human enamel did not depend on the loading rate in the diapason 10mm/min - 0.001mm/min under compression whereas the mechanical properties of human dentin depend on the loading rate in the same diapason under compression and bending. At that, no dependence of fracture behavior of dentin and enamel samples from the rate of loadings was observed. Both dentin and enamel samples were able to deformation at holding the constant load (creep). However, the deformation at compression creep test in enamel was lower than in dentin samples, ~ 0.3% and up to ~9%, respectively. The dependence of the properties of human dentin from the rate of loading under bending was more significant in comparison with dentin under compression. SEM observation of the fracture surfaces of pieces after bending was shown that all fracture surfaces are rough and no dependence of morphology of fracture surfaces from the rate of loadings is observed. On the fracture surface of the sample, which was destroyed during creep the test at stress more than 140 MPa, no features are observed which absent under bending at different conditions, for example, at different loading rates.

The reported study was supported by RSF, research project No. 15-19-10007.

Investigation of creep behavior of open cell ceramic Kelvin foam.

C. Settgast, M. Abendroth, M. Kuna

TU Bergakademie Freiberg, Institute of Mechanics and Fluid Dynamics, Lampadiusstraße 4, 09596 Freiberg, Germany

Email: Christoph.Settgast@imfd.tu-freiberg.de

Abstract. Ceramic foams are used as filters in metal melt filtration applications. During the casting process, the filters experience a complex thermo-mechanical loading, which is difficult to measure. Modern numerical methods allow the simulation of such complex processes. As a simplified foam structure, an open Kelvin cell is used as a representative volume element (RVE). The creep behavior of the bulk ceramic is taken from compression tests on novel carbon bonded alumina.

The results of this study describe the influence of the effective loading and the relative density of the ceramic foam on the creep behavior of a Kelvin cell.

Introduction. Open cell ceramic foams are widely used in industrial processes, e.g. as filters for metal casting. An open cell Kelvin foam [1] is often used as a simplified model. Settgast et al. [2] described a method to model such foams. The compressive deformation behavior at compact specimens of carbon bonded alumina (Al_2O_3-C) is tested at high temperatures [3].

In this paper, a creep power law suggested by [4] is used to describe the Al_2O_3-C creep behavior from [3] for a temperature of 1350°C. The effective creep behavior of the ceramic foam is investigated using a numerical analysis of the Kelvin foam model considering the influence of compressive stresses and relative density.

Methods and Materials. To generate a periodic finite element (FE) model as cubic RVE (see Fig. 1 middle) for a Kelvin cell foam, the procedure described in [2] is used. Thereby, the cavity in the interior of the foam struts is considered as well, which is due to the manufacturing process of these ceramic foams as shown in Fig. 1 (left). The relative density of the whole foam ϱ as well as the relative density of the inner cavity structure $\varrho_\mathrm{i} = 2.5\ \%$ can be adjusted.

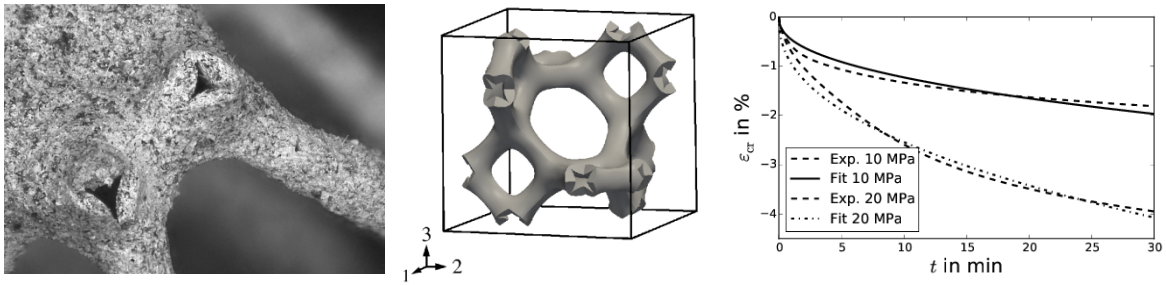

Figure 1. (left) Close-up view of a realistic ceramic foam, (middle) Kelvin cell as RVE with $\varrho = 10\ \%$. (right) Creep curves from creep testing at Al_2O_3-C from [3] and fitted creep power law.

Periodic boundary conditions for the displacements u_j ($u_j^{i+} - u_j^{i-} = \Delta u_j^i$) and tractions t_j ($t_j^{i+} + t_j^{i-} = 0$) are applied for corresponding points on opposite boundaries i+ and i-. The effective loading is given by the effective stress $\Sigma_{11} = t_1^1 / l^2$, where l denotes the RVE size.

The local creep behavior at $T = 1350°\mathrm{C}$ for a pressure of 10 MPa and 20 MPa is known from [3] and can be described using a creep power law of [4] $\dot{\varepsilon} = \left(\sigma / B\right)^n t^m \mathrm{s}^{-1}$, with the

equivalent creep strain rate $\dot{\varepsilon}$, the local von Mises stress σ, the stress factor B, the stress exponent n and the time exponent m. The parameters B, n and m are identified by numerical simulation and fitting of the experimental results. For the FE-model of the compression creep test, a friction coefficient of $\mu = 0.3$ is assumed between the pistons and specimen. The result is shown in Fig. 1 (right), with $B = 21450\ \text{MPa s}^{m/n}$, $n = 1.04$ and $m = -0.58$. The general course can be described by applying this creep power law. However, at the beginning the creep strain rate is underestimated and at the end of the creep tests the creep strain rate is overestimated.

Results and Discussion. The creep power law is applied to investigate the influence of Σ_{11} and ϱ on the Kelvin RVE foam. The results are shown in Fig. 2.

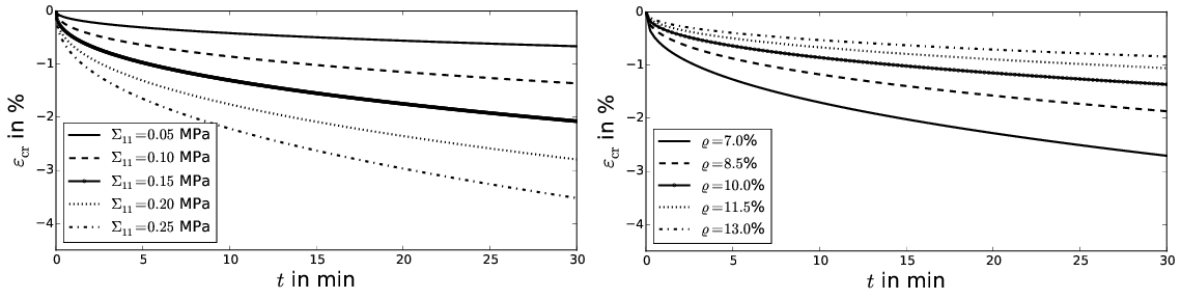

Figure 2. (left) Effective creep deformation for $\varrho = 10\%$ and different effective compression stresses Σ_{11}. (right) Effective creep deformation for compression stress $\Sigma_{11} = 0.1\ \text{MPa}$ and different ϱ.

With increasing Σ_{11} the local stresses increase as well. For small deformations it is a linear mapping [2], and so the effective creep deformation is increased, see Fig. 2 (left). For small deformations, the effective creep strain increases with the same stress exponent n and time exponent m as the bulk material.

As the relative density ϱ increases the effective creep deformation of the RVE decreases as shown in Fig. 2 (right), because more material is available to reduce the local stresses.

Conclusion. The effective creep behavior of open cell ceramic foam with carbon bonded alumina is investigated using a numerical approach. The effective creep behavior of the RVE can be described with the same power law as for the bulk material, whereby only the stress factor B depends on relative density ϱ.

Acknowledgement. The authors gratefully acknowledge the financial support by the German Research Foundation within the collaborative research center SFB 920.

References.

1. W. Thomson, *Acta Mathematica* **11**, pp. 121–134 (1887).

2. C. Settgast, M. Abendroth, M. Kuna, *Archive of Applied Mechanics* **86**, pp. 335-349 (2016).

3. J. Solarek, C. Bachmann, Y. Klemm, C.G. Aneziris and H. Biermann, *Journal of the American Ceramic Society* **99**, pp. 1390–1397 (2016).

4. K. Naumenko and H. Altenbach, *Modeling of Creep for Structural Analysis* (2007).

Harper-Dorn Creep in Lithium Fluoride Single Crystals

Shobhit P Singh[1], Michael E Kassner[2], Praveen Kumar[1]

[1]Department of Materials Engineering, Indian Institute of Science, Bangalore 560012, India

[2]Department of Aerospace and Mechanical Engineering, University of Southern California, Los Angeles, 90007 CA (USA)

Email: shopasi@platinum.materials.iisc.ernet.in

Abstract. Creep behavior of high purity LiF single crystals is critically examined in the Harper-Dorn (H-D) regime. Stresses, σ applied onto samples are of the order of 10^{-5} G, where G is the shear modulus of the material at high homologous temperatures of > 0.9 T/T_m. It is established that the creep occurs according to the classic H-D mechanism, showing a stress exponent of 1 and stress independent dislocation density. This is first study showing H-D creep in LiF, and the observations are discussed in terms of saturation dislocation density obtained after prolonged high temperature annealing.

Introduction. Harper and Dorn, in 1957, published a classical paper showing strain rates in steady state of creep as high as 1400 times greater than what was predicted by Nabarro-Herring model in high purity Al [1]. This phenomenon was observed in special class of high purity materials (single crystals or large-grain sized material) at very high homologous temperatures (> 0.9 T_m) and very low stresses (< 10^{-5} σ/G). The low-stress high-temperature creep, commonly referred to as the Harper-Dorn (H-D) creep, is constantly under debate and criticism since its advent. The salient features of Harper-Dorn creep include stress exponent of 1, independence of dislocation density, ρ to the applied stress and the activation energy equal to that of self-diffusion [2]. The observation of stress independence of ρ, which can then phenomenologically explain a stress exponent of 1, is particularly puzzling. Although dislocations are non-equilibrium defects, removal of all dislocations from a sample after prolonged annealing at high temperatures is generally not possible. Instead a saturation ρ may be observed. This leads to the question if the stress independence of ρ in the H-D creep regime is linked to this saturation limit of ρ.

Objective. This study investigates the occurrence of H-D creep in high purity LiF single crystals, *in lieu* of existence of exhaustion of ρ.

Experimental details and results. Compression creep of LiF single crystals is conducted at 1070 K (~0.95 T_m) at constant load starting from 0.042 MPa up to 3 MPa (i.e., 2×10^{-6} G to 1.5×10^{-4} G). In order to reduce friction between the sample and loading platens, hexagonal boron nitride powder was applied as lubricant.

Figure 1 compares creep data of LiF as obtained in this study with that reported in previous studies. The stress exponent of 1 is observed at low stresses, which concurs with the observation of H-D creep in LiF. Figure 2 shows variation of steady state ρ of creep tested LiF as function of stress. The stress independence of ρ can be clearly observed in the H-D creep regime, thus confirming occurrence of classic H-D creep in LiF single crystals. Fig. 2 also shows that the observed ρ in creep tested LiF single crystals were significantly higher as compared to that obtained after prolonged annealing at 0.92 T_m, thereby suggesting observation of ρ to be real outcome of testing under creep conditions and not due to exhaustion.

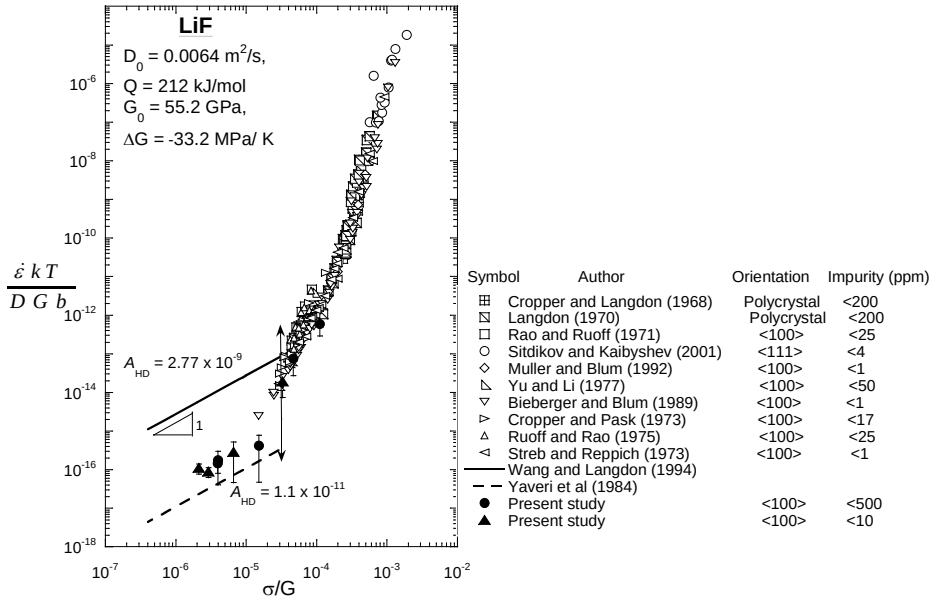

Fig. 1. Master plot of normalized stress versus normalized strain rate for LiF. The solid symbols represent the data from the present study.

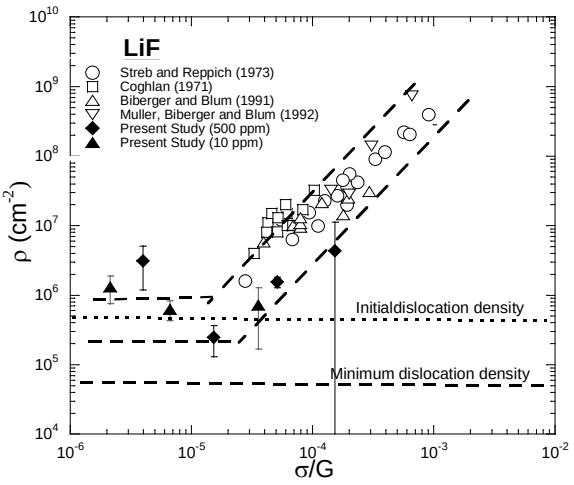

Fig. 2. Normalized stress versus the steady state dislocation density of LiF.

Conclusion. Classical Harper-Dorn creep is observed in LiF single crystals, wherein a stress exponent of 1 and the stress independence of ρ exists below a stress level of 2×10^{-5} G and at temperatures greater than 0.95 T_m.

References

1. J. Harper and J.E. Dorn, Viscous creep of aluminum near its melting temperature, *Acta Metallurgica*, **5(11)**, pp. 654-665 (1957).

2. M.E. Kassner, P. Kumar, and W. Blum, Harper–Dorn creep, *International journal of plasticity*, **23(6)**, pp. 980-1000 (2007).

Deformation behavior of polymerous liquid-crystalline films in a creep mode.

Karimov S.K., Abdumanonov A., Egamov M.Kh.

Khujand Scientific Centre AC of the RT, Khujand, Tajikistan.

E-mail: Sorbon_25@mail.ru

Structural changes and molecular processes happening in uniaxial tension of high-elasticity polymer systems in creep and stress relaxation modes are still in the center of scientists' attention. This problem is more urgent for compositional systems with dispersive medium which have anisotropy peculiarities. Dispersed with polymer nematic liquid crystal (DPNLC), which has lately been used as a photonics, can belong to the mentioned type of system. Optical transmission of the DPNLC in electric and magnetic field has enough been studied and there is a huge number of works on it. Studying deformation resistance properties of the given fields with regard to formation of new modification of configuration is however in the stage of overall investigation. The given article touches on the very direction of investigation.

Films with different concentration of microscopic droplet of liquid crystal were exposed to uniaxial deformation in the mode ε=const and the speed of the deformation were measured in a time interval of [1-10· 10^8] second. The outcomes of the measurement of deformation speed in time are depicted in a form of chart on the pic.1. It turned out that degree of deformation for the polymer matrix of polyvinyl alcohol (PVA) is twice as much than for polyvinylbutiral (PVB).

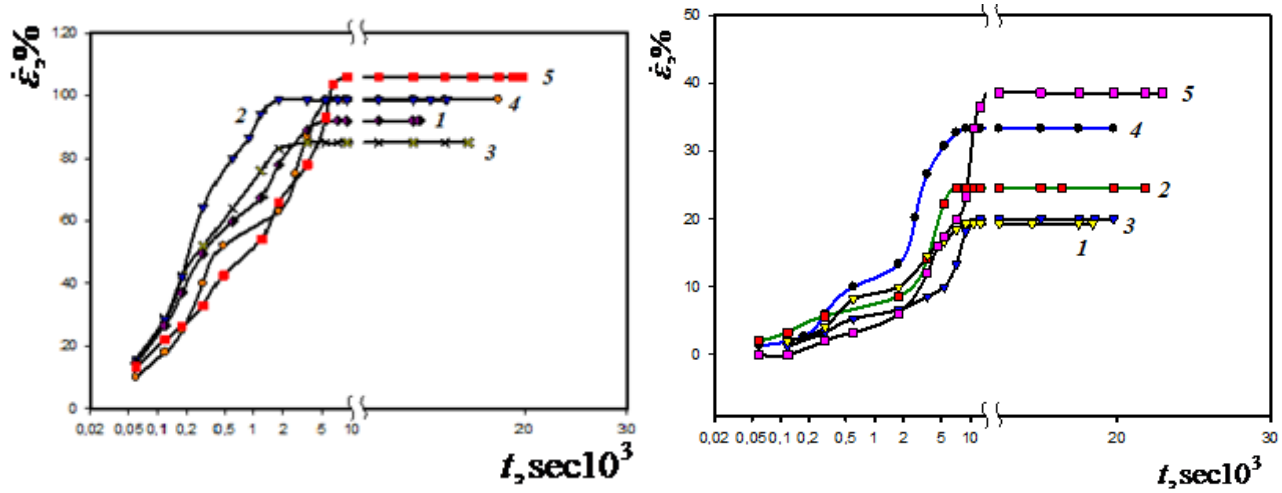

Fig. 1. Creep curve DPNLC film with 7CB (1-15%, 2-20%,3-25%, 4-30%, 5- 35%) and polymer matrix of polyvinyl alcohol PVA (a) and PVB (b)

Character of changes in creep curves deformation corresponds to the curves of polymeric systems in the highly elastic state, and is in good agreement with theoretical calculations.

The experimental results are interpreted on the basis of the nonlinear theory of viscoelasticity.

Why a Rock Never Creeps.

P. Panfilov[1], A.N. Kochanov[2]

[1] Ural Federal University, Yekaterinburg, Russia

[2] Research Institute for the Comprehensive Exploitation of Mineral Resources,Russian Academy of Sciences, Moscow, 111020 Russia
peter.panfilov@urfu.ru

The human history has shown that rock materials exhibit excelsior long-term mechanical properties in comparison with other structural materials of mankind. Indeed, “hard as a rock” is the highest strength characteristic of the substance. Some illustrations of this well-known statement are considered in this presentation. Deformation behavior of a wide circle of rock materials including granite, serpentine, quartzite and sand stone were studied on the small sized samples under compression and tension in air and water. In addition, the evolution of cracks on the macroscopic and microscopic scales was examined in these samples. Under tension, all rocks behave like a brittle substance, while under compression they demonstrate considerable elasticity, but a tiny irreversible deformation. Despite this, the dangerous cracks in the samples consist of a lot of pore-like microcracks. It means that there are two mechanisms of stress accommodation in these rock materials. An ability to considerable elastic deformation is the additional mechanism in comparison with such intrinsically brittle materials as SiO based synthetic crystals. However, the contribution of irreversible deformation to a crack stoppage in the rocks is almost zero. Therefore, a human never meet with the showings of creep of rocks under living conditions.

Acknowledgements

The reported study was supported by RSF, research project No. 15-19-10007.